

**Satellite Remote Sensing of snow cover over  
Northeast China**

**YAN, Su**

A Thesis Submitted in Partial Fulfillment  
of the Requirements for the Degree of  
Doctor of Philosophy  
in  
GeoInformation Science

The Chinese University of Hong Kong  
February 2011

UMI Number: 3492051

All rights reserved

INFORMATION TO ALL USERS

The quality of this reproduction is dependent on the quality of the copy submitted.

In the unlikely event that the author did not send a complete manuscript and there are missing pages, these will be noted. Also, if material had to be removed, a note will indicate the deletion.



UMI 3492051

Copyright 2011 by ProQuest LLC.

All rights reserved. This edition of the work is protected against unauthorized copying under Title 17, United States Code.



ProQuest LLC.  
789 East Eisenhower Parkway  
P.O. Box 1346  
Ann Arbor, MI 48106 - 1346

Thesis/Assessment Committee

Professor HUANG Bo (Chair)

Professor LIN Hui (Co-Supervisor)

Professor ZHANG Yuanzhi (Co-Supervisor)

Professor CHEN Jinsong (Committee Member)

Professor LI Xin (External Examiner)

## ABSTRACT

of thesis entitled:

Satellite Remote Sensing of Snow Cover over Northeast China

Submitted by YAN Su  
for the degree of Doctor of Philosophy  
at The Chinese University of Hong Kong  
in December 2010

Climate change becomes the hottest focus in the world at present as the tremendous increases of frequency of extreme weathers and natural disasters. It is not the problem only for government or scientists. Civilians start to concern about this issue when flooding, snow disasters and earthquakes are happening all over the world. The need to understand what is going, what will happen and why it happens on global climate becomes imperative. The study on snow cover provides us a possibility to fulfill the need.

Changes of snow cover is not only a result of global climate change, but also a contribute factor to the changes. The distribution and amount of snowfall play critical role in energy balance, heat release and atmosphere circulation. The changes on snow cover will lead to local, even global changes of climate, not to mention local disasters.

In this thesis, a systematic study on snow cover over Northeast China (Heilongjiang, Jilin and Liaoning provinces) is conducted. Firstly, study on the properties of local snow has been done by the method of insitu measurement and ground based field experiments. The result shows that, as one of the most sensitive parameters, snow grain size varies from 0.2mm to over 3mm. The range of snow grain size is too big to determine a fixed constant in passive microwave snow monitoring models. The followed experiments result on snow grain size and reflectance suggests that the problem can be solved by using a timely snow grain size retrieval model based on NIR reflectance data. Then the automatic process methods for mass of MODIS and AMSR-E data are discussed to get high quality input for snow covered area and snow depth model. By using the new process methods, the processing time of a 48 working days` job can be finished within two working days. After the preparation works, two improved models for snow covered area and snow depth monitoring are developed. To compare with MODIS snow products, the SCA monitoring accuracy

of improved model is better. Less errors on snow covered test sites can be found in improved model in the case study on SCA monitoring over Northeast China.

An initial data assimilation conception is introduced into SD estimation model. In improved model, snow grain size increase ratio that calculated by using MODIS band 4 and band 5 reflectance data are inputted into passive microwave SD estimation model to determine the value of constant which is changing according to the changes of snow grain size. Results show that, during the dry snow period, in new model the RMSE of estimation SD and measurement ones in 5 test sites are increased 24%, 0.4%, 23%, 65% and 16% respectively. This data assimilation method provides a bright new way in combination application of optical and microwave remote sensing technology in snow monitoring.

Although many achievements are obtained in the research, the investigation on snow properties and the preliminary application of remote sensing on snow monitoring during the 4 years from 2005-2009 shows us there are still some problems that need to be solved, they are:

1. Snow depth monitoring during wet snow period;
2. Snow depth monitoring on ice;
3. Specific snow grain size estimation by using MODIS data.

The future work on snow monitoring should go deeper for better estimation accuracy.

## 摘要

随着极端气候和自然灾害发生频率的猛烈增加,全球气候变化已经成为当今世界的焦点。全民都已经认识到了解气候变化、挖掘变化规律最终达到准确预测是当前唯一的应对方式。积雪作为对气候变化,尤其是气候变暖,最为敏感的因素之一,理所应当受到广泛重视。而积雪分布以及降雪量变化带来的大气环流、太阳辐照、热量释放和热量平衡的变化更是目前局部气候乃至全球气候变化的重要影响因子。可以说,积雪的变化与全球气候变化互为因果,对于积雪的监测是当前研究了解全球气候变化的有效方式之一。

本文以东北地区积雪研究为例,从地区积雪特性的研究到遥感监测模型的建立,对该地区季节性积雪首次进行了较为系统全面的研究。长期观察和测量显示,该地区积雪覆盖从每年 11 月起至次年 4 月止,其中干雪期大体从 11 月中旬至 3 月中上旬。在此期间,雪粒径变化非常显著,变化范围从新雪的 0.2mm 到陈雪的超过 3 mm,尤其深霜层的形成,对微波反演积雪厚度造成了巨大影响。不过地基试验显示,雪粒径与近红外区 ( $1.2\mu\text{m}$  -  $1.4\mu\text{m}$ ) 反射率比率有着很高的相关性 ( $R = 0.965$ ), MODIS 可以用于对该地区积雪粒径变化的估算。

接下来的章节里我对两个模型和两种遥感数据自动化处理系统的开发进行了探讨。这两个数据处理系统分别应用于海量 MODIS 数据和海量 AMSR-E 数据的自动化处理。实验结果表明,使用该系统可将人工处理需要 48 工作日的工作压缩至 2 工作日内完成。积雪覆盖面积及积雪深度的反演分别以 MODIS 和 AMSR-E 数据作为主要输入参数,其他多种数据相融合。积雪覆盖面积模型对辽宁省气象站的雪盖与否的监测结果表明,该模型探测雪盖误差低于 MODIS 积雪产品。数据同化思想首次应用于动态积雪深度反演的模型,MODIS 反演雪粒径变化率作为 AMSR-E 反演雪深模型的一个输入参数,将 5 个测试站点的估算雪深与实测雪深的 RMSE 分别提高了 24%, 0.4%, 23%, 65% 和 16%。

# TABLE OF CONTENT

|  |     |
|--|-----|
| ABSTRACT.....  | 1   |
| TABLE OF CONTENT .....   | IV  |
| LIST OF TABLES .....   | VI  |
| LIST OF FIGURES .....  | VII |
| ACKNOWLEDGEMENT .....  | X   |
| Chapter 1 INTRODUCTION .....   | 1   |
| 1.1 Significance of This Research.....   | 1   |
| 1.2 Research Questions and Objectives .....  | 3   |
| 1.3 Framework .....  | 4   |
| 1.4 Structure of This Thesis .....   | 6   |
| Chapter 2 LITERATURE REVIEW.....   | 7   |
| 2.1 Remote Sensing Data Applied in Snow Monitoring.....  | 7   |
| 2.1.1 Optical Remote Sensing Imagery.....  | 7   |
| 2.1.2 Microwave Remote Sensing Imagery .....   | 9   |
| 2.2 Effects on Estimation Accuracy.....  | 14  |
| 2.2.1 Vegetation .....   | 15  |
| 2.2.2 Large Water Body.....  | 19  |
| 2.2.3 Bared Land.....  | 21  |
| 2.2.4 Mountains.....   | 22  |
| 2.3 Snow Cover Monitoring Researches in China.....   | 22  |
| Chapter 3 METHODOLOGY.....   | 24  |
| 3.1 Study Area.....  | 24  |
| 3.2 Methods.....   | 26  |
| 3.2.1 SCA Monitoring Methods.....  | 27  |
| 3.2.2 SD Monitoring Methods .....  | 30  |
| 3.2.3 SWE estimation using remote sensing data .....   | 32  |
| 3.3.4 Researches on Effects of Estimation Accuracy and Corresponding<br>Algorithms .....           | 34  |
| Chapter 4 FIELD EXPERIMENT AND IN SITU DATA COLLECTION .....                                       | 35  |
| 4.1 Objectives of Field Survey.....  | 35  |
| 4.2 Field Survey and Field Experiments.....  | 36  |
| 4.2.1 Optical Remote Sensing Experiments.....  | 37  |
| 4.2.2 Field experiments on Microwave Properties of Snow .....                                      | 50  |
| Chapter 5 IN SITU DATA ANALYSIS.....   | 57  |
| 5.1 Introduction .....   | 57  |
| 5.2 Analysis of In Situ Data .....   | 57  |
| 5.2.1 Field Experiments Data.....  | 57  |
| 5.2.2 Analysis of Long Term Observation Data .....   | 88  |
| Chapter 6 SATELLITE REMOTE SENSING DATA PROCESSING.....  | 92  |
| 6.1 MODIS Data Processing.....   | 92  |
| 6.1.1 Introduction .....   | 92  |
| 6.1.2 Methodology .....  | 96  |
| 6.1.3 Snow Monitoring over Northeast China Based on MODIS L1B Data<br>during 2006-2007 Winter..... | 104 |
| 6.1.4 Snow Map Generation .....  | 107 |
| 6.1.5 Advantage of new Processing Method.....  | 110 |
| 6.2 AMSR-E Data Processing.....  | 110 |
| 6.2.1 Introduction.....  | 110 |

|   |            |
|---|------------|
| 6.2.2 Methodology .....   | 110        |
| 6.2.3 Comparison of Ascend and Descend data.....  | 115        |
| 6.2.4 Comparison between Estimation Results Based on AMSR-E and In<br>Situ Measurements ..... | 117        |
| 6.3 Breakthrough Points to Improve Remote Sensing Estimation Models.....                      | 124        |
| Chapter 7 DEVELOPMENT OF IMPROVED SNOW MONITORING MODELS                                      | 126        |
| 7.1 SD Retrieval Model.....   | 126        |
| 7.1.1 Introduction .....  | 126        |
| 7.1.2 Methodology .....   | 127        |
| 7.1.4 Conclusion .....  | 140        |
| 7.2 SCA Retrieval Model.....  | 141        |
| 7.2.1 Introduction.....   | 141        |
| 7.2.2 Methodology .....   | 143        |
| 7.2.3 SCA Estimation Results and Discussion .....   | 146        |
| 7.2.4 Conclusion .....  | 149        |
| Chapter 8 INNOVATIONS AND FUTURE WORKS.....   | 149        |
| 8.1 Innovations.....  | 149        |
| 8.2 Future Work .....   | 152        |
| <b>References .....</b>   | <b>154</b> |

## LIST OF TABLES

|   |     |
|---|-----|
| Table 2.1 Algorithms applicable to coniferous, deciduous, and sparsely forested landscape regions .....       | 19  |
| Table 3.1 Channel selection in NDSI calculation for different optical remote sensing sensors .....            | 27  |
| Table 3.2 Primary Algorithms to obtain snow properties by using passive microwave data .....                  | 33  |
| Table 3.3 SWE estimation algorithms based on passive microwave data .....                                     | 33  |
| Table 3.4 Summary of effects of land cover types on SD and SWE estimation .....                               | 34  |
| Table 4.1 Field survey record .....   | 40  |
| Table 4.2 Record for regular information .....  | 43  |
| Table 4.3 Record for spectrum .....   | 43  |
| Table 4.4 Parameters of SMZ-B4/T4 zoom expander stereomicroscope .....  | 44  |
| Table 4.5 Record for snow grain size .....  | 48  |
| Table 4.6 Snow information record for passive microwave experiment .....                                      | 53  |
| Table 5.1 Spectrum record in different test sites .....   | 63  |
| Table 5.2 Snow grain size in different position .....   | 65  |
| Table 5.3 Snow grain size in different layer .....  | 68  |
| Table 5.4 Slope of peak and trough in different test sites .....  | 70  |
| Table 5.5 Spectrum slopes of normal smooth snow .....   | 72  |
| Table 5.6 Spectrum slopes of uneven snow .....  | 73  |
| Table 5.7 Spectrum slopes of refrozen snow .....  | 74  |
| Table 5.8 Snow grain size and corresponding slope .....   | 76  |
| Table 5.9 NDSI of snow mixed with hay .....   | 78  |
| Table 5.10 Measurement result of TB and Radiance of three kinds of underlying surface .....                   | 81  |
| Table 5.11 Radiance measurement of different orientations in testing site A(the angle of incident is 0) ..... | 82  |
| Table 5.12 Brightness Temperature testing results on corn land .....  | 87  |
| Table 5.13 Brightness Temperature testing results on Ice surface .....  | 87  |
| Table 6.1 Interpretation key for 8-day snow covered mapping derived from MODIS L1B .....                      | 103 |
| Table 6.2 Spatial resolution of AMSR-E data .....   | 112 |
| Table 6.3 Location of test sites .....  | 117 |
| Table 6.4 Statistical data of long term observation in test sites .....                                       | 119 |
| Table 6.5 Summary of field measurements in two test sites in Northeast China .....                            | 120 |
| Table 6.6 The SD estimated from AMSR-E data compared with field data of 05-06 winter .....                    | 120 |
| Table 6.7 Correlations of estimation SD, measured SD and daily temperature .....                              | 122 |
| Table 6.8 The SWE estimated from AMSR-E data compared with field data of 05-06 winter .....                   | 123 |
| Table 7.1 In situ Precipitation on the time duration in corresponding to Figure .....                         | 135 |
| Table 7.2 RMSE of original and improved models .....  | 140 |
| Table 7.3 Example of Cloud Cover Duration .....   | 142 |

## LIST OF FIGURES

|  |    |
|--|----|
| Figure 1.1 Research Framework .....  | 4  |
| Figure 1.2 Research Flowchart .....  | 4  |
| Figure 1.3 Study procedures .....  | 5  |
| Figure 2.1 Spectral reflectance of optically thick cloud compared with snow<br>cover of two different grain sizes (adopted from Rees, 2005).....                               | 8  |
| Figure 2.2 <i>A multi layer system with a wave incident from above at an angle <math>\theta_{i,s}</math></i><br>(adopted from Christian Mätzler & Andreas Wiesmann, 2007)..... | 12 |
| Figure 2.3 <i>The parameters of a selected layer j</i> (adopted from Christian Mätzler<br>& Andreas Wiesmann, 2007).....   | 13 |
| Figure 3.1 Northeast China ( $38^{\circ}$ – $52^{\circ}$ N and $118^{\circ}$ – $134^{\circ}$ E).....   | 24 |
| Figure 3.2 Land cover types of Northeast China derived from<br>MODIS_NE_2000 Data Set (Provided by Dr. Kaishan Song).....  | 25 |
| Figure 4.1 Selected test sites during field experiment trip from west to east Jilin<br>.....   | 38 |
| Figure 4.2 Natural State of test sites .....   | 39 |
| Figure 4.3 Snow grain size measurement .....   | 41 |
| Figure 4.4 Grain size for both new fallen snow and sedimentary snow .....  | 41 |
| Figure 4.5 Snow grain sizes obtained from different snow layer on river ice ...  | 42 |
| Figure 4.6 Experiments on the relationship between snow grain size and<br>spectrum (20091222, night) .....   | 46 |
| Figure 4.7 Test sites located in Changling, Songyuan and Jilin .....   | 47 |
| Figure 4.8 Snow mixed with corn land(a) and vegetation(b).....   | 49 |
| Figure 4.9 Snow surfaces with different SDs .....  | 50 |
| Figure 4.10 Location of test sites for passive microwave experiments .....   | 52 |
| Figure 4.11 Natural stages of snow in test sites.....  | 52 |
| Figure 4.12 Experiments on underlying surface effects on microwave signals. ....   | 56 |
| Figure 5.1 Effects of vapors on spectral collected from field measurements ....  | 58 |
| Figure 5.2 Experiments on 20100126 .....   | 59 |
| Figure 5.3 Wavelet transformed spectrum collected from field experiment on<br>20100126.....  | 60 |
| Figure 5.4 Spectrum processing stages .....  | 61 |
| Figure 5.5 Processing procedure for spectrum that is strongly affected by vapor<br>.....   | 61 |
| Figure 5.6 Spectrum of surface snow.....   | 63 |
| Figure 5.7 Spectrum of snow body .....   | 63 |
| Figure 5.8 Comparison of new fallen snow and sediment snow.....  | 64 |
| Figure 5.9 Interface of snow grain size measurement software-- Tsview .....  | 64 |
| Figure 5.10 Snow particles in different position of snowpack.....  | 65 |
| Figure 5.11 Spectrum comparison of snow pack surface and snow body .....   | 66 |
| Figure 5.12 Comparison of new fallen snow and sediment snow.....   | 67 |
| Figure 5.13 Spectrum of different layers .....   | 67 |
| Figure 5.14 Slope comparison of different layers in the same testing site .....  | 68 |
| Figure 5.15 Slopes of spectrum peak and trough at wavelength range from<br>$1.2\mu\text{m}$ - $1.6\mu\text{m}$ .....   | 69 |
| Figure 5.16 Comparison of average slope of larger snow grain size and smaller<br>ones .....  | 69 |

|   |     |
|---|-----|
| Figure 5.17 Slopes of normal surface snow collected from different test sites   | 71  |
| Figure 5.18 Slope of refrozen snow grains   | 75  |
| Figure 5.19 slopes of heating or melting snow   | 75  |
| Figure 5.20 Comparison of slopes of snow surface in different status at near infrared range   | 75  |
| Figure 5.21 Mixed pixel of snow and grassland   | 78  |
| Figure 5.22 Effect of corn stalk on spectrum  | 78  |
| Figure 5.23 Spectrum comparison over sapling with different densities   | 79  |
| Figure 5.24 Spectrum of snow mixed with soil  | 80  |
| Figure 5.25 Microwave signal transmission   | 80  |
| Figure 5.26 Polarization Characteristics of Microwave radiance in three testing sites The upper-left one shows the H and V polarization $T_b$ s at incident angle from $30^\circ$ to $80^\circ$ of testing site A; the upper-right one shows the H and V polarization $T_b$ s at incident angle from $30^\circ$ to $70^\circ$ of testing site B; and the lower left one shows the H and V polarization $T_b$ s at incident angle from $30^\circ$ to $70^\circ$ of testing site C. | 82  |
| Figure 5.27 Brightness Temperature measurements on snow covered pasture   | 83  |
| Figure 5.28 Comparison of brightness temperature on shallow and thin snow covering test sites   | 84  |
| Figure 5.29 Brightness Temperature measurements on snow covered corn-land   | 84  |
| Figure 5.30 SD experiment on wet-field  | 85  |
| Figure 5.31 Brightness temperatures obtained from four test sites with typical underlying surfaces (Pasture, Corn-land, River ice and wet-field respectively)   | 86  |
| Figure 5.32 Brightness Temperatures of different incident angles over Corn-land   | 87  |
| Figure 5.33 Brightness Temperatures of different incident angles over River ice   | 87  |
| Figure 5.34 SD, SWE, and temperature data collected from these testing sites from 2005-2007   | 90  |
| Figure 6.1 Deformation of MODIS L1B image before and after geo-referencing  | 93  |
| Figure 6.2 The boundary caused by difference of light conditions and incident angles  | 95  |
| Figure 6.3 Flowchart of Mosaic  | 101 |
| Figure 6.4 Flowchart of mass MODIS data processing  | 104 |
| Figure 6.5 Flowchart of automated processing of MODIS L1B data in SCA monitoring  | 106 |
| Figure 6.6 Comparison of Snow covered percentage derived from in situ measurement, our model and MODIS daily snow product   | 108 |
| Figure 6.7 8-day snow covering map over Northeast China during 2006-2007 winter   | 109 |
| Figure 6.8 Process flowchart for AMSR-E L2 data   | 112 |
| Figure 6.9 Re-sampling spatial resolution according to specific usage   | 113 |
| Figure 6.10 Mosaic of AMSR-E data   | 114 |
| Figure 6.11 Interpolation Process   | 114 |
| Figure 6.12 Generation of daily snow covered map  | 114 |
| Figure 6.13 Preliminary estimation of SD in 6 testing sites in 2006-2007  | 116 |
| Figure 6.14 Comparison of estimation SD&SWE and in situ measurements  | 119 |

|   |     |
|---|-----|
| Figure 6.15 Temperature and snow parameters in Dehui ,05-06 winter.....   | 121 |
| Figure 6.16 Temperature and snow parameters in Jingyu, 05-06 winter.....  | 121 |
| Figure 6.17 Temperature and SWE in Dehui and Jingyu, 05-06 winter.....  | 124 |
| Figure 7.1 Diffuse albedo vs. grain radius (Adopted from Optical properties of<br>Snow, by Warren, 1982, pp.72) .....           | 128 |
| Figure 7.2 Relationship between snow grain size and scale area of optical<br>feature.....                                       | 129 |
| Figure 7.3 Model calculations of simi-infinite diffuse albedo as a function of<br>wavelength for various snow grain radius..... | 130 |
| Figure 7.4 Typical reflectance of snow, soil and vegetation and corresponding<br>detection channels of MODIS data .....         | 131 |
| Figure 7.5 Continuous Monitoring on Snow grain size .....   | 135 |
| Figure 7.6 Comparison of measurement SD and estimation result in 8 test sites<br>during 2007-2008 winter.....                   | 138 |
| Figure 7.7 Comparison of in situ SD, original estimation SD and improved SD<br>.....  | 139 |
| Figure 7.8 Statistics of Cloud Cover .....  | 142 |
| Figure 7.9 Flowchart of in situ snow covered map generation .....   | 144 |
| Figure 7.10 Snow maps on 5 <sup>th</sup> Mar., 2007 before and after the complement of<br>AMSR-E data .....                     | 147 |
| Figure 7.11 Comparison of daily SCA estimation result of improved model and<br>MODIS snow product .....                         | 147 |
| Figure 7.12 Comparison of 8-day SCA estimation results of improved model<br>and MODIS snow product .....                        | 148 |
| Figure 7.13 Comparison in numbers of snow covered stations that misjudged as<br>non-snow .....                                  | 148 |

## ACKNOWLEDGEMENT

Ph.D. study is not easy for everyone. It is even harder for me, who knew nothing about the new research direction when I turned major from computer science to remote sensing. If you could imagine how difficult it is to learn from a stranger to my research to finish this thesis, you will understand how deficient language is to express my gratitude now.

First of all, I would like to thank my co-supervisors: Professor Hui Lin and Yuanzhi Zhang. Thank you for everything you ever once gave to me: guidance when I lost; encouragement when I was upset; and support when I felt helpless. It is not academic knowledge but also courage to face difficulties and ability to solve the problems that I learned from both of you.

I would also express my gratitude by heart to Prof. Xin Li, Prof. Jian Wang, Prof. Long S Chiu, Prof. Bo Huang, Prof. Kai Zhao, Dr. KaiShan Song, Dr. Gareth Rees, and Dr. Tao Che. It is maybe a common happening when a student comes to you to seek answer to a question. And you, as usual, try to un-riddle for her the puzzles in a sincere, patient and painstaking manner like you do with your own students. You will never realize that what it does mean to someone in necessitous circumstances. Thanks a lot for your help and suggestion. Without you the thesis could not be finished.

Although it is difficult for me during the past three years, I still feel I am so lucky to have such great teachers as well as friends: Jia Du, Xinmin Zheng, Liyun Dai, Huilin Cheng, Ye Shen, Hongyan Xi, Yufei Wang, Ru Li, Biao Liu, Si Gao etc.. Some of you fought together with me against the bitterly cold when we were conducting field experiments in the wild; some of you are always there when I was in need of reassurance, comfort or a gentle helping hand. There is no word for me the express my appreciation for all of them.

In the end, I would like to say to my family: You are the motive that I work, no matter how many difficulties I met. Thank you!

# Chapter 1 INTRODUCTION

## 1.1 Significance of This Research

Climate changes are quite familiar to all of us nowadays. It is not only a conception in the book, but the daily life we take. The frequency of extreme weathers such as extreme cold or hot temperatures, abnormal snowfall and heavy rainstorm increased dramatically in the past ten years (IPCC 2007, Li *et al.*, 2010). The followed snow, rain, flood and dry disasters caused great casualties and financial losses throughout the world. Climatic deterioration becomes the great crisis that grabs the attention of the world. Since snow and ice are sensitive to the variations in amount of precipitation as well as the increase of temperature, cryosphere is the most sensitive indicator to climate change. Therefore, many studies on snow have attempted to assess the changes in distribution and quantity of seasonal snow under a warmer climate. Based on its control over agriculture, ecology and economic activities, snow cover is important in high and mid-high latitude regions (López-Moreno, 2009). Moreover, the role snow cover, especially seasonal snow cover, is more than an indicator of climate change. The change of snow cover is the result of global climate change, as well as the cause of many severe environmental problems in the following ways:

### 1. for local scale

- 1) Snow cover is significant for the area where is characterized by a thick seasonal snow during winter. As temporary water storage, snow cover is the main water resource for agriculture irrigation and soil moist in spring in semiarid areas like Northeast China. The quantity of snow is directly related to food productivity in these areas. And the insulation function of snow cover prevents the heat exchange from ground and atmosphere. Thus, vegetation could survive through the cold temperature in boreal zone.
- 2) On the other hand, seasonal snow cover is a risk that needs to be monitored timely in high or mid-high latitude area. The sudden runoff of melting snow raises the risk of flooding in certain areas. Moreover, in the areas such as Inner Mongolia, China, the thick snow cover also indicates lack of food that will lead to a big animal product industry disaster. Thus, accuracy snow cover monitoring

result is the efficient input of disaster prediction model, which will be very important for political decision making and disaster management.

## **2. for large scale**

The high albedo of snow is an important climatological factor that affects the earth's radiation budget for several months during the year. And the albedo together with radiation is the primary variables of global changes. For example, the changes in snow covered percentages in boreal areas will lead the extreme changes of monsoon during the spring, even summer, over south areas.

## **3. for the study area in Northeast China**

This study area, Northeast China, is one of main food grain bases of our country and one of the only three black-soil areas of the whole world. It means that as most important characteristics for hydrology and climatology which have great effects on soil conditions, Snow Covered Area (SCA), Snow Water Equivalent (SWE) and Snow Depth (SD) are significant parameters that need to be monitored in this region. However, seasonal snow cover & runoff models & algorithms based on remote sensing data over this area can hardly be found in the past decades, let alone researches on snow cover information over specific land cover types and latitudes (Song and Zhang, 2008; Song *et al.*, 2008; Zhang *et al.*, 2010). Thus, a systemic research on seasonal snow cover monitoring using remote sensing techniques is an urgent need over Northeast China.

## **4. potential significance of this study**

The methodologies, data processing systems and models can be generalized to snow monitoring over North China, even the whole high latitude regions. It is significant for snow disaster prevention work for the time such as the winters of 2007 and 2009, when snow disasters caused huge loss.

In conclusion, snow-cover information is important for a wide variety of scientific studies and political decision making. It plays a crucial role in food shortage, resource shortage, disasters prediction & monitoring and global climate changes studies as well as prevention of snow-caused disasters in pastoral areas.

As it is mentioned above, study on snow cover monitoring is significant, especially for our study area, Northeast China. Relevant research works have been done on seasonal snow cover estimation and monitoring during the past decades, but efficient research results over large scale areas were not obtained until satellite remote sensing technology was applied in this field.

## 1.2 Research Questions and Objectives

Because of the significance of snow, studies on snow monitoring are conducted over high latitude areas, such as Canada, Greenland, Finland and Russia, and mid-high latitude areas, for instance, North America, German, and Japan (Biancamaria *et al.*, 2008; Frei & Lee, 2010; Foster *et al.*, 2009; Pulliainen, 2006; Salomonson & Appel, 2004; Varhola *et al.*, 2010). Recently, preliminary research results on snow over Xinjiang and Tibet areas can be found on top-level remote sensing journal (Liang *et al.*, 2008; Wang *et al.*, 2008; Immerzee *et al.*, 2009). However, few researches have been done over Northeast China, where is the base of farming and animal husbandry of China (Zhang *et al.*, 2010; Song & Zhang, 2008). No systematical study was conducted over this area, which makes it a missing puzzle of the understanding of the whole North Hemisphere cryosphere, not to mention the support for decision making on local agriculture and animal husbandry. Therefore, in this dissertation a comparatively systematical research on snow monitoring over Northeast China will be conducted to fill the gap.

The objectives of this research are to:

1. Investigate snow cover properties in Northeast China. Based on in situ measurements and long-term observations, snow properties, such as snow grain size, will be well studied.
2. Analyze the sensitivity of snow properties to snow information via special designed ground based experiments.
3. Compare the results of snow cover monitoring and in situ measurements to find the most suitable application of multi-sources satellite remote sensing data. Each kind of remote sensing data has its own advantage in snow monitoring under different environmental conditions. In this thesis, snow cover estimation accuracy of each kind of data will be discussed according to different observation periods (wet-snow period and dry-snow period), land-cover types and other potential environmental factors to find an optimized combination of remote sensing data.
4. Investigate the unsolved problems that will bring great effect on accuracy of snow cover monitoring models.
5. Develop improved SCA and SD monitoring model to provide more accurate snow monitoring results for future applications.

### 1.3 Framework

The study of snow monitoring based on satellite remote sensing includes several contents that relate to different research fields: Knowledge of remote sensing theory, geography, computer science, and the ability of field experiments (see Figure 1.1).

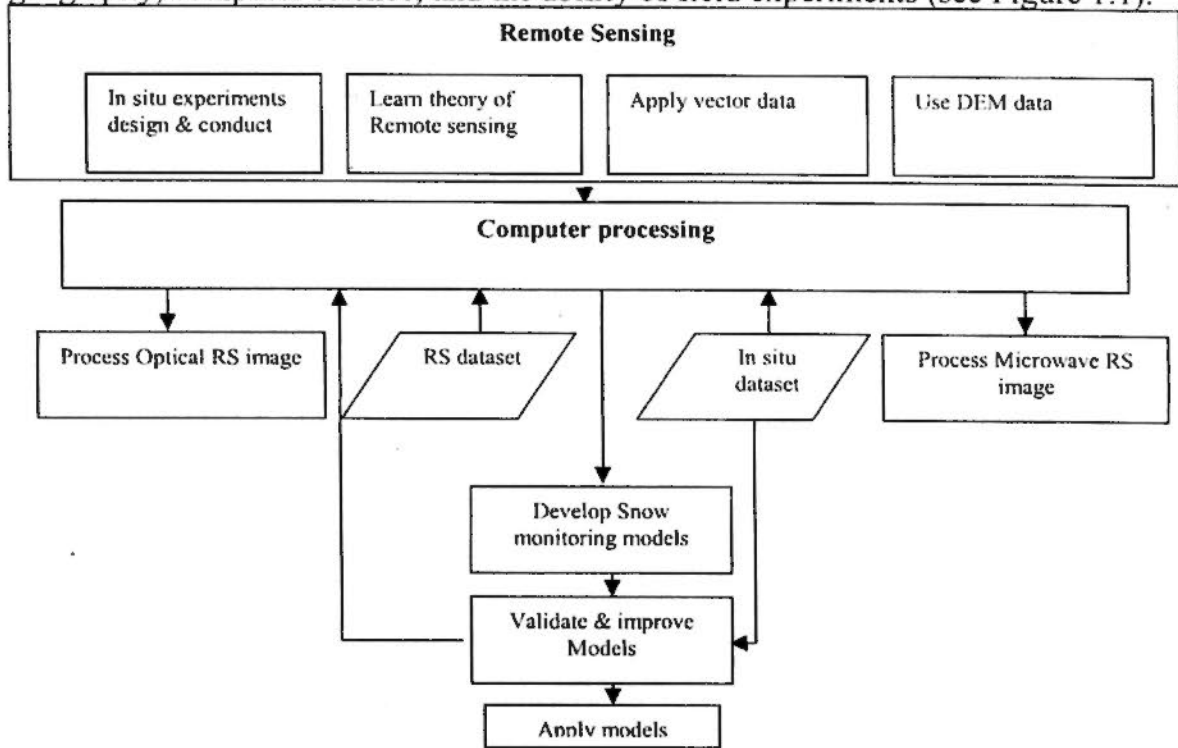


Figure 1.1 Research Framework

Since there are so many contents that need to be concerned in this study, a clear research flowchart will be helpful to sort out works that need to do (see Figure 1.2).

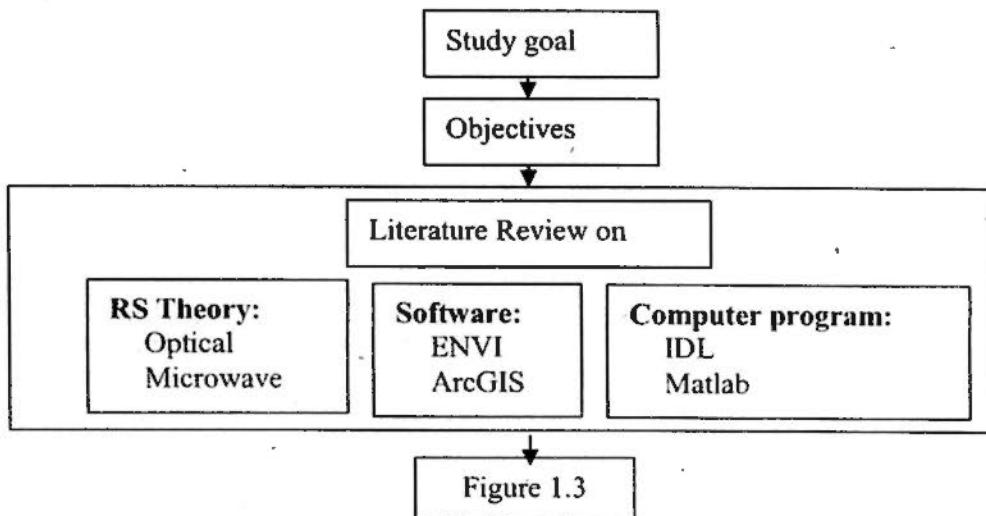


Figure 1.2 Research Flowchart

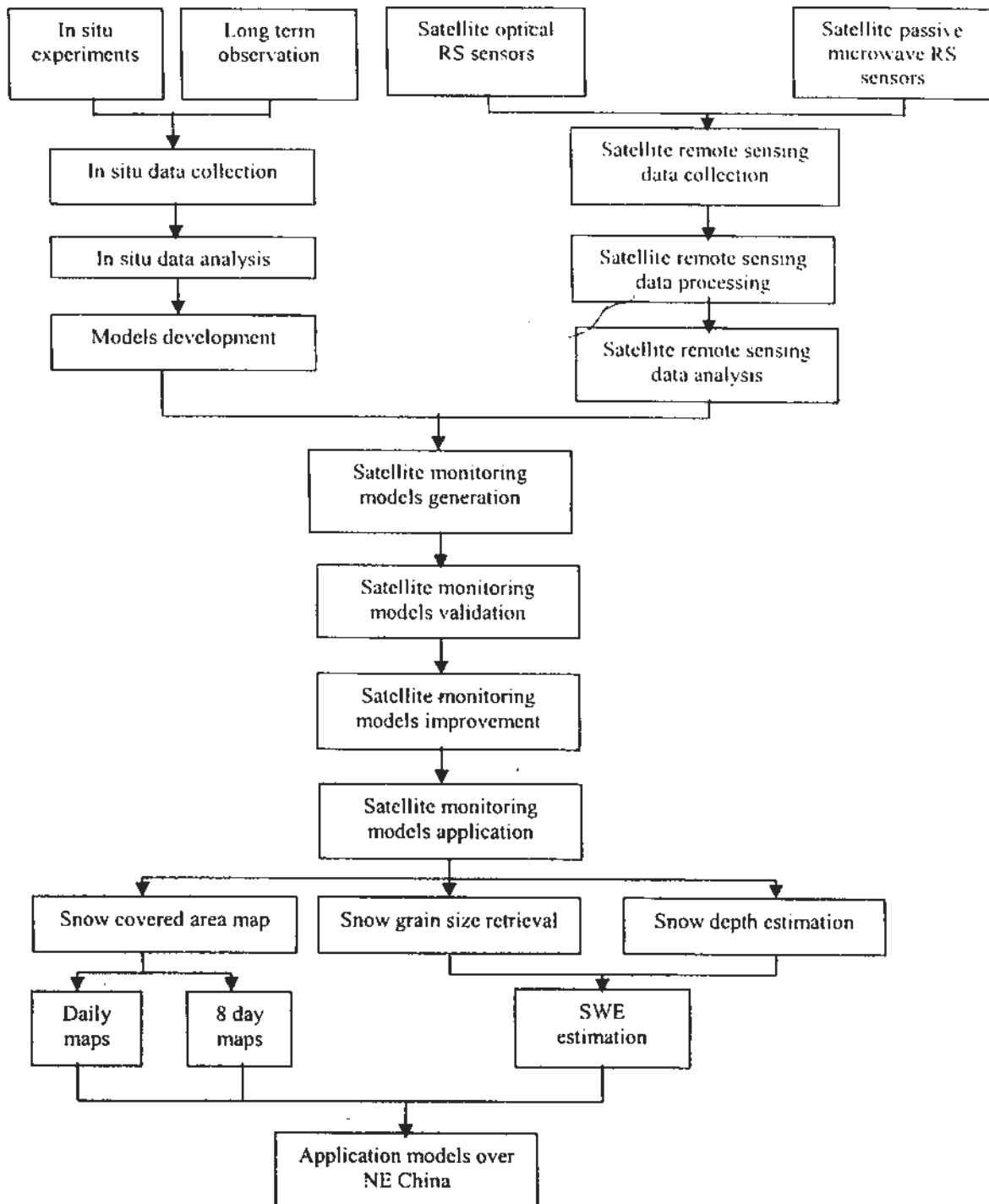


Figure 1.3 Study procedures

According to study procedures, this research work will be divided into two parts:

1. Field works
2. Satellite remote sensing related works

In the first part, field experiments and long term observations are introduced in details; while in the second part, the processing of satellite remote sensing data, modeling, validation and improvements of my monitoring models will be represented in the following chapters. Finally, the estimation results on SCA and SD over Northeast China will be analyzed.

## **1.4 Structure of This Thesis**

In this thesis, it will be started with an introduction to snow monitoring using remote sensing techniques (Chapter 2), then follows methodology that will be applied in this research (Chapter 3). However, not all the existing models work well over Northeast China, the further study on local snow properties need to be conducted, which will help to select or develop a new model. Thus, in Chapter 3, study area will be carefully studied. In Chapter 4, field experiments on snow properties are designed. And in Chapter 5, the results of field experiments are analyzed to find out a new solution for accurate model development. Then, the satellite remote sensing application part is given. In this part, the ideas on an efficient and accurate snow monitoring system will be explained in details. As it is known, the base of the whole model is high-quality input data. Thus, before modeling, another important work is discussed in Chapter 6. That is pre-processing of satellite remote sensing data. The processing method could be applied into all kinds of remote sensing applications but not limited in snow monitoring. With the using of high-quality input data, it will show the way to develop new models, which are more accurate than existing products in snow monitoring over Northeast China. Finally, it will briefly give snow monitoring results by using the new models and the contribution of this thesis (Chapter 8).

## Chapter 2 LITERATURE REVIEW

### 2.1 Remote Sensing Data Applied in Snow Monitoring

In the research of Matson *et al.* (1986), it was considered that snow cover has been routinely monitored by using satellite optical remote sensing data since 1966. But not until 1978, passive microwave imagery has been introduced into this area (Hall *et al.*, 2002). The two kinds of data are complementary approaches to each other in snow monitoring for both their advantages and disadvantages.

#### 2.1.1 Optical Remote Sensing Imagery

Generally, there are three kinds of components in snow body: air, water, and ice crystal, which is the chief constituent. Snow appears to be bright white because that it has very high reflectance in the whole range of visible region of spectrum. Only slight difference can be found when the composition ratio of the three components changes. The highest reflectance will be detected over fresh dry snow, in which no liquid water is contained. Generally, reflectivity of snow in visible region can reach 90%. With the increase of liquid water content contained inside snowpack, the reflectivity will decrease. However, water is not the only thing that affects reflectance of snow. Impurity and snow grain size can produce reactive changes in visible and near-infrared bands (Painter *et al.*, 2009; Rees, 2005). Recent researches show that, the shapes of snow particle do not have decisive effect on spectral albedo except in the modeling of radiance distribution (Jin *et al.*, 2008; Painter *et al.*, 2009). According to snow properties in visible and near-infrared regions, the commoner approach to distinguish snow from the other land surfaces is to use multispectral imagery (Rees, 2005). Figure 4 shows the spectrum properties of snow with two different grain sizes in comparison with optically thick cloud.

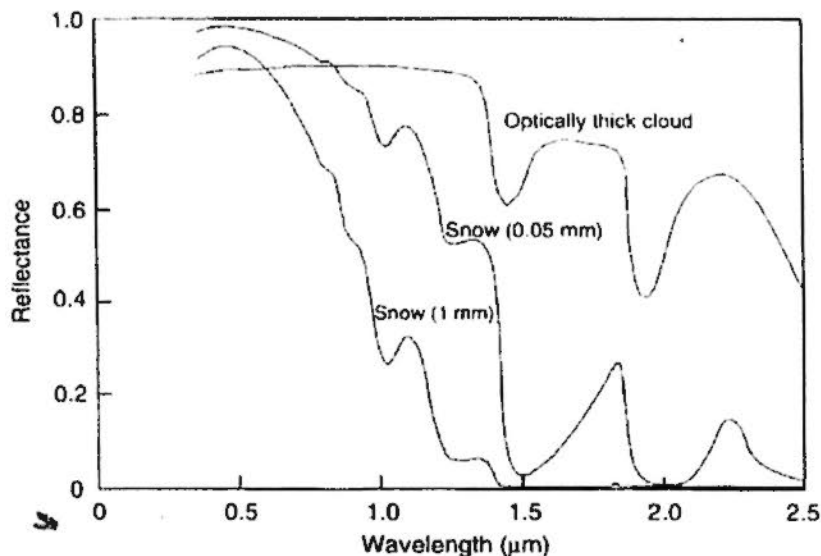


Figure 2.1 Spectral reflectance of optically thick cloud compared with snow cover of two different grain sizes (adopted from Rees, 2005)

It is clearly shown in Figure 2.1 that in visible region reflectance of snow is very high, almost 0.9, regardless of snow grain size. The other objects on earth surface can hardly reach the value, even get near of it. However, because of very similar components of snow and clouds, especially ice cloud, in the visible range comparatively high reflectance will be detected in the spectrum of optically thick cloud. But the reflectance of thick cloud does not drop as much as snow does at near-infrared region, because there is less water composition in ice cloud. A maximum difference between cloud and snow can be obtained at wavelengths between about 1.55-1.75 $\mu\text{m}$ . Therefore, these two bands of reflectance are used in snow interpreting: one is in the visible part of the spectrum, another is centered near 1.65 $\mu\text{m}$  are selected (Massom, 1991; König *et al.*, 2001). By using the difference, it is possible for us to detect snow from other land cover types and correct the topographic effect. The usual index to discriminate snow from other land cover types is called the normalized difference snow index (NDSI), defined in the following form:

$$NDSI = \frac{R_V - R_{NIR}}{R_V + R_{NIR}} \quad 2.1$$

Where  $R_V$  and  $R_{NIR}$  are reflectance of visible and near-infrared bands of remote sensing data respectively. Normally pixels are considered as snow covered when NDSI value of the pixels exceeds 0.4 (Dozier, 1989; Hall *et al.*, 1995).

Although the value of 0.4 is selected as the threshold in discrimination of snow generally, it is not universal for all kinds of land-cover types. Research results shows

that the optimum value of the threshold varies (Rees, 2005). Complement information is required to choose a suitable threshold value. For instance, over the surface with mixed land cover types, the value of threshold need to be properly lowered.

According to study results of Li and his team, the penetration of photon is only a few centimeters in visible range (Li *et al.*, 2001). To retrieve SD of snowpack by using optical remote sensing data, indirect relationship between snow depth and optical properties of snow should be utilized. In Romanov and Tarpley's research (Romanov & Tarpley, 2004) they have demonstrated that there is a relationship between snow depth and fractional snow cover. This relationship can be applied in SD estimation over open areas. It means that the snow covered fraction will change corresponding to the changes of SD caused by vegetation cover (Baker *et al.*, 1991). Therefore, the reflectance of land surface is directly proportional to SD until SD exceeds the penetrability of optical remote sensing signal, namely, land surface is completely covered by snow. This relationship provides a potential solution to retrieve SD by using optical satellite remote sensing images.

Although SCA can be obtained, snow water equivalent can hardly be derived by using optical remote sensing data (Tekel, 2005). Moreover, optical remote sensing data are greatly affected by cloud, weather condition and illumination. Alternative should be introduced into snow monitoring to make up the deficiency.

Be distinct in penetrability from visible and near-infrared ranges, the longer wave, such as microwave, is unaffected by cloud. Physical characteristics of snow, including snow grain size, liquid water content, SD, temperature, density, and land-over types, determine its microwave properties. Radiation measured at different wavelengths and at different polarizations enables the extraction of information related to SD and SCA by calculation of the areas with positive SD value because that the variable responses of snow in different states (Roshani *et al.*, 2008). In the next section, snow monitoring using microwave remote sensing imagery will be introduced briefly.

### **2.1.2 Microwave Remote Sensing Imagery**

Besides the capability of microwaves to penetrate clouds, the two characteristics of microwave signals make it possible to be used in snow monitoring: Microwave

remote sensing has the capability to penetrate dry snow, and the strengths of signals at different wavelengths vary according to their transmission capabilities in snowpack. It offers a chance to measure the SD and SWE of dry snow by using microwave remote sensing data.

The simplest situation in SD and SWE measurement is to measure the radiation energy from a flat snow surface. According to diffuse reflectance principle, the value of reflection is controlled by the angle at which the radiation strikes the surface and the dielectric constant of the snow. The greater the difference between the dielectric constant of snow and that of the air is, the greater the reflection coefficient is. Because of the low values of the absorption coefficient, transmission of microwave radiation through dry snow is generally dominated by scattering. The determining factors of scattering include dielectric constant of the surface, its roughness properties, and the geometry of the scattering (Rees, 2005). Among all of the scattering signals that passive microwave sensors obtained from snow, surface scattering is only a part of it. The major contributing factor to passive microwave remote sensor from snowpack is volume scattering by snow particles. With the increasing with SD, the brightness temperature of snow at microwave range decreases. However, the decrease which is considered as a result of volume scattering by snow particles can only be observed for dry snow (Hallikainen, 1984).

Both surface and volume scattering contribute to total backscattering observed by microwave radiometers. The difference between the two contributing parts is the change along with incidence angle. Strong peak can be found near normal incidence for surface scattering, while a very slow variation with incidence angle is shown in the measurement of volume scattering. Thus, it can be concluded that volume scattering dominates at large incidence angles except near zero, which is tends to be dominated by surface scattering (Rees, 2005).

The radiometric properties of snow were shown based on ground-based measurements. Strongly affected caused by snow grain size, snow depth and underlying surfaces are found during the experiments. The microwave properties at a the frequency range of 5 to 100 GHz of single and multi-layers snow layers are discussed by Weise (1996) and Christian Mätzler & Andreas Wiesmann (2007).

One of these physical models is Microwave Emission Model of Layered Snowpacks (MEMLS), in which horizontal layers of snow are considered stacks. of horizontal

layers. Snow depth, correlation length, density, liquid water content and temperature are all taken as effect factors and characterized in each layer. To apply multiple scattering radiative transfer theory in this model, layer interfaces are assumed as planar. In volume scattering part, multi-flux approach is used. Thus the absorption and scattering coefficients are functions of correlation length, density, frequency and temperature.

For general physical model, the up and down welling streams of snowpack radiation can be calculated via the following equations:

$$\begin{aligned}\frac{d}{dz}T^+(z) &= -k_{es}T^+(z) + F^+(z) + k_{as}T^- \\ \frac{d}{dz}T^-(z) &= k_{es}T^-(z) - F^-(z) - k_{as}T^+\end{aligned}\quad 2.2$$

Here:

$$k_{es} = k_e / \cos \theta_s, \quad k_e \text{ is scattering coefficient}$$

$$k_{as} = k_a / \cos \theta_s, \quad k_a \text{ is absorption coefficient}$$

$$\mu_s = \cos \theta_s, \quad \theta_s \text{ is refraction angle of layers}$$

$$T^+(z) = T(z, \mu_s, \phi_s),$$

$$T^-(z) = T(z, -\mu_s, \phi_s),$$

In the snowpack where temperature is independent on azimuth, and monotonic vertically, then

$$\begin{aligned}F^+(z) &= \frac{k_{ss}}{4\pi} \int_0^{2\pi} \int_0^1 P(\pm\mu_s, \mu, \phi_s - \phi) T^+ d\mu d\phi + \frac{k_{ss}}{4\pi} \int_0^{2\pi} \int_0^1 P(\pm\mu_s, -\mu, \phi_s - \phi) T^- d\mu d\phi \\ &= \frac{k_{ss}}{2} \int_0^1 P_0(\pm\mu_s, \mu) T^+ d\mu + \frac{k_{ss}}{2} \int_0^1 P_0(\pm\mu_s, \mu) T^- d\mu\end{aligned}\quad 2.3$$

Here

$$k_{ss} = k_s / \cos \theta_s, \quad k_s \text{ is volume scattering coefficient matrice}$$

For MEMLS, the model is designed for j-layer snow cover ( $j = 1, 2, \dots, n$ ). The boundaries between air-snow and snow-snow are planar (for a given frequency  $f$ , polarization  $p$ , and incidence angle  $\theta = \theta_n$ ) (Mätzler & Andreas Wiesmann, 2007):

(1). the snowpack brightness temperature  $T_b$ ,

- (2). the reflectivity at the bottom of the snowpack  $s_0$  and the temperature at the bottom  $T_0$ ,
- (3). the interface reflectivity on top of each layer  $s_j$ ,
- (4). the internal reflectivity  $r_j$ , emissivity  $e_j$ , transmissivity  $t_j$  temperature  $T_j$  of each layer due to volume scattering and absorption. Energy conservation requires  $r_j + e_j + t_j = 1$ ,
- (5). the downwelling (sky) radiation, given by the brightness temperature  $T_{sky}$ ,
- (6). the layer thickness  $d_j$  and the number of layers  $n$ .

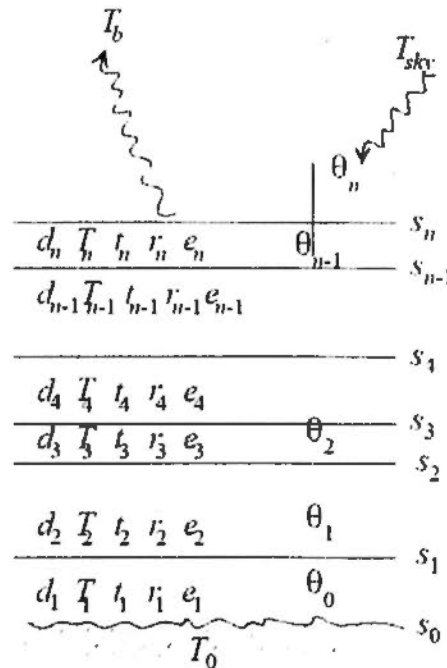


Figure 2.2 A multi layer system with a wave incident from above at an angle  $\theta_n$  s (adopted from Christian Mätzler & Andreas Wiesmann, 2007)

From Figure 2.2 it can be concluded that the radiation of snowcover can be described via the following equations( Mätzler & Andreas Wiesmann, 2007):

$$\begin{aligned}
 A_j &= r_j B_j + t_j C_j + e_j T_j \\
 B_j &= S_{j-1} A_j + (1 - s_{j-1}) D_{j-1} \\
 C_j &= (1 - s_j) A_{j+1} + s_j D_j \\
 D_j &= B_j + r_j C_j + e_j T_j
 \end{aligned}$$

2.4.

the parameters are shown in Figure 2.3.

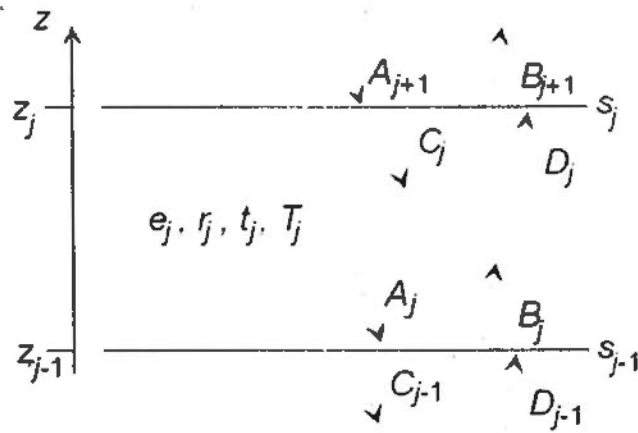


Figure 2.3 The parameters of a selected layer  $j$  (adopted from Christian Mätzler & Andreas Wiesmann, 2007)

When  $A_{n+1}=T_{sky}$  and  $D_0=T_0$ , the brightness temperature of snowpack is ( Mätzler & Andreas Wiesmann, 2007):

$$T_b = (1 - s_n)D_n + s_n T_{sky} \quad 2.5$$

Although microwave images can be used to monitor snow cover and SD without restrictions of cloud and light conditions in large scale, their usability in some certain kinds of local areas such as mountainous basins is limited because of their low spatial resolutions (Tekel, 2005).

Compared with passive microwave data, active remote sensing data can provide finer spatial resolution (e.g., Quikscat data with spatial resolution of 4.5km x 4.5 km while SAR can provide high resolution image with spatial resolution of 1m).

As it is mentioned above, passive microwave sensors can not detect shallow dry snow, which is one of the reasons that passive microwave techniques are always underestimating SCA. However, Monique Bernier and Fortin discussed the potential of times Series of C-Band Synthetic Aperture Radars (SAR) data in shallow dry snow detection (Bernier, 1998), and even before that, the capability of SAR in snow cover monitoring was analyzed by Goodison *et al.* (1980). C-band SAR was used as feasible tool in snow state determining. Furthermore, in cold regions space-borne microwave radars shows its advantage of regardless of cloud cover and lighting conditions in seasonal snow cover monitoring (Koskinen *et al.*, 1997). The problem in wet snow detection now can be solved by using C-Band data (Luoju et al., 2004). And at the same time, the possibility of using Ku-band data, such as Quikscat, was discussed by Nghiem and Tsai (2001) on global and regional scale respectively.

Linear regression and exponential regression of in situ data and Quikscat data are alternatively methods in SD and SCA estimation.

Hallikainen and his research team used data acquired from the QuikScat sensor in SCA calculation during the Snowmelt Period (Hallikainen *et al.*, 2005). The data is obtained from the SeaWinds satellite at 13.4 GHz, vertical and horizontal channels, with a spatial resolution of approximately 22.5 km and incidence angle of 46 for the horizontal channel and 54 for the vertical channel.

Pixel-wise percentage of snow-covered surface is calculated by using the backscattering coefficient  $\sigma^0$  against reference values for (a) wet snow (minimum value at the onset of snowmelt) and (b) snow-free ground (immediately after the end of snowmelt) (Hallikainen *et al.*, 2005):

$$SCA = 100 \frac{\sigma_g^0 - \sigma_{obs}^0}{\sigma_g^0 - \sigma_{ws,min}^0} \% \quad 2.6$$

where subscript 'g' refers to snow-free ground, 'obs' refers to present observed value, and 'ws, min' refers to the minimum value for wet snow.

By doing this, real-time monitoring of SCA is possible without requiring measurement of snow-free ground to obtain the reference value (Hallikainen *et al.*, 2005).

More recently, neural network method (NNW) is introduced into SWE retrieving models (Chang & Tsang 1992; Tsang *et al.*, 1992) based on passive microwave data. By using NNW, an acceptable result can be obtained, but large numbers of in situ measurement data are needed in NNW establishment and validation.

## 2.2 Effects on Estimation Accuracy

Remote sensing imageries provide us the possibility to monitor land surface from the space. However, it is such a long distance from satellites to the earth that errors caused by obstacles and modeling are inevitable. The accuracy of SCA, SD and SWE estimation is affected by several factors, among which, land cover types are considered as one of the most significant and unavoidable effects (Kurvonen & Hallikainen, 1997). The most common problem to all approaches in snow monitoring is forest effect because that much of the world's seasonal snow cover occurs there (Rees, 2005, Walker & Goodison, 1993; Vikhamar & Solberg, 2000; Klein *et al.*, 1998). Researches on vegetation cover as a second explanatory variable in snow

monitoring have been conducted (Forsythe, 1999; Stahli *et al.*, 2002). By doing this, they attempt to develop more accurate models in forested areas (Stahli *et al.*, 2002). In Rott and Mätzler (1989) study, it is concluded that the underlying surface should be well studied to understand the complex representation of snow.

Land cover types, which will significantly affect SD and SWE estimation results, are vegetation (include forest and agriculture), and large water body, such as rivers or lakes. There are still some other land cover types that will influence estimation results, for example, the bared land that covered by depth hoar or frozen ground, and complex mountainous terrain. In the following several sections, the effects of land cover types on snow information retrieval will be discussed in turn.

## **2.2.1 Vegetation**

Researches show that it is essential to develop algorithms and models to eliminate vegetation effect on snow monitoring. The optimum microwave response to SWE was 100 percent higher for farmlands than for forested areas. The necessary of reducing effects of vegetation on snow monitoring is considered in regional snow studies. However, it is not considered yet in global snow studies (Kurvonen & Hallikainen, 1997). On grasslands and croplands, studies were conducted and research results show that the SD/snow fraction relationship is most pronounced (Romanov & Tarpley, 2007). Since previous studies show that flat grasslands and croplands do not have significant effect on SD and SWE estimation, in this section, effects of forests on optical and microwave remote sensing techniques will be discussed.

### **2.2.1.1 Effects of Forest on Optical Remote Sensing**

In forests it has been demonstrated lower estimation accuracy will be found in snow mapping than that in non-forested areas (Vikhama & Solberg 2000). Tedesco and Miller (2007) in their study concluded that to improve the mapping of snow in forests, the effects of trees should be accounted for, while SCA may be underestimated in forested areas (Solberg *et al.*, 1997; Tedesco & Miller, 2007). In those models for SD estimation with snow reflectance, as it is mentioned in last section, the underestimation of snow mapping will lead to underestimation of SD. To increase estimation accuracy, vegetation index need to be considered along with

snow index. For instance, snow mapping from MODIS data uses bands 4 and 6 (0.56 and 1.64 $\mu\text{m}$ , respectively) to determine whether snow is present or not, and additionally uses a vegetation index calculated from bands 1 (0.64 $\mu\text{m}$ ) and 2 (0.86 $\mu\text{m}$ ) to improve detection accuracy in dense forests (Klein *et al.*, 1998). By doing this, underestimation of snow cover area will be eliminated to some extent.

### **2.2.1.2 Effects of Forest on Microwave Remote Sensing**

Because of lower reflectance of vegetation, SCA and SD estimated using visible range will be underestimated. Similarly, vegetation radiation properties are quite different from those of snow. The backscatter of snow will be affected by the proportion and underlying land cover, especially for shallow snow covered regions (Rees, 2005). Over non-forested areas, the reported accuracy range of SWE that derived from microwave remote sensing data is from 5mm to 45mm. When it comes to forest area, the range increases by 5–10mm. Thus, in the percentage expression, the error increases 40-100% corresponding to increasing range of SWE (Singh & Gan, 2000; Pulliainen *et al.*, 1999; Derksen *et al.*, 2003; Tait, 1998). For mostly forested locations Kelly *et al.* (2003a; 2003b) suggested an estimation accuracy of 50%–70% for microwave SD retrievals models. As to satellite remote sensing, there is much more uncertainty in SWE and SD retrievals because that the microwave signals from the other surface-emitted microwave radiation are too large to be neglected, besides the contribution of SD, snow grain size, density and stratification (Romanov & Tarpley, 2007).

The reason for the significant effect of forest to SD and SWE is the disturbing that trees and leaves caused to microwave signals.

Everything on the surface of observing area contribute to the total microwave measured radiation. In open prairies, snow cover exists between the ground and air. In the simplest case, ground under snow layer is the only radiation source. Theoretically, changes of signal are caused by different of snow states. While in the forest, the total microwave signals are complex. For example, in a forest area, the contribution of canopy in absorption, emission, and scattering of microwave energy is mixed with that of snow. It is not easy to distinguish which part of emitted energy is from snow, not to mention to derive snow information from the complex scattering environment (Foster *et al.*, 1991; Singh & Gan, 2000). In the research of Hallikainen

(1984), a measurement on forest effects show that a linear inverse relationship between the residual brightness temperature at 37 GHz and the thickness of snow cover up to 80 cm under the influence of trees can be found. There is the possibility that forested areas lower the difference between the brightness temperatures at 18 and 37 GHz in comparison with the values observed for farmland (Hallikainen, 1984).

Further researches on this issue show that it is more complex than underestimation. After a detailed analysis of the forest effect by classifying category of trees, results of both an underestimation and an overestimation of SWE can be found (Andreadis & Lettenmaier, 2006; Tait, 1998). Some researchers believe that it is the different tree densities that cause the underestimating or overestimating. It means that SWE in high tree density regions or linear algorithms under deep snow conditions will be underestimating. Otherwise, overestimating SWE will be found in low tree density regions (Armstrong *et al.*, 1993). However different conclusion was drawn from analysis of Tait's for both high and low density forests. In this study, the effect of forest is concluded as: estimation model will underestimate SWE when density of tree is relatively high or low. Thus tree density should be taken into account in SWE analysis (Tait, 1998). Similar results were found in Tedesco's study over comparatively open areas. While in dense vegetative covered area, the relationship seems to be weakened (Tedesco *et al.*, 2007).

Thus, more specific categories of tree and their densities should be found out to get better results. Different approaches were developed by researchers to reduce forest effects on estimates of the SD or the SWE:

In order to account for the masking effect of the forest cover, lots of studies were published. The improvement of NASA algorithm (Chang *et al.*, 1987) by introducing forest corrective factor into the original model is well adopted (Foster *et al.*, 1997). Furthermore, a more specific research on relationships for different forest types was conducted (Goita *et al.* 2003). For different remote sensing data, the combination of multiple microwave bands was studied to reduce forest effect (Tait, 1998; Kongoli *et al.*, 2004).

Therefore, improved SD and SWE retrieval algorithms over forest areas were developed:

For dry snow, as it is noted that attenuation of microwave radiation is dominated by volumetric scattering above 15 GHz, the difference between a high scattering

channel and a low scattering channel has been considered in most SWE retrieval algorithms. Finally, 18 GHz and 37 GHz are selected in SWE and SD retrieval because that there is a linear relationship between the difference of these two channels and SD or SWE. Generally horizontal polarization is more sensitive than that of vertical polarization. Therefore, SWE retrieval models based on passive microwave data were created (Rees, 2005):

$$SWE = K_1 + K_2(V_{19} - V_{37})$$

$$SWE = K_3 + K_4(H_{19} - H_{37})(1 - A_f)$$

$$SWE = K_5 + K_6[(V_{18_{SWE}} - V_{37_{SWE}}) - (V_{18_{SWE=0}} - V_{37_{SWE=0}})] \quad 2.7$$

where K1 to K10 are coefficients, V18SWE and V18SWE=0 are vertically polarized TB of 18 GHz at snow-covered and snow-free areas, AF is the fraction of forest cover, Ta is the air temperature, and ATUNDRA and AW are fraction of tundra and water body area within each SSM/I footprint, respectively.

Goodison and Walker (1995) assigned K1 and K2 as -2.07 cm (offset) and 0.259 cm/K (slope) for the application of SSM/I data. A year later, Chang *et al.* (1996) emended the expression and valued K3 and K4 by -2.5 cm and 0.48 cm/K for the negligible forest fraction. With an increase in the forest fraction, K4 tends to increase slowly and reaches a peak value as 0.96 cm/K while AF is increasing from 0 to the corresponding peak value of 50%. According to the increasing mode of K4 and AF, it is clearly that there is a linear relationship between the two parameters, which present the forest effect on SWE estimation. The research that had been done by Hallikainen (1989) in Finland modified the algorithm with K5 and K6. For northern the values for the two coefficients are -10.87 cm and 0.87 cm/K, and changes to be -9.8 cm and 1.01 cm/K for southern Finland, respectively. Here another relationship between the increase of forest and SWE is represented as K6, which is increasing associated with forest cover.

$$SWE = K_{10}(H_{18} - H_{37})/(1 - A_f) \quad 2.8$$

In the research of Chang *et al.* (1996), a mean snow density of 300 kg/m<sup>3</sup> is given as standard parameter for SWE models. Foster *et al.* (1997) applied the standard density into his algorithm and proposed K10 as coefficient of improved Chang's algorithm. For North America the value of K10 is 0.477 cm/K and for the inland area of Eurasia the value of K10 is 0.234 cm/K.

Tait (1998) emended the expression into two typical underlying surfaces:

$$\begin{aligned} K3 &= 1.29\text{cm} / K \\ K4 &= 0.31\text{cm} / K \end{aligned} \tag{2.9}$$

for area with non-forested, non-mountainous terrain of no depth-hoar and no melting snow.

$$\begin{aligned} K3 &= 2.64\text{cm} / K \\ K4 &= -0.13\text{cm} / K \end{aligned} \tag{2.10}$$

for a forested basin area.

In 1991 Chang and Chiu corrected the expression again for forest-covered areas:

$$SWE = a(T_{19H} - T_{37H}) + f(T'_{19H} - T'_{37H}) \tag{2.11}$$

Where T' is the brightness temperature measured for a snow-free forest-covered pixel and f is the fraction of a pixel covered by forest. The coefficient *a* can be determined empirically. It is following the same opinion that Hallikainen applied in the expression in 1984.

MSC algorithm classified land cover types into more detailed categories: open, deciduous, coniferous, and sparse forest. For different categories different values of the coefficients are used. Table 2.1 shows the research results of algorithms generated for coniferous, deciduous, and sparsely forested landscape regions (Goita *et al.*, 2003).

Table 2.1 Algorithms applicable to coniferous, deciduous, and sparsely forested landscape regions

| Cover type        | SSM/I SWE algorithm                  |
|-------------------|--------------------------------------|
| Open              | $SWE = -20.7 - 2.59[(37V - 19V)/18]$ |
| Coniferous forest | $SWE = 16.81 - 1.96(37V - 19V)$      |
| Deciduous forest  | $SWE = 33.5 - 1.97(37V - 19V)$       |
| Sparse forest     | $SWE = 1.95 - 2.28(37V - 19V)$       |

## 2.2.2 Large Water Body

### 2.2.2.1 Lake and River Nearby

The absorption of dry snow is  $10^5$  times lower than that of liquid water (Ulaby & Stiles, 1980b). Thus, 1% of water content increasing will lead to 105% increase of

absorption theoretically. While in the practical experiments, remote sensing estimation accuracy of SWE is within 10 or 20 mm. However, serious underestimates (30mm or more) can occur in areas where many lakes are present or in areas of exceptionally high SWE (Derksen *et al.*, 2003; Watker & Silis, 2002), which means large water body such as lakes will greatly affect remote sensing estimation of SWE. One of the important reasons for the error is the higher liquid water proportion in snow caused by water body because of its higher temperature and moisture, which will cause the increase of liquid water in snow body.

Researches show that small amount of liquid water has no directly effect on reflectance in visible and near-infrared ranges. The presence of liquid water will gather snow particles into a larger cluster and the changes of snow grain size can be manifested in  $1.03\mu m$  and  $1.24\mu m$ . Even in visible region, a slightly decrease in reflectance will be found. However, the presence of even very small amount of liquid water does have a great effect on microwave range (Rees, 2005). That is to say, the presence of wet snow (liquid water increases compared with dry snow) decreases the significance of volume emission, and increases the effective emissivity (Stiles & Ulaby, 1980a and 1980b). As a result of the increasing of liquid water content in snow body the brightness temperature increases dramatically at 37 GHz or higher channels (Hofer & Matzler, 1980; Hewison & English, 1999).

Researches proof that passive microwave radiation is inversely with the SWE (Kunzi *et al.*, 1982; Foster *et al.*, 1984). Water body will cause the changes of liquid water content or temperature changes of underlying surface (when water body is frozen and became the underlying surface). Both of water content and brightness temperature are sensitive to SWE detection. Therefore, water body near or under SCA will greatly affected SD and SWE estimation. Taking water effect into account, the calculation of SWE can be described as following expression:

$$SWE = K_7[(A_{TUNDRA})(H_{19} - H_{37})] + K_8(A_W)(T_a) + K_9 \quad 2.12$$

Here  $K_7$ ,  $K_8$  and  $K_9$  are determined based on the assumption that microwave emission from frozen water bodies is related to air temperature ( $T_a$ ). Comparison of SWE estimated from these algorithms with ground measurements showed a better estimate of SWE (Gan, 1996).

### **2.2.2.2 Lake Ice as Underlying Surface**

As a land cover with great effect on remote sensing signals, the other situation of lakes should be considered, that is lake ice being underlying when lake is frozen.

The physical properties of lake ice and ground are quite different. Estimation results of airborne passive microwave radiometer show that the brightness temperatures at 37 GHz can exceed 19 GHz with snow covered on the underlying surface. It is a phenomenon has never been observed over terrestrial surfaces. According to the existing research results, the brightness temperatures of snow covered ground-fast ice in shallow tundra ponds and floating ice on deeper lakes on is not known (Andreadis & Lettenmaier, 2006; Tedesco *et al.*, 2004).

In Singh and Gan's (2000) study, the absorption and emission of microwave radiation of ice layer on land surface and within the snowpack increase the difficulty of SD detection, which will lead to uncertainty of SWE estimation, because that crustal layers to increase the emissivity at high frequencies relative to low frequency. The energy deterioration during ice layer transmittance should be introduced into snow monitoring model to improve estimate of snowpack emissivity by considering thickness (Grody *et al.*, 1996). Unfortunately there is no calculation method for ice layer thickness based on remote sensing data yet. Thus, the correction of lake ice for snow monitoring based on passive microwave is still an unsolved problem till now.

### **2.2.3 Bared Land**

Under different natural environmental conditions, especially temperature and soil moisture, bared land can be different statuses. And the physical properties, such as emission of radiation, are greatly different. Effects on SD and SWE estimation is unpredicted if ground statuses are uncertain. One of the most significant descriptors affected SD and SWE estimates is depth hoar crystals, which are formed by the transfer of vapor from particle to particle along a strong temperature gradient within the snowpack. Compared with that of non-metamorphosed snow particle, the extent of scattering radiation of particles inside snow body is much greater at microwave range. And the growth of depth hoar crystal with larger extent of scattering makes it beyond description by using normal snow monitoring models, which are applicable when snow grain size are normal, because of the increasing of scattering

cross-section and the lowering of microwave brightness temperature caused by depth hoar particles in snow body. Therefore, the depth hoar crystals that grow large enough can significantly impact the microwave signal (Tail, 1998).

Singh and Gan (2000) conducted similar study on depth hoar. Experiments on depth hoar effect on microwave retrieval of snow cover parameters were conducted. Results show that a difference of 20°K has been observed between two snow packs of similar depth. The difference may be caused by thicker depth hoar inside one snowpack. Anyway, it is very difficult to accurately estimate the influence of depth hoar on microwave scattering (Rees, 2005).

## **2.2.4 Mountains**

The geometry surface under snow cover also plays an important role in the interaction of electromagnetic radiation, which will cause detection error (Rees, 2005). However, a digital elevation model of the terrain can be applied into monitoring models where the shadows presence to resolve the underestimation problem (Baral & Gupta, 1997).

## **2.3 Snow Cover Monitoring Researches in China**

Most of the snow monitoring application of remote sensing techniques in China started from early 1990s and focus on Xin jiang, inner Mongolia and Qinghai-Tibetan Plateau.

Optical remote sensing data, such as AVHRR and MODIS, were applied into monitoring of snow properties in Xinjiang area and the results are also compared with in situ observations during the four winters in northern Xinjiang. Comparison results show that the performance of MODIS is better than that of AVHRR in snow monitoring over Xinjing area. As it noted that in the area with SD less than 0.5 cm, it is not possible to detect snow cover with MODIS data. Therefore, one of the most important factor that lower the SCA estimation accuracy of MODIS product is SD. Analysis shows that with the  $SD \geq 3$  cm, the overall accuracy increases, vice versa. Another influence factor in the accuracy of MODIS snow cover maps is land cover types, which just proof the previous research results. Although daily snow cover products (as know as MOD10A1) is severely affected by cloud cover, the validation results show that 8-day composite products of (A.K.A. MOD10A2) can effectively

map snow in most cases. To be more flexible in composite period selection, a system that allows user to determine monitoring period was developed based on MOD10A1 for regional snow-caused disasters monitoring over Xinjiang area in their study (Ma, 2008; Liang *et al.*, 2008; Wang *et al.*, 2008). Tao Che applied the modified Chang's model in the Tibet Plateau (Che *et al.*, 2004; Li & Che, 2007), and found that the monitoring results by using SMMR data significantly overestimated SD of Qinghai-Tibetan Plateau. At the same time, Armstrong *et al.* found that snow free land marked by passive microwave monitoring results can be labeled as SCA by using optical remote sensing data (Armstrong *et al.*, 2002; Armstrong *et al.*, 2004). That may be cause by the existence of large-scale depth hoar. To solve the issue, GIS technique was introduced into snow monitoring to classify land cover types of SCA by Kc and his research team (Kc *et al.*, 1998). Che and his team applied SMMR data at 18 and 37 GHz in linear regression and got the regression form:

$$SD = 0.78(T_{b,18} - T_{b,37}) \quad 2.13$$

With the same method, SSM/I data at 19 and 37 GHz were applied in SD estimation and better results were obtained.

$$SD = 0.66(T_{b,19} - T_{b,37}) \quad 2.14$$

The standard deviation is 5.99 cm which is 0.23 cm less than that of SMMR.

However, a few studies have been done on seasonal snow cover monitoring in Northeast China (Song & Zhang, 2008; Song *et al.*, 2008; Zhang *et al.*, 2010). It is no doubt that a study on snow monitoring over this area is in urgent need.

## Chapter 3 METHODOLOGY

### 3.1 Study Area

Study area in this research is Northeast China, where is one of the three biggest food grain base and black-soil areas on the world. Because of the geographic position and environmental conditions, agriculture and animal husbandry are major pillar cornerstone industry in this region. The area is covered by snow for 5-6 months per year. The growth of vegetation and animals is directly affected by temperature and water sources, which is mainly from melting snow in the spring. Thus, the abnormal changes of snowfall and distribution will cause inestimable losses in the two fields. It makes snow monitoring extremely important here. In this chapter, a briefly introduction is given on physical geography of Northeast China. The information is essential for selection of snow monitoring models.

The eastern region of Inner Mongolia, Heilongjiang Jilin, and Liaoning, provinces are collectively called Northeast China (see Figure 4.1). Northeast China has a size of over 150,000 sq km. But in this study, most data collection and processing is focused on Heilongjiang, Jilin, and Liaoning Province.

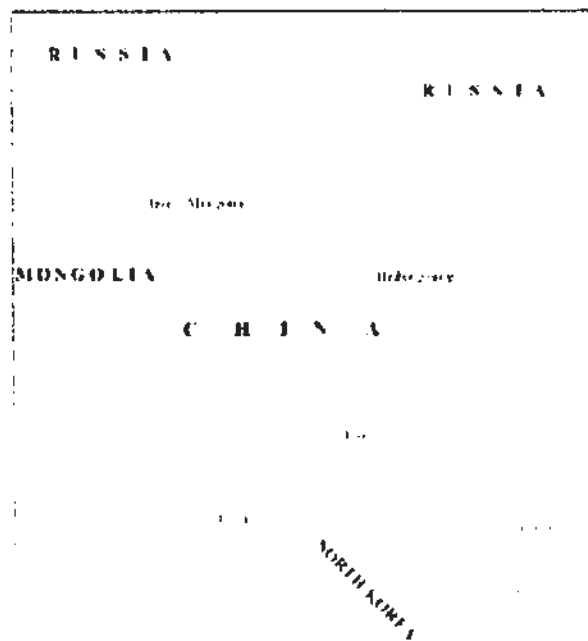


Figure 3.1 Northeast China (38°–52° N and 118°–134° E)

The study area is characterized by diverse land cover types. The ranges of vegetated areas are from temperate evergreen conifer-deciduous broad leaf mixed forests, deciduous broad leaf forests, woodlands to scrublands in the Changbai Mountain, the Daxing'an and Xiaoxing'an Mountain Ranges, grassland or meadow in the middle,

and agricultural lands (e.g., the Liao River Plain, the Songnen Plain and the Sanjiang Plain) (Song *et al.*, 2008). East boundary of Northeast China is roughed out by an irregular coast line. Rivers and lakes are distributing throughout the region (see Figure 4.2).

In summary, the area is mostly covered with forests. The typical land cover types in study area are:

1. Several kinds of forests (Changbai Mountain, the Daxing'an and Xiaoxing'an Mountain )
2. Agricultural and meadow lands (the Liao River Plain, the Songnen Plain and the Sanjiang Plain)
3. East boundary of Northeast China is roughed out by an irregular coast line. Rivers and lakes are included in the region.

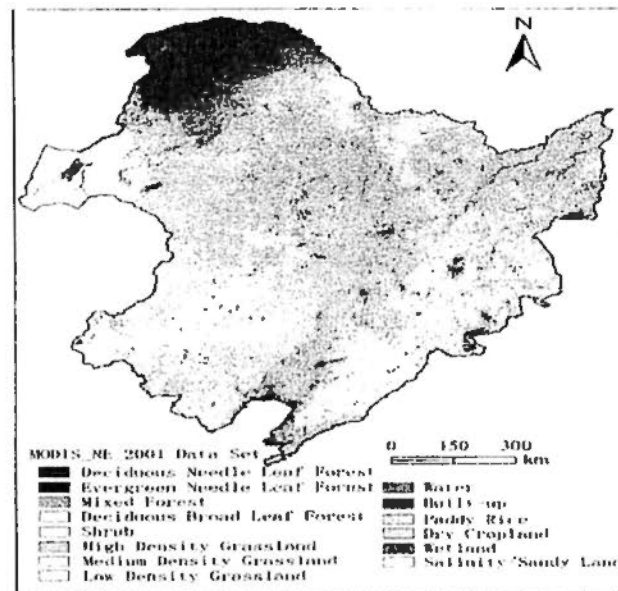


Figure 3.2 Land cover types of Northeast China derived from MODIS\_NE\_2000 Data Set (Provided by Dr. Kaishan Song)

Because of land types within the region, it is not surprisingly that agriculture and forestry are the biggest industries. Considering that winter in this region lasts more than six months and almost half a year the ground surface is covered by snow, which greatly affects the products of agriculture, forestry and animal husbandry, the study on snow monitoring is quite significant for this area.

### 3.2 Methods

There are two major research directions in remote sensing monitoring of snow cover. One focuses on the spectrum range of microwave, which is at wavelength of 1.5 mm to 3cm. Since 1970s, researchers started to discuss the capability of passive microwave data on snow cover detection. Among these studies (Choudhury, 1979; Chang *et al.*, 1982; Chang *et al.*, 1987; Chang *et al.*, 1991; Kelly *et al.*, 2003a; Kelly *et al.*, 2003b; Ashcraft & Long, 2005; Rees, 2005; Koenig & Forster, 2004), Chang and Foster's NASA retrieval algorithms used to calculate SD and SWE according microwave characteristics are widely accepted and introduced into snow monitoring work in China (Li *et al.*, 2007).

The theory is based on Geometrical configuration of the three layer medium (see Figure 3.1).

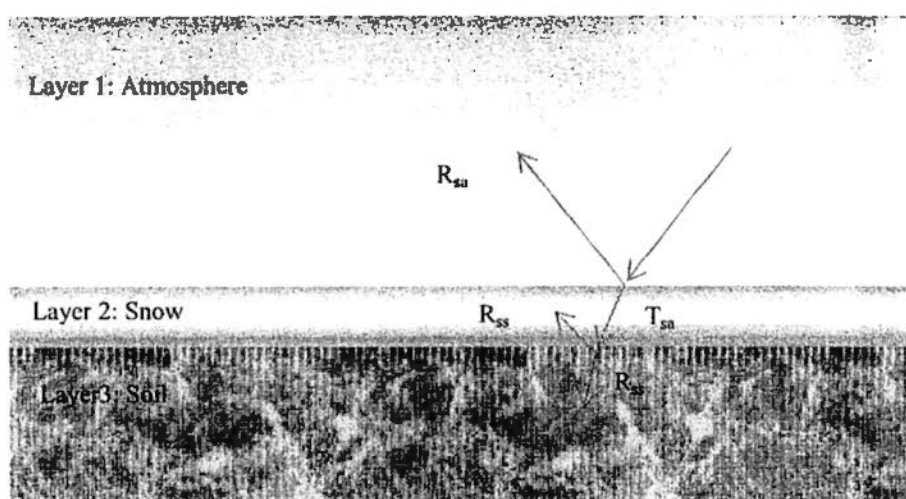


Figure 3.3 Three layer medium

A liner regression can be used to describe the relationship between SD and difference of brightness temperature.

MEMLS and HUT models that were developed by Bern University and HUT respectively, provide a better retrieve result under the condition of lesser transcendental information (Seidel & Martinec, 2004), which means the two models can be taken as complement of NASA's algorithms .

The second direction is the usage of optical remote sensing data (Rees, 2005; Derksen, 2008; Salomonson, 2004). MODIS data were utilized in snow cover monitoring in Xin jiang, China (Wang *et al.*, 2008). Generally, normalized difference of snow index (NDSI) can be used to distinguish snow and non-snow covered area (Rees, 2005; Ashcraft & Long, 2005; Armstrong *et al.*, 2004).

## 3.2.1 SCA Monitoring Methods

### 3.2.1.1 SCA Monitoring Using Optical Remote Sensing Data

As it is mentioned in Chapter 2, NDSI can be utilized to discriminate between non-snow and snow covered area. Originally, the method to calculate SCA can be described like this: check each pixel of image and count on the ones with  $NDSI \geq 0.4$ .

For different optical remote sensing data, different channels are selected to calculate NDSI.

For high resolution imagery, such as Landsat TM and ETM+ data, the reflectance in bands 2 and 5 ( $0.57\mu m$  and  $1.65\mu m$  respectively) were selected as  $R_V$  and  $R_{NIR}$  respectively (Dozier, 1984 and 1988; Vogel, 2002). Landsat TM and ETM+ data are selected for local SCA monitoring because the comparative fine spatial resolution. To improve estimation accuracy, digital elevation model (DEM) of the study area is suggested to be applied in SCA estimation models to correct shadows that caused by topography (Baral & Gupta, 1997).

For moderate resolution imagery: AVHRR with special resolution of 1.1km and MODIS with special resolution of 250m, 500m and 1km respectively are considered suitable for intermediate scales snow monitoring. In this thesis, MODIS data are selected as optical remote sensing source for SCA monitoring and snow grain size detection.

Table 3.1 shows the calculation channels for different optical remote sensing data.

Table 3.1 Channel selection in NDSI calculation for different optical remote sensing sensors

| Sensors             | $R_V$ | $R_{NIR}$ |
|---------------------|-------|-----------|
| Landsat TM and ETM+ | $R_2$ | $R_5$     |
| AVHRR               | $R_3$ | $R_5$     |
| MODIS               | $R_4$ | $R_6$     |

As it is discussed in Chapter 2, 0.4 is selected as the threshold in discrimination generally. However, a lower value needs to be assigned as threshold over forest area. With the increase of footprint, the likelihood that mixed land cover types that contained in one pixel is increased with the increased difficulties to determine threshold.

Previous studies show that, the largest effect factor is forest. Considering that canopy, even dead branches, will affect measurement spectrum in visible region by lowering NDSI, a corresponding lower threshold need to be defined over forest area. Therefore, before the determining of threshold for NDSI, forest detection needs to be conducted.

For MODIS data provide perfect channels for both NDSI and normal difference vegetation index (NDVI) detection. With the consideration of vegetation effect, snow covered land is determined by the following conditions: NDSI, NDVI and water eliminating condition.

The criterion for snow cover over not densely forested area with MODIS data is:

$$\text{NDSI} \geq 0.4 \text{ AND } R2 \geq 0.11 \text{ AND } R4 \geq 0.10 \quad 3.1$$

Here the thresholds in bands 2 and 4 help to eliminate effects of water, which can also show high values of NDSI. This algorithm generally performs well, though it seems to overestimate snow cover in areas or patchy snow (Hall *et al.*, 2002; Rees, 2005).

When the area is identified as forested by using vegetation index that calculated from bands 1 (0.64 $\mu\text{m}$ ) and 2, the detection conditions changes to be (Klein *et al.*, 1998):

$$\text{NDSI} \geq 0.2 \quad 3.2$$

In Rees's overview, there is another approach to solve the mixture pixel problem. That is the use of spectral mixture modeling based on high spectral resolution. Nolin *et al.* (1993) successfully applied the model by using airborne AVIRIS data (Nolin *et al.*, 1993). However, data source is still a problem for large scale application.

### **3.2.1.2 SCA Monitoring Using Microwave Remote Sensing Data**

Because of coarser resolution (e.g., the footprint of the 19GHz band of the SSM/I is 70km x 45 km; and that of 18.7 GHz band of the AE L2A-2 is 51 km x 29 km), passive microwave data can be utilized in SCA monitoring for large scale. In comparison with non-snow covered ground, the emission of radiation properties of snow cover obviously vary with frequency, based on which, multi-frequency bands in microwave ranges have been selected in SD and SWE retrieval models (Rees, 2005). Grody and Basist *et al.* (Basist *et al.*, 1998; Grody & Basist, 1996) in their series of researches introduced a method to identify scattering materials and then to

eliminate those with similar scattering property but not one of snow cover by the following steps (Rees, 2005):

1. Identifies a scattering medium by using the judgement of  $(T_{22v} - T_{85v} > 0)OR(T_{19v} - T_{37v} > 0)$ ,
2. And then indicates precipitation by using  $(T_{22v} > 257)OR(T_{22v} - 0.49T_{85v} > 165)$ ,
3. The third step is to eliminate cold desert by  $(T_{19v} - T_{19h} > 17)AND(T_{19v} - T_{37v} < 10)AND(T_{37v} - T_{85v} < 10)$
4. Finally, indicates areas of frozen ground by  $(T_{22v} - T_{85v} < 8)OR(T_{19v} - T_{37v} < 8)AND(T_{19v} - T_{19h} > 7)$ .

If passive microwave data are used alone, a problem with the removal of precipitation still exists because that snow cover and precipitation have very similar scattering properties (Standley & Barrett, 1999; Negri *et al.*, 1995; Bauer & Grody, 1995). It is suggested that thermal infrared data should be utilized as one of an auxiliary dataset (Rees, 2005).

Another way to achieve SCA is to calculate the pixels where SD is greater than 0 (or a practical threshold for a certain region). The place where snow exists can be considered as SCA. By doing this, SD estimation algorithms or models should be performed first. For example, followed the SD calculation algorithm of Chang, Foster, and Hall, Hall *et al.* (2002) brought out a modification algorithm on snow detection. The calculation method of SD will be detailed introduced in next section. The determining conditions of snow is:

$$SD > 80(\text{in mm}) \text{ AND } T_{37v} < 250 \text{ AND } T_{37h} < 240 \quad 3.3$$

The third approach for SCA estimation involves several steps (details can be found in *Remote Sensing of Ice and Snow* by Rees, 2005, pp. 137):

1. Estimating the land surface temperature from passive microwave data,
2. using this temperature to deduce the effective emissivity at different frequencies and polarizations,
3. then applying a set of rules to the emissivity to determine whether snow is present.

## 3.2.2 SD Monitoring Methods

### 3.2.2.1 Optical Remote Sensing Data Applied in SD Retrieval

Optical remote sensing data, which have no penetrability as microwave ones, can not be utilized in SD estimation directly (Stahli *et al.*, 2002). However, the indirectly method was worked out to estimate SD with a snow depletion model (Cline *et al.*, 1998). The model relates the SCA to its mean depth and SCA to runoff during the melt season (Rees, 2005). As it is noted in Chapter 2, DEM is regresses as altitude information to improve the estimation accuracy of snow depletion model (SDM) (Konig *et al.*, 2001). However, the environmental conditions are too complex while the reflectance is affected by diverse contribution factors, the accuracy of SD retrieval by using satellite optically remote sensing data is questionable.

### 3.2.2.2 Microwave Remote Sensing Data Applied in SD Retrieval

Since 1970s, passive remote sensing started to be applied in SD estimation. A series algorithms and models were developed, included: NASA algorithms originally by Chang; Microwave Emission Model of Layered Snowpacks (MEMELS); HUT model and Advanced Integral Equation Method (AIEM) model (Chao *et al.*, 2006).

#### 1. NASA Algorithms

This algorithms was originally developed by Alfred T. C. Chang and his research group in 1987 (Chang *et al.*, 1987) according Mei scattering theory. The difference of 18 GHz and 37GHz was calculated and results show that there is linear correlation between SD and the difference of brightness temperature. That is:

$$SD = 1.59(T_{b,18} - T_{b,37}) \quad 3.4$$

Where  $T_{b,18}$  and  $T_{b,37}$  are H polarization brightness temperature of 18 GHz and 37 GHz of SMMR, respectively. The Brightness temperature of H polarization is selected but not that of V polarization because the former is more sensitive to the differences of SD (Chang *et al.*, 1987). The model can be applied only over the regions with SD lower than 1m and higher than 2.5cm.

Considering the grain size differences and depth hoar, Chang's algorithm was emended like this (When grain size is larger than 0.4 mm):

$$SD = a(T_{b,18} - T_{b,37}) \quad 3.5$$

Where  $a$  is a coefficient that will be given different values in different regions (e.g., 1.59 in North America and 0.78 in Eurasia).

And if we take forest effects into account, further modification should be performed (Forster *et al.*, 1997)

$$SD = \frac{a(T_{b,18} - T_{b,37})}{1.00 - f} \quad 3.6$$

However, SD and SCA underestimation was found by using this model because shallow snow can not be detected by using microwave data (Robinson *et al.*, 1993; Tait & Armstrong, 1996; Armstrong *et al.*, 2002).

AMSR data were introduced into SD retrieval model since 1999. For better application, Chang's algorithm experienced another improvement, in which precipitation, grain size, forest and wet snow were taken into account:

$$SD = b(\Delta T_b)^2 + c\Delta T_b \quad 3.7$$

where  $\Delta T_b$  is the H polarization brightness temperature difference of 19GHz and 37GHz,  $b$  and  $c$  are two empirical coefficients, which are functions of grain size and proportion respectively (Chang & Rango, 2000; Kelly *et al.*, 2003a).

However, in the algorithm only aged snow particles are considered. When new snow occurs, the physical properties are quite different from old snow layers. The accuracy of this algorithm is not reliable anymore in the circumstances.

## 2. MEMLS

MEMLS was developed by University of Bern. It is considered as a model for passive microwave in multilayer snow monitoring, with an applied frequency range of 5~100 GHz. The original model can not be applied in all kinds of regions because it is a regression results of absorption coefficient, efficient Dielectric Constant, reflectance and refractive index and snow density and all these parameters are obtained through in situ measurement in certain area. Mätzler (Mätzler, 1994; Mätzler & Wiesmann, 1999) improved the model by extending its application scope. Research results show that SD can be approximately described with linear function of brightness temperature of 19and 37 GHz when SD is less than 50cm.

## 3 HUT Model

Helsinki University of Technology (HUT) semi-empirical radiation transfer model was developed by Hallikainen and his research team (Pulliainen *et al.*, 1999; Pulliainen & Hallikainen, 2001), and latter improved by extending its application into forested areas (Wiesmann & Mätzler 1999; Roy *et al.*, 2004; Pulliainen, 2006). In Pulliainen's further research, it is proved that by applying ground based observations into non-linear models, estimation accuracy of SWE and SD is significantly improved (Pulliainen, 2006).

Using the HUT model, SD was estimated with the comparison of simulation data and remote sensing observation brightness temperature.

To sum up, although more accurate estimation results could be obtained by using local models, such as HUT and MEMELS, NASA algorithm developed by Chang *et al.* is still the most popular one because of its universal applicability and requirement on ground based observation. Thus, timely snow monitoring over large scale, even global scale is possible by applying NASA algorithm. And passive microwave data become the favorite with researchers in SD retrieval models. Table 3.2 shows the often-used algorithms.

However, the global model for SD retrieval is still need to be improved in estimation accuracy and for different land cover types.

### **3.2.3 SWE estimation using remote sensing data**

SWE can be calculated by using SD, SCA and snow density as well as estimated from remote sensing estimation model. SWE retrieval models are similar to SD retrieval models. Linear relationship between the difference of 18 and 36GHz and SWE amount is found because that volume scattering reduces the brightness temperature of the radiation emitted from the underlying ground and the attenuation at different frequencies is different (Rees, 2005). NASA's series algorithms were developed based on the relationship between brightness temperature and volume scattering. However, the extract approach can only be utilized on dry snow. Table 3.3 shows some of SWE estimation algorithms. These generally use the difference in emissivity between two frequencies, typically 18 (or 19) GHz and 36 (or 37) GHz (Rees, 2005).

Table 3.2 Primary Algorithms to obtain snow properties by using passive microwave data

| Sensor | Algorithms  |
|--------|---|
| SMMR   | Uses brightness temperatures of 18H and 37H GHz to discriminate dry and melting snow over Northern Hemisphere (Chang, 1982; Chang <i>et al.</i> , 1987; Choudhury, 1979; Rees, 2005)        |
| SMMR   | SD retrieve by using difference between brightness temperatures of 18H and 37H GHz (Chang <i>et al.</i> , 1987; Rees, 2005)   |
| SMMR   | Uses brightness temperatures of 18H and 37H GHz in SD estimation with the considering of fractional boreal forest cover (Foster <i>et al.</i> , 1991)                                       |
| SSM/I  | Utilizes 19V, 37V, and 85V data to determine European SD. Inclusion of 85-GHz channel improved identification of thin snow cover (Chang <i>et al.</i> , 1991; Derksen <i>et al.</i> , 2008) |
| SSM/I  | Brightness temperature of 19 and 37 GHz are utilized in SWE model over fractional forest type (Goita <i>et al.</i> , 1997)  |
| SMMR   | A modified model of NASA algorithm (Foster <i>et al.</i> , 1997)  |
| AMSR-E | Uses AMSR-E in Global Snow Area and SD estimation (Kelly <i>et al.</i> , 2003a; Kelly <i>et al.</i> , 2005)   |

Table 3.3 SWE estimation algorithms based on passive microwave data

| Sensors | Algorithms  |
|---------|---|
| SMMR    | Uses brightness temperatures of 18H and 37H GHz for SWE estimation (Chang <i>et al.</i> , 1987)   |
| SMMR    | Uses brightness temperature difference between 18V and 37V GHz with considering of forest effect (Pulliainen & Hallikainen, 2001)               |
| SSM/I   | Estimation SWE with various frequency and polarization combinations and subdivides Northern Hemisphere regions based on snow state (Tait, 1998) |
| SSM/I   | derive SWE for Northern Finland based on snow emission inversion algorithm (Kelly <i>et al.</i> , 2005; Seidel & Martinec, 2004)                |
| SSM/I   | Retrieves SWE by using brightness temperatures of 19V and 37V GHz for North American Prairie (Walker <i>et al.</i> , 1995)                      |

In the following research, the existing algorithms and models will be applied on study area firstly. And then in situ measurements will be used as validation data to find out the drawbacks of these models. Based on the results new models will be developed or modification will be applied onto existing models to obtain more accurate estimation results over study area.

### 3.3.4 Researches on Effects of Estimation Accuracy and Corresponding Algorithms

Although various algorithms were developed for SCA, SD and SWE retrieval, estimation accuracy is not satisfying enough, especially those over local scales. Snow parameters, with the water content and state (frozen or thawed) of the underlying ground will affect retrieval accuracy. For instance, the responses of remote sensing signals to SWE and SD are higher for open areas than for forested areas (Tait, 1998). The existing researches on effects of land cover types show that among all the land cover types, forest is considered as the most influenced one. Because of effects of the liquid water proportion in snow body on penetrability of microwave, effects of water body can not be ignored. Not much research on effects of frozen ground under shallow snow can be found, however, according to the experimental results over Northeast China, the effects do exist and may cause the underestimation of SD. Topography effects on SD and SWE estimation over mountain areas can be reduced by using DEM. Table 3.4 shows a brief summary of effects of different land cover types according these researches mentioned above.

Table 3.4 Summary of effects of land cover types on SD and SWE estimation

| Land cover types | effects  | Memo  |
|------------------|--|---|
| Forest           | Both overestimation and underestimation  | NDVI will be applied to acquire accurate results                            |
| Water body       | Underestimation  | Special test sites will be selected to figure out effects of lake ice on SD |
| Bared land       | Depth hoar may cause overestimation and frozen ground probably lead to a underestimation | Snow grain size study will be conducted to reduce the effect                |
| Mountains        | Underestimation over deep snow area  | DEM application may eliminate the effect                                    |

In the following research, special strategies or algorithms will be developed to solve the problems that caused by certain land cover types listed above to improve estimation accuracy.

## **Chapter 4 FIELD EXPERIMENT AND IN SITU DATA COLLECTION**

### **4.1 Objectives of Field Survey**

As it is mentioned above, the aim of this research is to solve research problems that are directly related to the most important factors that hinder the practical use of satellite sensing data to monitor snow properties.

The objectives are to:

Investigate snow cover properties in Northeast China. According to the daily measurement of snow properties in the test sites, the difference of snow structure and crystal particle between Northeast China and other high latitude areas will be well described and found. The more suitable modified simulation models in snow cover monitoring in Northeast China can be chosen by using remote sensing data. Since passive microwave data could only provide coarse resolution images, multi-source remote sensing data fusion techniques are needed to obtain a fine grid monitoring result.

Analyze the sensitivity of snow properties to snow information. Different channel signal is sensitive to the changes of different snow properties. In order to improve the accuracy of snow cover monitoring in Northeast China, most suitable remote sensing data and algorithms should be found from the sensitivity analysis.

Compare the results of snow cover monitoring and find the most proper application of different kinds of remote sensing combination data. Each kind of remote sensing data has its own advantage in snow monitoring under different environmental conditions. In this project, snow cover estimation accuracy of each kind of data will be discussed according different observation periods, land cover types, topography and other potential environmental factors to find an optimized combination of remote sensing data.

Investigate the unsolved problem that will bring great effect on accuracy of snow cover monitoring. Huge errors that almost reach 200% still exist in the estimation results of snow cover monitoring models. Besides those of snow properties, the environmental impacts could not be underestimated. The frozen soil or ground is an important issue that will greatly affect the accuracy of SD and SCA estimation. Froze

soil or ground has a very similar emission and scattering properties as snow itself. In order to distinguish the two land cover substance, multi-polarization, multi-sources and multi-channel remote sensing data will be applied in the project to retrieve SCA, SWE and SD.

To accomplish this, two kinds of in situ data are necessary. They are:

1. In situ data of snow properties collected from field experiments;
2. Daily in situ data acquired from weather stations and testing sites.

The first kind of in situ data includes information derived by using optical and microwave equipments, natural properties, weather conditions, land surface types and other relative information. These in situ data will be used in investigation and analysis of snow cover properties, snow structure and crystal particle over Northeast China. To get these data, field experiments need to be designed carefully. Moreover, repetitive experiments are conducted to eliminate experiment errors. This kind of data is used to understand snow properties of our research area, analyze the sensitivity of different wavelength to snow status.

The second kind of in situ data is long time series elementary snow parameter, such as SD, precipitation, locations, temperature, elevation and other relative information of our testing sites. We can collect these data through a long term observation. These data are mainly applied in model validation and improving.

In this chapter, in situ data collection methods are introduced.

## **4.2 Field Survey and Field Experiments**

To obtain snow properties of Northeast China, field experiments on optical and microwave properties are conducted. There is less constraints when microwave experiments were conducted because that light conditions do not have such huge effect on experiment results as it does to optical remote sensing. Thus, during the experiment design, one of the most important rules is to consider the nature light conditions. For this reason, only a few spectrum data collected during the two months-long field work are applied in the final construction of grain size retrieval model. In the following section, the design and conducting of optical remote sensing experiments will be introduced.

## 4.2.1 Optical Remote Sensing Experiments

The distinct difference optical property of snow in visible and near-infrared regions makes it possible to classify snow from the other land surface, based on which we can distinguish SCA from non-snow covered areas. In visible wavelength, the measured reflectance is mostly sensitive to snow purity while in near-infrared and shortwave-infrared, all of grain size, temperature and humidity have significantly effect on the spectrum curve. And among all these effect factors, snow grain size has two observable absorption peaks near  $1.03\mu m$  and  $1.25\mu m$ . Generally, newly fallen snow has a finer grain size in comparison with that of sedimentary snow because of metamorphism and sintering. Part reason for the decrease trend in reflectance in wavelengths beyond about  $0.8\mu m$  is dust, which increases the impurity of snow, while the growth of grain size is another contributing factor. These properties of snow are important indicator in snow monitoring for hydrologic and climate models. Understanding of the relationship between snow's physical properties and the resulting changes on spectrum will greatly helpful in accuracy improvement on these models (Dozicr *et al.*, 2009). The following experiments were designed to understand optical properties of snow.

To figure out optical properties of snow over Northeast China, the following three experiments are designed:

1. experiments on grain size
2. experiments on mixed pixel
3. experiments on SD

### 4.2.1.1 Experiments on Grain Size

The goal of this experiment is trying to quantitatively and qualitative analyze the effect of grain size on snow reflectance. As we know, there are two kinds of methods that can increase the grain size of snow in the nature:

1. Metamorphism caused by gravitation
2. Refrozen after melting

Generally, the larger size of grain caused by refrozen can only be found on the surface of a snow pack. However, grains both on the surface and in the snow body can be changed by gravitation. The longer it takes, the larger the grain size will be.

To understand the optical properties of both of the two kinds of snow structure, two series of field experiments are conducted.

## **Experiments on Metamorphosis of Snow Grain Size Caused by Gravitation**

### **Design and Methods**

The series experiments are designed to figure out the effects of different sizes of snow grain on snow spectrum.

### **Testing sites selection**

Snow grain size and spectrum with different grain sizes are collected in 6 testing sites in 4 cities (see Figure 4.1). The experiments trip was started from west of Jilin province to the east.

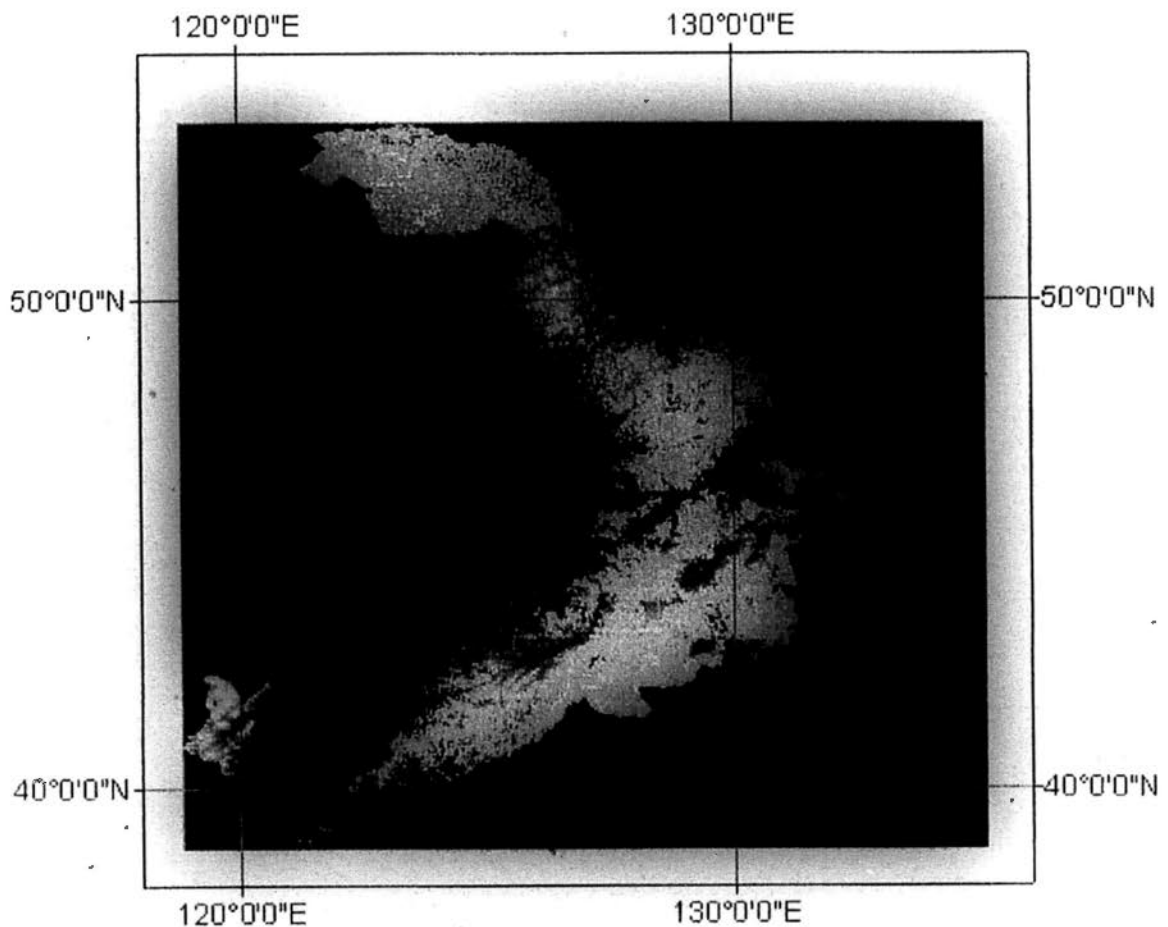


Figure 4.1 Selected test sites during field experiment trip from west to east Jilin

The SD of out testing sites is decreasing gradationally, which provides us the chance to find out the effect of SD on grain size metamorphism under gravity. Figure 4.2 shows the status of testing sites.

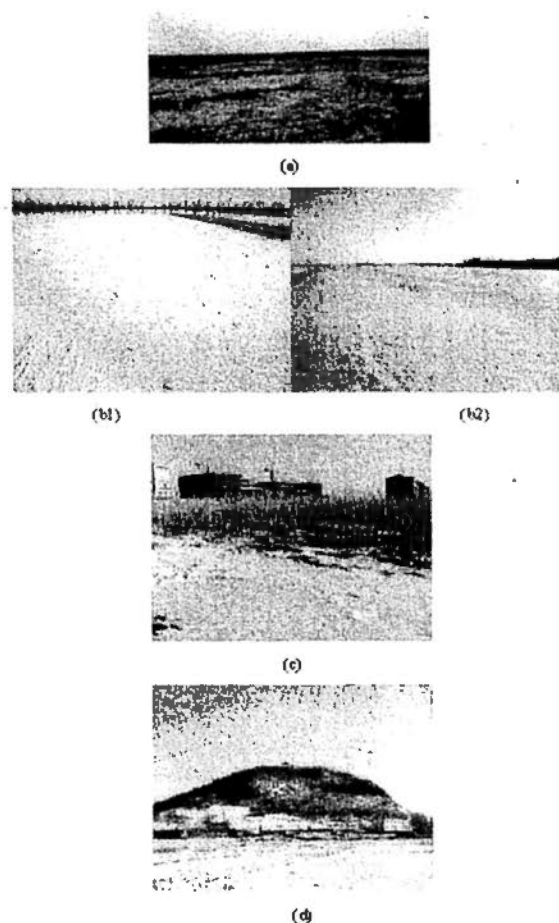


Figure 4.2 Natural State of test sites

(a) –(d) are pictures of testing sites which were taken in Changling, Songyuan, Changchun and Jilin respectively. Here, the underlying surfaces of b1 and b2 are cropland and ice on Songhua River.

The maximum SD in the 4 test cities are 3cm, 13cm, 13cm and 22cm respectively.

### Testing time

To get the best nature light source for our experiments, we need to start at 10: 30 and finish before 14:30.

### Experiments Methods

The in situ data we need to collect in these experiments include SD, temperature, snow grain size, GPS-based location and spectrum. Wetness of snow is one of effect

factors on reflectance, especially when the surface temperature is higher than melting point. To obtain all these data, instruments need to be prepared before the experiments.

a) Electronic map: since we took a comparatively long way from one testing sites to the other, maps are important for our field trip. Maps of highways, electron map of land covers are selected via internet.

b) Recording form: to list out all the parameters should be record in the field survey (See Table 4.1).

Table 4.1 Field survey record

|                      |  |                       |  |
|----------------------|--|-----------------------|--|
| Date                 |  | Recorder              |  |
| Record No.           |  | Snow depth            |  |
| Grain size photo No. |  | Sample Photograph No. |  |
| Spectrum No.         |  | Surface Temperature   |  |
| Ground Temperature   |  | Snow Temperature      |  |
| Wetness              |  | Land cover type       |  |

c) Instruments preparation:

**Global Positioning System (GPS):** horizontal accuracy is 3-5 m, for recording the accurate location of each sample site;

**Digital camera:** for recording the sampling objects;

**Ruler and tape:** accuracy is 1mm. For measuring the SD and the length from sensor to objects respectively;

**Weatherglass and geothermometer/JM624u Digital thermometer:** for measuring the temperature of air, snow surface, snow body and ground. The accuracy of these Weatherglass and geo-thermometer is  $\pm 1^\circ\text{C}$  with Working temperature of  $-40^\circ\text{C} \sim 50^\circ\text{C}$ . For JM624u Digital thermometer, the range is extended to  $-199.9 \sim 199.9^\circ\text{C}$  and the accuracy is  $\pm 0.1^\circ\text{C}$

**Spectroradiometer:** for acquiring spectral reflectance of snow, it can measure the reflectance for wavelengths from  $0.35\mu\text{m}$  to  $2.5\mu\text{m}$ . The reflectance curves are calculated using the reflectance from a white plate of barium sulfate powder.

**Snow fork:** for the measurement of the electrical parameters: resonant frequency, attenuation and 3-dB bandwidth. The measuring results are used to calculate

accurately the complex dielectric constant of snow. Further, the liquid water content and density of snow are calculated using semi-empirical equations;

**Snow grain size measurement device:** for the measurement of snow grain size. The device is composed of electron microscopy at high magnification, notebook installed with packaged image processing Software, and photographic paper sacred to snow grain size measurement (see Figure 4.3).



Figure 4.3 Snow grain size measurement

### Experiment procedures

The experiment can be divided into two parts. In the first part, difference detection of new fallen snow and sedimentary snow is discussed. In Northeast China, the grain size of new fallen snow is smaller in comparison with that of sedimentary snow (see Figure 4.4). On 17-12-2009 and 19-12-2009, we conducted two field experiments in Changchun. It snowed on 17-12-2009, which means that via the measurement we can get spectrum and grain size for both new fallen snow and sedimentary snow.

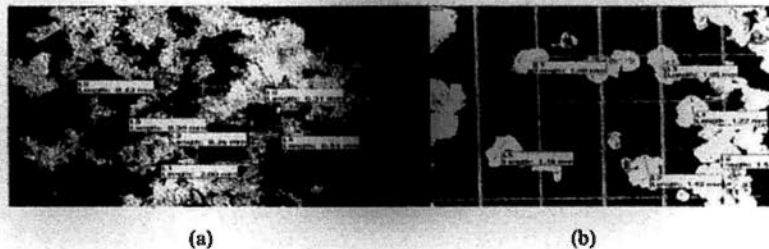


Figure 4.4 Grain size for both new fallen snow and sedimentary snow

(a) shows the grain size of new fallen snow and in (b) sedimentary snow grain is measured.

The second part of the experiment was conducted in the following 3 cities: Changling, Songyuan and Jilin. In the rest four testing sites, testing snow packs are straight-cut to find out the relationship between grain size and spectrum in different snow layers on transverse sections. For each layer, spectrum and grain size were measured before the snow on this layer was removed.

Figure 4.5 shows snow grain sizes from different layers measured (from top to bottom: (a) to (f)) on Songhua River in Songyuan city.

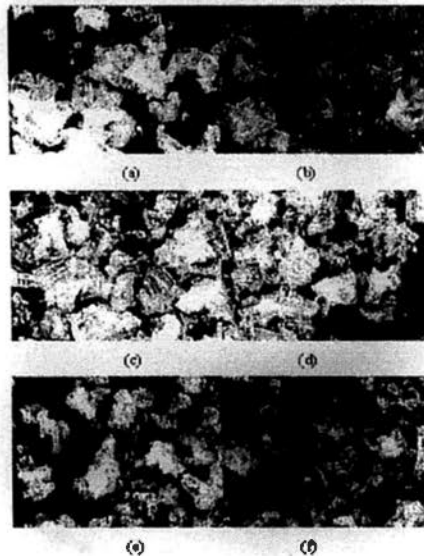


Figure 4.5 Snow grain sizes obtained from different snow layer on river ice

## Experiments on snow grain size affected by melting and refrozen

### Design and Methods

When the temperature is higher than melting point, snow starts to melt on the surface. The small melting snow grain will refreeze into a larger one when temperature falls below the freezing point. It is difficult to simulate the fluctuated temperature in nature. On the other hand, although we can control temperature in an isolated laboratory, the artificial snow layers are far different from those in nature.

Thus, field experiments are absolutely necessary. Long term observation will be one option, however, it will take more than one cycle of temperature fluctuation

### Testing sites selection

In the experiments, high power experiment instruments to heat the air like sun does. Thus two testing sites are selected in the suburb that is near Northeast Institute of Geography and Agroecology (NEIGAE) in Changchun.

### Testing time

To get the best nature light source for our experiments, we need to start at 10:30 and finish before 14:30. For those experiments that do not need sun as their light source, the experiments were conducted not until 18:00 to eliminate the effect of natural light.

## Experiments Methods

- a) Recording forms: to list out all the parameters should be record in the field experiments (see Table 4.2 and 4.3).

Table 4.2 Record for regular information

|                                  |  |                       |  |
|----------------------------------|--|-----------------------|--|
| Date                             |  | Recorder              |  |
| Testing site No.                 |  | Refrozen Spectrum No. |  |
| Grain size photo No.             |  | Time                  |  |
| Testing site Surface Temperature |  | Surface Temperature   |  |

Table 4.3 Record for spectrum

|                                  |  |                      |  |
|----------------------------------|--|----------------------|--|
| Date                             |  | Recorder             |  |
| Testing site No.                 |  | Heating Spectrum No. |  |
| Grain size photo No.             |  | Heating Time         |  |
| Testing site Surface Temperature |  | Surface Temperature  |  |

Parameters in the two tables are similar. However they are used in different periods of the experiment. Table 4.2 is the form used for analysis of refrozen grain, while Table 8 is used to understand the properties of wet snow.

- c) Instruments preparation:

**Weatherglass and Non-Contact Infrared Thermometer:** for measuring the temperature of snow surface. The accuracy of these Weatherglass and thermal infrared thermometer is  $\pm 1$  °C;

**Spectroradiometer:** for acquiring spectral reflectance of snow, it can measure the reflectance for wavelengths from  $0.35\mu m$  to  $2.5\mu m$ . The reflectance curves are calculated using the reflectance from a white plate of barium sulfate powder;

**Hot air generator:** to heat snow of testing sites in the first part of experiment, the power of the two hot air generators are 1500Kw and 1000kw;

**Snow grain size measurement device:** for the measurement of snow grain size, the device is composed of SMZ-B4/T4 zoom expander stereomicroscope (Table 4.4),

notebook installed with packaged image processing Software, and photographic paper sacred to snow grain size measurement.

Table 4.4 Parameters of SMZ-B4/T4 zoom expander stereomicroscope

|                                   |                            |
|-----------------------------------|----------------------------|
| Zoom Ratio                        | 1 : 6.5                    |
| Magnification                     | 7-45                       |
| Zoom Range                        | 0.7×-4.5×                  |
| Working distance                  | 110mm                      |
| Interpupillary distance           | 54-76mm                    |
| Diopter regulation                | ±5 diopter                 |
| Input voltage                     | 220V, 50Hz                 |
| Vertical fluorescence illuminator | LED cold light illuminator |
| Transmission illuminator          | LED cold light illuminator |

**Lowel Pro-Lamp Interior Light Source Assembly/ A128932:** for lighting in the second part of experiment, which were conducting in the night to avoid obvious light sources and effects of water vapor. It could be used both in the visible and near infrared regions. Two lamps were used to avoid shadows.

### Experiment procedures

In this experiment, we try to figure out how does the spectrum change when temperature or wetness changes, and how does the grain size change caused by melting and refrozen affect the spectrum.

In nature, melting and refrozen processes will happen only under certain environmental conditions, which make it hardly to acquire repeatability data for analysis. Thus, imitated experimental environment is needed.

In the first part, we tried to figure out snow spectrum of different grain size that formed by natural variation of temperature. To do this, we need to:

1. acquire the spectrum of new fallen snow ;
2. compare the spectrum of new fallen snow with that of accumulated snow;
3. compare the spectrum of undisturbed snow with that of disturbed snow with footprint on it.

The second step is to simulate environmental temperature change. The freezing and thawing process generated under artificial temperature controlling in an open environment will make the changes of grain size and wetness of snow in control to a

certain extent. In this part, we try to establish the relationship between grain size and spectrum.

Hot air generators were used to simulate the rise and fall of temperature. To avoid heat exchange, heating isolation materials are used as adiabatic walls and baffle. The experiment procedure of this part is:

1. Select a plot on which is not destroyed by footmarks;
2. Gage the temperature of snow surface with glass thermometer and Non-Contact Infrared Thermometer;
3. Measure the grain size of surface snow;
4. Calibrate Non-Contact Infrared Thermometer with glass thermometer;
5. Heat the air above testing plot with hot air generator;
6. Adjust heating altitude and power to get a better result according the change speed of air temperature;
7. Measure the temperature of snow surface with Non-Contact Infrared Thermometer;
8. Acquire snow spectrum while snow thaw;
9. Stop heating to refreeze snow;
10. Acquire the spectrum of refrozen snow;
11. Measure the grain size of refrozen surface snow;
12. Compare the spectrum of artificial refrozen snow and natural one;
13. compare the snow grain sizes before and after freezing and thawing process;
14. Compare the snow spectrum of different grain sizes.

However, the effects of water vapor are still existing if the experiments conducting in the day time. Thus, a derivative experiment is designed for eliminating these influence factors:

1. Experiment time for derivative experiment is changed to 7 pm, when it is dark.
2. A pair of Lowel Pro-Lamps was used as light source in stead of sunlight.
3. Because of the big power of Lowel Pro-Lamp, in the derivative experiment the two lamps replace hot air generators as air temperature controller, which makes the control of experiment easier and more efficient.

Figure 4.6 shows the grain size of snow under different artificial conditions.

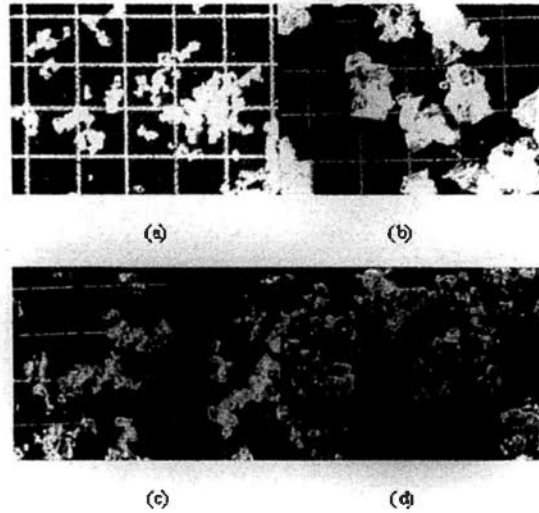


Figure 4.6 Experiments on the relationship between snow grain size and spectrum (20091222, night) (a) and (b) are snow grain size photos of original snow surface and refreezing snow taken for the day time experiment. (c) and (d) show the grain size of original snow surface and refreezing snow taken for the derivative experiment.

#### 4.2.1.2 Experiments on Mixed Pixel

Mixed pixel is the common issue people met in snow monitoring based on satellite remote sensing data. Misjudged pixel occurs in the area of complex land cover types. To solve the problem, one approach is the use of mixture modeling (A.K.A. spectral un-mixing of imagery with high spectral resolution). Pixels in the image representing "end-members" that are believed to represent homogeneous land cover types is identified. Pixels in the image are assumed to consist of linear mixtures of these pure land cover types, of which reflectance spectra are determined. Thus, the reflectance  $r_i$ , observed in spectral band  $i$  is modeled as (Rees, 2005)

$$r_i = \sum_{j=1}^N f_j r_{ij} + e_i \quad 4.1$$

Where  $f_j$  is the fraction of land cover type  $j$  present in the pixel,  $r_{ij}$  is the band- $i$  reflectance of land cover type  $j$ , and  $e_i$  is the error in the linear model.  $N$  is the total number of land cover classes. The spectral un-mixing process involves determining the set of coefficients  $f_j$  that minimize the sum of the squares of the errors  $e_i$ , (Rees, 2005).

## Design and Methods

Here in our experiments, we aim to acquaint the spectra properties of mixing pixel on main land cover types in Northeast China. Therefore, the testing sites of the series experiment are selected in several cities where typical land cover types can be found.

### Testing sites selection

The series experiment was conducted in five testing sites located in Changling, Songyuan and Jilin respectively (Figure 4.7).

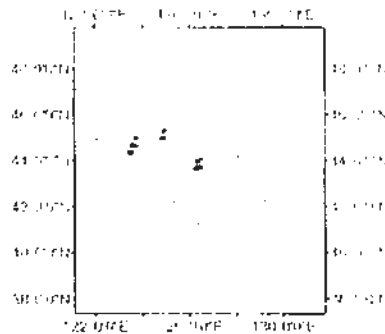


Figure 4.7 Test sites located in Changling, Songyuan and Jilin

The underlying surfaces of testing sites are pasture, corn land, river ice, rice land and sapling land.

### Testing time

The optimum time for optical remote sensing experiments is 10:30-14:30 in Northeast China. In this series experiment, we aimed for that time frame.

### Experiments Methods

We attend to study the spectra properties of mixing pixels composed with snow and a certain major land cover type. Consequently three kinds of spectrum are locked on:

1. Spectra of snow;
2. Spectra of a certain bared underlying surface;
3. Spectra of the mixture of snow and underlying surface.

To acquire the information, we need to prepare the following instruments and documents.

The experiments on mixing pixel and grain size are performed in turn. The in situ data we need to collect in these experiments include SD, temperature, snow grain size, GPS-based location and spectrum. Wetness of snow is one of effect factors on reflectance, especially when the surface temperature is higher than melting point. To obtain all these data, instruments need to be prepared before the experiments.

a) Electronic map: before we start the trip, we need to locate the plots with topical underlying surfaces. The map of land cover type over Northeast China is necessary. Besides, the maps of highways and urban map are prepared.

b) Recording form: to list out all the parameters should be record in the field survey (see Table 4.5).

Table 4.5 Record for snow grain size

|                    |  |                     |            |
|--------------------|--|---------------------|------------|
| Date               |  | Recorder            |            |
| Record No.         |  | Altitude of sensors |            |
| Spectrum No.       |  | Sample No.          | Photograph |
| Underlying surface |  | Memo                |            |

c) Instruments preparation:

**Global Positioning System (GPS):** horizontal accuracy is 3-5 m, for recording the accurate location of each sample site;

**Digital camera:** for recording the sampling objects;

**Ruler and tape:** accuracy is 1mm. For measuring the altitude of sensor to objects;

**Spectroradiometer:** for acquiring spectral reflectance of snow, it can measure the reflectance for wavelengths from  $0.35 \mu m$  to  $2.5 \mu m$ . The reflectance curves are calculated using the reflectance from a white plate of barium sulfate powder;

**Flag:** to mark the testing plots.

### Experiment procedures

In this experiment, the difference between the spectra of testing plots with different proportion of component parts is compared. By doing this, the relationship between reflectance spectral and snow proportion can be deduced, and the relationship will be applied in snow map accuracy improvement for the models based on satellite optical remote sensing data, such as MODIS. In order to achieve this aim, the following experiment steps are designed:

1. Select testing plots;
2. Measure spectra of snow surface, bared underlying surface and mixing area;
3. Mark the plot;
4. Take photos of testing plots;

Figure 4.8 shows the mixture status of testing sites.

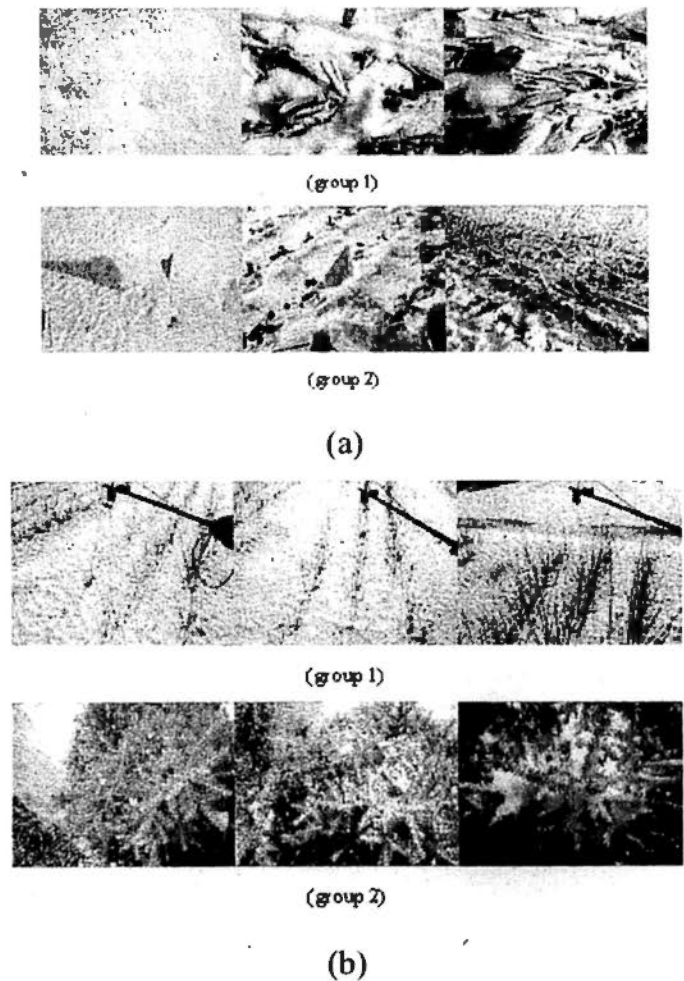


Figure 4.8 Snow mixed with corn land(a) and vegetation(b)

### 4.2.1.3 Experiments on SD

Remote sensing of snow is based on the idea that is to use measurements in specific wavelength regions to estimate the physical properties of the snow. To detect SD with optical remote sensing data, models are generated based on the following two theories:

The relationship between snow grain size and SD, based on the assuming that grain size increases with depth, SD can be retrieved from grain size (Dozier *et al.*, 2009)

In the visible part of the spectrum, snow reflectance is dominated by the absorption of dust, soot, or algae inside snow pack. Snow grain size is not as sensitive as it is in

near-infrared range. Therefore, to estimate snow grain size, near-infrared range should be selected (Dozier *et al.*, 2009). However, the growth of snow grain size on the surface layer of a snowpack is not only determined by SD. The metamorphism is complicated, which involve temperature gradients, vapor gradients, and many other environmental effects.

Another hypothesis bases on spectrum of thermal infrared. SD may have influence on heat emission in snowpack. To study the changes at thermal infrared range, there may be a chance to calculate the changes of SD.

However, both of the two scientific hypothesizes are still in its infancy. In this study, the experiment is designed to dig out the relationship between SD and its optical properties.

The series experiment is embedded in the other optical experiments. The parameters in all the three experiments are correlative. Thus, these experiments were performed in turn. The same preparing work and procedures that mentioned in above experiments also can be used for this one. Furthermore, to obtain direct information, three testing plots on a snow slope are compared in this experiment, which are on the top, half-way up the slope and the foot of the slope. The SD of the three plots are 26 cm, 20cm and 15cm respectively (see Figure 4.9).

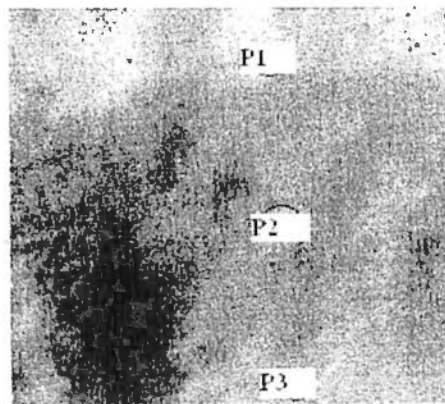


Figure 4.9 Snow surfaces with different SDs

## 4.2.2 Field experiments on Microwave Properties of Snow

As it is noted in literature review and methodology section, passive microwave snow cover algorithm development efforts have been varied, with focus on the retrieval of SCA, SD, and SWE (Pulliainen & Hallikainen, 2001; Tait, 1998; Derksen *et al.*, 2005; Pardé *et al.*, 2007). Among all these studies, it is of vital importance to estimate SD. Since 1970s, passive remote sensing started to be applied in SD

estimation. A series algorithms and models were developed. Among these models, the following four are most popular: NASA algorithms originally developed by Chang's group; MEMEL model; HUT model and AIEM model.

However, the accuracy of SD estimation is still affected by several other factors, among which, land cover types are considered as one of the most significant and unavoidable effects as it is discussed in Chapter 2 and 3. Therefore, in the experiments design, we focus on the relationship between microwave radiation signals and snow status, and try to find out the effect factors on snow information estimation:

1. Microwave Radiation Characteristics and SD;
2. Effects of underlying surface on Microwave Radiation Characteristics;
3. Microwave Radiation Characteristics and snow density/SWE;
4. Microwave Radiation Characteristics and SCA.

Here in this thesis, SD estimation over different underlying surfaces was focused on. Thus the design and data analysis for microwave radiation characteristics and SCA, snow density and SWE will not be covered in the following sections.

#### **4.2.2.1 Microwave Radiation Characteristics and SD**

##### **Design and Methods**

The series experiments are designed to figure out the sensitivity of  $T_{b,18}$  and  $T_{b,37}$  to SD.

##### **Testing sites selection**

7 testing sites in 4 cities (see Figure 4.10). In the 7 testing sites, Jingyue district belongs to Changchun, while three testing plots with different underlying surfaces were selected.

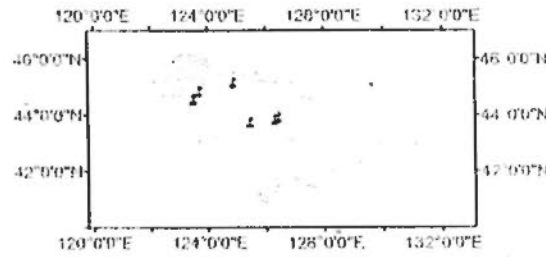


Figure 4.10 Location of test sites for passive microwave experiments

The series experiment is lasting for more than one year. The experiment selected in Jingyue District of Changchun was conducted in 2009. The rest part of the experiment is conducted in Changling, Songyuan and Jilin in 2010 (see Figure 4.11). The underlying surface, SD and snow grain size are varied in different testing plots.

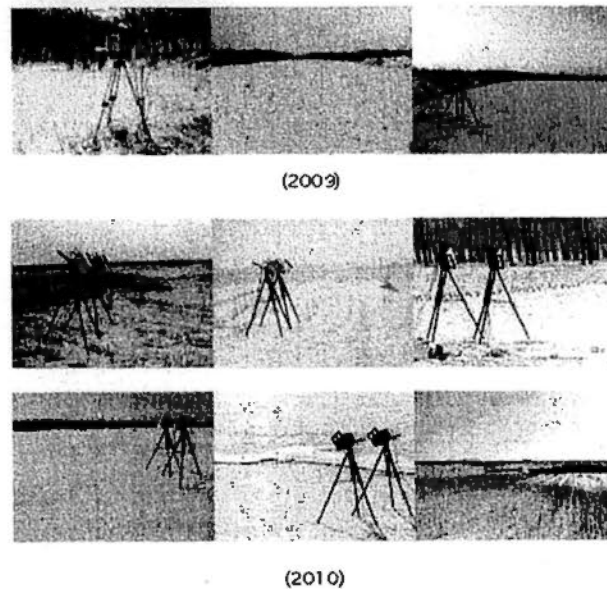


Figure 4.11 Natural stages of snow in test sites

(2009) – (2010) are two group photos of testing sites which were taken in Changchun, Changling, Songyuan and Jilin respectively. Here, the underlying surface of these testing sites includes pasture, glabe, lake or river ice, paddy fields, bush field and grove.

### Testing time

The advantage of microwave remote sensing is its penetrativity and independence on light source. It makes us extend our working time from sunshine period to the whole day in comparison with that of optical remote sensing experiments.

## Experiments Methods

In this experiment, we mainly focus on the brightness temperature of 18GHz and 37GHz. To get accurate measurement results, we will do the following prepare work:

- a) Electronic map: since we took a comparatively long way from one testing sites to the other, maps are important for our field trip. Maps of highways, electron map of land covers are selected via internet.
- b) Recording form: to list out all the parameters should be record in the field survey (see Table 4.6).

Table 4.6 Snow information record for passive microwave experiment

|                      |  |                       |  |
|----------------------|--|-----------------------|--|
| Date                 |  | Recorder              |  |
| Time                 |  | Snow depth            |  |
| Grain size photo No. |  | Sample Photograph No. |  |
| Surface Temperature  |  | Snow Temperature      |  |
| Ground Temperature   |  |                       |  |
| Wetness              |  | Land cover type       |  |
| Polarization         |  | Incident Angle.       |  |
| BT(18.7)             |  | BT(36.5)              |  |

### c) Instruments preparation:

**Global Positioning System (GPS):** horizontal accuracy is 3-5 m, for recording the accurate location of each sample site;

**Digital camera:** for recording the sampling objects;

**Ruler and tape:** accuracy is 1mm. For measuring the SD;

**Cryogenic thermometers and Geological thermometer:** for measuring the temperature of air, snow surface, snow body and ground. The accuracy of these geo-thermometer is  $\pm 1$  °C with Working temperature of  $-40$  °C  $\sim$   $50$  °C.

**Snow fork:** for the measurement of the electrical parameters: resonant frequency, attenuation and 3-dB bandwidth. The measuring results are used to calculate accurately the complex dielectric constant of snow. Further, the liquid water content and density of snow are calculated using semi-empirical equations;

**Snow grain size measurement device:** for the measurement of snow grain size. The device is composed of electron microscopy at high magnification, notebook installed with package image processing software, and photographic paper sacred to snow grain size measurement;

**Electronic balance and snow shovel:** for the measurement of snow density. The accuracy of Electronic balance is 0.05g.

**Test-tube:** for the measurement of snow water equivalent. Quantitative snow with natural state was put into the test tube or beaker for melting, then the snow water equivalent can be calculate by counting the water left in the container. The accuracy of test tube is 1ml.

**Microwave radiometer:** for the measurement of brightness temperature of 18 GHz and 37 GHz. The height of microwave radiometer shelf is 1.5m. Liquid nitrogen is used to calibrate the microwave radiometer.

### **Experiment procedures**

In the experiment, the following steps are conducted:

1. we will calibrate microwave radiometer with blackbody;
2. change the angle of shelf to obtain the brightness temperature in different incident angles. The range of incident angle is from 30 to 60°;
3. change the polarization to get the polarized properties;
4. measure the environmental temperature synchronously;
5. survey the snow grain size via SMZ-B4/T4 zoom expander stereomicroscope;
6. measure snow density and SWE.

### **4.2.2.2 Effects of underlying surface and snow grain size on SD estimation**

#### **Design and Methods**

The effects of underlying surface are one of the hottest research focuses in snow monitoring study, because the influence result of these effects is still imponderables. Meanwhile, the effect of snow grain size on SD estimation is widely accepted by the researchers. However, it is still a difficult problem to determine the exact coefficient that depends on snow grain size in SD retrieval model in Northeast China. In this

section, the design of two experiments, from which the answer for the problems mentioned above may be found, is introduced.

### **Testing sites selection**

In selection of testing sites for the two series experiments, we consider both underlying surface and SD. The major underlying surfaces include farmland, ice and woodland. Because of the different moisture content of the underlying surface, both paddy fields and dry fields are selected as testing sites. Considering the thickness of ice, we conducted experiments on both frozen fish pond and frozen driver (Songhua River with the boundary of Songyuan). Bush field and grove are taken as test sites.

### **Testing time**

Testing time for the two experiments is 9:00-22:00.

### **Experiments Methods**

The preparing works for these experiments are very similar as those in experiment for estimation of SD. Actually the two series experiments were conducted together. Thus, in this section the differences between the two experiments will be mentioned.

### **Experiment procedures**

The first several steps for underlying surface effects are the same as those of SD retrieval experiment. But something new in this experiment is that the microwave signals of uncovered land surface need to be recorded to analyze the physical properties of underlying surface. Thus, the final step for this experiment is to sweep away the covered snow. Here it needs to be emphasized that, the brightness temperature will be greatly affected by the surface temperature. And the temperature of underlying surface is generally a few degrees' higher than that of air temperature because of the insulation function of covering snow. To reduce the errors that caused by temperature, the radiation brightness temperature of underlying surface should be measured half hour's later after the snow is swept off. Figure 4.12 shows the start and final stage of test plot.

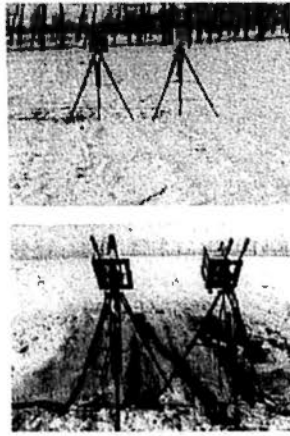


Figure 4.12 Experiments on underlying surface effects on microwave signals

### 5.1 Introduction

In this chapter, the processing method of in situ data collected from field experiments and long term observation will be processed into a standard format and then analyzed to figure out the relationship between snow physical properties and SD/snow grain size.

### 5.2 Analysis of In Situ Data

After the collection stage, in situ measurement results need to be pre-processed for analysis. This is in situ data preparing stage.

#### 5.2.1 Field Experiments Data

As it is noted, the most difficult part of field experiment is to control the environmental conditions during the experiments. The effects of vapors in the atmosphere, sunlight and temperatures can hardly be eliminated because the experiments are conducted in the open area. To get the in situ data with higher quality, some process procedures will be conducted.

##### 5.2.1.1 Optical experimental data

The most valuable optical experimental data collected during series experiments are snow grain sizes and corresponding spectrum. However, the veracity of data is highly depended on environmental conditions.

According to the theory of atmospheric window, the atmosphere is composed of gases and aerosols which selectively absorb and scatter electromagnetic radiation at particular wavelengths. Both of solar and earth surface radiation are filtered by the atmosphere. The sensors on satellites outer space can only detect the energy that transmit atmosphere. Therefore, no accurate results can be derived from reflectance that recorded with satellite sensors without considering the loss of energy that is absorbed by atmosphere but not earth surface. Still there are three ranges of wavelength through which there is less loss of energy caused by atmosphere

absorption. They are visible and reflected infrared (0.4 - 1.2 $\mu\text{m}$ ), thermal infrared (3 - 5 $\mu\text{m}$  and 8 - 14 $\mu\text{m}$ ), radar and microwave (1 mm - 1 m) ranges. All the three ranges are atmosphere window.

For this reason, spectrum data measured with Spectroradiometer in field survey are usually affected by water vapor outside the range of atmosphere window, especially at infrared range (see Figure 5.1).

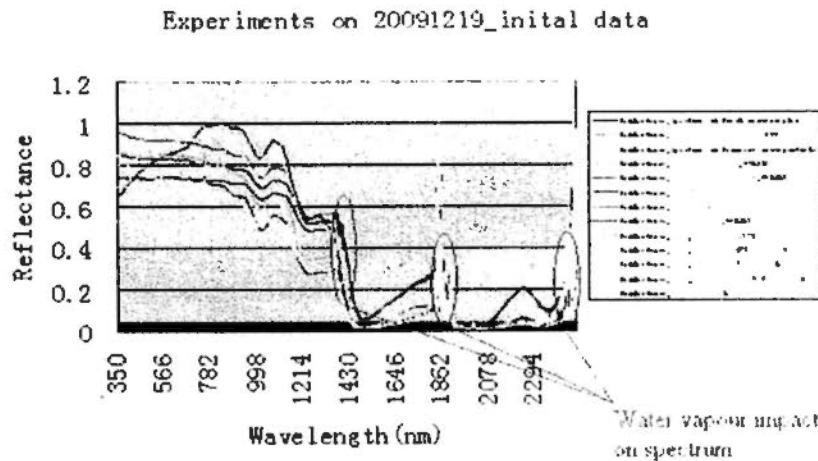


Figure 5.1 Effects of vapors on spectral collected from field measurements

The smoothing process has become an indispensable feature of modern data handling programs.

At present, under the general name "smoothing", different mathematical algorithms and filter functions are included.

Localization is the most typical feature of field collected spectrum, which means that its intensity and frequency change greatly during the whole collection spectrum range. Therefore, in most of cases these disturbed bands will be removed in feature extraction. The immediate sequel to the discarding is large number of deficiency.

In this research, the feature of different distribution of energy on the frequency domain is used to separate useful signals from noise: Generally, most noise distribute on high frequency region while useful information on the low frequency region. Wavelet transform is one of the efficient methods for noise reduction. Meanwhile, the fine detail of de-noised spectral is well preserved.

### 5.2.1.1.1 De-noising processing

The reflectance acquired from field experiments are measured by comparison method. That is to say, the reflectance can be calculated as the following expression (Zhou *et al.*, 2009):

$$R = \frac{REFLECTANCE_{object}}{REFLECTANCE_{whiteboard}} \times 100\% \quad 5.1$$

Here  $REFLECTANCE_{object}$  and  $REFLECTANCE_{whiteboard}$  are reflectance of target object and standard board respectively.

Considering the noise, the formula can be emended as (Zhou *et al.*, 2009):

$$R = \frac{REFLECTANCE_{object} + error_{object}}{REFLECTANCE_{whiteboard} + error_{whiteboard}} \times 100\% \quad 5.2$$

Here  $error_{object}$  and  $error_{whiteboard}$  are the random errors generated during measurements. In this study, the measurement errors caused by absorption of water vapor in atmosphere near wavelength  $1.45\mu m$  and  $1.8\mu m$  are much higher than those of object reflectance (Zhou *et al.*, 2009).

$$\log(R) = \log(REFLECTANCE_{object} + error_{object}) - \log(REFLECTANCE_{whiteboard} + error_{whiteboard}) \quad 5.3$$

As it is mentioned above, wavelet transform can be applied to de-noise the spectrum. Here in this step, wavelet transform will be applied to reduce the noise. Figure 5.2 shows spectrum measured on 20100126. It is obvious that noise caused by water vapor around  $1.3\mu m$  and  $1.9\mu m$  in near-infrared band appears at each spectral curve. However, near-infrared range is most significant for the study on snow grain size because that it is more sensitive to energy absorption of snow particles than visible range. These noises need to be eliminated before the analysis of optical in situ data before the calculation of extreme values in grain size sensitive range, which has, unfortunately, overlap with that under the effect of vapor.

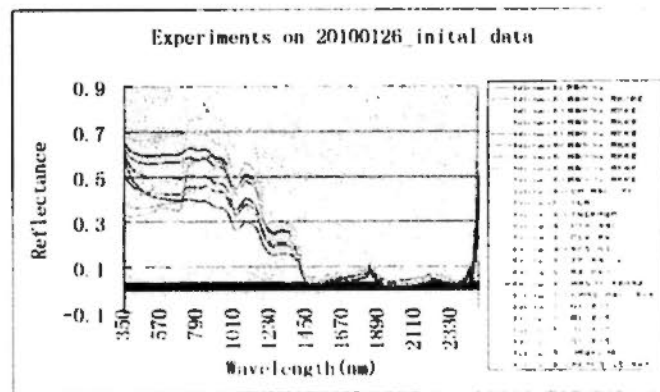


Figure 5.2 Experiments on 20100126

To eliminate the noise, logarithm operation should be performed on the initial data as it is described in formula 24. However, sometimes zero value can be found at troughs of reflectance spectrum. Thus, a declination value is added to initial data before logarithm operation.

Then Wavelet transform can be applied on logarithmic data to de-noise the high frequency noise. Figure 5.3 shows the same group of in situ spectrum as those in Figure 32. The noticed effect of wavelet transform is obviously:

1. The trembling noises around  $1.3\mu m$  are smoothly filtered,
2. The strong noise neared  $1.9\mu m$  are basically removed. However, since the noises at  $1.9\mu m$  are too strong, the processed curves are undergoing a slightly metamorphosis.

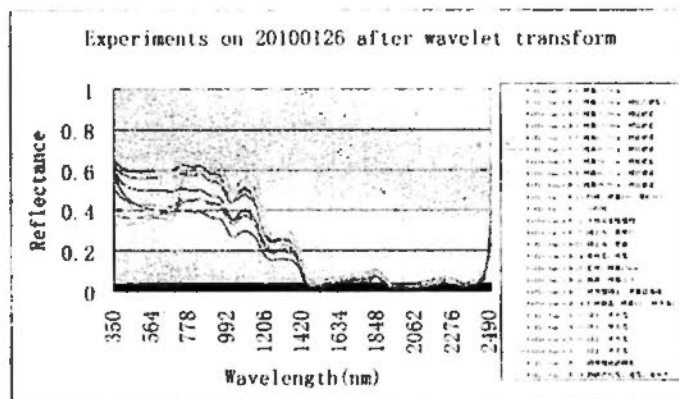


Figure 5.3 Wavelet transformed spectrum collected from field experiment on 20100126

To guarantee data quality, the part of spectrum at the wavelength between  $1.6\mu m$  and  $2.5\mu m$  is abandoned.

### 5.2.1.1.2 Smooth processing

The second step for spectrum pre-processing is smooth processing. Since it is unavoidable that fluctuation appear in reflectance curve after wavelet transform, further processing is necessary to smooth the curve before analysis. The basic idea for spectrum smooth is to (1) select several points before and after focus point, (2) and average the reflectance of selected points or simulate focus point with selected points. This method can be used to eliminate noise only when the mean value of random noise is 0 in processing window.

Figure 5.4 shows the final processing result of the group of spectrum measured on 17<sup>th</sup> Dec. 2009. Compared with their initial data (see Figure 5.4 (a)), most of the effects of noises are removed.

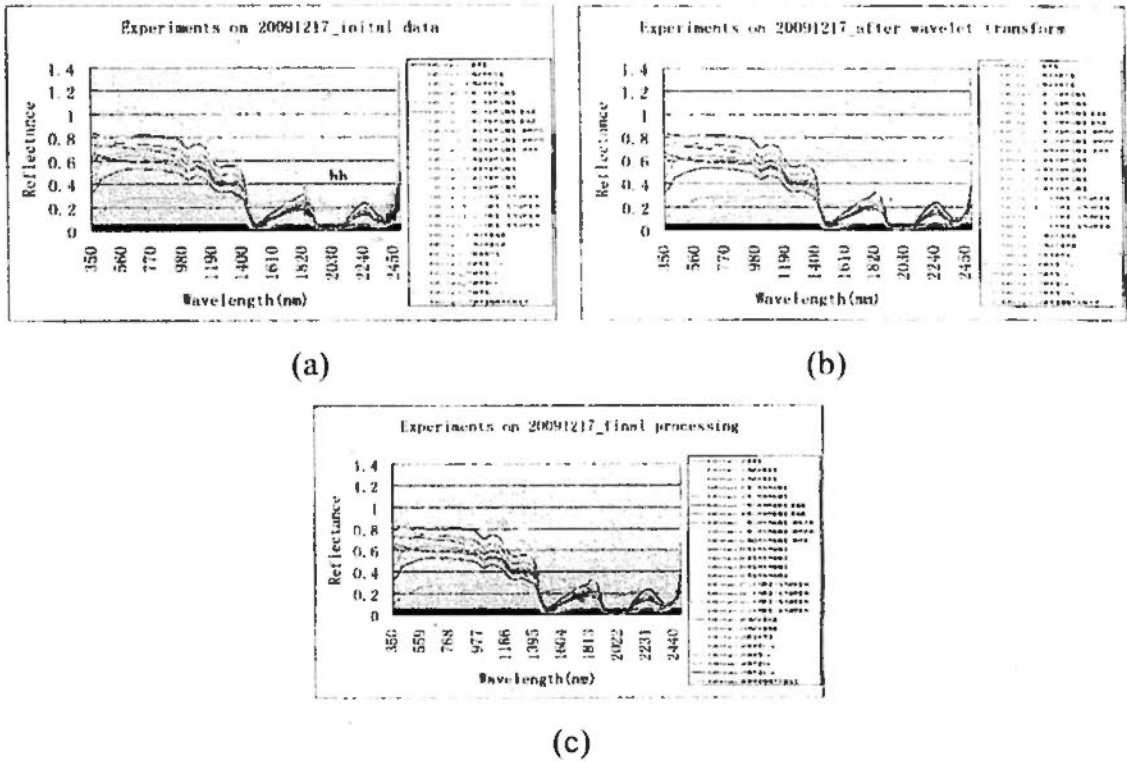


Figure 5.4 Spectrum processing stages

The group of pictures in Figure 5.5 shows the strongly affected measured spectrum of the same group of snow samples after each processing steps:

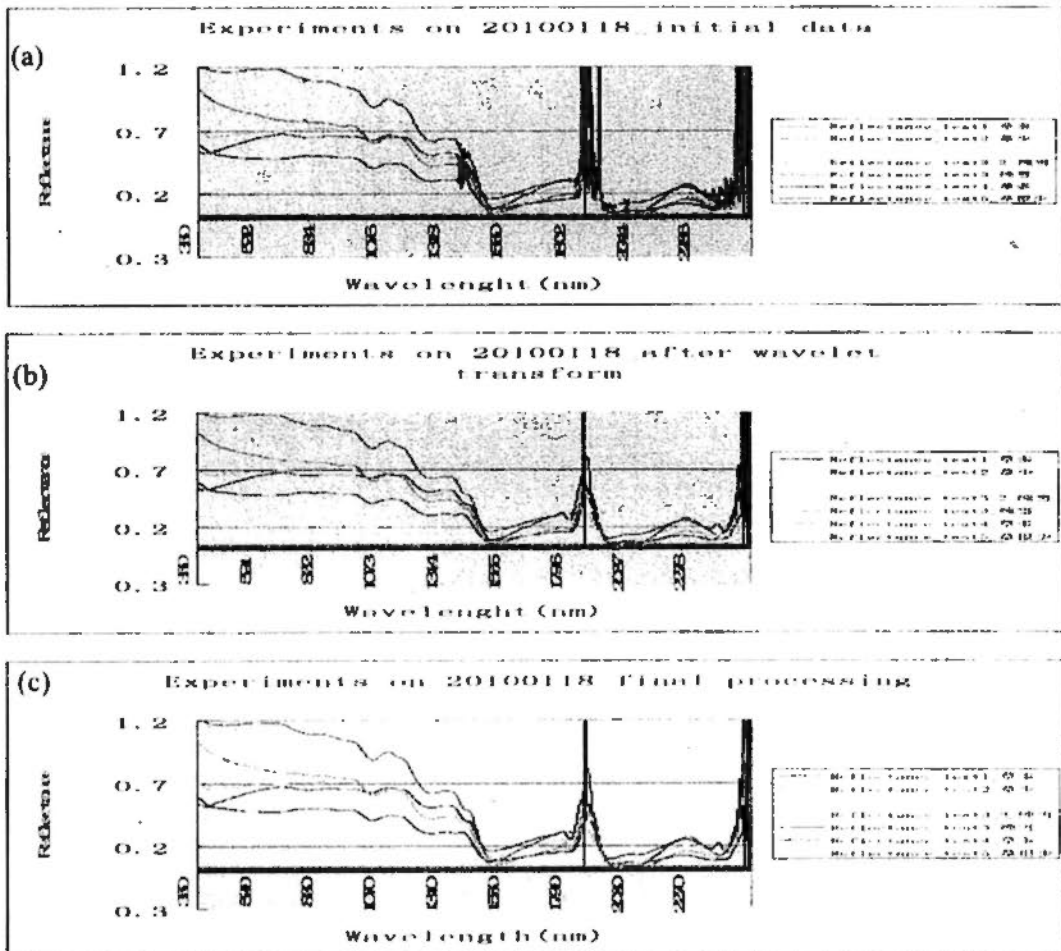


Figure 5.5 Processing procedure for spectrum that is strongly affected by vapor

Here (a)-(c) are the spectrum of the same group of snow samples after in situ measurement, wavelet transform and smoothing processing respectively.

Although the reflectance at near  $1.9\mu m$  are still under the influence of high frequency noise, the spectrum curves as a whole can be used in analysis.

### **5.2.1.1.3 Experiments on grain size**

As it is mentioned in chapter 4, the most contribution of optical remote sensing data to snow monitoring is its ability on obtaining of snow grain size. There are two different series experiments designed for determining the relationship between snow grain size and reflectance of the same snow sample. In the following section, in situ data obtained in the two series experiments are analyzed, and preliminary results on the relationship of snow grain size and reflectance are concluded.

#### **5.2.1.1.3.1 Experiments on metamorphosis of snow grain size caused by gravitation**

##### **Data processing**

In this part, optical spectrum data are divided into two groups:

1) new snow, and 2) old snow.

Considering the effects of gravitation on different snow layers, snow grain sizes and spectrum both on the surface of snowpack and inside snowpack body are studied.

##### **Spectrum of snow particles**

Figure 5.6 shows the spectrum measured in different testing sites (see Table 5.1) in experiments on snow grain size metamorphosis caused by gravitation. These spectrums are used to obtain the optical property of normal snow surface, which means the testing sites for these data need to remain in its naturally flat state when we conducted our experiments. Among the 7 spectrums, three of them are measurements of new fallen snow (see Table 5.1 Memo) and the rest are measured on sediment snow surfaces.

To compare with the surface snow, corresponding spectrums inside snowpack are measured too (see Figure 5.7). There are two kinds of snow samples in this group:

1. Natural formed snow particles under the thin coating of ice. To measure the spectrum of this kind of snow particles, we need to lift up the ice cover very carefully without invasion of the snow particles beneath the ice.



To analyze the difference of snow spectrum caused by naturally formed snow grain size, spectrums of new fallen snow and sediment snow are compared in this research (see Figure 5.8).

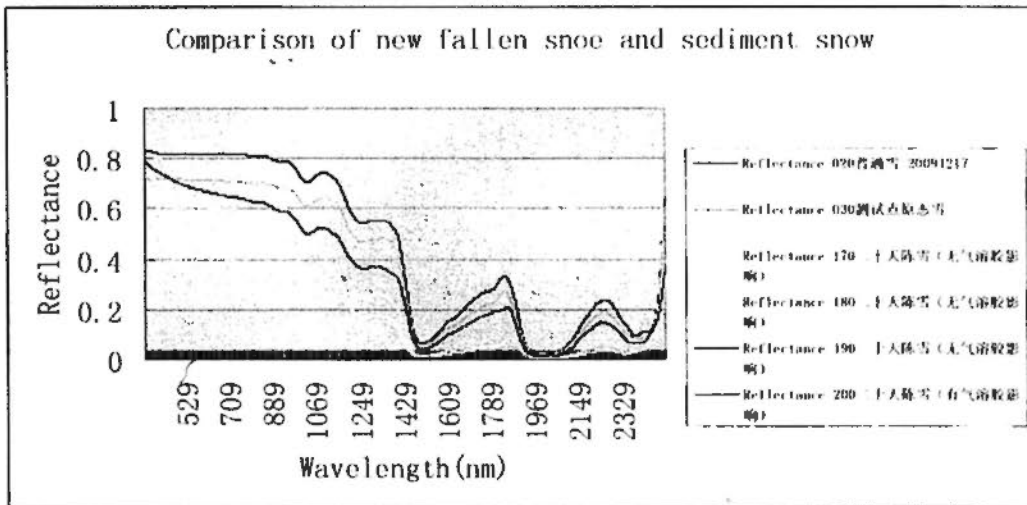


Figure 5.8 Comparison of new fallen snow and sediment snow

### Snow grain size

Another part of this experiment is the measurement of snow grain size. Tsview is used in snow grain size measurement (see Figure 5.9). The first tag presents us the parameters used in taking photos of snow grain size by electron microscopy. And the second tag shows the operations for geometrical measurements.

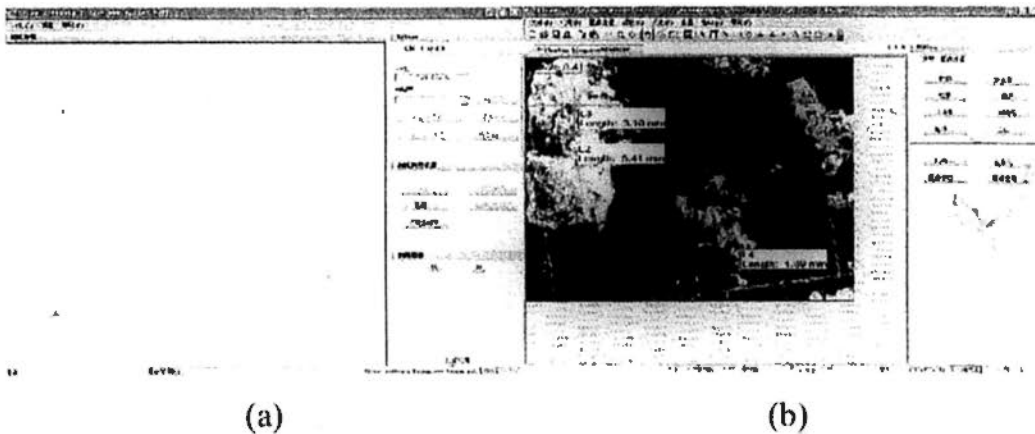


Figure 5.9 Interface of snow grain size measurement software-- Tsview

Here (a) and (b) are photos of user surfaces of taking photos of snow grain and analyzing.

Snow samples are carefully collected from testing sites with a piece of special photographic, which was separated into squares with sides of 2mm by red lines. By doing this, snow grain size can be calculated with red square as the reference substance.

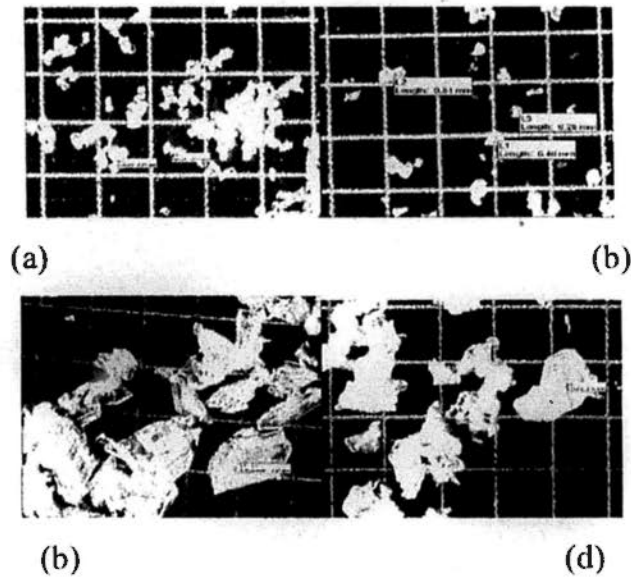


Figure 5.10 Snow particles in different position of snowpack

Here (a) and (b) show the snow particles of surface snow. And (c) and (d) present the naturally formed snow particles inside snow body.

In Figure 5.10, it is clearly that the grain size of middle layer snow is much larger than that of surface one's. The specific numbers of snow grain size in different layers are listed in Table 5.2.

Table 5.2 Snow grain size in different position

| Date     | Time  | Grain size(mm) | Grain size(mm) | Grain size(mm) | Grain size(mm) | Average (mm) | Position |
|----------|-------|----------------|----------------|----------------|----------------|--------------|----------|
| 20091219 | 10:21 | 0.54           | 0.76           | 0.59           | 0.74           | 0.66         | surface  |
|          | 10:25 | 2.03           | 2.43           | 2.05           | 2.89           | 2.35         | body     |
|          | 10:49 | 0.92           | 1.05           | 0.64           | 0.6            | 0.80         | surface  |
|          | 11:35 | 0.58           | 0.58           | 1.27           |                | 0.81         | surface  |
|          | 11:50 | 0.28           | 0.46           | 0.81           |                | 0.52         | surface  |
| 20091221 | 11:50 | 3.07           | 1.75           | 2.1            |                | 2.31         | body     |

Generally , the range of grain size of surface snow (new fallen snow or short-time sediment snow) is from 0.52mm to 0.80mm; while the grain sizes of middle layer snow are larger than 2.3mm (2.35mm and 2.31mm respectively), which are significantly larger than those of surface snow.

### Data analysis

As it is observed in situ spectrum processing results, there are significant differences between the average snow grain sizes of surface snow and that of middle layer's, and

between new fallen snow surface and sediment snow surface. In this section, the relationship between of snow grain sizes and snow spectrum is analyzed.

Average spectrums derived from snow surface and snow body are shown in Figure 5.11. As it is observed, the snow grain size inside snowpack ( $>2.3\text{mm}$ ) is larger than that on snow surface ( $<1\text{mm}$ ). From the spectrum curve, it is clearly that reflectance of snow body is lower than that of snow surface.

Moreover, the reflectance of new fallen snow on the surface of snow pack is higher than that of sediment snow surface (To make it more precise, the experiment was conducted in the same testing sites, Changchun. A pair of cross-references testing plots is selected. One plot was covered with plastic film with an altitude of half meter over snow surface. Another plot was exposed to the air. This ensures that the grain of snow surface of testing plot 1 is naturally formed sediment snow. When experiment was conducted the on snowy day, the grain of snow surface in testing plot 2 is new fallen snow. ).

Figure 5.12 shows the spectrums of new fallen snow and sediment snow. It is obvious that at near infrared range the spectrums of these two kinds of snow are quite different from each other.

However, absolute value of reflectance is determined by several factors, such as grain size, wetness and the incident angle of light from light source. Thus, to find out the qualitative changes corresponding to the changes of snow grain sizes, the changes of wave crests and troughs need to be carefully studied.

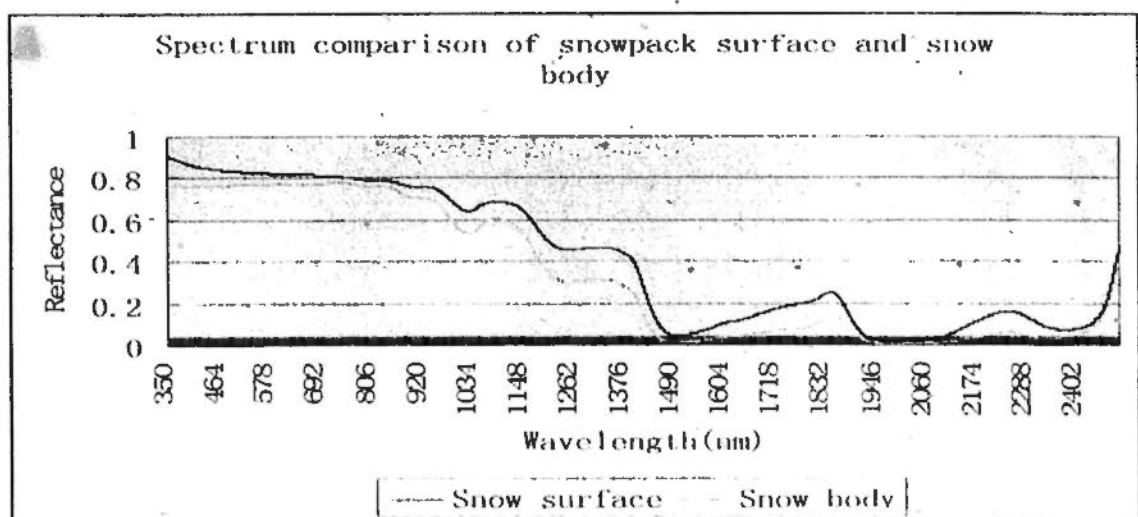


Figure 5.11 Spectrum comparison of snow pack surface and snow body

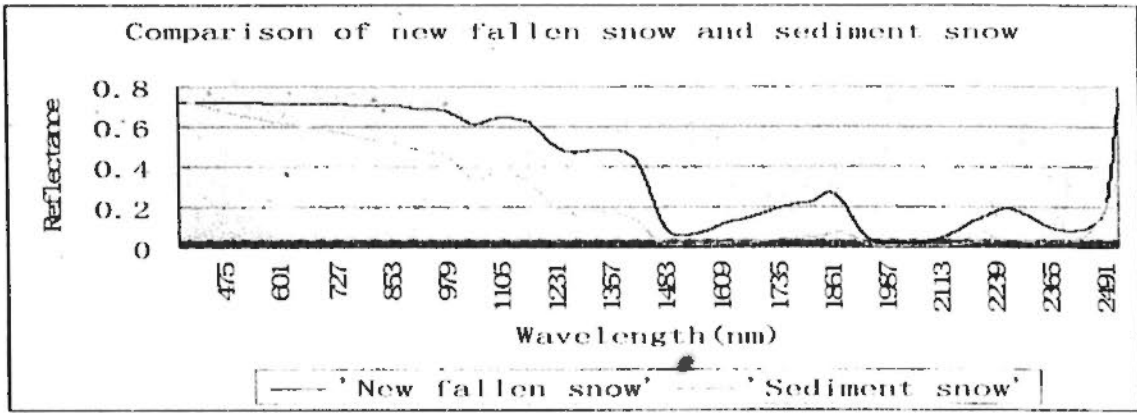


Figure 5.12 Comparison of new fallen snow and sediment snow

As it is mentioned in data pre-processing part, the most sensitive band to snow grain size changes is near infrared range. However, after wavelet transform, only the water vapor noise at range from  $1.28\mu\text{m}$  to  $1.6\mu\text{m}$  (which can be found in MODIS channels) can be removed successfully. Thus, in this section, snow properties within this range will be discussed.

To visually explain the relationship between snow grain size and snow sampling spectrum, in situ data derived from the experiment measured on separated snow layers are illustrated in Figure 5.13. The spectrums of five layers are drawn from  $1.25\mu\text{m}$  to  $1.6\mu\text{m}$ . And a pair of crest and trough is contained in this figure. Figure 5.13 shows three groups of reflectance that composed of five spectrums curves. The upper curve with higher reflectance in this range is that of surface snow's, which is followed by the reflectance of the fifth layer's. The lowest reflectance group is composed of spectrum curves of layer 2-layer 4.

The snow grain sizes of the five different layers' are shown in Table 6.3.

It is easy to deduce that there are at least two snowfalls over the testing site, since the grain size of lowest layers is smaller than that of upper ones', which will never happen if there is only one snowfall according to the deformation laws under gravity.

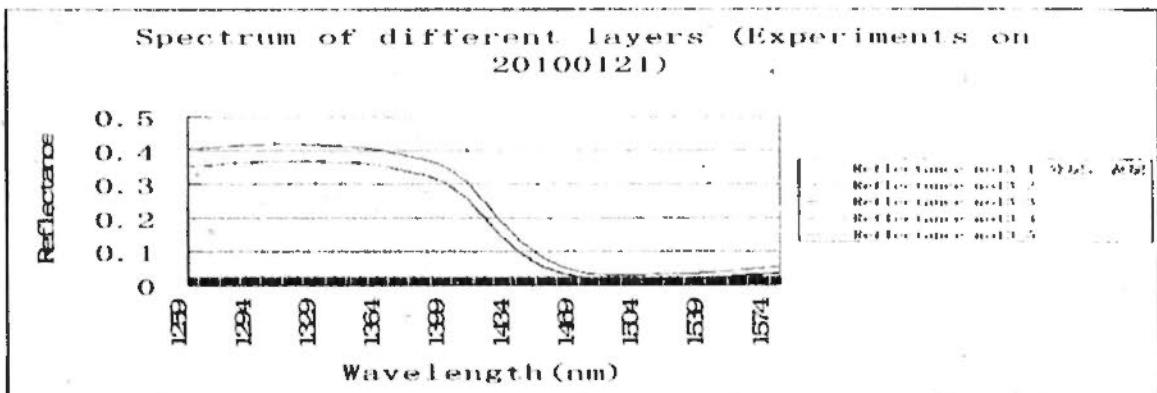


Figure 5.13 Spectrum of different layers

Table 5.3 Snow grain size in different layer

| Layer | SD(cm)           | Grain sizes(mm) |      |      |      | Average Grain Size(mm) |
|-------|------------------|-----------------|------|------|------|------------------------|
|       |                  |                 |      |      |      |                        |
| 13_1  | 6.7-6.8<br>(6.5) | 2.28            | 1.76 | 1.8  |      | 1.95                   |
| 13_2  | 5.50             | 2.15            | 2.12 | 2.06 | 1.94 | 2.07                   |
| 13_3  | 4.50             | 2.62            | 1.53 | 2.01 |      | 2.05                   |
| 13_4  | 3.50             | 2.38            | 1.72 | 1.80 |      | 1.97                   |
| 13_5  | 2.50             | 1.50            | 1.50 |      |      | 1.50                   |

Comparing the snow grain sizes in table 15 and the spectrum curves in Figure 44 , it is obvious that the reflectance with smaller grain sizes is higher than those with larger grain size (reflectance curves of the first layer and the fifth layer are lying over those of second, third and the fourth lays’).

However, from the curves we can hardly draw a conclusion that there is any displacement on the wavelength of crest and trough.

To solve this problem, the slope of the pair of crest and trough is calculated. In Figure 5.14, the grain sizes of first layer and second layer are selected to represent the two groups of snow grain samples. After the calculation, a much more obvious result can be found. That is the slope calculated from the peak and trough within  $1.2\mu\text{m}$  and  $1.3\mu\text{m}$  with larger grain size is bigger than that with smaller grain size.

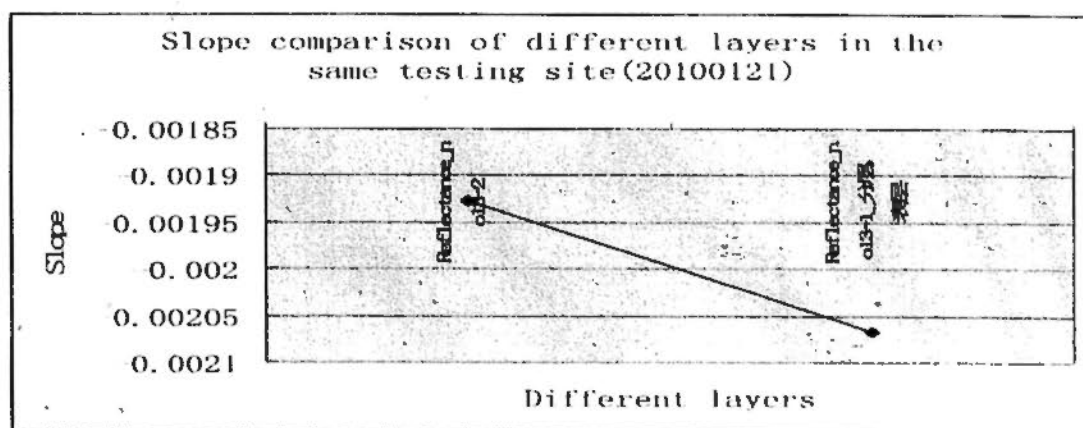


Figure 5.14 Slope comparison of different layers in the same testing site

According to slope calculation results (see Table 5.4), it can be concluded that although the absolute value of the slope difference is light (0.00013959), the relative difference is quite big (6.7%). It indicates that slope of peak and trough at the range of  $1.2\mu\text{m}$  -  $1.3\mu\text{m}$  can represent the changes of snow grain size to some degree.

Follow the same idea, slopes of wave peak and trough are calculated for spectrums measured in different testing sites (see Figure 5.15).

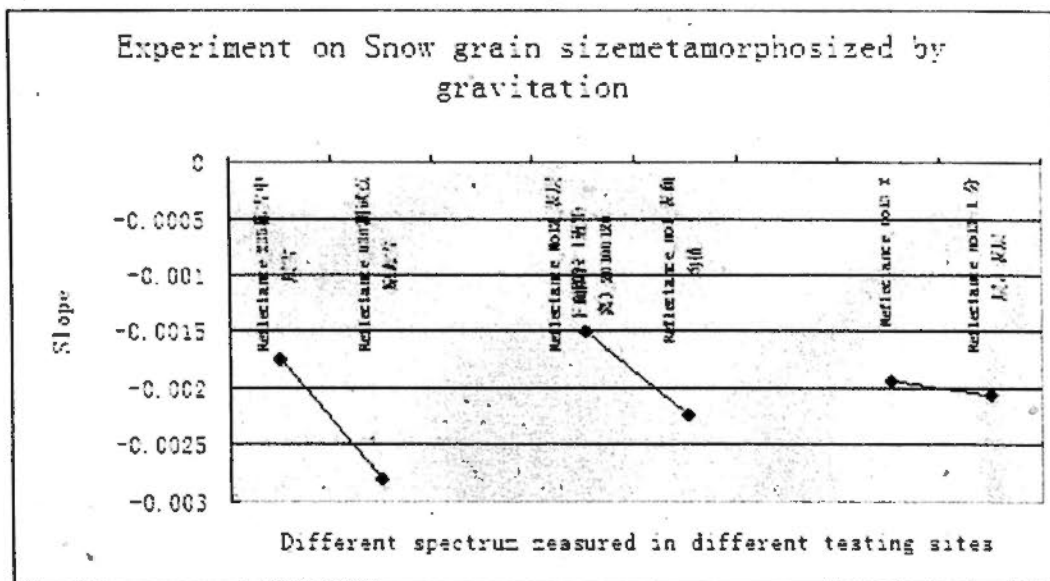


Figure 5.15 Slopes of spectrum peak and trough at wavelength range from  $1.2\mu\text{m}$  -  $1.6\mu\text{m}$ . Similar results can be obtained in different testing sites with different environmental conditions. That is:

1. The snow grain size of snow surface is smaller than that inside snow body,
2. The snow grain size of new fallen snow is smaller than that of sediment snow,
3. The slope of snow with smaller grain size is lower than that with larger snow grain size (see Figure 5.16).

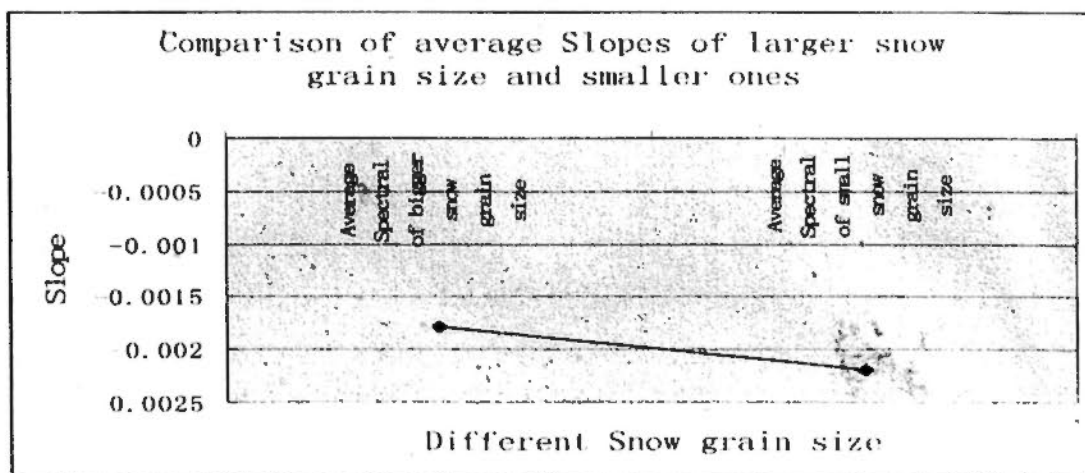


Figure 5.16 Comparison of average slope of larger snow grain size and smaller ones

Table 5.4 Slope of peak and trough in different test sites

| Spectral Name                     | Reflectance_23<br>5 层雪中层雪 | Reflectance_冰<br>下大颗粒雪均<br>值 (不含 090) | Reflectance_No<br>12_表层下面颗<br>粒 (近距<br>离)_20100120 | Reflectance_<br>no13-2 | Reflectance_17<br>0 二十天降雪<br>(无气溶胶影<br>响) | Reflectance_no<br>1_平整表面<br>_20100121 | Reflectance_no<br>2_平整表面 | Reflectance_no<br>3_平整 | Reflectance_<br>no13-1_分层,<br>表层 |
|-----------------------------------|---------------------------|---------------------------------------|--|------------------------|---|---------------------------------------|--------------------------|------------------------|----------------------------------|
| Index of<br>Reflectance<br>peak   | 55                        | 109                                   | 83   | 55                     | 55  | 56                                    | 82                       | 55                     | 56                               |
| Value of<br>Reflectance<br>peak   | 0.3287                    | 0.3746                                | 0.2380   | 0.3672                 | 0.1747                                    | 0.4055                                | 0.3752                   | 0.4813                 | 0.4130                           |
| Index of<br>Reflectance<br>trough | 236                       | 237                                   | 236  | 237                    | 235                                       | 236                                   | 236                      | 236                    | 236                              |
| Value of<br>Reflectance<br>trough | 0.0147                    | 0.0137                                | 0.0076   | 0.0163                 | 0.0112                                    | 0.0331                                | 0.0362                   | 0.0418                 | 0.0408                           |
| Slope                             | -0.0017                   | -0.0028                               | -0.0015  | -0.0019                | -0.0009                                   | -0.0021                               | -0.0022                  | -0.0024                | -0.0021                          |

### 5.2.1.1.3.2 Experiments on snow grain size affected by melting and refrozen

#### Data processing

In this experiment, the pre-processing of in situ optical remote sensing data is similar with that of last section (include Wavelet transform and smoothing). Table 5.5-5.7 list three groups of slopes calculated by using peak and trough at wavelength from  $1.2\mu\text{m}$  to  $1.5\mu\text{m}$  of three groups of snow:

1. Snow with smooth surface
2. Snow with uneven surface
3. And refrozen snow.

From the analysis results (Table 5.5-5.7) we can conclude that the wave peak and trough of the three kind of snow surface are very similar. That is to say, just like what is mentioned in the analysis of last experiment, there is no significant difference between the original snow and refrozen snow seemingly. However, when we go through the slopes of these spectral, the difference appears.

#### Data analysis

Figure 5.17, and 5.18 show the slopes of normal surface snow, refrozen snow and the slopes of spectrum while we heating the testing plots' surface.

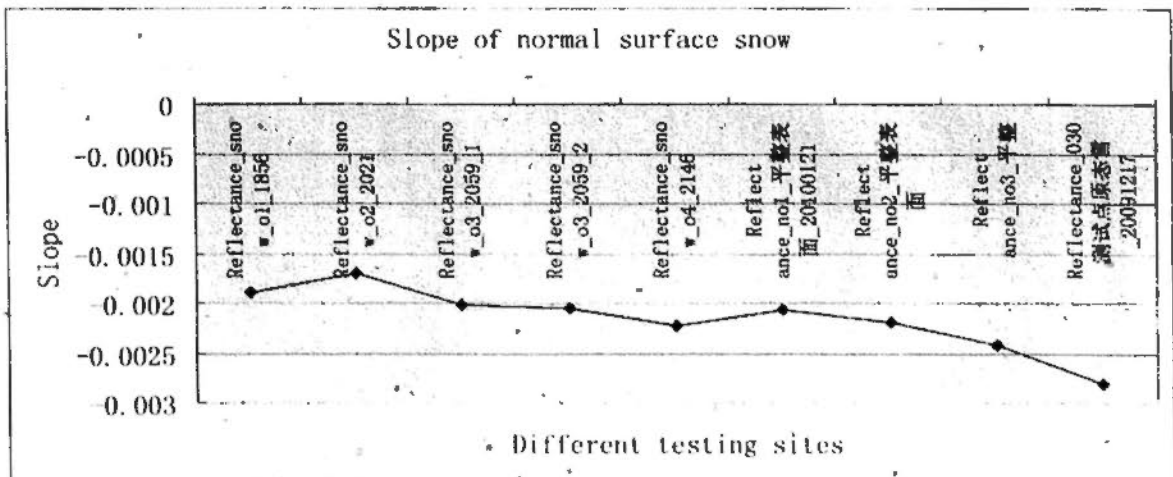


Figure 5.17 Slopes of normal surface snow collected from different test sites

Table 5.5 Spectrum slopes of normal smooth snow

| Spectral Name               | Reflectance <sub>sn</sub><br>ow_o1_1856 | Reflectance <sub>sn</sub><br>ow_o2_2021 | Reflectance <sub>sn</sub><br>ow_o3_2059_1 | Reflectance <sub>sn</sub><br>ow_o3_2059_2 | Reflectance <sub>sn</sub><br>ow_o4_2146 | Reflectance <sub>no</sub><br>1_平整表面<br>_20100121 | Reflectance <sub>no</sub><br>2_平整表面 | Reflectance <sub>no</sub><br>3_平整 | Reflectance_03<br>0 测试点原态<br>雪_20091217 |
|-----------------------------|---|---|---|---|---|--|-------------------------------------|-----------------------------------|---|
| Index of Reflectance peak   | 53                                      | 51                                      | 50  | 46  | 37                                      | 56   | 82                                  | 55                                | 86                                      |
| Value of Reflectance peak   | 0.36                                    | 0.33                                    | 0.39                                      | 0.40                                      | 0.46                                    | 0.41   | 0.38                                | 0.48                              | 0.48                                    |
| Index of Reflectance trough | 234                                     | 234                                     | 234                                       | 233                                       | 232                                     | 236  | 236                                 | 236                               | 238                                     |
| Value of Reflectance trough | 0.017                                   | 0.016                                   | 0.017                                     | 0.018                                     | 0.022                                   | 0.033  | 0.036                               | 0.042                             | 0.058                                   |
| Slope                       | -0.0019                                 | -0.0017                                 | -0.0020                                   | -0.0021                                   | -0.0022                                 | -0.0021  | -0.0022                             | -0.0024                           | -0.0028                                 |

Table 5.6 Spectrum slopes of uneven snow

| TableSpectral<br>Name             | Reflectance_<br>No2_不平雪 | Reflectance_n<br>01_坑雪(半<br>米)<br>_20100125 | Reflectance_No2<br>4_有坑雪, 纯雪<br>_20100126 | Reflectance_no4<br>_距(半米) | Reflectance_no6<br>_大距(半米) | Reflectance_no8<br>_混合(平+深<br>点, 半米) |
|-----------------------------------|-------------------------|---|---|---------------------------|----------------------------|--------------------------------------|
| Index of<br>Reflectance<br>peak   | 56                      | 54  | 53  | 57                        | 56                         | 54                                   |
| Value of<br>Reflectance<br>peak   | 0.29                    | 0.34  | 0.27                                      | 0.39                      | 0.43                       | 0.43                                 |
| Index of<br>Reflectance<br>trough | 233                     | 234   | 233                                       | 236                       | 236                        | 236                                  |
| Value of<br>Reflectance<br>trough | 0.012                   | 0.027                                       | 0.019                                     | 0.034                     | 0.040                      | 0.040                                |
| Slope                             | -0.0016                 | -0.0018                                     | -0.0014                                   | -0.0020                   | -0.0021                    | -0.0022                              |

Table 5.7 Spectrum slopes of refrozen snow

| TableSpectral Name          | Reflectance_ No1_融过雪_20100120 | Reflectance_ No14_融化雪(半米) | Reflectance_2 15 测试点重结晶 | Reflectance_2 25 测试点重结晶 | Reflectance_ 测试点重结晶均值_091217 | Reflectance_r efrozen2_20 56_1 | Reflectance_r efrozen2_20 57_1 | Reflectance_r efrozen2_20 57_2 | Reflectance_r efrozen3_21 43_1 | Reflectance_r efrozen3_21 43_2 |
|-----------------------------|-------------------------------|---------------------------|-------------------------|-------------------------|------------------------------|--------------------------------|--------------------------------|--------------------------------|--------------------------------|--------------------------------|
| Index of Reflectance peak   | 57                            | 56                        | 56                      | 55                      | 55                           | 53                             | 50                             | 47                             | 51                             | 50                             |
| Value of Reflectance peak   | 0.26                          | 0.23                      | 0.34                    | 0.22                    | 0.28                         | 0.22                           | 0.23                           | 0.23                           | 0.31                           | 0.30                           |
| Index of Reflectance trough | 233                           | 232                       | 233                     | 231                     | 232                          | 234                            | 234                            | 233                            | 233                            | 233                            |
| Value of Reflectance trough | 0.0145                        | 0.0078                    | 0.0226                  | 0.0092                  | 0.0158                       | 0.01425                        | 0.01454                        | 0.0141                         | 0.0126                         | 0.01264                        |
| Slope                       | -0.0014                       | -0.0013                   | -0.0018                 | -0.0013                 | -0.0015                      | -0.0012                        | -0.0011                        | -0.0012                        | -0.0016                        | -0.0015                        |

Most of slopes of spectrums of original surface snow are less than -0.002, while all of the slopes of spectrums of refrozen snow are greater than -0.002.

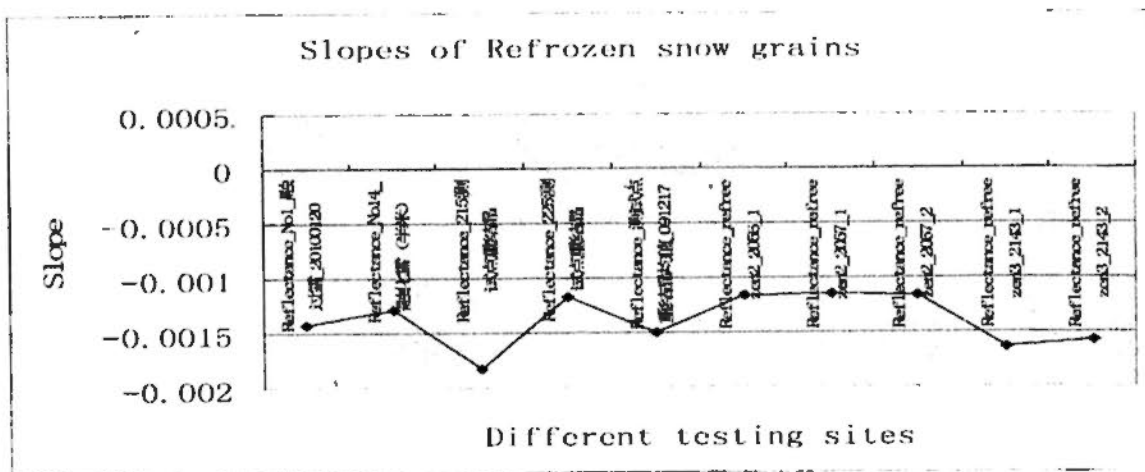


Figure 5.18 Slope of refrozen snow grains

As to the heating/melting plots, the values of slope changes with the temperatures (Figure 5.19).

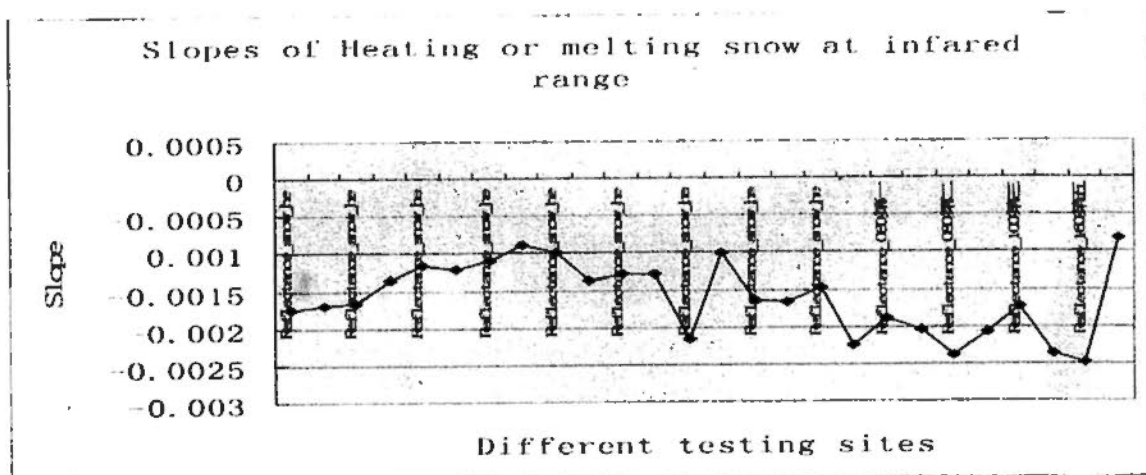


Figure 5.19 slopes of heating or melting snow

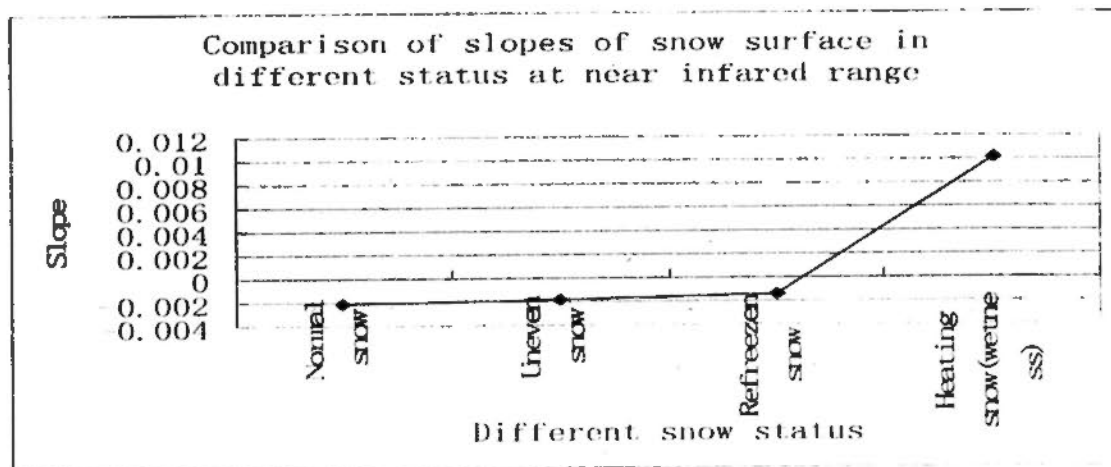


Figure 5.20 Comparison of slopes of snow surface in different status at near infrared range

The average slopes of the four kinds of surface snow are described in Figure 5.20:

1. Slope of normal snow is the lowest one;

2. The slope of uneven snow is a bit greater than that of normal snow maybe caused by the refrozen part of the testing plots. Or there is still another possibility: the effect of dappled shade;
3. Slope of refrozen snow is, definitely, greater than normal snow, even the uneven snow.
4. The heating or naturally melting snow has the highest slope. However, the biggest contributor to the high slope maybe is the temperature but not wetness. To validate the assumption, more field experiments should be conducted in the future.

### 5.2.1.1.3.3 Snow grain size retrieval model based on hyperspectra data

To sum up, strong correlation between snow grain size and slope can be found. To select most sensitive expression for snow grain size

To apply the model in MODIS data, two troughs are selected as alternative in slope calculation. The comparing result tells us, the two slopes perfect match each other. That is to say, calculation of band5 and band7 can be used in this grain size retrieval model.

Table 5.8 Snow grain size and corresponding slope

| Grain size (mm) | Slope_peak&trough | Slope_double_trough |
|-----------------|-------------------|---------------------|
| 0.6575          | -0.0031452        | -0.000716           |
| 0.85            | -0.0026257        | -0.000684           |
| 1.946667        | -0.0020673        | -0.000533           |
| 2.35            | -0.0017348        | -0.000382           |
| 2.0675          | -0.0019278        | -0.00048            |
| 2.053333        | -0.0019278        | -0.00048            |
| 1.966667        | -0.0019327        | -0.000474           |
| 1.5             | -0.0021284        | -0.00054            |

By using the in situ measured reflectance in the range from  $1.2\mu\text{m}$  to  $1.5\mu\text{m}$  and snow grain size, a regression formula as:

$$\text{Grain size}(y) = 4.55 + 5364.57 * \text{slope\_peak\_trough} \quad 5.4$$

Here *slope\_peak\_trough* is the slope of peak point and trough point at range from  $1.2\mu\text{m}$  from  $1.5\mu\text{m}$ .

However, in the application of MODIS data, the reflectance of band 5 and band 7 are the closer bands to slope peak and trough derived from in situ measurements, respectively. But they are not exactly the peak and trough points. Errors can be found in slope calculation using band 5 and band 7. Therefore, the formula can not use to detect the specific grain size if the two bands are applied in the regression formula. But the change trend of grain size can be estimated. The correlation between snow grain size and slope is as high as 0.97. It indicates that snow spectrum at NIR range is extremely sensitive snow grain size.

#### **5.2.1.1.4 Experiments on mixed pixel**

Mixed pixel is a common problem that we will meet in snow monitoring based on satellite remote sensing data for both microwave and optical techniques. The in situ experiments on mixed pixel are designed to solve this issue.

##### **5.2.1.4.1 Data processing**

For spectrum data, the pre-processing work for this experiment is the same as that of experiments on snow grain size. Wavelet transform and smooth processing need to be performed on initial data to remove all kinds of noise, and improve the quality of in situ measurement data.

##### **5.2.1.4.2 Data analysis**

There are four major mixed pixels in Northeast China:

1. Mixed pixel of snow and dry-field;
2. Mixed pixel of snow and grassland;
3. Mixed pixel of snow and trees or shrub;
4. Mixed pixel of snow and soil.

In this section pixel with more than one kind of land cover types in the field of view will be analyzed. To ensure that the FOV can contain more than one land cover types, the measurement altitude is determined as 1 meter or 50cm. The FOV area is:

$$S = \pi \times (50(\text{or}100) \times \tan(25^\circ))^2 = 1017(6828)\text{cm}^2 \quad 5.5$$

##### **Mixed pixel of snow and grassland**

The grass turns yellow in winter in Northeast China. The greatest effect of mixture of hay on snow spectrum is in the visible range. The highest value of reflectance can be

found in pure snow spectrum. And with increase amount of hay, the reflectance decreases gradually (Figure 5.21).

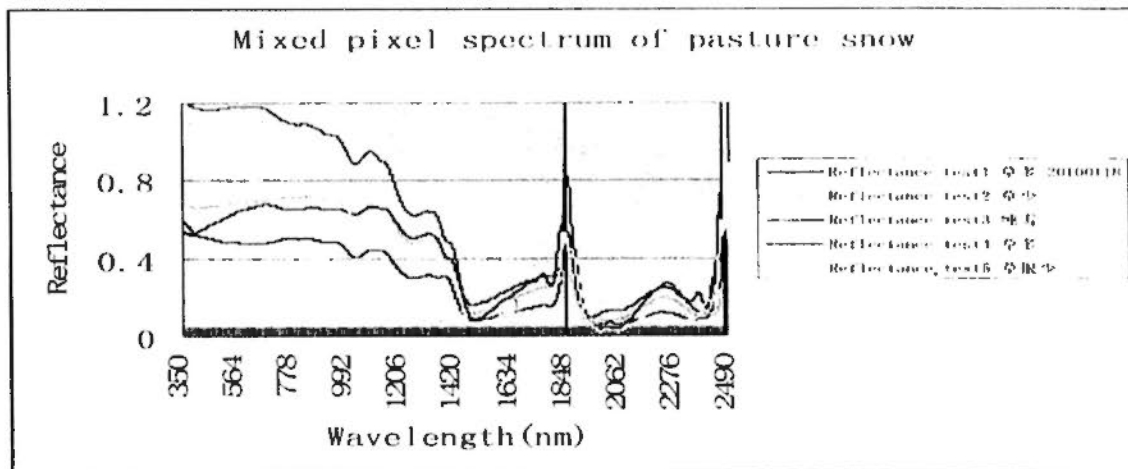


Figure 5.21 Mixed pixel of snow and grassland

Because of the emission of hay, the spectrum is not only affected at visible by the color of impurities band but also at near infrared band by the emission of impurities. Generally, with the increase of hay, the NDSI has a decline trend (see Table 5.9).

Table 5.9 NDSI of snow mixed with hay

|      | More hay | Less hay | Pure snow | Lots of hay | Litter hay |
|------|----------|----------|-----------|-------------|------------|
| NDSI | 0.722329 | 0.705634 | 0.861604  | 0.599609    | 0.88746    |

### Mixed pixel of snow and cornstalk

Generally, the typical characteristics of snow can be found in the spectrum of mixed pixel, the differences between these spectral curves are values of reflectance. All in all, spectrums of snow samples have the characteristics of snow spectrum, except two of them. In these curves, corn stalk dominates the reflectance. To figure out the effect of corn stalk on spectrum, three typical spectrums are selected (see Figure 5.22).

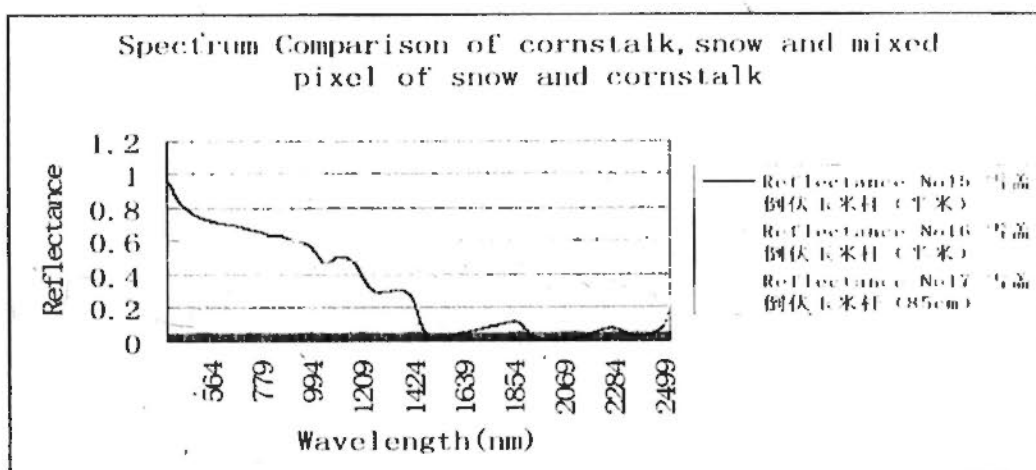


Figure 5.22 Effect of corn stalk on spectrum

The pink curve shows the spectrum that dominates by corn stalk and the blue one shows the reflectance mainly contributed by snow. Yellow line is situated between the two.

In the visible band the reflectance is degraded because of the lower reflectance of corn stalk, while the reflectance is elevated in near infrared band in comparison with that of pure snow.

Thus, we can conclude that the NDSI will be reduced if the pixel is a mixture of snow and corn stalk, which is the common sight in Northeast China.

### Mixed pixel of snow and trees and shrubs

Northeast China is surrounded by the Great Xing'an Mountain. Effect of forests is always considered as one the most difficult problems in snow monitoring, since the deciduous forest and coniferous forest, which are the most common trees on mountains of Northeast China, have great effect on spectrums measured from satellite sensors.

In this experiment, the mixed pixel of snow with forest is simulated by using the seed plot. The testing plots selected are covered with sapling of different densities.

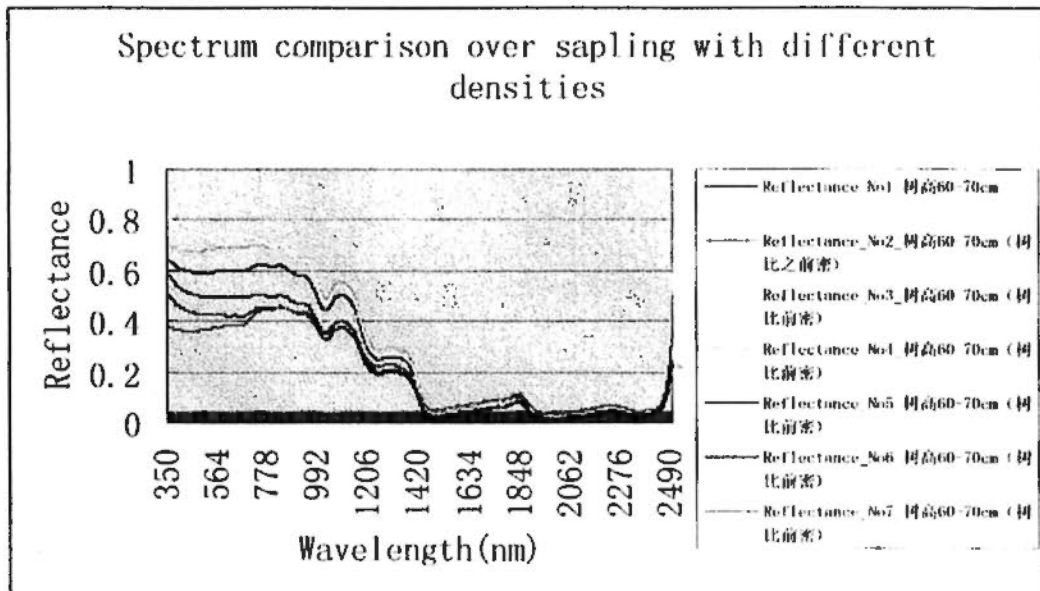


Figure 5.23 Spectrum comparison over sapling with different densities

From Figure 5.23 a down trend of reflectance at visible band can be found. The trend basically meets the ascend tendency of sapling density,

In near-infrared band, the spectrums of snow samples with different sapling densities are consistent. It indicates that the NDSI in forest area must be lower than that of pure snow covered area.

### Mixed pixel of snow and soil

The decrease trend of mixed pixel of snow and soil in reflectance at visible range is similar with that of snow with corn stalk in some degree (Figure 5.24). Soil, as the impurities, will decrease the reflectance at visible band. Moreover, more effect of soil on snow spectrum can be found at near infrared band because of the special emission property of soil. With the increase of soil proportion, the NDSI will decrease correspondingly.

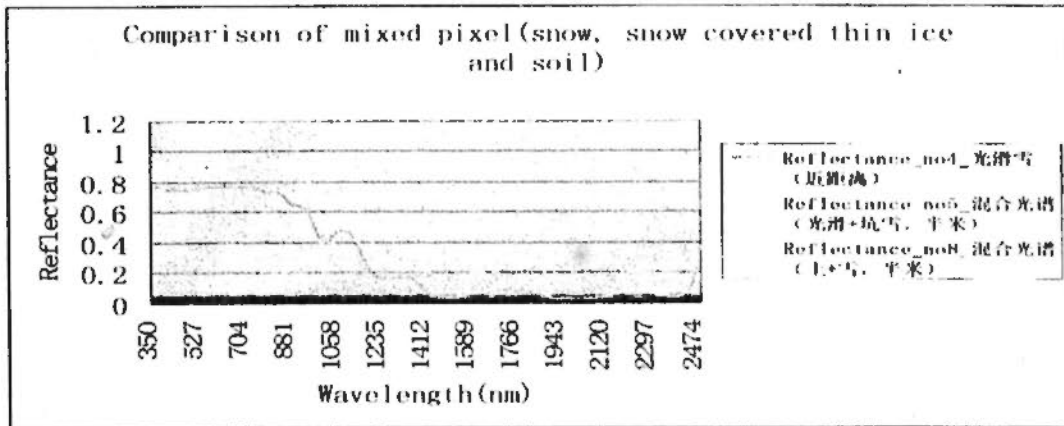


Figure 5.24 Spectrum of snow mixed with soil

### 5.2.1.2 Field Experiments on Microwave Properties of Snow

The first step of the research is measurement and analysis of snow parameters. By doing this an optimizing method for snow monitoring based on microwave remote sensing data over Northeastern China can be developed.

#### 5.2.1.2.1 Pre-experiment

In the study, Chang's algorithm is the basic theory applied to the snow monitoring model based on microwave satellite remote sensing data. Before establishing the model, the algorithm for in deeper snow monitoring (SD greater than 20cm) needs to be performed.

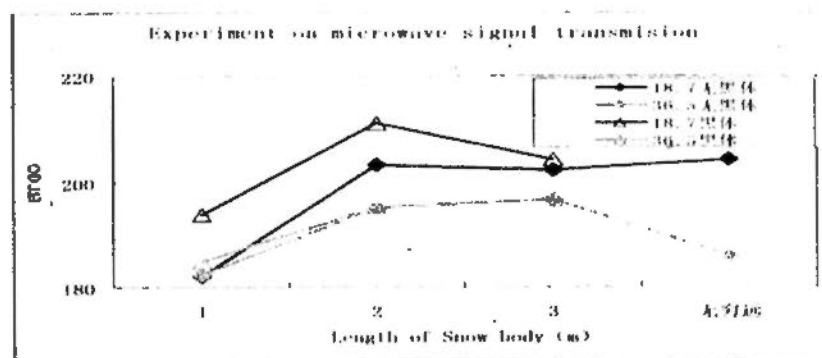


Figure 5.25 Microwave signal transmission

This part of pre-experiment on signal transmission of 18.7GHz and 36.5GHz is aimed to figure out their signal transmission distance. From the result (see Figure 5.25) it can be concluded that for 18.7GHz, the signal can penetrate more than 3 meter's distance, while for 36.5 GHz, the longest distance from where we can receive the signals is 2 meters. That is to say, 2 meters is the largest SD that can be detected by using 18.7GHz and 36.5GHz.

The second part of pre-experiment for passive microwave model is to get an outline of physical properties of snow and the potential effect factors. In the field experiments conducted in 2008-2009 winter is to fulfill the goal. Table 5.10 shows the experiment results of 18GHz and 37 GHz brightness Temperature over three different underlying surfaces.

Table 5.10 Measurement result of TB and Radiance of three kinds of underlying surface

| Underlying surface       | 18V    |          | 18H    |          | 37V    |          | 37H    |          |
|--------------------------|--------|----------|--------|----------|--------|----------|--------|----------|
|                          | TB (K) | Radiance |
| Forest frozen ground (A) | 263.4  | 0.992    | 256.9  | 0.968    | 253.2  | 0.954    | 248.8  | 0.937    |
| Farmland (B)             | 256.9  | 0.967    | 247.0  | 0.929    | 245.7  | 0.925    | 238.3  | 0.897    |
| Lake ice (C)             | 240.3  | 0.913    | 209.8  | 0.798    | 247.4  | 0.942    | 205.8  | 0.783    |

Three common underlying surfaces were selected, which are forest frozen ground (site A), Farmland (site B) and Lake ice (site C) respectively. The mean SD is 10 cm and the snow layer is mixture of new snow with grain size of 0.2 mm and old snow with refrozen grain size of 0.5mm. Figure 5.26 shows the experiment results of 18GHz and 37 GHz brightness Temperature over three different underlying surfaces. The underlying surface temperatures for testing site A, B and C are  $-7.5^{\circ}\text{C}$ ,  $-7.25^{\circ}\text{C}$  and  $-10.25^{\circ}\text{C}$  respectively.

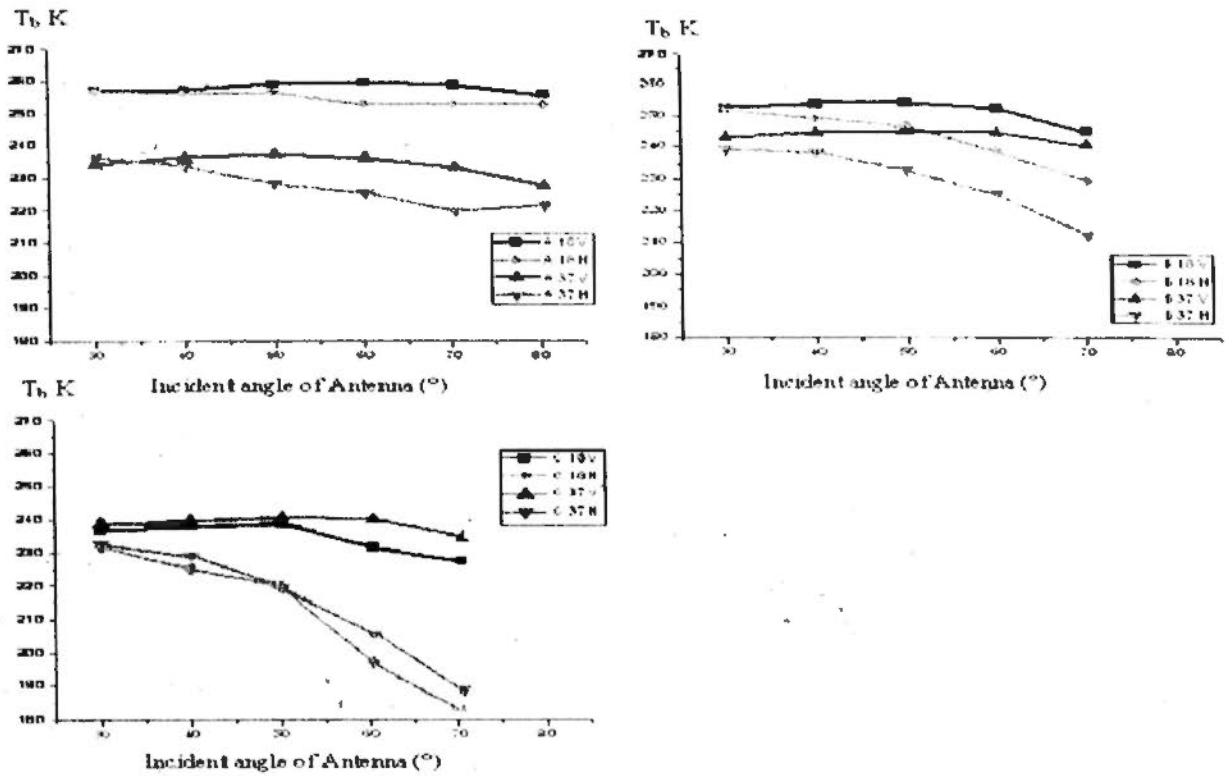


Figure 5.26 Polarization Characteristics of Microwave radiance in three testing sites The upper-left one shows the H and V polarization  $T_b$ s at incident angle from  $30^\circ$  to  $80^\circ$  of testing site A; the upper-right one shows the H and V polarization  $T_b$ s at incident angle from  $30^\circ$  to  $70^\circ$  of testing site B; and the lower left one shows the H and V polarization  $T_b$ s at incident angle from  $30^\circ$  to  $70^\circ$  of testing site C.

From the results in Figure 5.26 and Table 5.10, we can find that there are differences between radiances of the three underlying surfaces, but no significant difference found between the vertical (V) polarization radiances of testing site A and B, especially in those of 18 GHz. In testing B, difference of V and horizontal (H) is diminished because of the geometric effects of ground surface, especially in high frequency. Thus, H polarization data should be utilized in distinguishing of underlying surfaces. The curves of V polarization for three testing sites are comparatively smooth, while larger variation can be found in H polarization data, which is not as smooth as that of V polarization.

Forest background does bring significant effect on TB, which can be figured out from experimental result of TB obtained from different orientations (see Table 5.11).

Table 5.11 Radiance measurement of different orientations in testing site A(the angle of incident is 0)

| Orientation             | 18V TB (K) | 37V TB (K) |
|-------------------------|------------|------------|
| East                    | 244.1      | 226.1      |
| Southeast               | 242.3      | 227.4      |
| South                   | 250.8      | 227.7      |
| Southwest               | 250.5      | 230.6      |
| Northeast( $10^\circ$ ) | 250.3      | 230.4      |

All the field experiment results show that underlying surfaces do have effects on passive microwave signals we obtained from remote sensors. However, data derived from H polarization can be used as primary monitoring dataset over Northeast China according to our experiment results.

To validate these results, further series field experiments are designed for 2009-2010 winter.

### 5.2.1.2.2 Microwave Radiation Characteristics and SD

SD is always the research focus of snow monitoring, since it is the most significant input parameter for SWE calculation and hydrological models. In the series experiment, the obstacles that prevent the improvement of snow monitoring accuracy will be found.

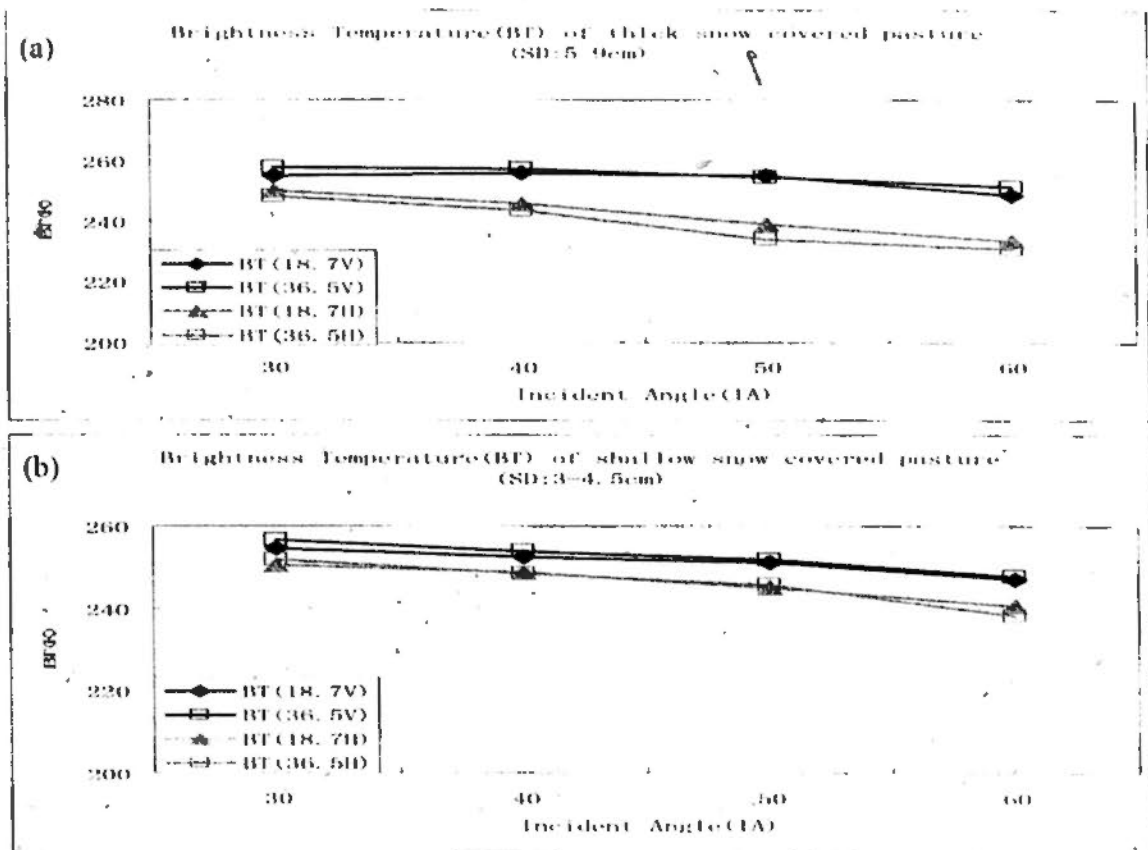


Figure 5.27 Brightness Temperature measurements on snow covered pasture

Here (a) is the measurement of 18.7GHz and 36.5GHz on a comparative deeper testing plot, where SD is 5-9cm; (b) is the experiment result on another testing plot, where covers thinner snow (3.5-4cm).

Figure 5.27 shows experiment results on the same testing sites, Changling. The underlying cover types of the two testing plots are both pasture. From the figure we can see that on the thinner snow covered plot, it is hardly to calculate SD by using

Chang's algorithm (the difference of 18.7GHz and 36.5 GHz). On the other hand, on the deeper snow covered plot, SD can be calculated by using H polarization data. Moreover, the most sensitive incident angle is  $50^\circ$ , which matches the incident angle of satellite remote sensor.

To make it more clear, two pairs of channels are drawn together in Figure 5.28. When the temperature of ground is similar,  $T_b$  of 18.7 GHz and 36.5GHz are decreasing. And the decline trend of 36.5GHz is more violent than that of 18.7GHz.

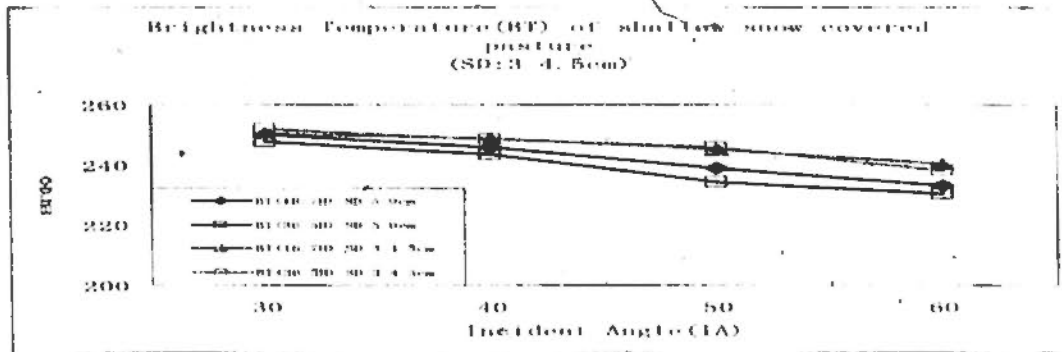


Figure 5.28 Comparison of brightness temperature on shallow and thin snow covering test sites

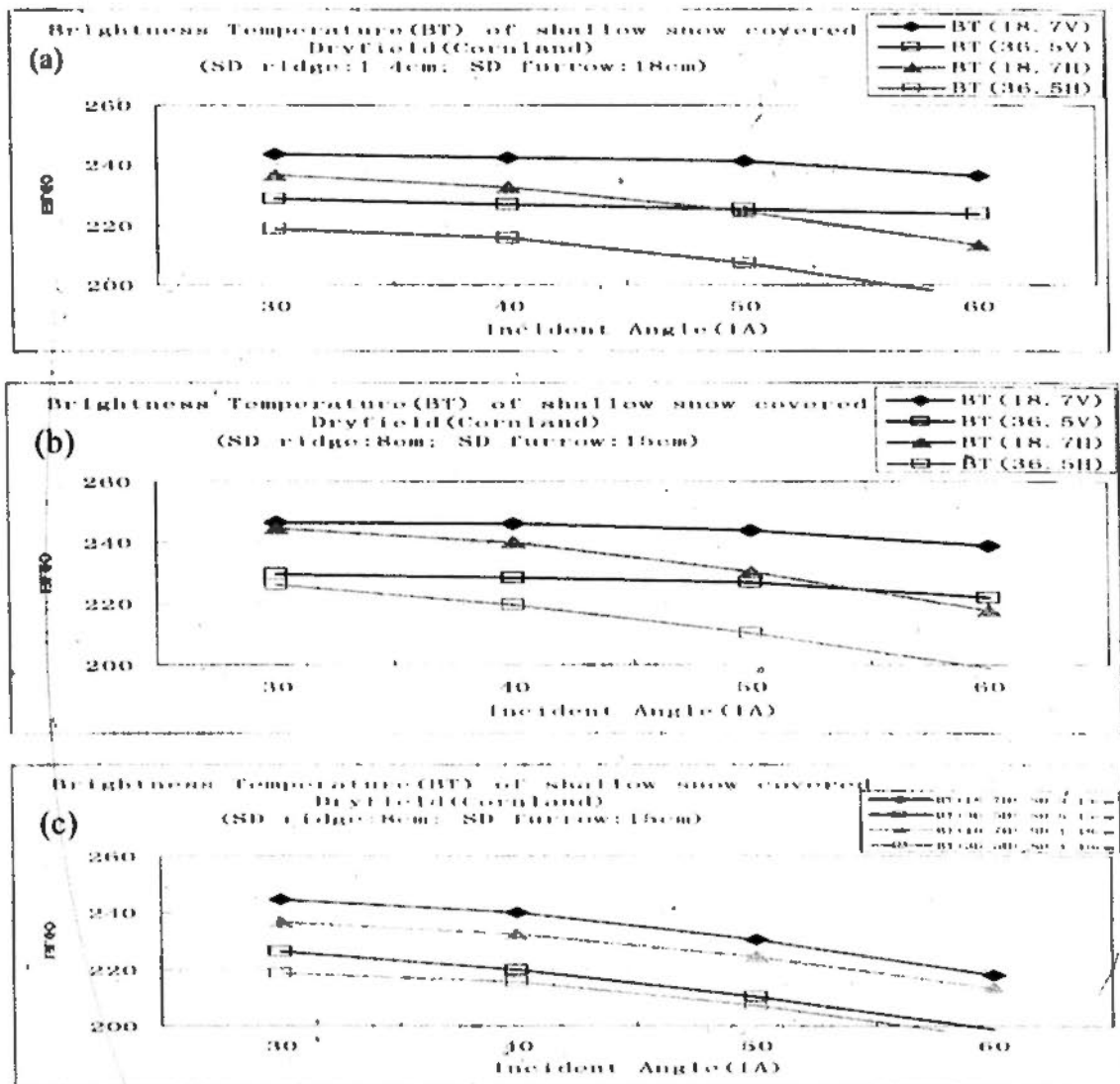


Figure 5.29 Brightness Temperature measurements on snow covered corn-land

On the other hand, to the testing plots with similar snow covered depth (average SD is larger than 4cm), the differences of brightness temperature of 18.7GHz and 36.5GHz are similar. It proves that SD is one of the obstacles that affect retrieval accuracy. For those areas with SD less than 4cm, Chang's model can not be applied to obtain accurate snow information.

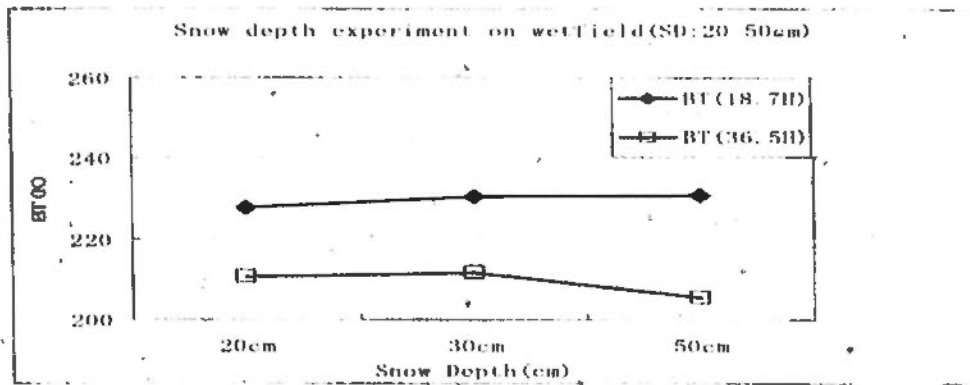


Figure 5.30 SD experiment on wet-field

Figure 5.30 shows the experiment conducted on wet field. With the increasing of SD from 20cm to 50cm, the difference of 18.7GHz and 36.5GHz increases. Moreover, the brightness temperature of 18.7GHz keeps increasing while 36.5 GHz start to decrease when SD is larger than 30cm. That is to say, SD detection model should be modified when SD is larger than 30cm.

### 5.2.1.2.3 Effects of Underlying Surfaces on Microwave Radiation Characteristics

As it is mentioned in chapter 2 and chapter 3, underlying surface is the well known issue in snow monitoring. Microwave signal's transmission will be greatly affected by the underlying surface.

There are four typical underlying surfaces in Northeast China, which are:

1. Pasture,
2. Dry-field,
3. Wet-field,
4. And river ice.

Figure 5.31 shows the experiment results of 18.7GHz and 36.5GHz on the four kinds of underlying surfaces.

The average SD of the four testing plots are very similar, which are 7.5cm, 9.5cm, 6.5cm and 9cm. however, the differences of 18.7GHz and 36.5GHz are quite different in these testing plots.

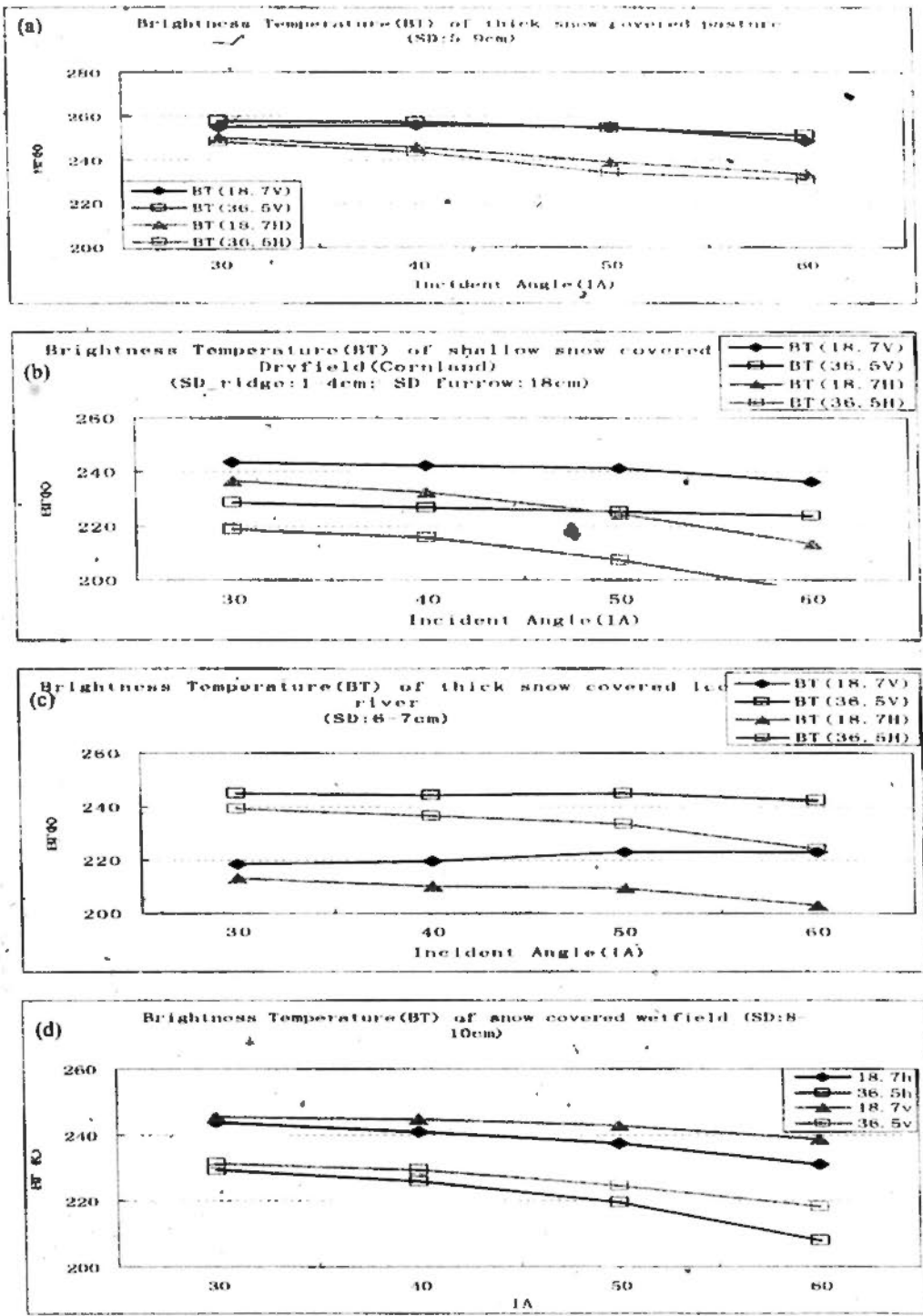


Figure 5.31 Brightness temperatures obtained from four test sites with typical underlying surfaces (Pasture, Corn-land, River ice and wet-field respectively)

It is to say, the difference is caused by underlying surface. The reason for the difference is that 18.7GHz mainly represents the brightness temperature of underlying surface because of its penetrability while the 36.5GHz is more sensitive to SD. When the underlying surfaces change, the signals derived from 18.7GHz changes (see Table 5.12-5.13 and Figure 5.32-5.33).

Table 5.12 Brightness Temperature testing results on corn land

|     | BT(18.7)_corn-land Ground | BT(36.5)_corn-land Ground |
|-----|---------------------------|---------------------------|
| 30h | 251.52                    | 255.68                    |
| 40h | 248.06                    | 252.89                    |
| 50h | 241.91                    | 249.72                    |
| 50v | 251                       | 255.88                    |
| 40v | 253.1                     | 256.84                    |
| 30v | 254.05                    | 256.94                    |

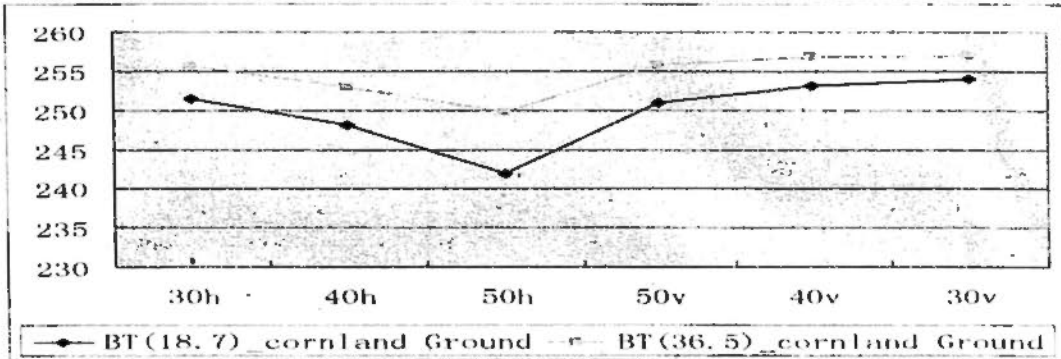


Figure 5.32 Brightness Temperatures of different incident angles over Corn-land

Table 5.13 Brightness Temperature testing results on Ice surface

|     | BT(18.7GHz)_Ice | BT(36.5GHz)_Ice |
|-----|-----------------|-----------------|
| 50h | 195.22          | 220.78          |
| 40h | 201.03          | 229.81          |
| 30h | 206.39          | 239.51          |
| 60h | 188.99          | 215.77          |
| 60v | 224.17          | 244.99          |
| 50v | 222.11          | 245.57          |
| 40v | 218.02          | 245.38          |
| 30v | 215.18          | 242.69          |

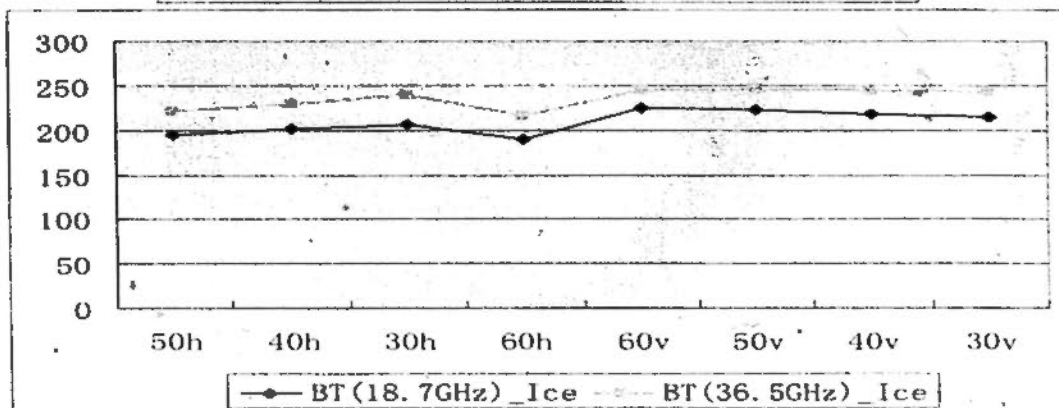


Figure 5.33 Brightness Temperatures of different incident angles over River ice

Here is still a big problem. That is the minus value of difference between 18.7 and 36.5 GHz on river or lake ice.

Both for V polarization and H polarization, the differences of 18.7 and 36.5GHz are minus. The reason for the minus value is thermal loss of the ice. The temperature of water under the thick ice is a constant (about  $-4^{\circ}\text{C}$ ), with the increases of thickness of ice, the quantity of thermal loss is increased. The signals of 18.7GHz can penetrate the ice with a certain thickness, while that of 36.5GHz can not.

### 5.2.2 Analysis of Long Term Observation Data

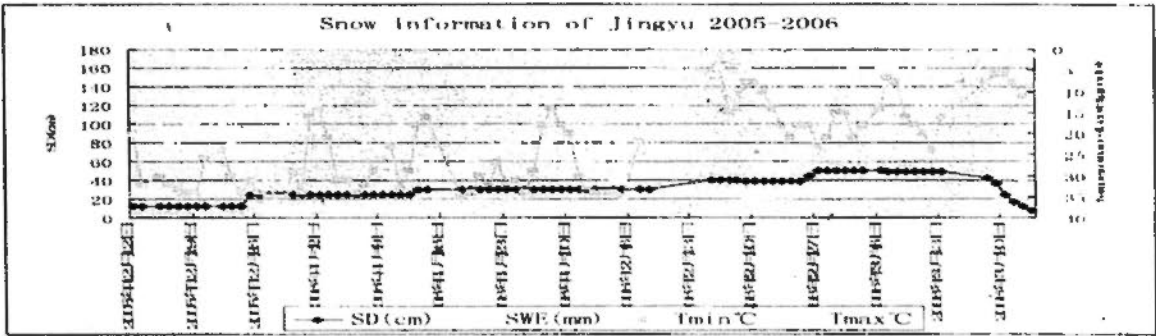
The ground data include daily morning and afternoon air temperatures and precipitation. In addition, SD, SWE and snow grain size were measured. SWE were estimated via the snow density, which is determined by melting a snow column and dividing the melted water height by the snow column height.

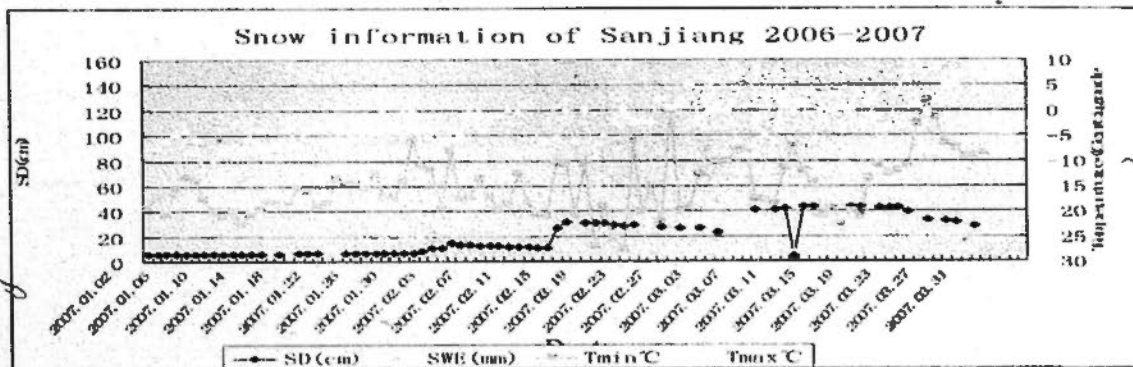
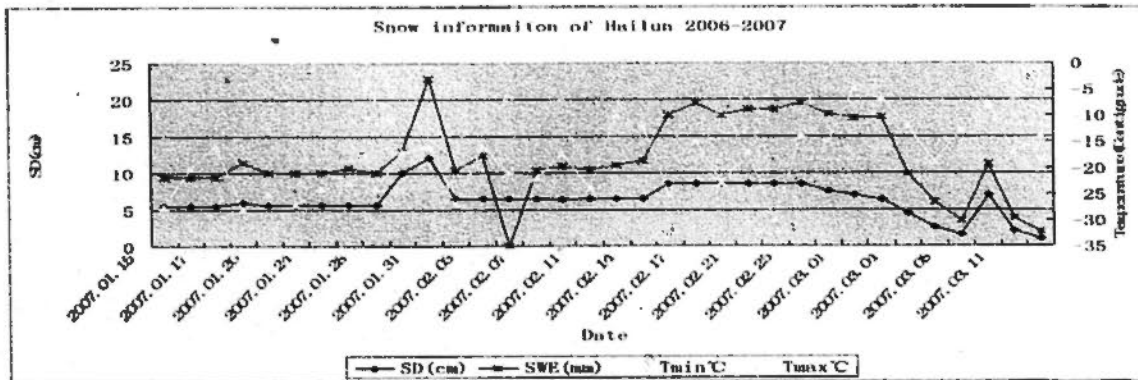
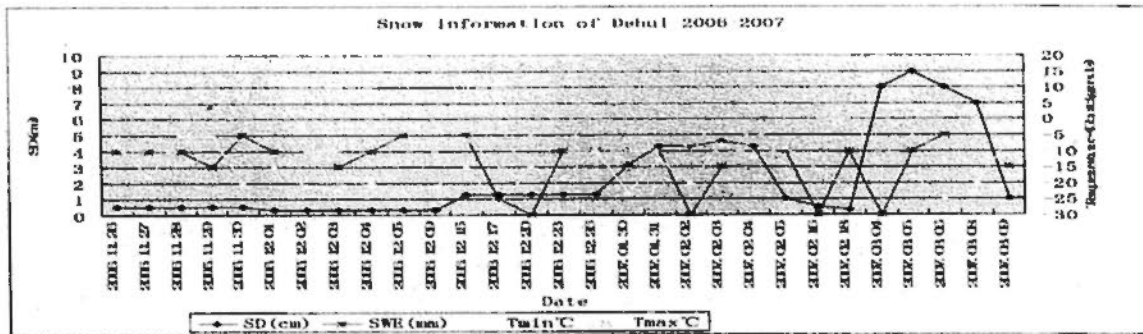
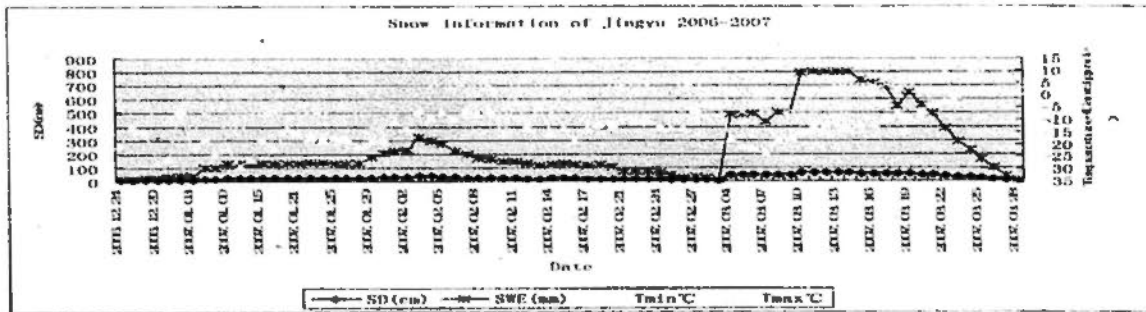
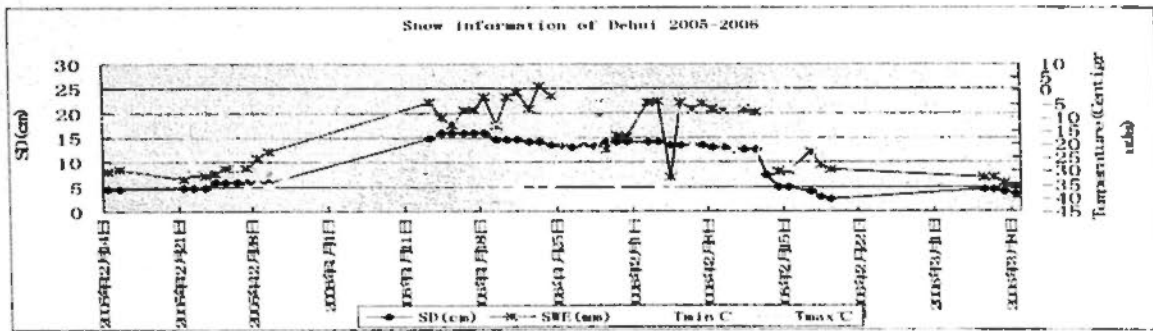
To validate the SD retrieval results and SWE estimation, long term observation data were collected from several testing sites, which are:

1. Jingyu,
2. Dehui,
3. Yinchun,
4. Hailun,
5. Sanjingzhan,
6. Muling.

Among all the six long-term observation testing sites, underlying surface of two of them are forest (Jingyu and Muling), the rest of them is cropland.

Figure 5.34 shows SD, SWE, and temperature data collected from these testing sites from 2005-2007.





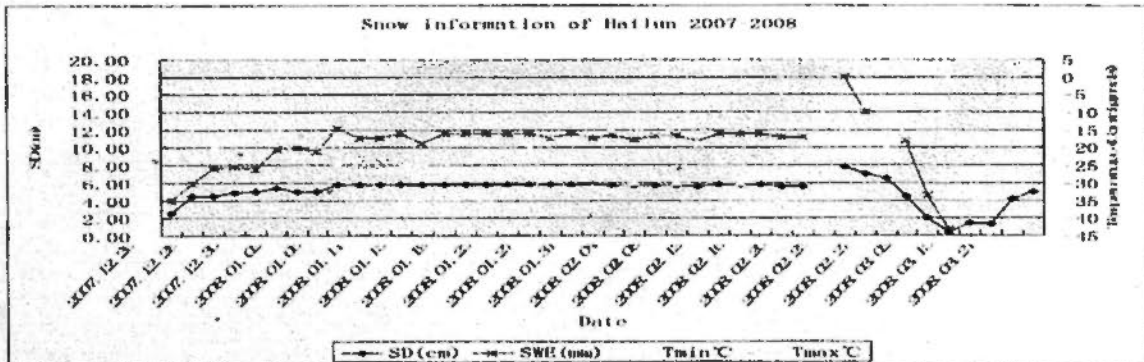
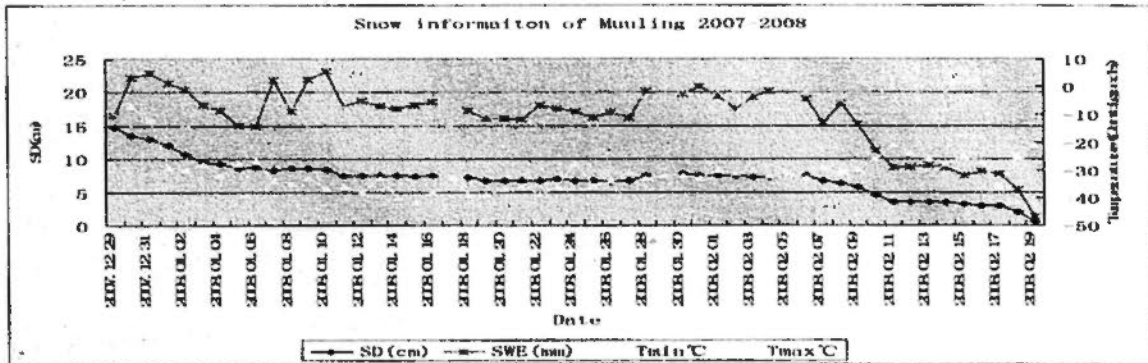
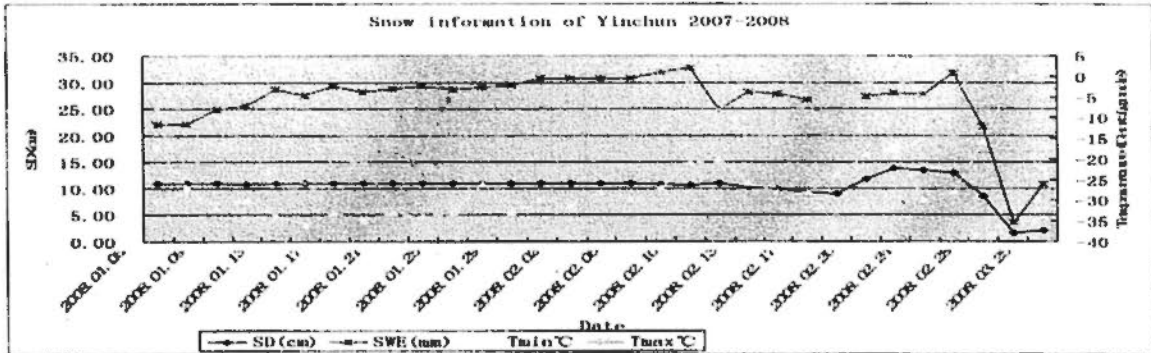
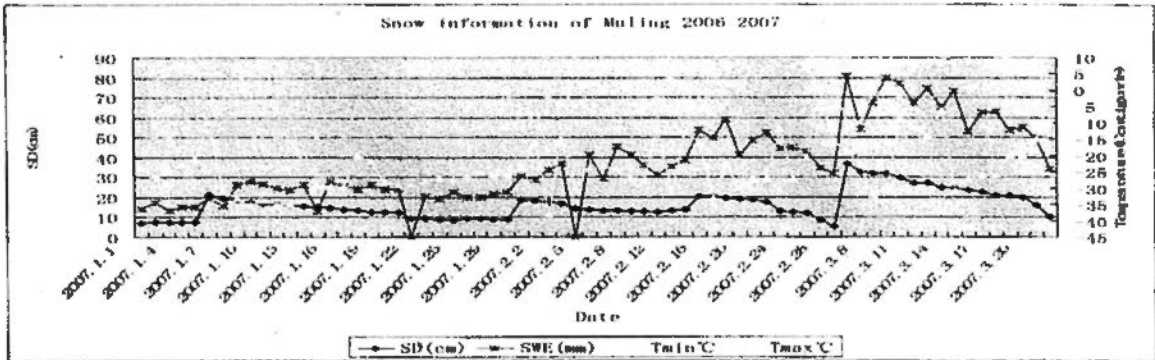
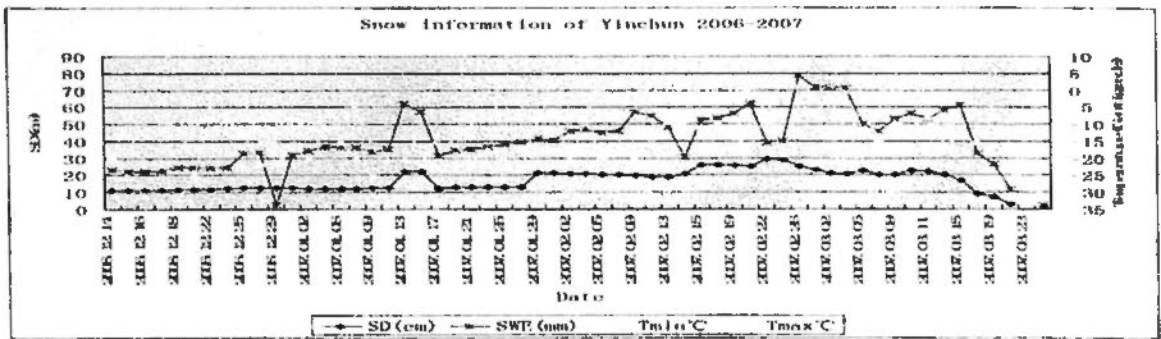


Figure 5.34 SD, SWE, and temperature data collected from these testing sites from 2005-2007

Confined to the length of this thesis, here observation data of 2005-2006 will be taken as example to analyze snow cover status. More detailed analysis will be given in modeling section (Chapter 7) as validation data and results discussion.

## **Chapter 6 SATELLITE REMOTE SENSING DATA PROCESSING**

High quality satellite remote sensing data as input parameters is the base of SCA and SD estimation system. As it is noted, there are still some manual differences during the processing of satellite images besides the unavoidable system errors. Compared with spectral feature of earth objectives, these errors are quite huge. To get reliable estimation results which can be used to dig deep during the causal nexus analysis, we need to pay more attention in satellite data processing procedures. In this chapter, the preparing methods for mass of MODIS, AMSR-E, and land-cover type data will be discussed.

### **6.1 MODIS Data Processing**

#### **6.1.1 Introduction**

Satellite images are widely applied into all kinds of earth observation related researches since 1960s. People try to take the advantage of remote sensed data to monitor the large and un-traversed regions where can hardly be measured in the past. One of the extensively applied data for Earth Observing System (EOS) is MODIS. MODIS data play more and more important role in a variety of aspects in EOS, such as vegetation monitoring, fire detection, ocean color monitoring, and snow cover monitoring.

The researchers who focus on long-term global observations need to process at least 4 MODIS images per day. For a ten years' long observation, totally 14,600 images are needed to be deal with. Moreover, data pre-processing is always the first and fundamental step, based on which the analysis can be conducted. The quality of processed data will directly affect the analysis results (Durbha, 2002). The processing of mass MODIS images became a tremendous task, which requires accuracy, reliability and timeliness for all the long term earth observation researchers based on MODIS data, no matter which fields they focus on.

In this thesis, normal method for MODIS data processing is discussed. The procedure is designed for in all kinds of researches based on MODIS L1B data, however, here snow monitoring over Northeast China based on MODIS L1B data is

presented as a practical example of MODIS products application during the methodology illustration.

Generally, the pre-preparation phase includes the following processing steps:

1. Geo-reference of original images;

Geo-reference processing is utilized to adjust the rectangle images we obtained from remote sensing sensors to the irregular earth surface. Only after geo-referencing, can MODIS L1B images be located with relative pinpoint ground area and each pixel on the image is corresponding to the surface position with unique pair of longitude and latitude. And for MODIS snow products, a projection transform processing will be performed as well.

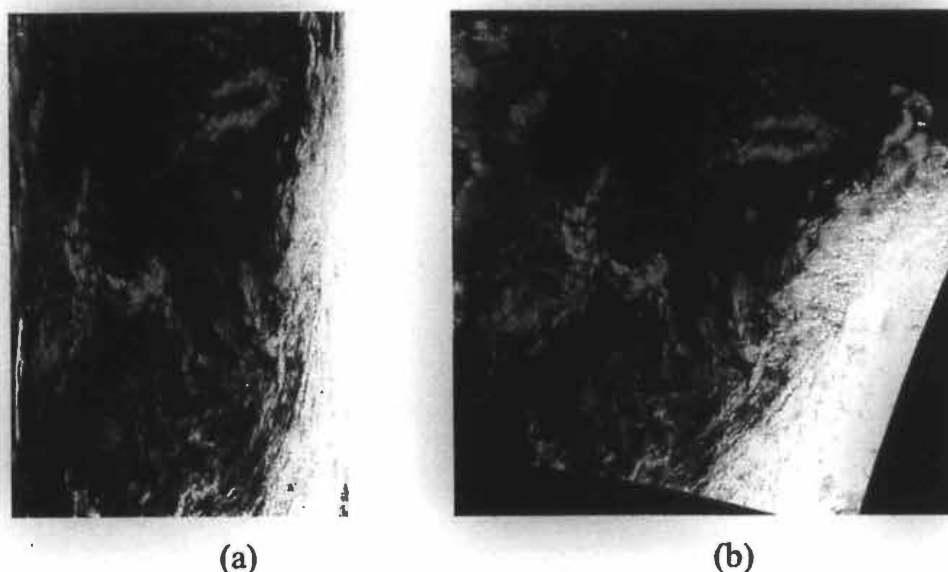


Figure 6.1 Deformation of MODIS L1B image before and after geo-referencing

(a) and (b) are images before and after geo-referencing respectively.

The shape of geo-referenced images will change to a greater or lesser extent. Figure 6.1 shows the shape changes of MODIS L1B image before and after geo-referencing processing.

In many cases, the geo-referenced images can only cover such a small part of research area that researchers have to abandon them to save processing time. However, it is hard to tell which image covers more area via macroscopically observable in manual processing. To find out suitable images, geo-referencing should be conducted to all images, even if most of them can not be applied in further analysis. It greatly reduces the working efficiency. For example, in each MODIS L1B image, there are 2,748,620 pixels that need to be located. An experiment shows that, by using ENVI 4.5, the geo-reference processing of one scene of 22 Channel MODIS L1B image with 1 km spatial resolution takes approximately 12'20" on Inter

® Core™2 Duo CPU T7300 (at)2.00GHz, 777MHz, 2 GB Rom Lenovo ThinkPad (For further comparison, the other experiments on processing time are conducted on the same notebook).

The spaces to save the image before and after processing are approximately 165MB and 450MB respectively.

In traditional, manual processing way, an inexperienced researcher can select suitable images only after he identifies the location of images. Therefore, it will take 48 working days ( $12.33(\text{minutes/image}) / 60 * 1865(\text{pieces}) / 8(\text{hours/day})$ ) to do the geo-referencing work before selection the proper MODIS L1B images (1 km spatial resolution) for snow map generation of 2006-2007.

## 2. Mosaic of geo-referenced images;

In most of cases, research area is much larger than that can be covered by only one MODIS image. For a larger region, such as Northeast China (as large as 787,300 square kilometers), which usually needs several scenes of MODIS image to cover the whole region. Thus, mosaic becomes an essential processing step, through which several images will be pieced together to create a new image that can cover the whole research region. These images are selected according to research requirements, such as research location and periods. And then they need to be spliced together according to the latitude and longitude of each pixel.

Mosaic can be conducted at different processing stages, which is determined by actual requirements of specific research. Generally there are two ways to conduct Mosaic:

### (a) Right after geo-referencing;

In this way, researchers will mosaic those images that accord with the certain conditions without any further process. However, sometime the images that applied in mosaic process are obtained at different days, even different years. Zenith angles and light conditions are quite different for each image. In some cases reflectance values are different even if images are obtained on the same day and from the same sensor. The software used in image processing is not intelligent enough to reduce the decided boundary of different images caused by environmental conditions.

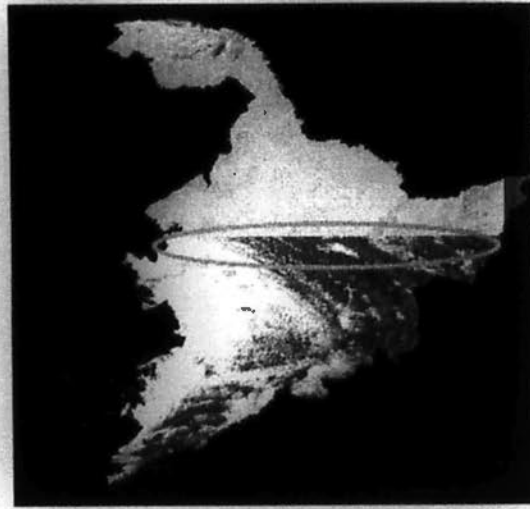


Figure 6.2 The boundary caused by difference of light conditions and incident angles

Figure 6.2 is an image of Northeast China, which is processed with three MODIS L1B images collected at different time. In Figure 6.8 we can clearly see the boundary of different images after mosaic processing by using ENVI 4.5.

(b) After map generation.

Another way to combine several images into a whole view is Mosaic of completely processed images. Researchers need to completely finish the process of each piece of images, including Geometrical Correction, Atmospheric Correction and map generation. Finally, several pieces of maps are Mosaic into a whole one.

### 3. Clipping of mosaic results.

After mosaic, most of images cover the whole research area. However, a MODIS L1B image, especially the mosaic one, is always covering a larger area than that is required, which will be an effect on statistic accuracy in analysis section. It is the reason that we still need to delimit areas. The processing is clipping, which is the final processing procedure in pre-preparation phase.

Normally, all the three pre-preparation steps are manual processed. The traditional processing way poses a couple of problems:

- (a) To deal with these works, most research members have to sit in front of computers, interacting with processing software, processing each image step by step. Besides, during the time of computer processing for one image, researchers have to sit there for several minutes, doing nothing but waiting for the next interaction. It is waste of time and manpower.
- (b) Most of the selections are done by researchers manually according to their subjective experiences:
  - a) Does the image cover interested area?

b) Is the image covered by cloud?

Rich experience, patience and carefulness are required during the whole processing procedures, which will take months in many cases. Subjective factors determine the quality of processing results.

To increase working efficiency and processing quality, studies on remote sensing data processing emerged in the past several years. Leptoukh and his NASA colleague introduced a series of desktop and on-line tools to remote sensing data users, such as HDF\_reader (Masuoka *et al*, 2001; Leptoukh *et al*, 2003). A few researchers tried to focus on a special issue such as geo-reference algorithms, geo-reference automation or mosaic automation processing (Fu *et al*, 2007; Wang *et al*, 2004; Xin *et al*, 2007) for their separate processing purposes.

Although the ideas of lighten the load of the data processing and improving processing quality have already become a consideration for all researchers who need to apply MODIS data in their projects (Sonntag, 2008), very few studies can be found on the whole three-step pre-processing steps of large number of MODIS data based on ENVI/IDL environment.

In this section, the problems which lead to decreased efficiency in mass MODIS data processing are solved by providing an automatic and intelligent processing system. The whole processing procedures will be presented and an automatic processing system for mass MODIS data based on ENVI/IDL environment will be introduced in snow cover monitoring case study over Northeast China.

### **6.1.2 Methodology**

Pre-processing is the procedure to prepare data for analysis. For remote sensing data, especially optical remote sensing data like MODIS, more factors need to be taken into account when we arrange processing procedures.

As it is mentioned above, three steps compose of the processing procedure:

1. Geo-reference;
2. Mosaic;
3. Clip.

## **6.1.2.1 Data**

### **6.1.2.1.1 MODIS L1B Data**

MODIS L1B data are generated from the MODIS Level 1A scans of raw radiance and in the process converted to geophysical units of  $W/(m^2 \mu m sr)$ .

The Moderate-resolution Imaging Spectroradiometer (MODIS) provides 36 channels, 20 of which locates in the visible and near-infrared bands and 16 of which belongs to thermal infrared bands. The spectrum range it holds is from  $0.4\mu m$  to  $14.3\mu m$ . Because of its acceptable time, spatial and spectral resolution (Zhao, 2003), MODIS data were selected for SCA monitoring in this study.

### **6.1.2.1.2 MODIS Snow Products**

MOD10A1 data, MOD10A2 data are snow covered products. They provide fractional snow cover, and snow albedo map daily and every 8-day respectively.

## **6.1.2.2 Geo-reference**

Geo-referencing is the first step of the whole processing, which is used to locate image pixel with relative pinpoint ground area via unique pair of longitude and latitude.

Generally, a reference map or a group of ground control points are needed to calibrate the corresponding pixels on image. Then triangulation based interpolation algorithms are applied to calculate the location of nearest neighbor points of these calibrated pixels.

For MODIS L1B data, two methods can be applied in geo-referencing:

1. One way is to plot each pixel of the L1B data using the latitude and longitude stored in the corresponding MODIS Geo-location file (MOD03);
2. Another way is to use the geo-location information attached in Swath structure of MODIS L1B or higher level MODIS data. Geo-locations of every fifth pixel are stored in the structure, with which a table of ground control points can be generated. This method has the advantages of faster calculating speed and less occupation of memory and hard disk.

In the study, the second method is selected to process 1km MODIS L1B data.

As it is mentioned above, because of the huge locating computation, geo-referencing is the most time consuming procedure. Unfortunately, not all of geo-referenced images can be used in further research. Two kinds of data will be removed from dataset during the images quality control for Mosaic:

1. The images with very small coverage of our interested area;

A threshold of interested area coverage is 25% in our research (considering that there are 4 images provided on our study area by NASA daily).

2. The images with unacceptable cloud covered part.

Another problem that will lead to low efficiency and quality is the effect of cloud. Those images covered with large cloud need to be removed from dataset before feature extraction of ground objects. However, it is difficult to distinguish the cloud from snow cover by naked eyes, especially for inexperienced analysts.

To improve processing efficiency, algorithms for rough estimation of interested area coverage and cloud detection are introduced as image selection in geo-referencing step to avoid wasting of time on useless data and low quality of processing images.

### 6.1.2.2.1 Image Detection

#### 6.1.2.2.1.1 Location Estimation

Generally, only after geo-referencing images selection procedure by location can be robot-icized. During the selection of MODIS data with requirement of specific period of time and particular location from the website: <http://ladsweb.nascom.nasa.gov/data/search.html>, all the images will be listed, even if only 1% of the image is involved in the research region.

This means that a great deal of time will be wasting on useless data if most of images with less than 25% overlapping area with the interested region are geo-referenced. To solve this problem, a rough but efficient detecting method is needed to apply in our research. During the location detecting, geo-location information of MODIS swath is obtained from the header of MODIS data. By doing this, those images with less than 25% overlapping area can be removed from datasets before geo-referencing. The proportion calculation can be described as the following

$$overlap\_proportion = \frac{n_o}{n_{all}} * \frac{A_M}{A_i}$$

6.1

Where  $n_o$  and  $n_{all}$  are the number of overlapping units and number of all units in MODIS images, respectively;  $A_M$  and  $A_i$  represent the covered area of one MODIS image and the area of interesting region.

#### 6.1.2.2.1.2 Cloud Detection

Optical remote sensing data are usually affected by lots of environmental factors, such as the angle of sun, aerosol, topography, and clouds. When a suitable MODIS image is selected by research projects, the cloud factor needs to be considered.

In manual processing method, research workers are always making the judgment according to their experiences. Errors caused by visual fatigue can hardly be avoided during mass data processing.

In the automatic processing method, cloud detection via band calculation applied to remove those images covered by cloud automated. According to the research results of Chen, Junhui (Chen, 2007), reflectance of band 1, band 6 and band 26 can be applied in cloud detection. After the analysis of large amount of cases, the following detection thresholds were obtained in her thesis:

$$0 < \frac{band_1 - band_6}{band_1 + band_6} \leq 0.4 \quad \text{or} \quad band_{26} \geq 0.1 \quad 6.2$$

$band_1$ ,  $band_6$  and  $band_{26}$  are reflectance from channel 1, channel 6 and channel 26 respectively.

#### 6.1.2.2.2 Channel Selection

In MODIS, there are 36 channels. Extra processing time is required to process more channels than needed. The experiment results shows that it will take 9.15 minutes to process visible and near infrared bands, but only 2 minutes to process 500m resolution bands (channel 3-6) by using automatic program. By manual processing on ENVI 4.5, 12.22 minutes to process visible and near infrared bands, 5.24 minutes to process band 1, band 4, band 6 and band 26 and 4.63 minutes to process band 4 and band 6. To calculate Normalized Deference of Snow Index (NDSI), reflectance of band 4 and band 6 is needed. Similarly, data from band 1 and band 26 are still important in cloud detection.

### **6.1.2.2.3 Equilibrium Selection**

Depending on the research requirements, researchers need to find a balance between processing speed and details during data processing. In the research of long term snow cover monitoring, million of images need to be processed to generate daily snow covering maps. Both processing speed and images quality need to be considered. The processing time will be reduced by applying image selection and channel selection.

Generally 4 MODIS L1B images that pass through Northeast China are provided by NASA per day (some times 3 or 5 images per day). In this study, those images will be removed according to determined thresholds:

1. The MODIS image will be removed if its overlapping proportion is less than 25% in case study section.
2. Those images with 25% pixels covered by cloud are removed from analysis dataset automatically.

More accurate cloud coverage of interested area will be obtained after geo-referencing. However, considering the research is a long term observation and total cloud amount over Northeast China is comparatively small, both location and cloud detections can be conducted before geo-referencing by using the location information in swatch structure to reduce processing time. Thus geo-referencing will be performed on the bands that will be used in NDSI calculation and the images selected for snow monitoring according location and cloud detections. Working time is greatly shortened by doing this.

### **6.1.2.3 Mosaic**

For the cases that interested regions covered by more than one image, a mosaic processing of multi-images is necessary. Because of different zenith angles and light conditions, reflectance values are different even if images are obtained on the same day or from the same sensor. To maintain optical consistency of most interested areas, mosaic sequence needs to be taken into account. The images with a better definition and larger covered area will be put on the top of mosaic queue of MODIS images. Acquisition time of images is another considering condition. Besides, during Mosaic procedure for more than one images, the light condition of different images

need to be considered. Several algorithms are designed to reduce the boundary effect (Ye *et al.*, 2007):

1. Replace;
2. Taking max value;
3. Taking average;
4. Add priority average.

During images selection, size, time and cloud effects are taking as conditions before Mosaic. In most of cases, Mosaic images are smooth in our study. However, “boundary” effect happens sometimes. To improve processing quality, a new method is developed to reduce the boundary in this thesis:

If the difference between DN values of the same location in different images is larger than a certain threshold which can be decided by analyst according to research requirement, DN adjustment processing by calculating the average value will be applied before Mosaic.

Figure 6.3 shows the processing flowchart of Mosaic.

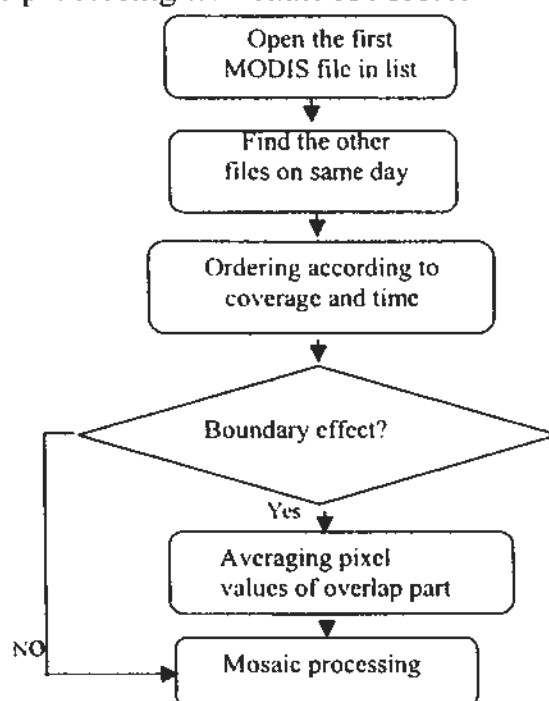


Figure 6.3 Flowchart of Mosaic

After Mosaic processing, a comparative smooth Mosaic image is generated.

#### 6.1.2.4 Clip

In most cases, the mosaic result is larger than the research area. To make the statistic calculation result more precise, a masking processing to limit the computing in

certain region will also be performed. There are two kinds of methods to clip interested area:

1. Clip the interested area with vector;
2. Clip the interested area by application of mask.

#### 6.1.2.4.1 ROI

Region of interested (ROI) is the processing method of clipping research area by using a vector. To conduct the process, a polygon vector will be generated according to research area. Each pixel on Mosaic images will be judged whether it is in/on the vector or outside the vector. If the pixel is outside the vector, it will be assigned a fix value which will never appear as DN value in interested pixel.

$$\text{Pixel on Mosaic image} \quad \left\{ \begin{array}{l} ND_{new} = DN_{original}; \text{Pixel} \subseteq \text{polygon\_vector} \\ ND_{new} = \text{Fix\_value}; \text{Pixel} \not\subseteq \text{polygon\_vector} \end{array} \right.$$

6.3

#### 6.1.2.4.2 Mask

Another method to cut research area from a Mosaic image is application of mask. Before the processing, a mask image with the same size and spatial resolution as those of images that need to be processed need to be generated. The value of each pixel on mask image is assign following the rules:

$$\text{Pixel on Mask image} \quad \left\{ \begin{array}{l} ND_{new} = 0; \text{Pixel} \subseteq \text{polygon\_vector} \\ ND_{new} = \text{Fix\_value}; \text{Pixel} \not\subseteq \text{polygon\_vector} \end{array} \right.$$

6.4

Then the mask image will be processed with each Mosaic image that need to be clipped. “See-through” value is set as 0 during Mosaic.

Both of the two algorithms can be used as efficient clipping methods. After all these procedures, MODIS data are ready for further data analysis.

### 6.1.2.5 Map

Once the pre-processing work is done, snow covering maps of Northeast China will be generated by using NDSI and Normalized difference of vegetation index (NDVI). The thresholds can be determined according to vegetation coverage and vegetation types. In the research on snow covered mapping over Liaoning province (Zhang, Yan and Lu, 2010), the NDSI thresholds of forest and non-forest areas are 0.2 and 0.4 respectively, NDVI threshold is 0.4. Then the pixel values of snow map can be assigned according to the following formula:

$$\text{Pixel on image} \begin{cases} ND_{snow} = 1; (NDSI > 0.4) OR (NDVI > 0.4 \& 0.2 < NDSI) \\ ND_{snow} = 0; (NDVI \leq 0.4 \& NDSI \leq 0.4) OR (NDVI > 0.4 \& NDSI \leq 0.2) \end{cases}$$

6.5

Although rough cloud detection by using the reflectance of band 26 was applied before geo-referencing, the effect of atmosphere can not be eliminated completely. Because band 26 is sensitive only to water vapor and cirrus clouds. To reduce the effect of atmosphere, 8-day Mosaic method is needed in our long term observation system. Daily snow maps of 8 continuous days are overlapped to generate an 8-day snow covering map. The value of each pixel on mosaic image is assigned as one of the following numbers (Table 6.1) (Zhang *et al.*, 2010).

Table 6.1 Interpretation key for 8-day snow covered mapping derived from MODIS L1B

| <i>Value</i> | <b>Meaning</b>            |
|--------------|---------------------------|
| 1-3          | Possible SCA              |
| 4-8          | SCA                       |
| 0            | Nun Snow-Covered area     |
| -2           | Cloud Obscured            |
| -1           | Outside Liaoning Province |

### 6.1.2.6 Flowchart

According to MODIS data processing procedures mentioned above, seven basic data processing procedures are discussed in a flowchart. Figure 6.4 shows the flowchart. The first step is to download MODIS data from <http://ladsweb.nascom.nasa.gov/>.

Then, geo-location information and DN values of selected channels will be obtained from MODIS images for the detection of reference location and cloud coverage.

Those images selected through the detection of location and cloud will be geo-referenced for mosaic processing.

According to the mosaic requirements (e.g., date or zenith angles), MODIS images will be jointed together to form an integrated map of the whole research area.

The next step of data pre-processing is masking, through which the superfluous area of mosaic images will be removed during statistic analysis.

Finally, snow covered maps are generated by using NDSI, NDVI and 8-day Mosaic technology, based on which further analysis on long term snow covering changes can be conducted.

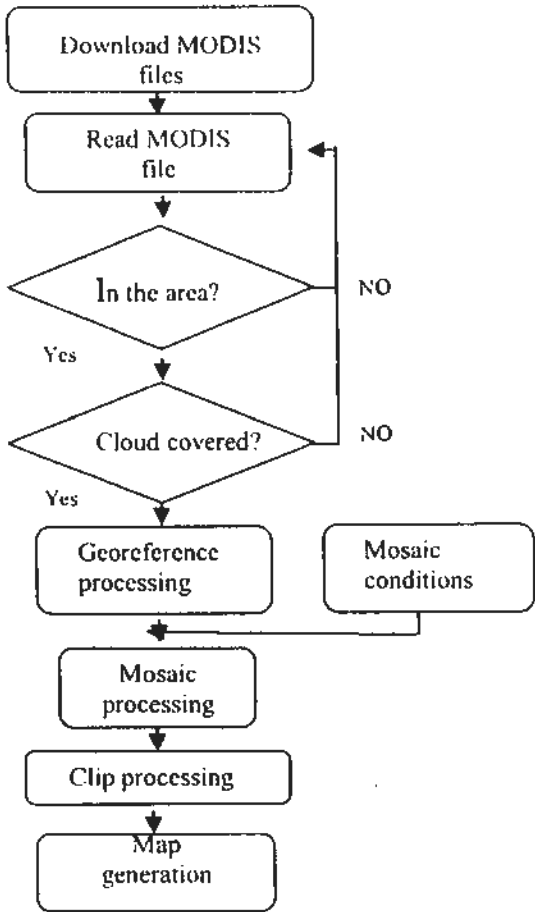


Figure 6.4 Flowchart of mass MODIS data processing

### 6.1.3 Snow Monitoring over Northeast China Based on MODIS L1B Data during 2006-2007 Winter

In this part key codes of snow monitoring map generation over Northeast China will be discussed step by step.

In the traditional way, the processing time of 1865 pieces of MODIS L1B images is 48 working days.

In our automatic processing method, we followed the following steps:

1. Download MODIS files-totally 1865 pieces of MODIS L1B images;
2. Automated processing to select useful images is conducted according to location and cloud detections. The advantage of this automated method is that researchers are freed from the bored and automatic work.

To apply the method mentioned above, the following processing will be performed for the specific research (Figure 6.5).

3. 651 files were removed because only emission data but no reflectance value can be found in those files.

The key point to handle this issue in ENVI/IDL is:

- (a) To open MODIS file.
- (b) If reflectance is unreasonable, then start to process the next MODIS file

270 geo-referenced NDSI files are generated from the rest of 849 files. The others are removed because of their location (420 files), cloud (1 files), invalid data (21 files), and lack of transformation points.

The total geo-referencing time for processing of 270 images are 9 hours.

The corresponding code is

```
fid=EOS_SW_OPEN(filename, /READ)
SWATH_L2_STD_LowRes = 'Low_Res_Swath'
SWidlowres=EOS_SW_ATTACH(fid, 'MODIS_SWATH_Type_L1B')
;read Geolocation fields
ret= EOS_SW_READFIELD(SWidlowres, "Latitude", lat)
ret= EOS_SW_READFIELD(SWidlowres, "Longitude", lon)
envi_open_data_file, filename, /modis, dims=dims, ns=ns, nl=nl, r_fid=fid
envi_file_query, fid, dims=dims, ns=ns, nl=nl, nb=nb, bnames=bnames
if nb EQ 7 then begin
; use to distinguish files with spatial resolution of 500m from those with 1km
if float(n_elements(index))/float(n_elements(lat)) LT 0.07
```

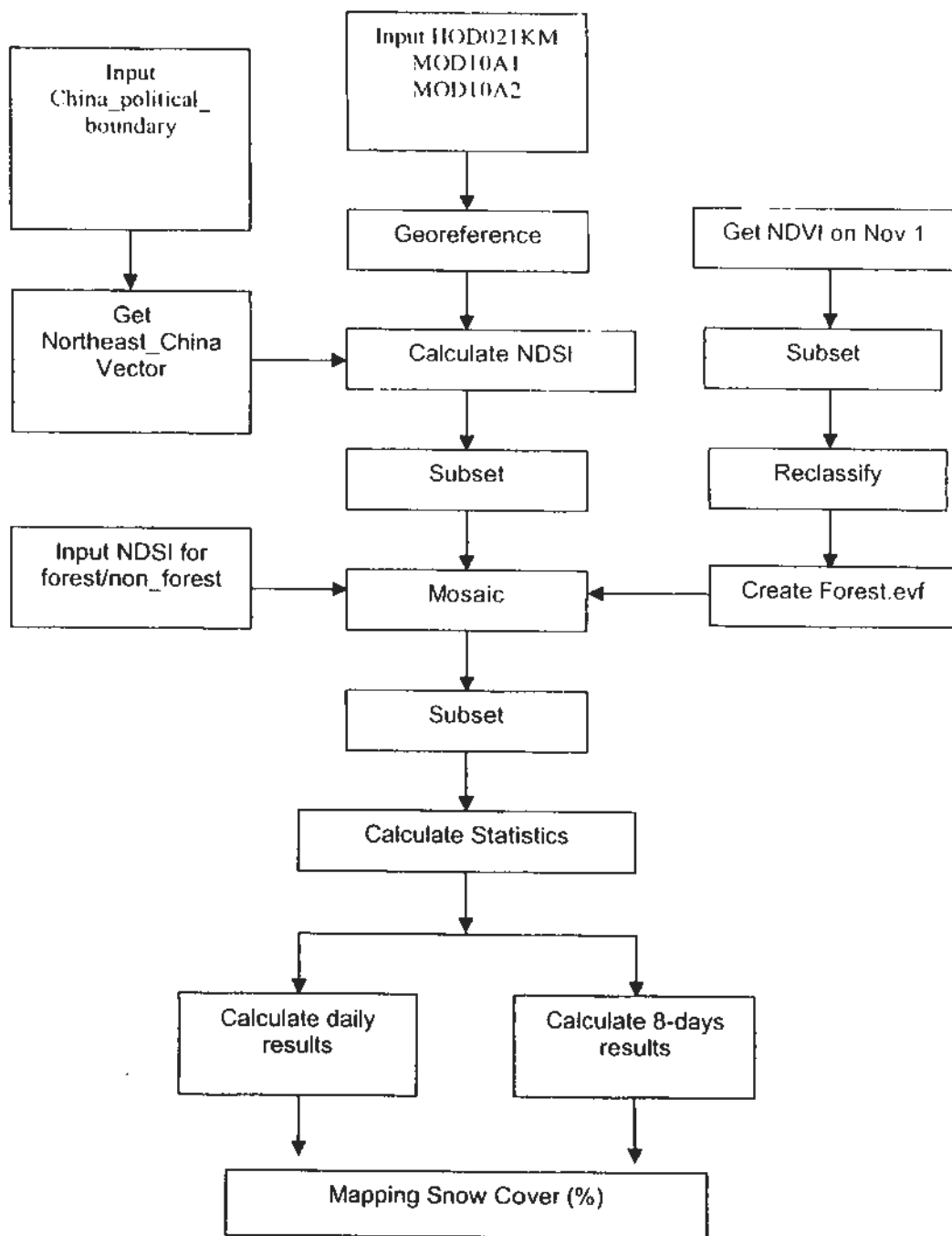


Figure 6.5 Flowchart of automated processing of MODIS L1B data in SCA monitoring

Then begins calculate by using the following equation:

$$\frac{\text{area\_of\_research\_region}}{\text{covered\_area\_of\_MODIS\_image}} \times 25\%$$

6.6

Besides, to reduce the performance time, a new file of our interested data was created. Thus, unnecessary computing to those not interested pixels can be elided. Approximately 8-10 seconds and 5/6 storage space can be saved for each MODIS geo-referenced image in mosaic processing.

4. 5 and 11 8-day mosaic images are created in late 2006 and early 2007, respectively. These images of eight successive days were pieced together and the one with larger

covering area is put on the top. About 5 minutes are needed to mosaic sub-set NDSI images. Totally 1.33 hours are needed in this step.

5. 16 files of masking in the research area are the final output of results. To do this, ROI is applied on each Mosaic image. All reflectance values outside Northeast China were assigned as -1. By doing this, the calculation of SCA will be limited in our research region.

0.08 hour is needed for clipping processing in this case.

Totally processing time of MODIS LIB data for snow cover monitoring in 2006-2007 are 10.41 hours, which are 2 working days by using automatic processing method introduced in this paper.

Clearly, the automated method can greatly increase the efficiency of MODIS data processing by saving manpower and time.

## **6.1.4 Snow Map Generation**

### **6.1.4.1 Daily Snow Cover Mapping**

The processing method removes the images of which more than 25% is covered by cloud. However, cloud is still taken as the major effect on monitoring results according to the research of Frei and Lee (2010). Thus, a cloud mask is needed to reduce the error-judgment of SCA monitoring model.

The compared results of in situ measurements and remote sensing estimation show that estimation values of our model are much more closer to those of in situ measurements in comparison with MODIS snow products over Liaoning(See Figure). However, estimation value of our model is larger than that of in situ data in a few days in late fall or early spring, when temperatures are higher than 0 °C. Only in few days estimation results are larger than those of in situ ones. The errors may be caused by cloud effects (Zhang *et al.*, 2010).

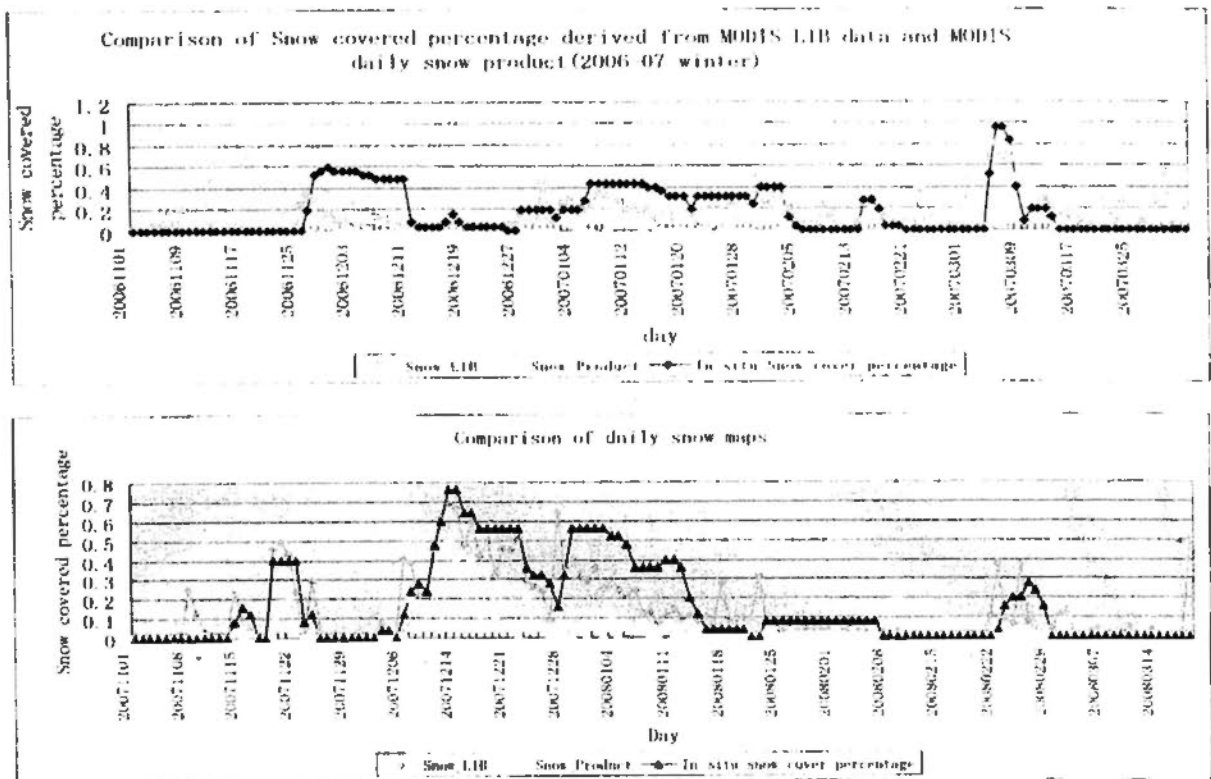


Figure 6.6 Comparison of Snow covered percentage derived from in situ measurement, our model and MODIS daily snow product

#### 6.1.4.2 8-day Maximum Snow Covered Extend Mapping

Generally the pixels with values larger than 1 are snow covered ones. However, snow can hardly melt within one day when the temperature is lower than  $0^{\circ}\text{C}$ . Since lower cold clouds and snow are very similar in the optical properties, the result of SCA based on NDSI is usually mixed with lower cold cloud covered area. Empirically, a pixel can be considered as SCA only when it is marked as SCA the day before the judgment-day and the day after judgment-day. Thus, during an 8 day period, the threshold of snow covered marks is 6. However, the thin snow covered should be considered particularly because the wind and gravitational processes will lower SD. And the snow cover with SD less 2.5cm is invisible to MODIS sensors. Therefore, it is more reasonable to assign the threshold as 4 or 3 (Zhang, Yan, and Lu, 2010).

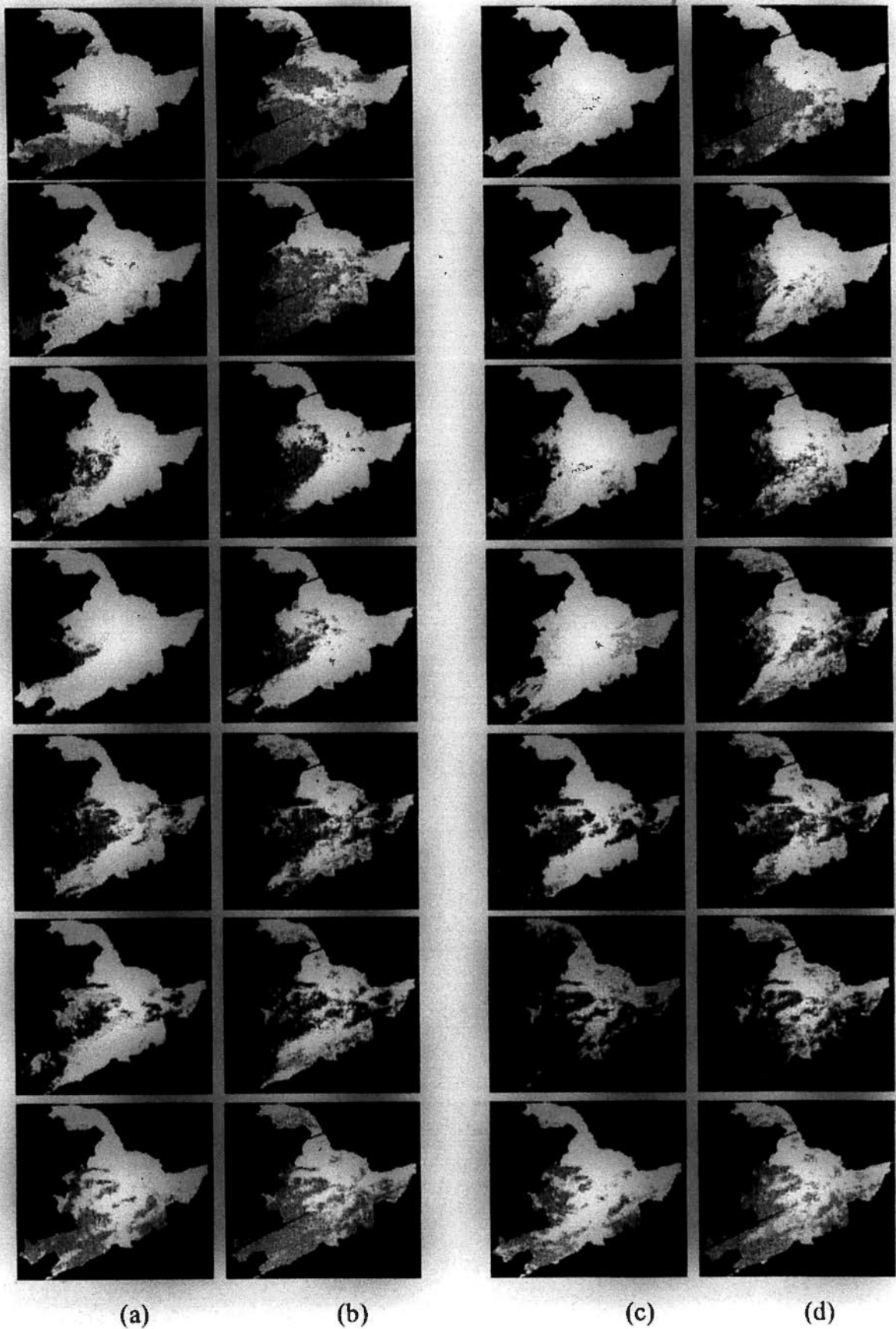


Figure 6.7 8-day snow covering map over Northeast China during 2006-2007 winter (a) and (c) presents snow covered map that produced by NASA while (b) and (d) is the map the generated by using my processing method. In (b) and (d), the muddy color marks the pixels that are not covered by snow; light grey presents the pixels may be covered by cloud or snow (pixel value is less than 4). The pure white shows SCA.

## 6.1.5 Advantage of new Processing Method

The new automated MODIS data processing method is presented for researches related to the long time series. Seven processing procedures are included in the method. A case study of snow cover monitoring over Northeast China shows that by using the new method very similar results as NASA snow products is obtained (Figure 73), moreover, the processing time is reduced from about 48 to 2 working days (10.41 hours), which greatly improves the working efficiency of our data pre-processing in SCA monitoring over Northeast China.

## 6.2 AMSR-E Data Processing

### 6.2.1 Introduction

The Advanced Microwave Scanning Radiometer - Earth Observing System (AMSR-E) L2A data and its high level product- AE\_DySno data are widely used in snow monitoring since 2002.

Brightness temperature can be derived from AMSR-E data in the following way:

$$T_b (\text{kelvin}) = (\text{stored data value} * 0.01) + 327.68 \quad 6.7$$

To calculate SD, brightness temperatures of 18.7 GHz and 36.5 GHz with spatial resolution of approximately 20km from 1st Nov 2005 to 1st Apr 2009 over Northeast China are acquired in this study.

To acquire Snow Water Equivalent (SWE), AE\_DySno data from 1st Nov 2005 to 1st Apr 2009 over Northeast China are applied in our study.

These Level-3 SWE data sets contain SWE data with spatial resolution of 25 km, and are available from 19 June 2002 to the present. Three kinds of datasets are provided by National Snow and Ice Data Center, they are AMSR-E/Aqua Daily L3 Global Snow Water Equivalent EASE-Grids (AE\_DySno), AMSR-E/Aqua 5-Day L3 Global Snow Water Equivalent EASE-Grids (AE\_5DSno), and AMSR-E/Aqua Monthly L3 Global Snow Water Equivalent EASE-Grid (AE\_MoSno).

### 6.2.2 Methodology

Comparing with optical remote sensing data, microwave remote sensing data have the capacity of penetrating, which means that cloud detection can be omitted in

microwave data processing. The processing steps for cloud will be neglected during AMSR-E data preparing.

### **6.2.2.1 Data**

#### **AMSR-E L2A**

The AMSR-E Level-2A data provides brightness temperatures at 6.9 GHz, 10.7 GHz, 18.7 GHz, 23.8 GHz, 36.5 GHz, and 89.0 GHz, respectively. The spatial resolution for different channels corresponds to the footprint sizes of the observations, which are 56 km, 38 km, 24 km, 21 km, 12 km, and 5.4 km, respectively. Since 2002, the daily AMSR-E data are available. All these data can be downloaded free charge from National Snow and Ice Data Center.

#### **AE\_DySno**

To acquire Snow Water Equivalent (SWE), AE\_DySno data from 1st Nov 2005 to 1st Apr 2009 over Northeast China are applied in our study.

These Level-3 SWE data sets contain SWE data with spatial resolution of 25 km, and are available from 19 June 2002 to the present. Three kinds of datasets are provided by National Snow and Ice Data Center, they are AMSR-E/Aqua Daily L3 Global Snow Water Equivalent EASE-Grids (AE\_DySno), AMSR-E/Aqua 5-Day L3 Global Snow Water Equivalent EASE-Grids (AE\_5DSno), and AMSR-E/Aqua Monthly L3 Global Snow Water Equivalent EASE-Grid (AE\_MoSno).

### **6.2.2.2 SD Calculation**

Since AMSR-E L2A data provide us 12 channels with re-sampling and without re-sampling data (See Table 6.2). To reduce computational complexity, the channels that are sensitive to SD according to our field experiments are selected and processed before geo-referenced processing, which means among the 6 channels without re-sampling, only 18.7GHz and 36.5GHz are selected for the further processing.

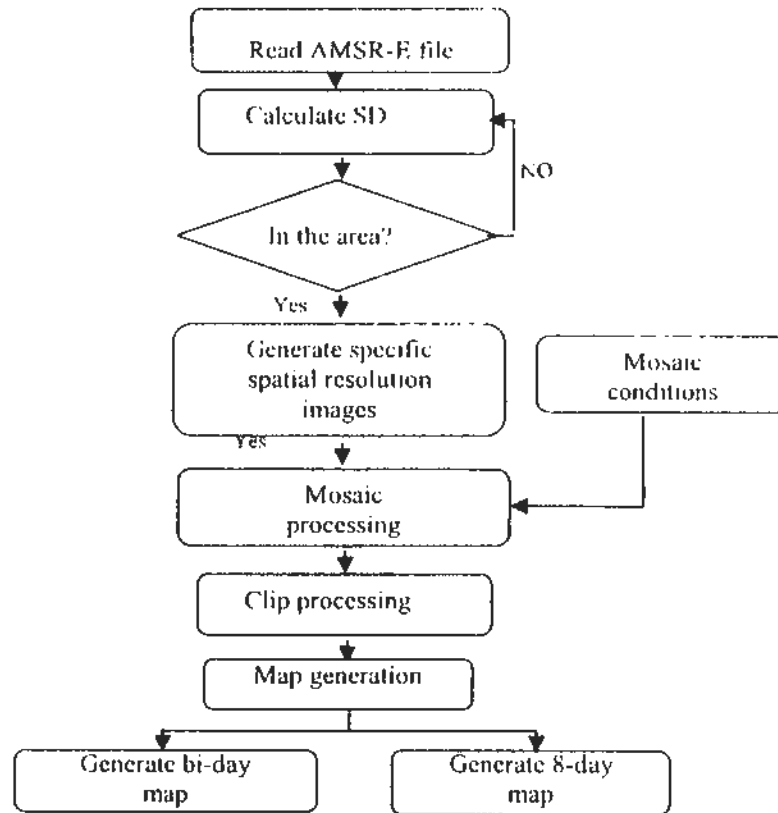


Figure 6.8 Process flowchart for AMSR-E L2 data

Table 6.2 Spatial resolution of AMSR-E data

|                              |         |         |         |         |         |       |
|------------------------------|---------|---------|---------|---------|---------|-------|
| Center Frequencies (Ghz)     | 6.925   | 10.65   | 18.7    | 23.8    | 36.5    | 89.0  |
| Mean Spatial Resolution (Km) | 56      | 38      | 21      | 24      | 12      | 5.4   |
| Ifov (Km X Km)               | 74 x 43 | 51 x 30 | 27 x 16 | 31 x 18 | 14 x 8  | 6 x 4 |
| Sampling Rate (Km X Km)      | 10 x 10 | 5 x 5 |

From Table 6.2 we know that each channel has its corresponding special resolution. Although the special resolution of 36.5GHz is 12km, that of 18.7GHz's is 21km. Thus for geo-referencing location (pair of longitude and latitude coordinate) with low spatial resolution is selected.

### 6.2.2.3 Geo-referencing

In the original image that NISDC provides us, geo-information are not linked to brightness temperature. Thus, geo-referencing processing is required.

Geo-referencing of AMSR-E L2A data is quite different from that of MODIS data processing since AMSR-E L2A data are swatch data. AMSR-E data are composed of dispersion point with brightness temperature and location information.

To fix each point into its corresponding location for my study, the boundary of the research area is simply defined by the use of a rectangle with upper-left and down-right corner candidate of Northeast China on the map. Only those points locate in my interested area are registered into geo-referenced file.

#### 6.2.2.4 Spatial Resolution Selection

After Geo-referencing, the rectangle image is transformed into an anomalous formation (see Figure 6.9). The corner coordinates of black background are (118E, 54N) and (136E, 38N).

One of the advantages of this processing method is optional spatial resolution. The distribution without re-sampling point is not as regular as that of grid data's. When the sampling spatial resolution increases, number of points found in one pixel will decrease.

Therefore, the selection of re-sampling spatial resolution is important. On one hand, a finer spatial resolution is required for accurate monitoring of snow. On the other hand, post processing to fill vacancy where no sampling point can be found is necessary.

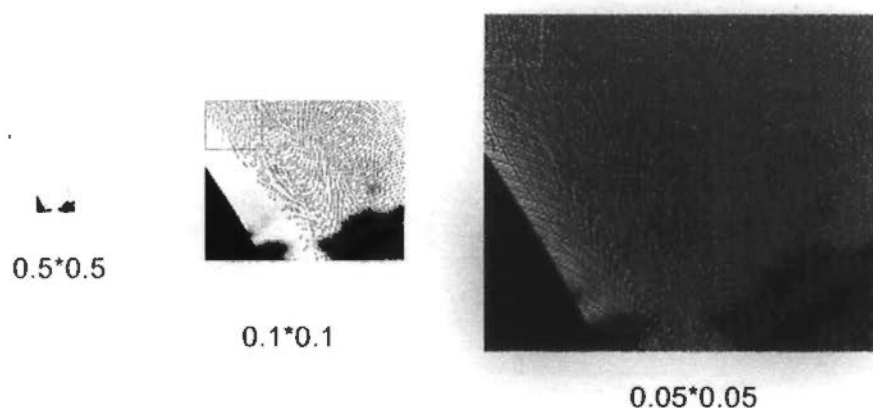


Figure 6.9 Re-sampling spatial resolution according to specific usage

Accuracy will be deteriorated if the re-sampling spatial resolution is defined higher than  $0.05*0.05$ .

#### 6.2.2.5 Mosaic

In most of cases, only one piece of swatch can not cover the whole Northeast China. Mosaic of several swatch data within one day or two days are needed here to generate a map for the whole research area (Figure 6.10).

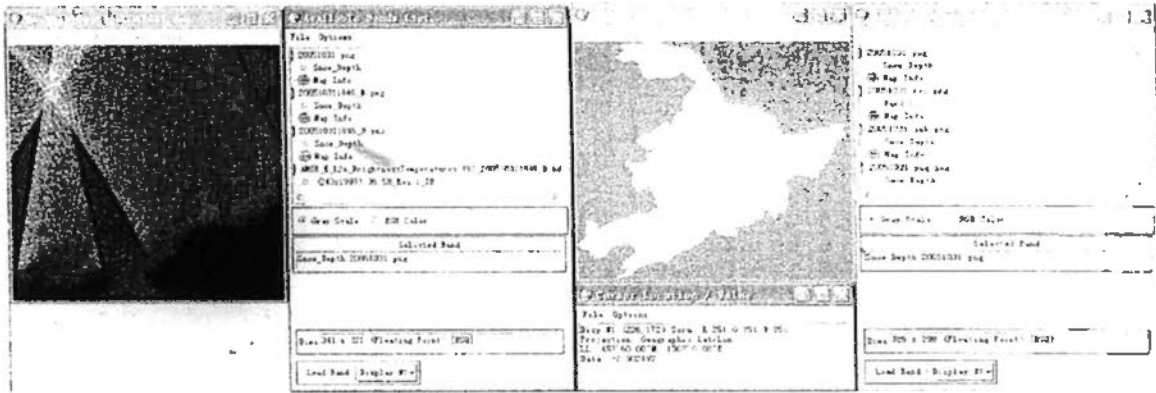


Figure 6.10 Mosaic of AMSR-E data

Figure 6.11 Interpolation Process

### 6.2.2.6 Subset and Interpolation

Then, a vector of the research area is needed to border the data interested. However, there are lots of blank pixels within which no sampling point can be found in the interest of research area map (see Figure 6.11). An additional processing is to apply Algorithms on processing result of boundary delimiting.

Values of blank points on the map are generated with 8 neighbor points. By doing this, each point in our research area is assign a value.

### 6.2.2.7 Generation of Snow Mask Map

Finally, snow mask is generated from the interpolated map. Those pixels with value over 0 are SCA, while those pixels with zero values are bared land.

However, it is noticed in Figure 6.12 that most of pixels have minus values (the dark blue pixels). On this kind of pixels, we can hardly determine whether or not it is a SCA according to the analysis of field experiment. That is to say, further researches on snow covering on different underlying surfaces are in urgent need.

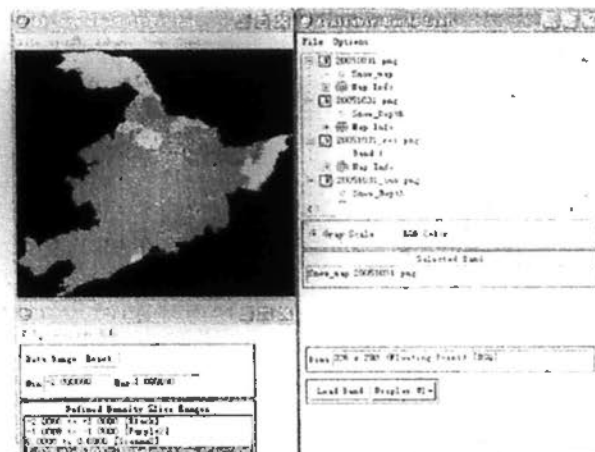


Figure 6.12 Generation of daily snow covered map

Sometimes, 8-day Mosaic of snow covered map can provide us a more accurate result on snow covered monitoring. However, the radiation properties of some kind of underlying surfaces are uncertain, which doubtless increases the difficulty in land cover discrimination.

### **6.2.3 Comparison of Ascend and Descend data**

Besides all the procedures mentioned above, there is still one thing that we need to considerate. That is the change of incident angle. Generally, there are 4 piece of swatch data that we can obtain from satellite remote sensors per day. Two of them are Ascend images, the others are Descend images. The incident angles of the two types of satellite images are around  $50^\circ$ , which is considered are the best performed angle.

Another effect factor that will influence retrieval accuracy of the two kinds of AMSR-E data is snow wetness. The transit times of Ascend and Descend satellites are 16-18pm and 2-4 am respectively. Basically, in the winter of Northeast China, minimum temperatures will occur in both of two time frames except very few days. It means that unless the snow is melting during the whole day, there is no big difference between the two time frames, especially in snow covered judgment calculation.

Figure 6.13 shows the preliminary estimation of SD in 6 testing sites in 2006-2007. The estimation results of Ascend and Descent satellites are similar.

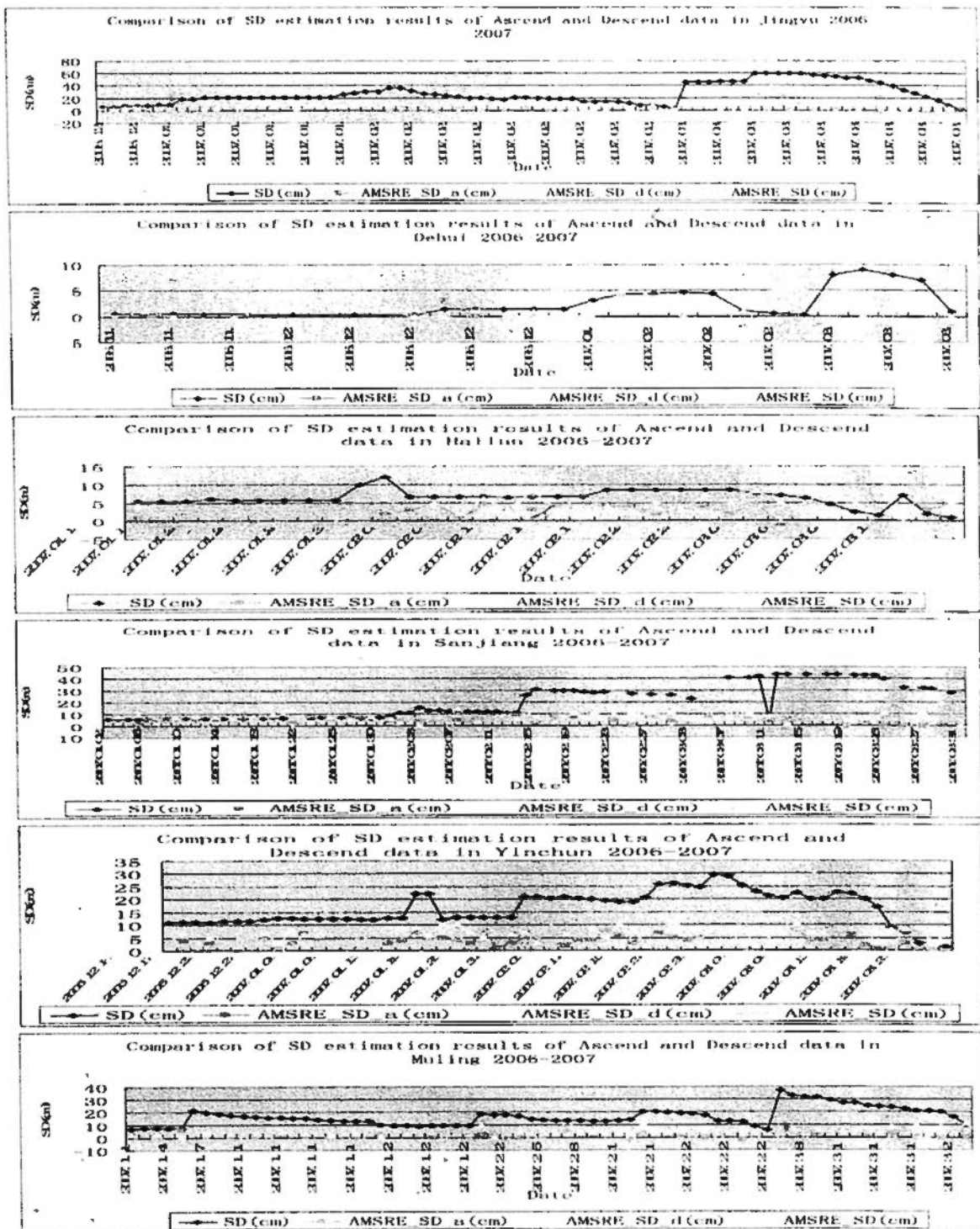


Figure 6.13 Preliminary estimation of SD in 6 testing sites in 2006-2007

However, we can see that the estimation results of AMSR-E data are quite different from that of in situ measurements. The estimation model is not accurate enough in practical use. More researches should be done to improve the model.

## 6.2.4 Comparison between Estimation Results Based on AMSR-E and In Situ Measurements

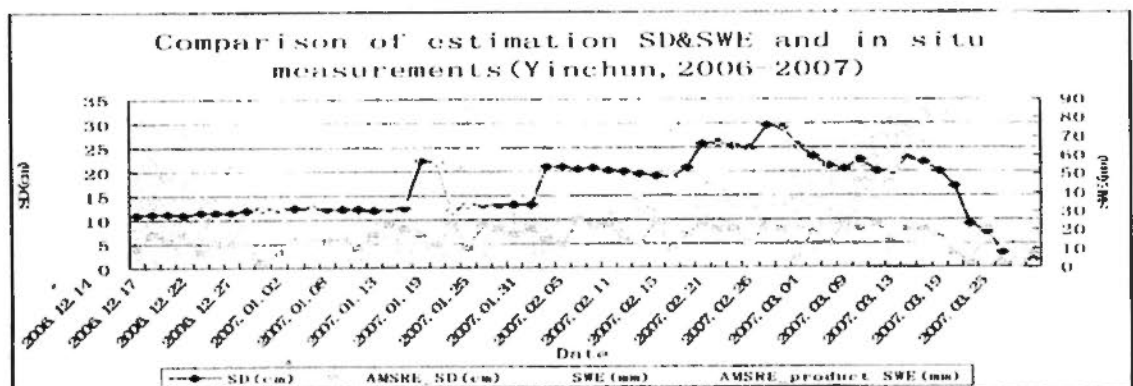
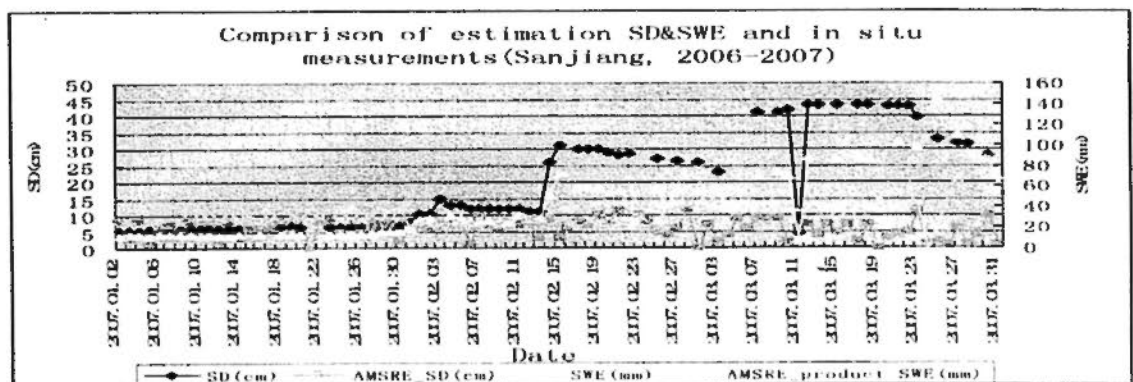
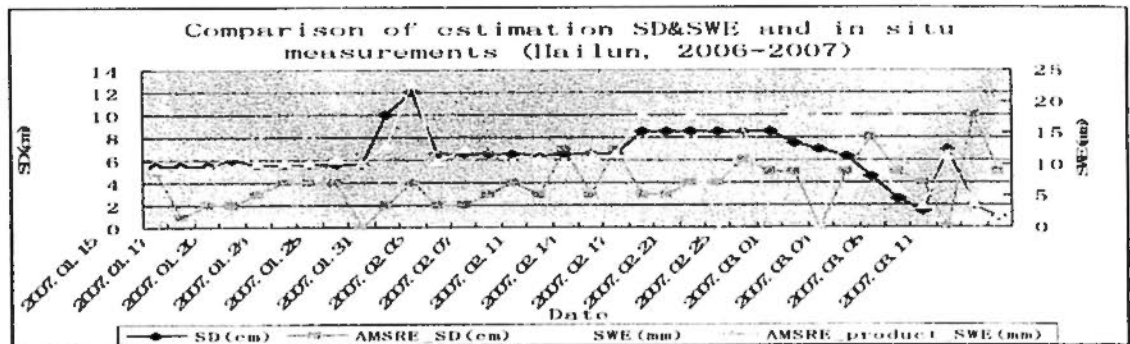
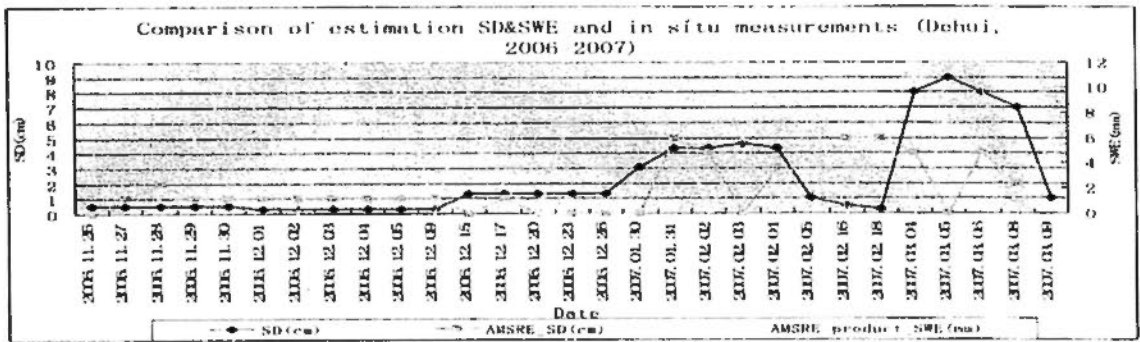
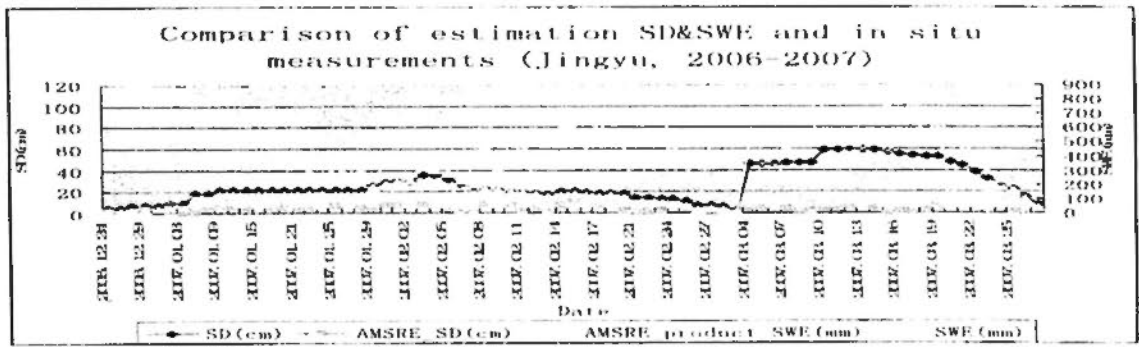
### 6.2.4.1 SD Estimation

To develop an accurate SD retrieval model, field experiments and long term observation are essential. Table 6.3 shows the location of test sites, where long term observation conducted.

Table 6.3 Location of test sites

| lat   | lon    | Test sites name |
|-------|--------|-----------------|
| 49.43 | 127.35 | Sunwu           |
| 46.82 | 130.28 | Jiamusi         |
| 43.37 | 128.2  | Dunhua          |
| 45.63 | 122.83 | Baicheng        |
| 41.98 | 122.83 | Xinmin          |
| 41.55 | 120.45 | Chaoyang        |
| 47.28 | 126.57 | Hailun          |
| 47.42 | 128.56 | Yichun          |
| 44.9  | 130.5  | Muling          |

The measurement results of SD and SWE are compared with that of estimation results by using AMSR-E L2 and AMSR-E L3 data. Figure 6.14 shows us the comparison results in selected test sites from 2006 to 2007.



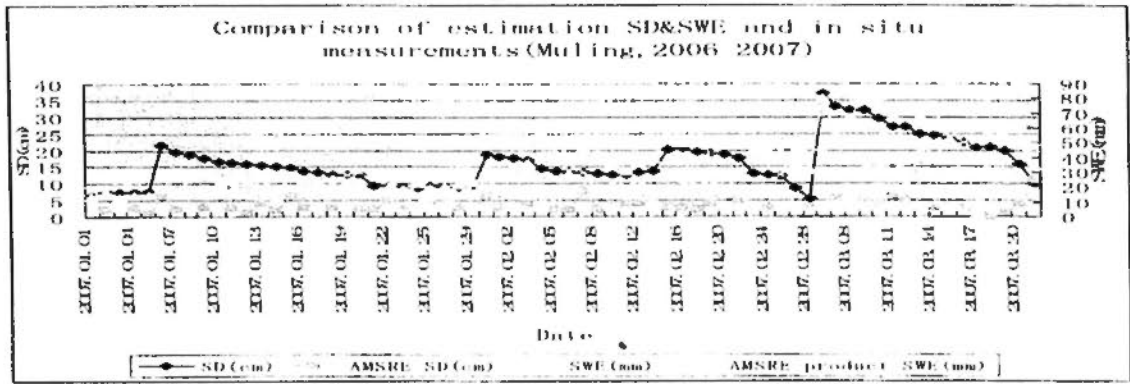


Figure 6.14 Comparison of estimation SD&SWE and in situ measurements

Table 6.4 shows the RMSE of estimation results and measurements.

Table 6.4 Statistical data of long term observation in test sites

| Average_SD(cm) | RMSE_SD(cm) | RMSE_SWE(mm) | Test Sites | Year    |
|----------------|-------------|--------------|------------|---------|
| 30.33          | 28.13       | 42.89        | Jingyu     | 2005-06 |
| 10.22          | 5.60        | 23.56        | Dehui      | 2005-06 |
| 27.66          | 18.70       | 28.97        | Sanjiang   | 2006-07 |
| 26.55          | 28.97       | 313.58       | Jingyu     | 2006-07 |
| 2.28           | 2.81        | 3.37         | Dehui      | 2006-07 |
| 6.31           | 4.33        | 8.67         | Hailun     | 2006-07 |
| 16.98          | 11.85       | 28.72        | Yichun     | 2006-07 |
| 16.25          | 15.52       | 22.70        | Muling     | 2006-07 |
| 5.10           | 3.98        | 16.34        | Hailun     | 2007-08 |
| 10.38          | 6.63        | 15.07        | Yichun     | 2007-08 |
| 7.11           | 10.54       | 541.81       | Muling     | 2007-08 |

The figure and table clearly shows us that generally, the estimation values are lower than that of in situ data. However, there are crosses of estimation curves and in situ ones. The under estimation is higher in the test sites with underlying surfaces of farmland, grassland and the wetland. While in the forest area where SD is less than 35 cm, less underestimation can be found (see results of Muling).

The crosses between estimation and measurement curves make the modification of SD retrieval model more difficult, since the relationship is not linear. If I want to find out a better matched relationship, the first thing we need to do is to figure out what is the cause of crosses.

In the following part, test sites of Jingyu and Dehui (2005-2006) are selected as typical example of forest and farmland. The major effect factor of the crossing curves is discussed by analysis of the two typical test sites.

Ground data collected from two testing sites (Jingyu and Dehui) from Dec. 2005 to Mar. 2006 are listed in Table 34. As mentioned above, the underlying surface of testing site Dehui is farmland, where directly exposures to the sun and fluctuation air temperature due to the open terrain. In comparison with Dehui, there is more snowfall in testing site Jingyu, where the land cover type is forest with less difference in temperature during day and night (see Table 6.5). The mean grain size of new snow is below 3.0 mm in both two sites and the largest SD(49 cm) is far less than the penetrability limitation of passive microwave signal (100 cm) , which mean that NASA model developed by Chang's group can be applied in SD and SWE estimation of the two testing sites by using AMSR-E data.

Table 6.5 Summary of field measurements in two test sites in Northeast China

| Sites  | Tmin<br>℃ | Tmax<br>℃ | Dsize<br>(mm) | SD<br>(cm)  | SWE<br>(mm)  | SWE<br>mean(mm) |
|--------|-----------|-----------|---------------|-------------|--------------|-----------------|
| Dehui  | -39       | 5         | 0.30-1.30     | 4.50-15.80  | 5.18-25.48   | 13.75           |
| Jingyu | -35       | -1        | 1.00-2.00     | 11.70-49.00 | 20.57-171.50 | 81.70           |

According the analysis of remote sensing data (AE\_L2A, AE\_DySno) and in situ measurements of the two test sites, we find that SD estimation result with modified Chang's algorithm is lower than those of in situ measurements (see Table 6.6). A clear trend of under estimation can be found in SD retrieve in both of two test sites.

Table 6.6 The SD estimated from AMSR-E data compared with field data of 05-06 winter

| Test site | Mean_<br>measured<br>(cm) | Mean_<br>AMSR-E<br>(cm) | RMSE<br>(cm) | Error_relative | Correlation<br>(r) |
|-----------|---------------------------|-------------------------|--------------|----------------|--------------------|
| Dehui     | 10.2176                   | 8.72811                 | 4.74921      | 46.4805        | 0.536825           |
| Jingyu    | 30.3294                   | 7.65008                 | 25.0182      | 82.4882        | 0.454089           |

The underlying surfaces of the two test sites (Dehui and Jingyu) are farmland and forest respectively. According analysis results in Table 6.4 and 6.5, it is obviously that retrieval result of Dehui is better than that of Jingyu by using AE\_L2A data when we compare the estimation accuracies of two test sites during the whole winter. Figure 6.15 and 6.16 show the max and min surface temperatures, measured SD, and estimation SD by calculating the difference of 18 GHz and 36 GHz derived from AE\_L2A data. From the figures we can see that during the period of early spring, estimation results of SD start to fluctuate with temperature. That is to say, temperature becomes one of the most important factors that will greatly affect remote sensing estimation.

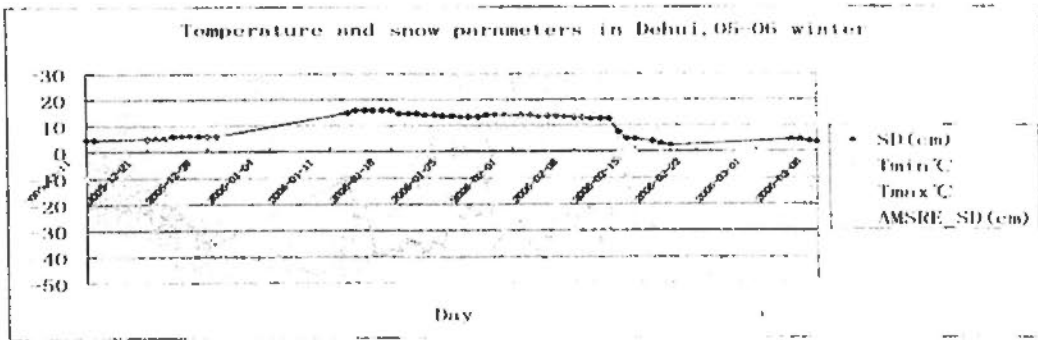


Figure 6.15 Temperature and snow parameters in Dehui ,05-06 winter

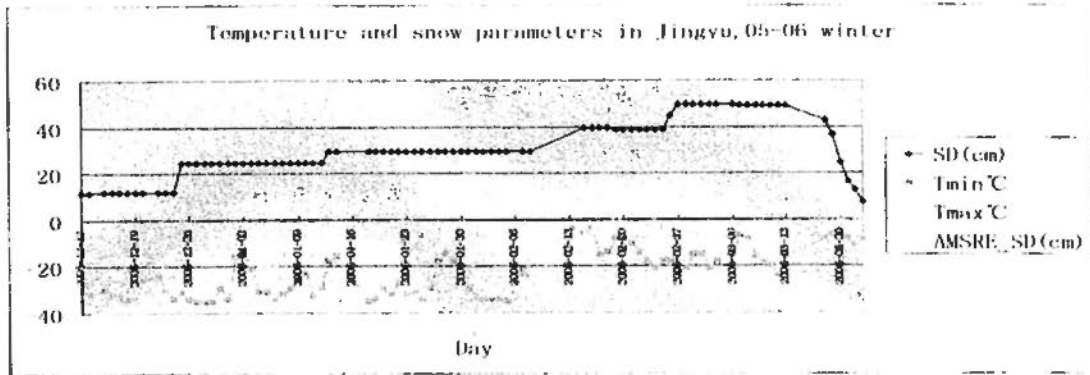


Figure 6.16 Temperature and snow parameters in Jingyu, 05-06 winter

The influence research of temperature on SD estimation results was conducted by the correlations between estimation SD, measured SD and snow surface temperature. Table 6.16 shows the correlation between estimation SD and measured SD and correlation between estimation SD and max/min temperature. As it is noted, both of grain size and water content in snow body have great impact on microwave signals. Only when temperature reaches melting point, rapid changes of grain size and water content will happen. In Rees's review on snow, he defined that melting point is 0°C (Rees, 2005). In researches on SD and SWE estimation in Finland, -3°C is taken as the key point. Actually, melting point is different in different region because that the impurities in snow changes in different area. The only way to define a suitable melting point for Northeast China is figure out the clue from errors between estimation SD and measured one. From Figure 6.15-6.16 we can find that in most of days, SD is underestimated by AMSR-E data, except the days followed a temperature fluctuation with sudden elevation and rapid drop. The overestimation is caused by a refrozen snow layer with larger grain size on the top of snowpack. The grain size of new fallen snow is 0.2 mm in Northeast China while the refrozen one is 0.5 mm according our field work. Based on Mei theory, the larger refrozen grain size will cause an overestimation if the same coefficient is utilized in Chang's model as for new fallen snow. Thus, -6°C can be taken as the proper melting point for the two

test sites. By using the point, the whole winter can be divided into two period, which are dry snow period and melting period. For the two test sites, 15<sup>th</sup> Feb 2006 and 7<sup>th</sup> Feb are selected as the Segmentation points of test sites Jingyu and Dehui, respectively. However, the solution method requires more in situ measurements. More efficient way should be designed to solve the problem. In Chapter 7, an improved model for SD retrieval will be discussion on this issue.

Table 6.7 Correlations of estimation SD, measured SD and daily temperature

| Test sites | Dry snow period |               |               | Melting period |               |               |
|------------|-----------------|---------------|---------------|----------------|---------------|---------------|
|            | $R_{e\_m}$      | $R_{e\_Tmax}$ | $R_{e\_Tmin}$ | $R_{e\_m}$     | $R_{e\_Tmax}$ | $R_{e\_Tmin}$ |
| Dehui      | 0.70            | 0.43          | -0.27         | 0.53           | -0.54         | -0.79         |
| Jingyu     | 0.85            | -0.12         | 0.05          | 0.56           | -0.45         | -0.39         |

(Here  $R_{e\_m}$  is the correlation of estimation SD and measured SD,  $R_{e\_Tmax}$  is correlation of estimation SD and daily max temperature and  $R_{e\_Tmin}$  is correlation between estimation SD and daily min temperature)

From Table 6.7 we can find that in dry snow period, high correlations can be found between estimation SD and measured SD in both two testing sites, which means that modified Chang's model can be applied in SD monitoring over Northeast China where underlying surfaces are forest and farmland during dry snow period. However, temperature becomes the most important factor in Dehui during melting period and the important factor in Jingyu. The less effect on SD estimation in Jingyu may be caused by the deeper SD and smaller temperature fluctuation.

Furthermore, minus values of SD appear in estimation results with AE\_L2A data during melting period in two testing sites, which are caused by water percentage contained in snow body.

In conclusion, because of the property of passive microwave meters, fluctuations in temperature will lead to the estimation errors, if temperature is higher than -6 °C. Besides the effect of land cover types, temperature become the major effect on SD estimation during melting and larger effect will be caused over comparatively open area like farmland than that of forest.

#### 6.2.4.2 SWE Estimation

Similar results can be found in SWE analysis in two test sites. By using AMSR-E L3 data, SWE estimation results can be obtained according to NSIDC:

$$SWE = SD \text{ (cm)} * \text{density (g cm}^{-3}\text{)} * 10.0 \text{ (mm)}$$

Table 6.8 shows the analysis of SWE estimated from AMSR-E data compared with field data in the winter of 2005-2006.

Table 6.8 The SWE estimated from AMSR-E data compared with field data of 05-06 winter

| Test-sites | Mean_measured (mm) | Mean_AMSR-E(mm) | RMSF (mm) | Error_relative | Correlation(r) |
|------------|--------------------|-----------------|-----------|----------------|----------------|
| Dehui      | 14.76              | 7.70            | 10.53     | 71.33          | 0.16           |
| Jingyu     | 77.7               | 16.36           | 69.57     | 89.36          | 0.74           |

A very low correlation is found between SWE estimation and in situ measurements in Dehui, which means estimation accuracy of SWE derived from AMSR-E L3 is far from the requirement for practical application. A new model for SWE retrieve is badly needed. Generally, there is a linear relationship between the difference of 18GHz and 37GHz, which are quite sensitive to snow grain size, and SWE. The higher relationship (0.7) between the difference of 18GHz and 37GHz and measured SD in Dehui can be obtained. And the in situ SWE is calculated by using measured SD. Thus, it can be concluded that by using the difference of 18GHz and 37GHz we will get a more accurate SWE estimation in comparison with AMSR-E L3.

According to the preliminary work on SWE estimation here, a negative correlation can be found between SWE estimation and temperature, which may lead to the low accuracy in SWE retrieval. Another factor that affects the retrieval accuracy may be SD. In Jingyu, a better result is obtained compared with that in Dehui, although the SWE was wildly underestimated (see Figure 6.17).

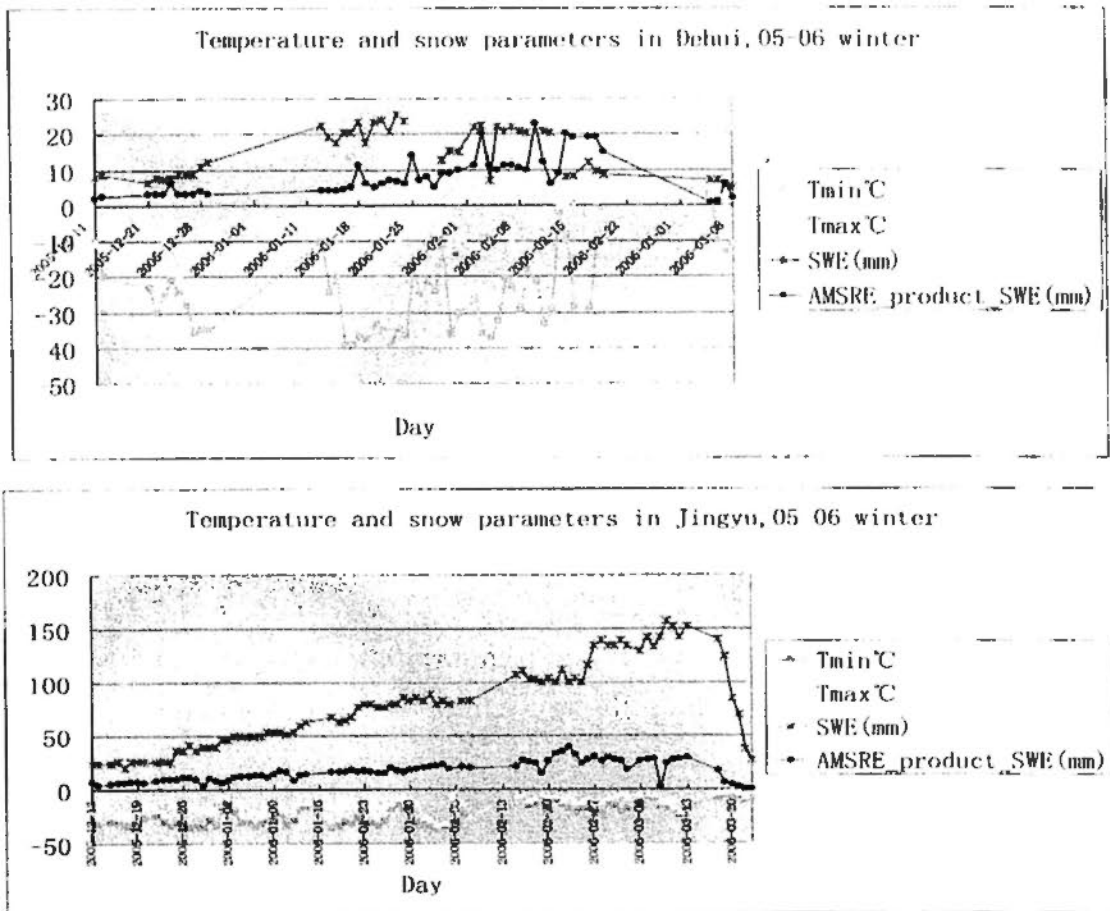


Figure 6.17 Temperature and SWE in Dehui and Jingyu, 05-06 winter

The comparison of SWE estimation between two test sites shows that AMSR-E L3 product can be utilized in SWE trend estimation, in spite of it is underestimated in both of two sites.

To sum up, it is a practical way to roughly divide snow covered period into dry snow and wet snow parts to improve estimation accuracy for both SD and SWE. But here still be other problems that need to be explained. That is: what happens in the cross points during the dry snow period? And how dose the temperature affect SD estimation?

### 6.3 Breakthrough Points to Improve Remote Sensing

#### Estimation Models

Field experiments and the comparisons of SCA, SD and SWE between remote sensing estimation results and in situ measurements are conducted in this study. Results suggest the following conclusions.

1. Effect of cloud is always that major problem for optical remote sensing. To

make models practicable, the effect must be eliminated.

2. Different underlying surfaces will affect SD and SWE estimation results by using passive microwave remote sensing data. For instance, vegetation on the ground surface masks partly the emission from the ground and snow.
3. Difference of V and H is diminished because of the geometric effects of ground surface, especially in high frequency
4. SWE and SD were underestimated in retrieval model by using AMSR-E data over agriculture area and forest in different degree.
5. Unlike the other researches, estimation results over agriculture underlying surface are worse than those over forest, especially in early spring, which means temperature may become prior effect factor in SD and SWE estimation in the period of early spring.
6. Minus value in estimation results of SD is found over the regions near rivers and lakes or in the period of late autumn and early spring, which can be considered as the proof of effects of water body to SD and SWE estimation.
7. There are crosses or trend that will lead to cross in the curves of estimation results and measurements ones in both dry and wet snow periods. The phenomena makes it more difficult to find the exact way to interpret snow information by using AMSR-E data, because the linear model for SD retrieve is seems to be destroyed now. To improve estimation accuracy, the first thing is to explain the cross.

## **Chapter 7 DEVELOPMENT OF IMPROVED SNOW MONITORING MODELS**

In chapter 5 and chapter 6, the estimation results of SD, the effect of land cover types on estimation accuracy and the physical properties of snow were analyzed briefly. The preliminary results show us that the existing models for SCA and SD estimation are not good enough in retrieval of snow information, which is usually applied as very important input parameters in hydrology and climatology models. Another message brought by these results is that there is a great potentiality in satellite remote sensing data to provide more accurate estimations which will meet the requirements of hydrology and climatology models. Deeper research on the inherent relationship between snow properties and satellite remote sensing data need to be conducted to accomplish the goal. In this chapter, improved snow monitoring models with which more accurate SCA and SD estimations can be acquired over Northeast China will be developed and discussed.

### **7.1 SD Retrieval Model**

#### **7.1.1 Introduction**

In Chapter 2, SD retrieval models based on both optical and microwave remote sensing data were expounded. Optical remote sensing data are not dominant in this area because they do not have the penetrability as microwave remote sensing signals do. With microwave remote sensing data, popular models are applied in SD estimation within different scales. With abundant and timely input parameters, HUT and MEMELS models achieve comparatively high precision but more limitation for large scale application. The requirements of abundant and timely input parameters greatly whittle away the advantage of models based on remote sensing, which are supposed to work efficiently and timely without intervention from in situ measurement and to be applicable to large, even global scale. Chang's algorithm is successfully applied in global scale monitoring. However, the fixed coefficient in this model lead to huge errors when it is performed in different regions where snow properties diverge greatly. The difference in snow properties is mainly in snow grain size, which has great effect on SD estimation by changing the scattering with in snow

packs. To solve the problem, assigned value of the constant is suggested to be different in different location because of diversity in snow grain size in different continent. The value of constant ' $a$ ' is changed from 1.59 (in America) to 0.78 when this model is applied in Eurasia.

Nevertheless, even in the same location, snow grain size varies. In situ measurements in Chapter 5 shows that, snow grain size varies from 0.2mm to more than 2mm. Researches show that, under certain temperature and humidity circumstances, snow grain size can increase tenfold. The huge snow particles inside snowpack body are referred to as deep hoar, which is considered as one of the unsolved problem that dramatically reduces retrieval accuracy (see Chapter 2 and 3). Further reversions have been made on Chang's original algorithm to deal with the growth of grain size over time (see Formula 3.8).

But new fallen snow mantled the old snow layer is not considered in this modification. For the new layer, snow grain size is small. Therefore, the scattering property changes again. But the time counting for the reversion model will keep running in the old mode without intervention of ground observation, even if there is new snowfall. Here comes the problem: snow grain size is constantly changing while the parameters and constant for global SD retrieval models remain static. In the following section, an improved model which addresses to solve this problem is developed.

## **7.1.2 Methodology**

### **7.1.2.1 Original SD Retrieval Model**

Till now, there is no widely accepted model for SD retrieve by using optical remote sensing data. The most universal algorithm in SD estimation is Alfred T. C. Chang's model. According Mei scattering theory, it is suggested that the difference of 18 GHz and 37GHz can be used in SD estimation and series experiment results confirm the linear correlation between SD and the difference of brightness temperature ( $T_b$ ) (see Formula 3.5)

In Formula 3.5,  $a$  is a coefficient that will be assigned different values in different regions according to snow grain size (e.g., 1.59 in North America and 0.78 in Eurasia).

In this study, the Chang's original algorithm is applied in SD retrieval to make a comparison between the SD estimation results of original algorithm and that of improved model. The value of  $a$  is assigned as 0.78 according to Li and Che's researches for original algorithm.

### 7.1.2.2 Changing Trend of Snow Grain Size Estimate Model

Study on snow grain size detection started from research on scattering and absorption of radiation by single ice particle. Calculation results show that scattering light is mostly due to refraction but not reflection within snowpack (Warren, 1982). With the increase of snow grain size, path direction of light photon inside ice particle is increasing, which gives more chances to ice molecules for absorption. However, at different wavelength, absorption shift is different.

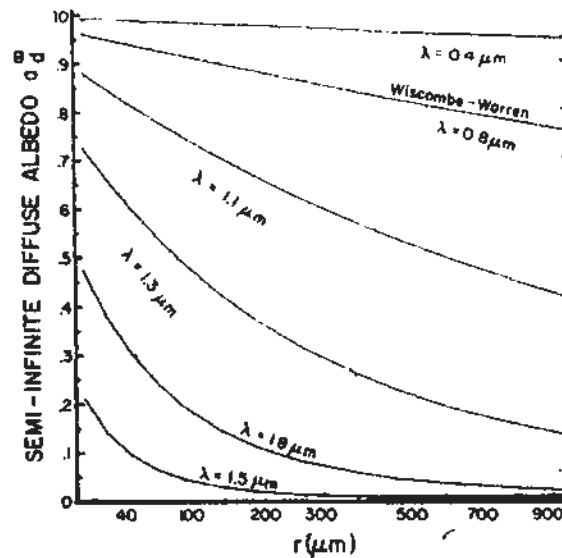


Figure 7.1 Diffuse albedo vs. grain radius (Adopted from Optical properties of Snow, by Warren, 1982, pp.72)

Here  $\lambda$  present wavelength and  $r$  is grain radius.

By using WWI model, changing rate of albedo according to increase of snow grain radius is calculated at different wavelength (see Figure 7.1). At visible region, linear relationship with slightly downward slope can be found between diffuse albedo and square root of grain radius. When it comes to near-infrared range, the changing rate is more like exponential curve. It indicates that at near infrared range, albedo is more sensitive to the changes of snow grain size than at visible range. However, at wavelength of  $1.5\mu\text{m}$ , change of albedo is close to saturation when  $r$  reaches  $200\mu\text{m}$ . At  $1.1\mu\text{m}$  a comparatively obvious inverse relationship between albedo and

grain radius can be found. Based on which, Dozier *et al.* calculate snow grain size by using the scaled area of the absorption feature near  $1.1\mu\text{m}$  (see Figure 7.2) (Dozier *et al.*, 2009).

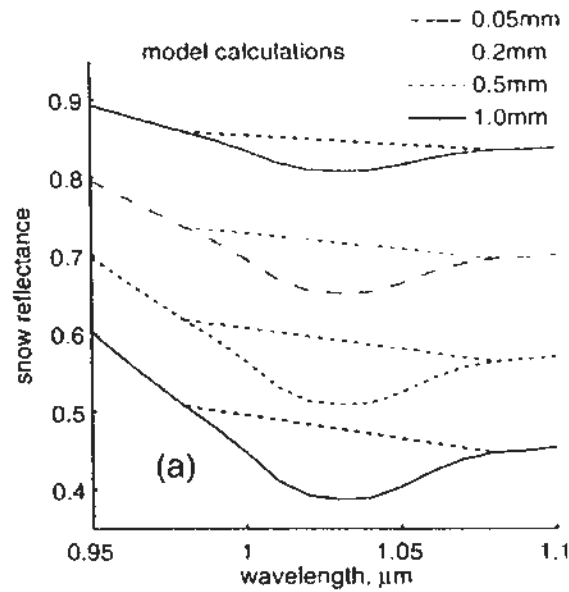


Figure 7.2 Relationship between snow grain size and scale area of optical feature

Figure 1. (Adopted from Dozier, J., Green, R., Nolin, A., Painter, T.(2009). Interpretation of snow properties from imaging spectrometry. Remote Sensing of Environment, 113 (2009), S25–S37.)

However, the most notable and monotonic decreasing of albedo can be found near  $1.3\mu\text{m}$ . Therefore, in this thesis, the wavelength with which snow grain size will be retrieved is selected from  $1.2\mu\text{m}$  - $1.3\mu\text{m}$ , that can be provided by MODIS sensors. The analysis result of in situ measurements (see Chapter 5) perfectly matches the conclusion.

Compared with the dramatic decline of reflectance caused by larger scattering at  $1.2\mu\text{m}$  - $1.3\mu\text{m}$  with increase of snow grain size, the reflectance shift at  $0.4\mu\text{m}$  - $0.6\mu\text{m}$  is much less. The calculation results on snow grain radius and reflectance (or albedo) in both Figure 7.1 and Figure 7.3 clearly show the flagrant contrast for reflectance decline.

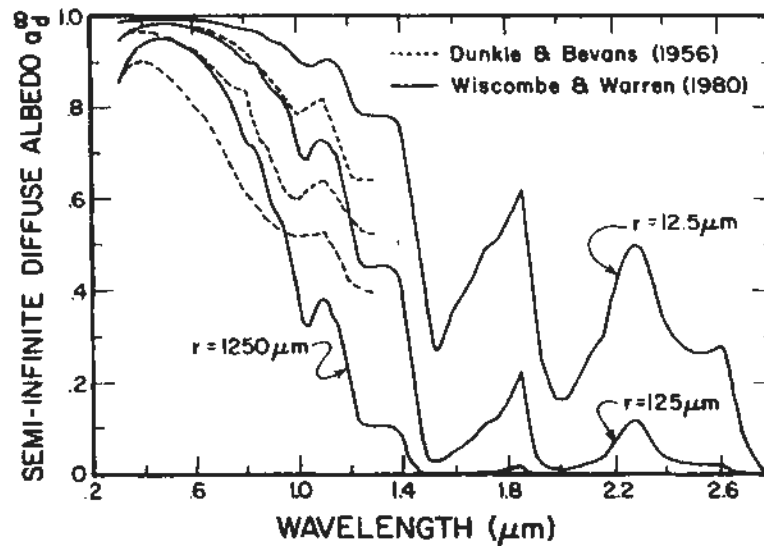


Figure 7.3 Model calculations of semi-infinite diffuse albedo as a function of wavelength for various snow grain radius

Figure 2. (Adopted from Optical properties of Snow, by Warren, 1982, pp.71)

The reflectance at  $1.5\mu\text{m}$  remains comparatively static when snow grain radius is larger than  $200\mu\text{m}$ . However, in most cases the grain size of natural snow is larger than  $200\mu\text{m}$  (Rees, 2005). The insitu measurement over Northeast China is a proof of that (see Chapter 5). Therefore, it can be concluded that with the increase of snow grain size, the reflectance at  $1.2\mu\text{m} - 1.3\mu\text{m}$  will dramatically drops, while the reflectance at  $0.4\mu\text{m} - 0.6\mu\text{m}$  and  $1.5\mu\text{m}$  are relatively stable. Consequently the difference between reflectance at  $0.4\mu\text{m} - 0.6\mu\text{m}$  and  $1.2\mu\text{m} - 1.3\mu\text{m}$  significantly decreases, and that between  $1.2\mu\text{m} - 1.3\mu\text{m}$  and  $1.5\mu\text{m}$  obviously increases with the growth of snow grain size. The change regularity derived from in situ measurement in Chapter 5 is the result of this.

Thus, an expression can be drawn out from above theory for detection on snow grain size changes:

$$T = \frac{R_{0.5\mu\text{m}} - R_{1.25\mu\text{m}}}{R_{1.25\mu\text{m}} - R_{1.5\mu\text{m}}} \quad 7.1$$

Here  $C_T$  is the threshold for change detection and  $R$  represents reflectance at different wavelength. The subscript is wavelength selected according to sensitivity to snow grain size. In this thesis, the three wavelengths are selected according to both snow physical properties and channels that MODIS can provide.

To compare the values of  $C_T$  calculated for same location but in different dates, the change trend of snow grain size can be deduced.

The model can be applied into imagery pixels that fully covered by pure snow. However, there are still some other issues that need to be considered. Although ice particles are highly transparent in the visible, which lead to a weak dependence on the grain size, it does no mean snow reflectance at visible range is always as high as new fallen snow because of the absorption by impurities, which have very high effect on reflectance in this region. The value of  $C_T$  may be degraded by lower reflectance at  $0.5\mu m$  but not the changes at  $1.25\mu m$ . Besides, other land cover types, such as soil and vegetation, also have effect on reflectance (see Figure 7.4).

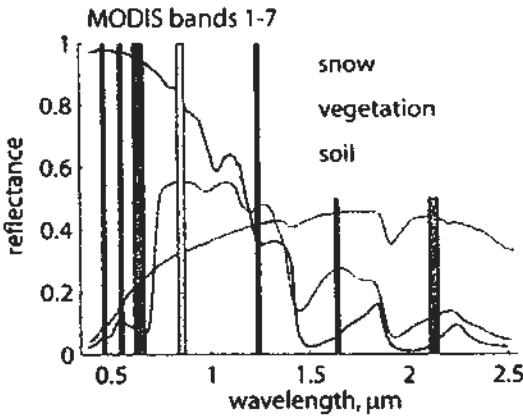


Figure 7.4 Typical reflectance of snow, soil and vegetation and corresponding detection channels of MODIS data

Figure 3. (Adopted from Retrieval of subpixel snow covered area, grain size, and albedo from MODIS. By Painter, T., Rittger, K., McKenzie, C., Slaughter, P., Davis, R., Dozier, J. (2009). Remote Sensing of Environment, 113 (2009), 868–879)

The mixture of soil or vegetation and snow will lead to the decrease of reflectance in band 2 (near  $0.5\mu m$ ) as well as increase in band 6 (near  $1.5\mu m$ ). There is a slightly increase on reflectance at  $1.25\mu m$  (band 5) can be found. It means that mixed pixel or impurity will decrease the value of  $C_T$ . Thus, in the practice the effects on  $C_T$  from mixed pixel and impurity need to be considered. The experiments on mixed spectrum confirm the conclusion (see Chapter 4 and 5).

Painter *et al.* (2009) solve the problem by establishing a spectral database of all kinds of typical, mixture spectra and comparing the measured spectra with samples in database.

In this thesis, the ratio of  $C_T$  and NDSI is performed to reduce the effects of mixture and impurity on spectrum. Consequently, the criteria can be modified as:

$$C_T = \frac{R_{0.5\mu m} - R_{1.25\mu m}}{R_{0.5\mu m} + R_{1.25\mu m}} / NDSI \tag{7.2}$$

Here the ratio used in formula can reduce the effects both from solar and sensor

zenith and topography. The wavelengths selected for calculation are less affected by water vapor.

### 7.1.2.3 Improved SD Retrieval Model

In the algorithm of original Chang,  $a$  is taken as constant in certain area. In North China, the value of  $a$  is assigned as 0.78 (Li & Che, 2007). However, the estimation results of both ascend or descend AMSR-E data show that RMSE of estimation SD is huge (see Chapter 5). Compared with the underestimation over forest areas, the situations for meadow and cropland are more complex. Crosses or trend that will lead to cross in the curves of estimation results and measurements once are found in both dry and wet snow periods. Linear model for SD retrieve based on passive microwave data is seems to be destroyed by the comparatively large changes on snow grain size inside snowpack. As it is discussed above, the problem is cause by the fixing value of ‘ $a$ ’, which is not static. Actually, the value of ‘ $a$ ’ is changing according to the changes of snow grain size. According to previous research results, the value of ‘ $a$ ’ is originally assigned as 1.59 when the model is applied in North America, and changed to be 0.78 in Eurasia because that snow grain size in the two continents is changing from coarser to finer. But actually, snow grain size over Northeast China varies from 0.2mm to over 2mm, and changes over time and snow status.

To solve the problem, an addition model to detect the change of snow grain size based on MODIS data is introduced into NASA algorithm (see Formula 3.5) to determine the value of ‘ $a$ ’:

$$SD = A_{gs} (T_{b,18} - T_{b,37}) \quad 7.3$$

Where  $A_{gs}$  is the function of  $T$  and original  $A_{gs_o}$ :

$$A_{gs} = A_{gs_o} / (1 + \Delta T / 5) \quad 7.4$$

Here  $\Delta T$  is the difference of  $T$  calculated from images obtained on different dates.

### 7.1.2.4 In Situ Snow Parameters Measurement

The ground data include important weather conditions (daily morning and afternoon air temperatures) and significant snow parameters (SD, SWE and snow grain size). SWE were estimated via the snow density, which is determined by melting a snow

column and dividing the melted water height by the snow column height. To develop an accurate SD retrieval model, field experiments and long term observation are essential (see Chapter 4 and 5). The in situ measurements will be used in assessment of Chang's SD retrieval model and the improved model developed in this thesis.

### **7.1.2.5 Data**

#### **7.1.2.5.1 AMSR-E L2A Data**

In this study, data from several sources are applied. They are AMSR-E L2A data, MODIS data, and in situ measurement of snow parameters.

The AMSR-E Level-2A product contains brightness temperatures at 6.9 GHz, 10.7 GHz, 18.7 GHz, 23.8 GHz, 36.5 GHz, and 89.0 GHz. Two channels required for snow monitoring are 18.7 GHz and 36.5 GHz. By using brightness temperature ( $T_b$ ) for the two channels together with location information, SD map will be generated. Brightness temperature can be calculated by using formula 7.7.

To calculate SD, brightness temperatures of 18.7 GHz and 36.5 GHz from 1st Nov 2007 to 1st Apr 2008 over Northeast China are acquired by using equation 3.5 with spatial resolution of approximately 0.1 degree in this study.

#### **7.1.2.5.2 MODIS L1B Data**

MODIS image provides 36 channels. Reflectance from band 4, band 5 and band 6 is needed in snow grain size monitoring.

#### **7.1.2.5.3 In Situ Data**

In situ measurements on SD from 8 test sites, daily precipitation and temperature data from 101 weather stations are applied in this research as validation of improved model.

### 7.1.3 SD Estimation Results and Discussion

#### 7.1.3.1 Snow Grain Size Estimation Results and Discussion

Figure 7.5 shows the continuous monitoring of snow grain size from 27<sup>th</sup> Feb., 2007 to 14<sup>th</sup> Mar., 2007. The value of  $T$  is classified into five levels:

$$T' = \begin{cases} 1, & 0 < T \leq 0.1 \\ 2, & 0.1 < T \leq 0.3 \\ 3, & 0.3 < T \leq 0.5 \\ 4, & 0.5 < T \leq 0.8 \\ 5, & 0.8 < T \leq 1 \end{cases} \quad 7.5$$

The value for pixels where is identified as non-snow covered or lack of data is assigned as -1. From the Figure we can found that snow grain size over northwest of study area increased slightly from 27<sup>th</sup> Feb., 2007 to 3<sup>rd</sup> Mar., 2007. On 4<sup>th</sup> Mar., 2007, it seems to change greatly in comparison with previous day. On most of the area that covered by snow a day before, snow grain size decreases from 2 to 1, and over the area that is identified as non-snow covered, snow grain size appears. From in situ precipitation data (see Table 7.1), it can be found that there was a snow storm on 4<sup>th</sup> Mar., 2007. The storm lasted for 2 days in most of stations from which the in situ data were collected. When it comes to 6<sup>th</sup> Mar., 2007, snow grain size decreased in comparison with that on 3<sup>rd</sup> Mar., 2007. Because that when there is a snow storm, the accuracy of optical remote sensing data trend to be declined. Therefore, the snow grain size on 6<sup>th</sup> Mar. need to be compared with that on 3<sup>rd</sup> Mar.. On 8<sup>th</sup> Mar., snow grain size increased slightly. While on 10<sup>th</sup> it declined again because there is a snowfall that day (see Table 7.1). On the following days, snow grain size keeps increasing when snow stopped in most of stations.

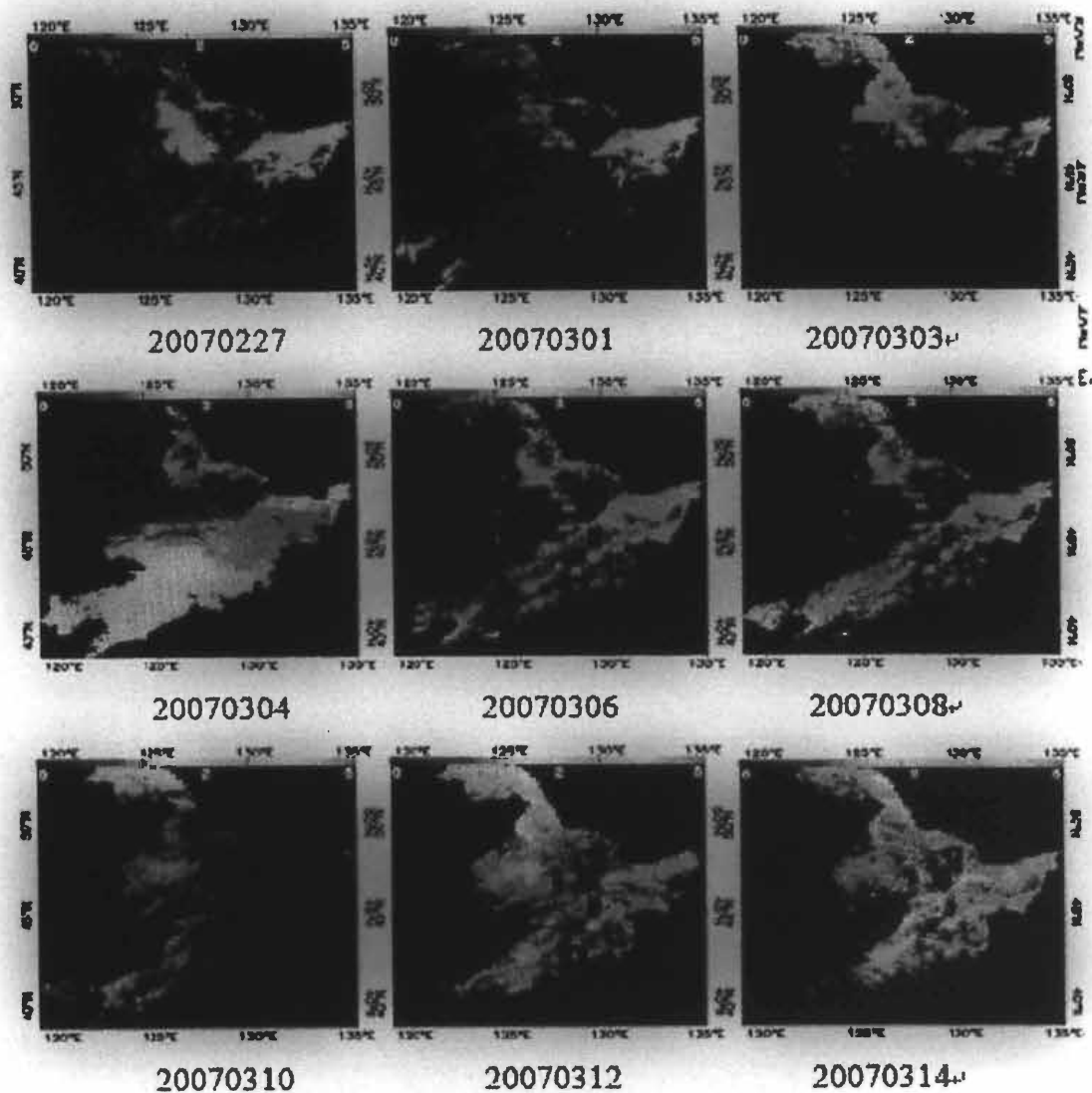


Figure 7.5 Continuous Monitoring on Snow grain size

Table 7.1 In situ Precipitation on the time duration in corresponding to Figure

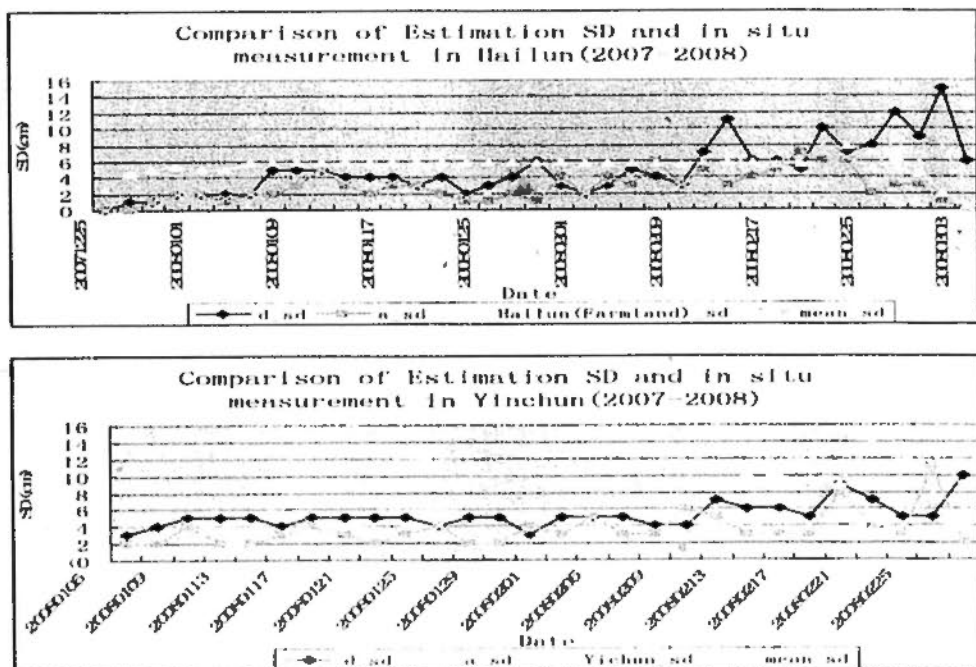
| Date     | Average Precipitation (mm) | Numbers of Precipitation stations (Among 101) |
|----------|----------------------------|---|
| 20070227 | 0.18                       | 8   |
| 20070228 | 0                          | 0   |
| 20070301 | 0.25                       | 15  |
| 20070302 | 0.05                       | 4   |
| 20070303 | 0.16                       | 6   |
| 20070304 | 11.13                      | 54  |
| 20070305 | 4.77                       | 45  |
| 20070306 | 0.05                       | 3   |
| 20070307 | 0                          | 0   |
| 20070308 | 0                          | 0   |
| 20070309 | 0.17                       | 10  |
| 20070310 | 2.41                       | 53  |
| 20070311 | 0.24                       | 5   |
| 20070312 | 0.01                       | 1   |
| 20070313 | 0                          | 0   |
| 20070314 | 0                          | 0   |

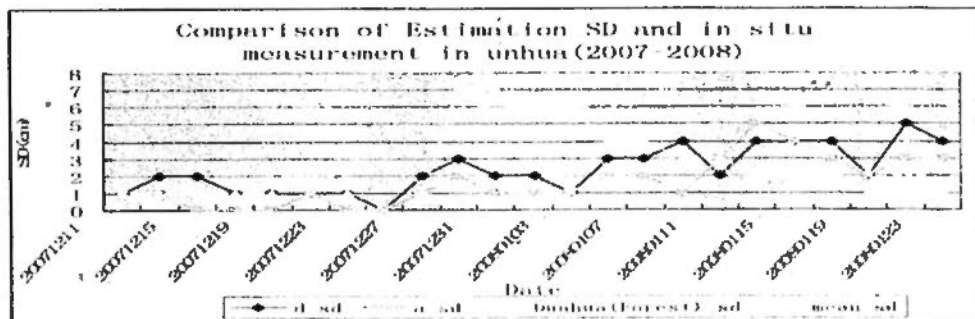
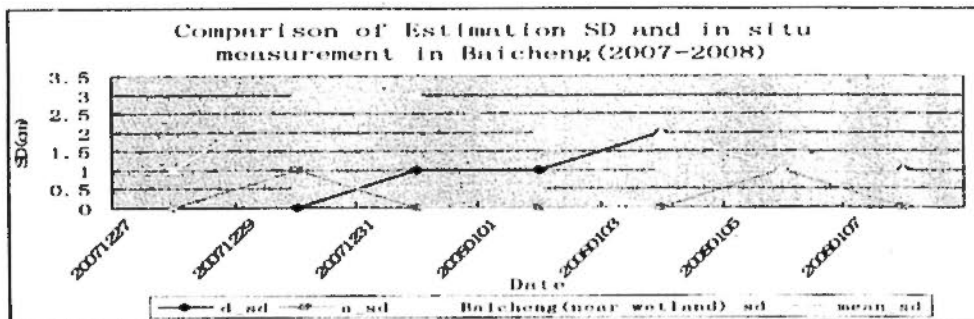
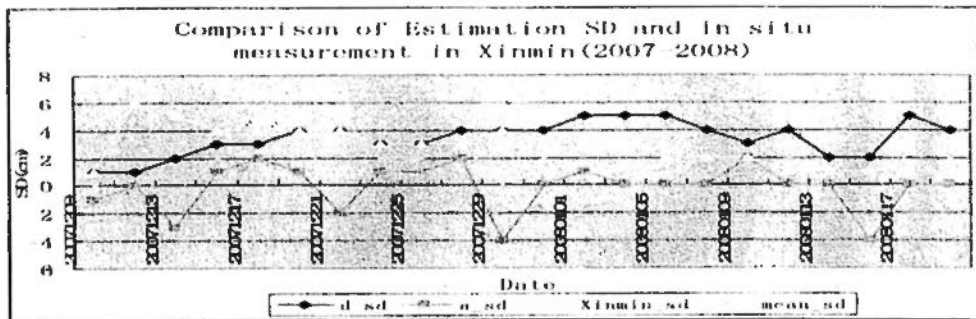
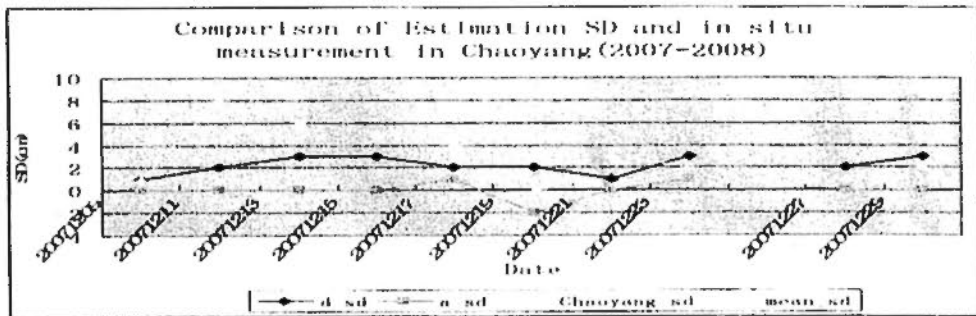
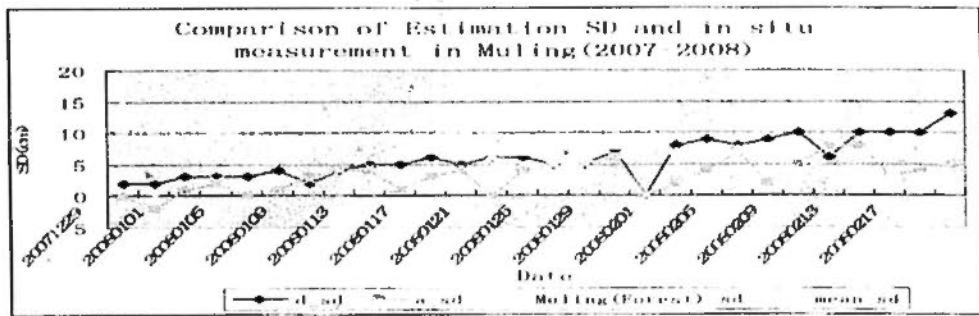
From the comparison of monitoring results and in situ precipitation, it is obviously that the grain size detection model can provide an accurate monitoring result on the changes of snow grain size. According to in situ measurement, the grain size of new fallen snow is approximate 0.2mm. Therefore, the value of  $a$  can be deduced by using the initial value and level of grain size change provided by the detection model.

### 7.1.3.2 Discussion on SD Retrieval Results of Original Model and Improved Model

Figure 7.6 shows the comparison of estimation SD and measurements in 8 test sites by using original SD retrieval model developed by Chang *et al.* (1987). It is obviously that during the dry snow season, SD is underestimated over both forest and cropland. The underestimate over cropland is larger than that of forest. While in the wet snow season, the estimation result is more complex because of the effect of liquid water contained in snow body.

From both ascending and descending satellite estimation, the retrieval SD are lower than that of measured, in most cases. It is similar to the results discussed in Chapter 5 and previous sections. It is to say, the improved model should be applied.





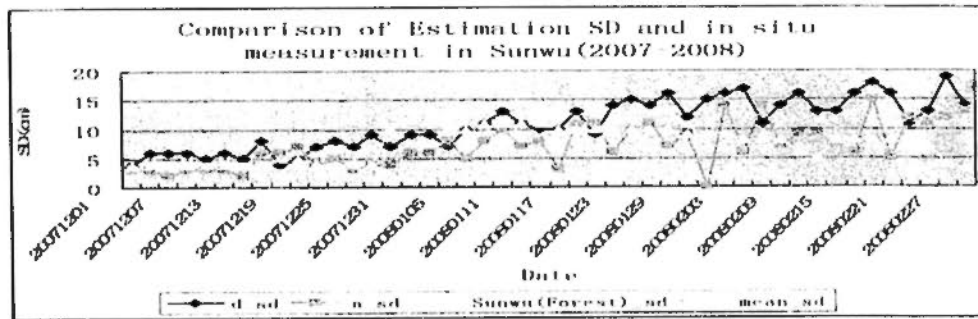
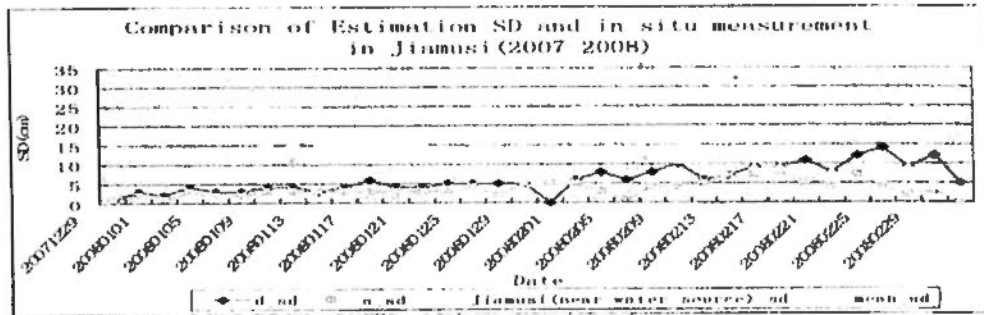
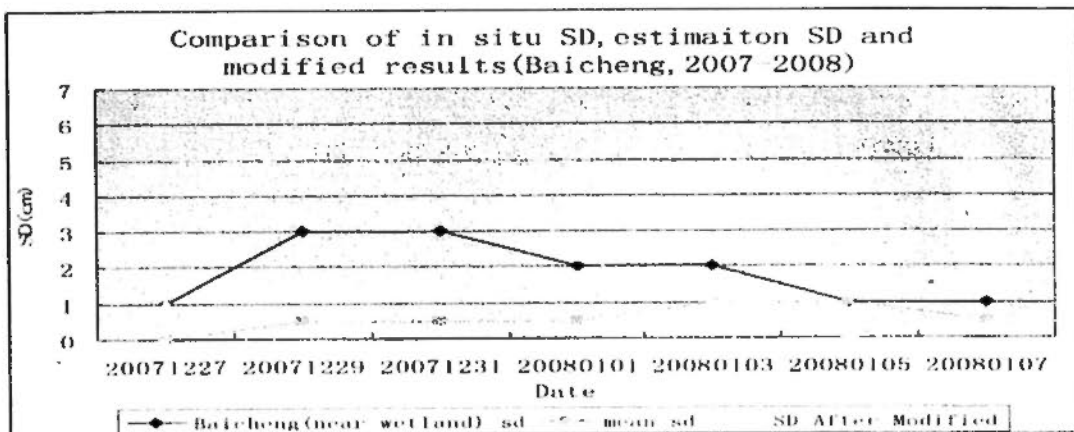
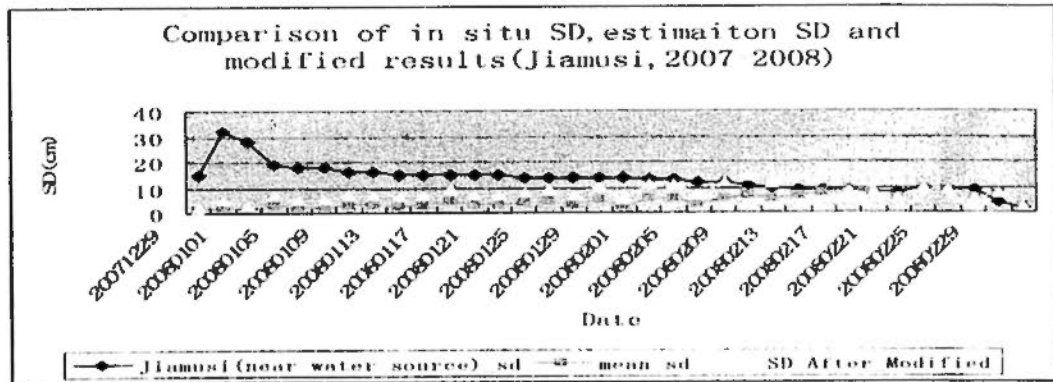


Figure 7.6 Comparison of measurement SD and estimation result in 8 test sites during 2007-2008 winter. Results in Figure 7.7 and Table 7.2 show that, the improved SD retrieval model can provide a more efficient and accurate results in comparison with existing ones.



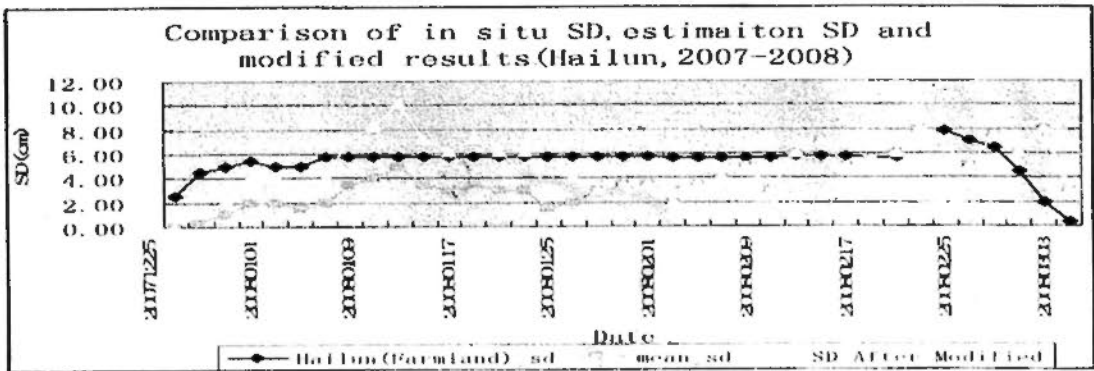
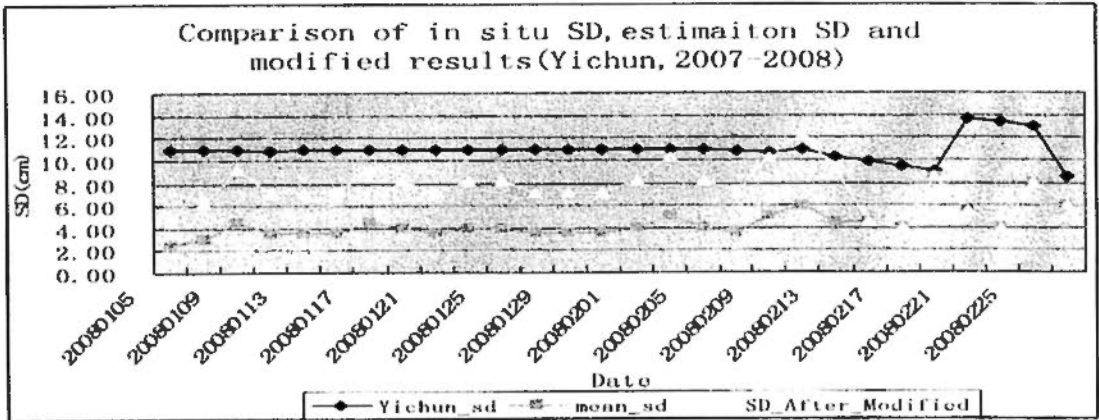
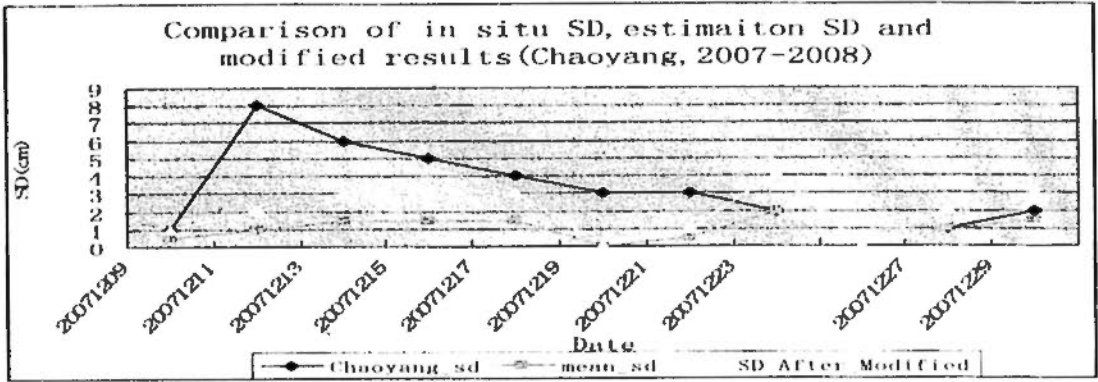
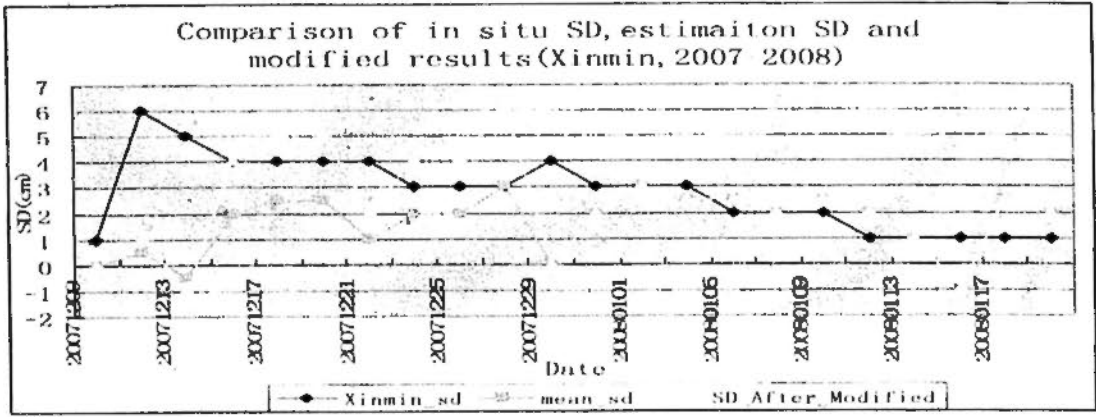


Figure 7.7 Comparison of in situ SD, original estimation SD and improved SD

Table 7.2 RMSE of original and improved models

| Test Sites | RMSE_original model | RMSE_new model | Memo   |
|------------|---------------------|----------------|--------|
| Sunwu      | 4.21                | --             | Forest |
| Jiamusi    | 10.93               | 8.86           | --     |
| Dunhua     | 2.39                | --             | Forest |
| Xinmin     | 2.21                | 2.20           | --     |
| Chaoyang   | 3.07                | 2.49           | --     |
| Muling     | 5.64                | --             | Forest |
| Yichun     | 6.64                | 4.03           | --     |
| Hailun     | 2.97                | 2.56           | --     |

### 7.1.4 Conclusion

The breakpoints mentioned in Chapter 5 show that there is a great potential in the accuracy improvement for snow information, such as SD and SCA, monitoring. In this section, an improved SD retrieval model is developed by creating a snow grain size detection model. For the application of the improved model, following rules should be noted:

1. According to the in situ measurements and experiments, the major effect on difference of 18GHz and 37GHz is frozen ice. The difference of the two channels is minus over ice underlying surface. Minus value can also be found in the experiments on pasture. However it only happened where the SD of test site is shallow. The estimation result is generally lower than in situ measurements in both forest and farmland. But the correlation of Jingyu is higher than that of Dehui. Thus, classification of land cover types is introduced into improved model. During the estimation, forest area, ice and agricultural land are separated. And the performance of improved model over cropland is the best.
2. Temperatures of 10 selected test sites are analyzed. Result shows that more than 80% of test sites were explored under below -3 in the period of 11-15~03-15. Then the dry snow period is defined from 11-15 to 03-15 the next year.
3. After careful analyzing, the crossing trend is found to appear in the following 2 situations:
  - a) When the measured SD increases dramatically (new fallen snow)
  - b) When it does not snow for a few days since last snow (accumulated snow)

Now it is easier to understand the reason that causes these crosses. Brightness temperature of snow is very sensitive to snow grain size. As it is noted Chapter 5, the grain size of new fallen snow in Northeast China is about 0.2mm. But the accumulated snow has much larger grain size, which can be ten times of new fallen snow. As accumulated time goes by, the grain size is increasing. When snow grain size becomes smaller, the trend of under estimation on SD appears; vice versa, especially in the area deep hoar appeared.

To reduce the estimation errors caused by naturally changes of snow grain size, a branch model to monitor snow grain size timely need to be applied to determine the value of the changeable constant  $a$ .

4. The comparing results show that, the improved model can efficiently

## **7.2 SCA Retrieval Model**

### **7.2.1 Introduction**

Snow cover mapping is significant for global albedo estimation, which is directly related to global climate, and hydrology monitoring. In the past two decades, research on SCA is mainly focusing on optical and passive microwave remote sensing. Satellite optical remote sensing data provide finer spatial resolution for snow monitoring in comparison with passive microwave data, however, cloud cover is an insolvable problem in application at visible region. Statistics on cloud cover status from 6 weather stations (2 in Heilongjiang, 2 in Jilin, and the last 2 are selected from Liaoning according to different land cover types) for totally 279 days, when selected station is covered by snow, show that, only more than half of observation days the selected station is covered by cloud (see Figure 7.8), and the duration of cloud cover could last for more than 8 days (see Table 7.3). Percentage of Lower cloud cover, which could be a main factor of overestimation of snow cover with optical data, is 17.56%. The statistical results show that over Northeast China, cloud cover is still a big problem in SCA estimation using optical remote sensing data, which will cause both overestimation and underestimation of snow extent. The SCA estimation results shown in Chapter 6 just confirm the conclusion. And the conclusion is similar to that Frei & Lee (2010) got in their study on optical-band based snow extent products.

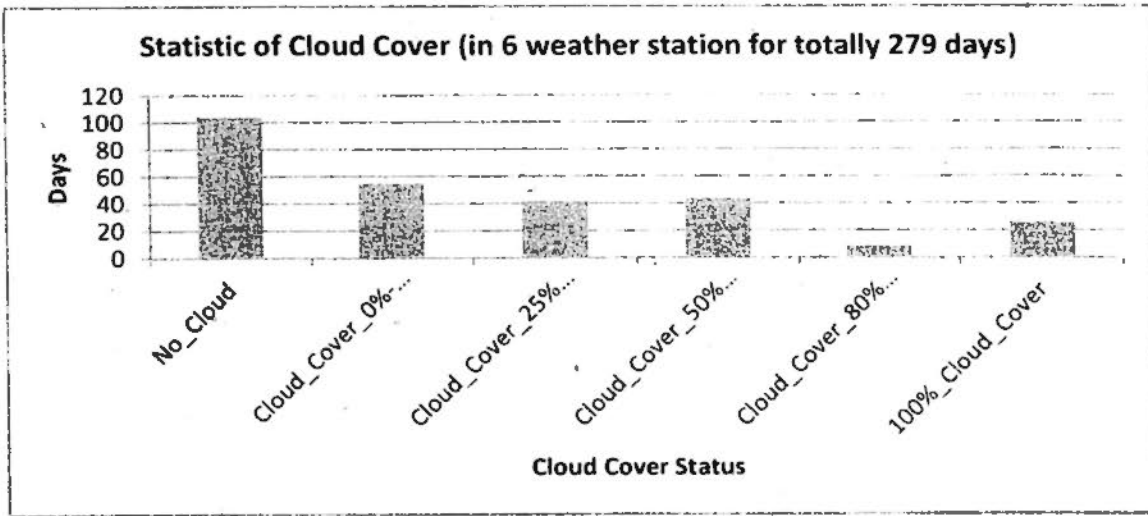


Figure 7.8 Statistics of Cloud Cover

Table 7.3 Example of Cloud Cover Duration

| Station Name | Date     | SD (cm) | Cloud Cover Status (%) |
|--------------|----------|---------|------------------------|
| Sunwu        | 20071224 | 4       | 5                      |
| Sunwu        | 20071225 | 4       | 30                     |
| Sunwu        | 20071226 | 4       | 75                     |
| Sunwu        | 20071227 | 4       | 65                     |
| Sunwu        | 20071228 | 4       | 63                     |
| Sunwu        | 20071229 | 10      | 100                    |
| Sunwu        | 20071230 | 12      | 100                    |
| Sunwu        | 20071231 | 12      | 75                     |

Another approach to monitoring SCA is to detect SD by using passive microwave data (detailed explain can be found in Chapter 2 and 3). Snow is the only object on the earth that can provide decline emission with the increase of frequency (Rees, 2005). Based on this property, algorithms and models are generated to distinguish snow from other land surfaces. However, the effect of underlying surface sometimes is stronger than emission of radiation of snow on the surface. Rees conclude that thick lack ice or frozen ground may cause the radiation attenuation at 18 GHz. Field experiments on lake ice and thin snow covered meadow and processing results of AMSR-E data prove the theory (see Chapter 5 and 6). It is obviously that over Northeast China, where great amount of area are covered by thin snow with frozen ground or lake ice as underlying surface, estimation accuracy of SCA by using AMSR-E data is not convincing enough for practices application, regardless the overestimation and underestimation caused by coarse spatial resolution. In this section, improved model for SCA monitoring based on the combination of MODIS and AMSR-E data will be discussed. The improved model takes advantage of higher spatial resolution of MODIS data and the penetrability of AMSR-E data to eliminate

the effects of cloud and underlying surface on optical and passive microwave remote sensing data, respectively.

## **7.2.2 Methodology**

### **7.2.2.1 Data**

#### **7.2.2.1.1 MODIS L1B Data**

Daily MODIS L1B data, MOD10A1 data, MOD10A2 data from Nov. 1<sup>st</sup>, 2007 to Apr. 1<sup>st</sup>, 2008 were applied in SCA monitoring in this study. The former is used as input of the improved model, but the later two are utilized as comparison.

#### **7.2.2.1.2 AMSR-E L2A Data**

Re-sampled AMSR-E L2A data are applied in this research as complement of MODIS L1B data in SCA monitoring. The spatial resolution of re-sampled AMSR-E data is  $0.05d \times 0.05d$  after the special designed processing (see Chapter 6). The finer microwave data will provide a better estimation result by reducing the overestimation and underestimation caused by coarse resolution in comparison with original data provided by NSIDC.

#### **7.2.2.1.3 In Situ Data**

In situ precipitation data and temperature data observed from 107 weather stations over Northeast China are applied in this study as Criterion on performance in the comparison between improved SCA monitoring model and MODIS snow products.

### **7.2.2.2 In Situ Precipitation Processing Method**

In situ precipitation data will be applied in the study to confirm the presence of snow. However, precipitation can not be translated into snow covered map information without temperature condition analysis in test station. Thus, a special designed processing method for translation of daily precipitation into snow cover status is needed to pre-process these in situ obtained from weather stations to get in situ snow covered information in selected stations. If temperature of selected station is higher

than 0, daily precipitation is considered as rain. Under the circumstances that temperature is lower than 0 and daily precipitation is more than 0, the ground is absolutely covered by snow. Between the two states, the presence of snow is uncertain. Figure 7.9 shows the flowchart of snow map generation.

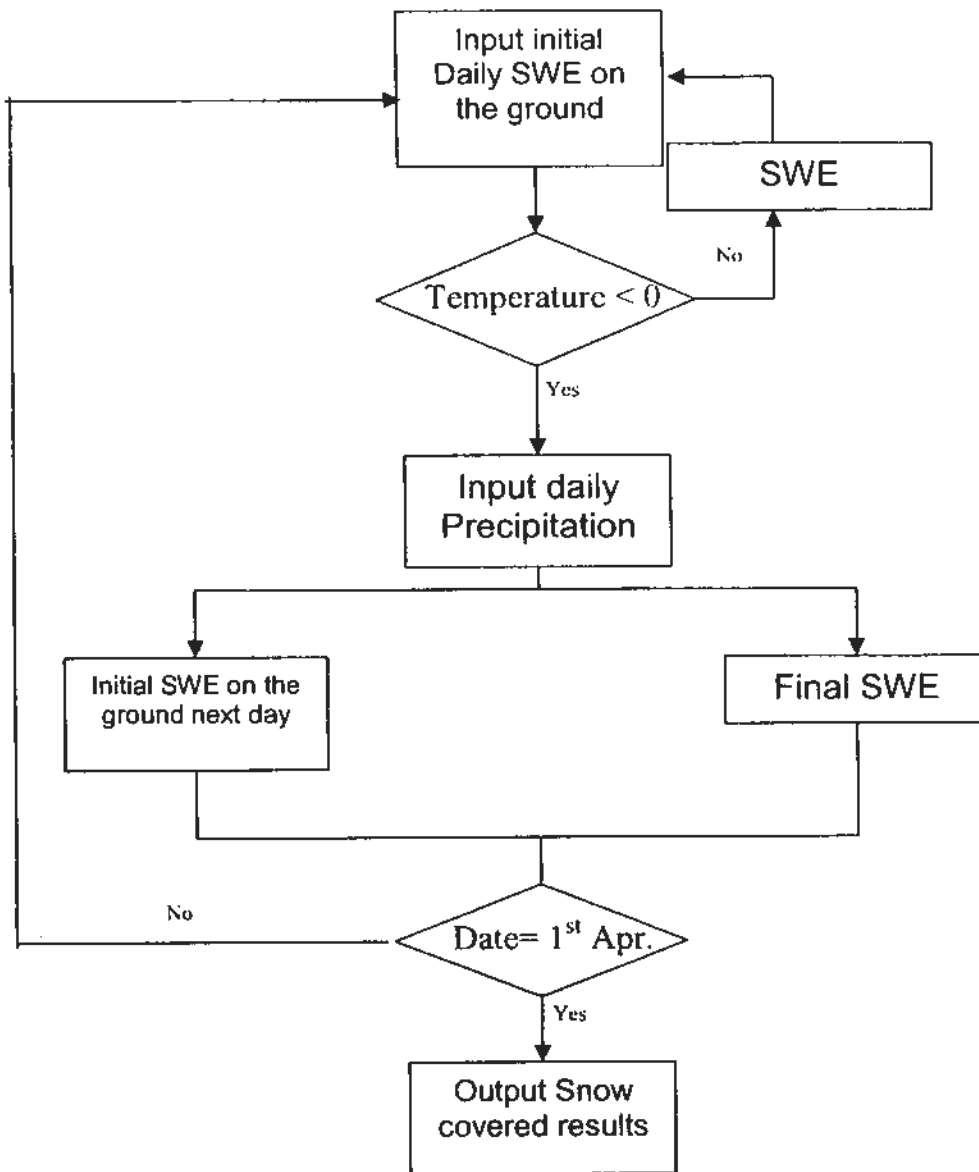


Figure 7.9 Flowchart of in situ snow covered map generation

8-day maximum snow extends of in situ measurements are derived from daily in situ snow map. The pixels with precipitation value greater than 0 during the period of eight successive days are marked as snow covered state.

### 7.2.2.3 Improved SCA Estimation Model

#### 7.2.2.3.1 Cloud Detection Model

During the processing of MODIS data, cloud presence need to be detected. Although NDSI can distinguish most of kinds of cloud from snow, however, it can not tell cloud from other land surface. In this study, cloud detection model is applied to mark all of the pixels that covered by different kinds of cloud:

For lower thick cloud of which reflectance is as high as almost 1 at visible range and slowly declines with increase of wavelength at near-infrared region, band 1 and band 6 can be applied in detection; for higher cold cloud, less liquid water is contained inside cloud body, which makes reflectance of this kind of cloud comparatively high in near-infrared region than all the other land surface. Band 26 is designed for the detection of high cold cloud. To sum up, clouds can be detected by using the following model:

$$0 < \frac{R_1 - R_6}{R_1 + R_6} \leq 0.4 \quad \text{For lower thick cloud}$$

$$R_{26} \geq 0.1 \quad \text{For high cold cloud}$$

7.6

$R_1$ ,  $R_6$  and  $R_{26}$  are reflectance from Band 1, Band 6 and Band 26 of MODIS data, respectively. The pixels that satisfy the judgment can be identified as cloud.

#### 7.2.2.3.2 Threshold Definition of Non-Forest and Density Forestry Area

For those pixels that are not covered by cloud, NDVI is calculated. Both ground based experiments on mixed pixels and previous researches (see Chapter 2 and 5) show that the threshold of NDSI over snow covered forest areas is supposed to be lower than 0.4. Klein, Hall and Riggs (1998) suggested that the threshold of NDSI in the pixel with value of NDVI larger or equal 0.4 should be 0.2.

In our study area, grassland and farmland tend to present a low value of NDVI during late autumn and winter because that deciduous tree contributes a large part of forest in this region. To figure out the threshold for NDSI, the threshold of NDVI for density forest can be deduced in following method:

$$DensityForest\_proportion = \frac{NDVI_{threshold} - NDVI\_MIN}{NDVI\_MAX - NDVI\_MIN} \quad 7.7$$

Here NDVI MAX and NDVI MIN are the values of minimized and maximal pixels of NDVI map. And the Density Forest\_proportion is statistic of density forest coverage rate of study area.

According to the study of Ji *et al.* (2007), the covering of forestry in Liaoning Province is 31.84 percent. By using the NDVI maps of maximal extended NDVI of 10 days (downloaded from Environmental and ecological science data center for west China (westdc.westgis.ac.cn) freely), the threshold for density forest in Liaoning is 0.4 by using NDVI map derived on 1<sup>st</sup> Nov., 2007. Considering that the vegetation condition over the whole Northeast China is very similar with that of Liaoning, in this research, threshold of NDVI is assigned as 0.4. Therefore, for the pixels with NDVI equal or great that 0.4, threshold of NDSI is 0.2.

### 7.2.2.3.3 AMSR-E Complement

AMSR-E snow map with spatial resolution of 5km generated by using the method mentioned in Chapter 6 is applied as supplement in last procedure to improve modeling accuracy by eliminating effects of cloud. Besides, for daily snow mapping, neither MODIS nor AMSR-E data can always cover the whole area everyday, the combination of MODIS and AMSR-E data provide the possibility to generate the complete daily map. For those pixels that marked as cloud covered or lack of data, locations are calculated to capture snow presence information from exact the same location on AMSR-E snow map.

## 7.2.3 SCA Estimation Results and Discussion

Figure 7.10 shows the snow maps on 5<sup>th</sup> Mar., 2007 before and after the complement of AMSR-E data. 20% of area is covered by cloud, which makes it impossible to determine the snow presence under clouds. And the proportion that covered by cloud is too large to be accepted in practices application. After the supplement of AMSR-E data, the effect of cloud is eliminated.

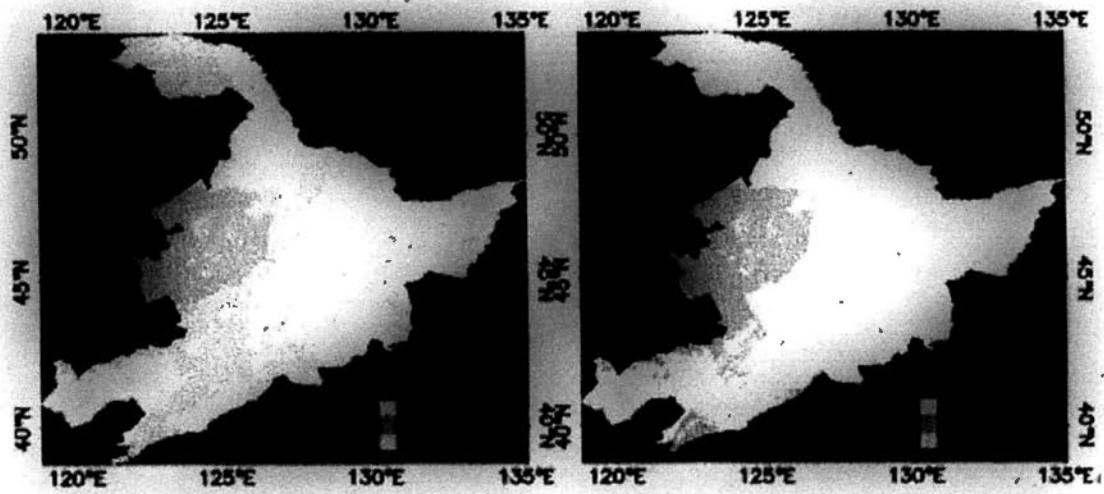


Figure 7.10 Snow maps on 5<sup>th</sup> Mar., 2007 before and after the complement of AMSR-E data

Therefore, the application of improved SCA retrieval model provides better estimation results by reducing the underestimate caused by cloud and data missing from MODIS sensors.

Daily snow maps show that on most of days, estimation SCA percentage of improved model is higher than that of MODIS snow product, except two days: 3<sup>rd</sup> Feb., 2007 and 19<sup>th</sup> Feb., 2007, on which days there are no MODIS images available (Figure 7.11).

8-day MODIS snow product is generated to reduce the effect of cloud by the greatest extend using optical remote sensing data, however, as it is discussed in introduction and previous researches, the effect still exists. Only the application of multi-sources remote sensing data can really solve the problem. Although there are still other effect factors, such as underlying surface, the underestimate is improved (see Figure 7.12).

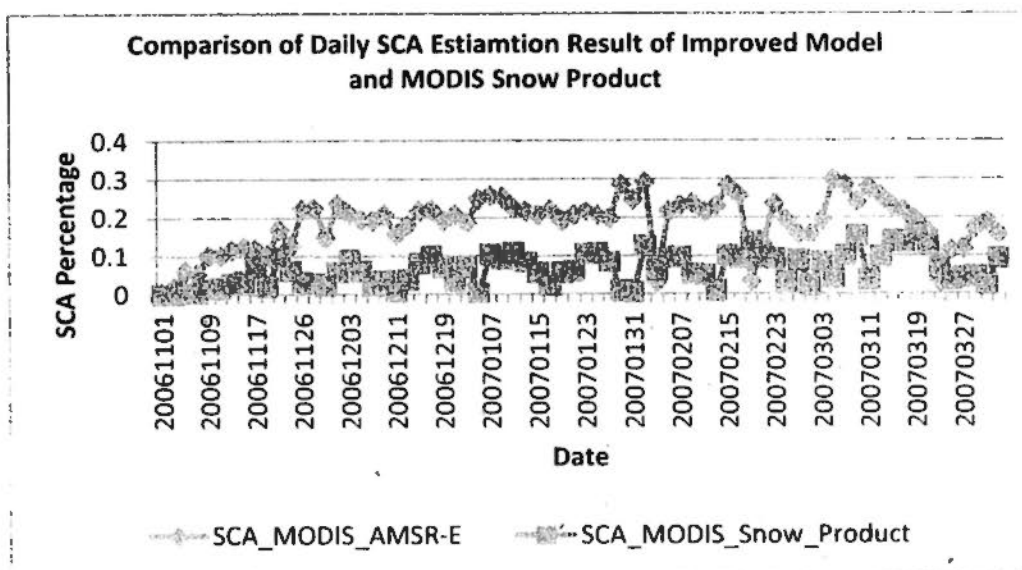


Figure 7.11 Comparison of daily SCA estimation result of improved model and MODIS snow product

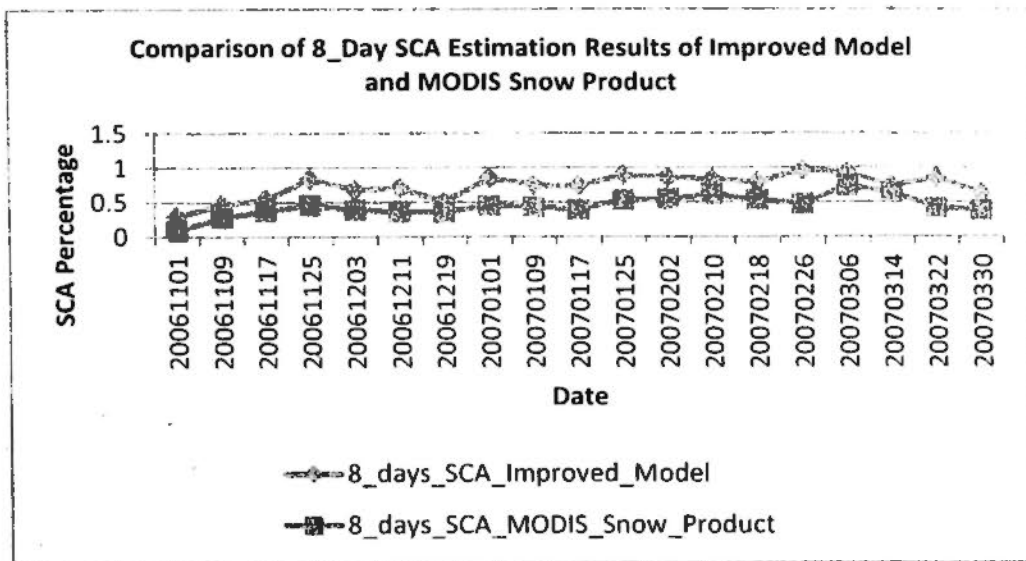


Figure 7.12 Comparison of 8-day SCA estimation results of improved model and MODIS snow product. In situ snow presence map generated by using of precipitation is utilized as validation source to assess the performance of improved model in comparison with 8-day MODIS snow product (see Figure 7.13). From the figure it can be observed that the most misjudged as non-snow stations can be found by using MODIS snow product. And the best performance is found for improved model. The model mentioned in Chapter 6 by using an unconvincing empirical judgment on cloud frequency will produce more errors than the improved model by using combination of MODIS and AMSR-E data.

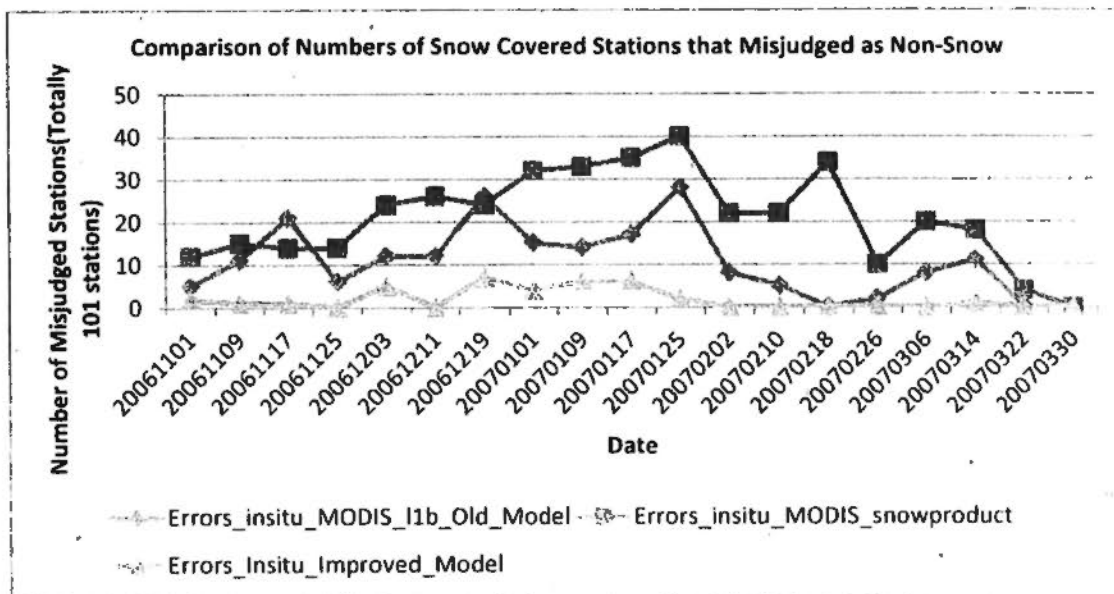


Figure 7.13 Comparison in numbers of snow covered stations that misjudged as non-snow

## **7.2.4 Conclusion**

The combination of MODIS and passive microwave data in previous research is mainly focused on spatial resolution. Here in this study, the problem that caused by coarse spatial resolution of AMSR-E data is partly solved via using re-sampling procedure. However, the minus value over lake ice, frozen ground and shallow snow covered meadows are much bigger problems that urgently need to be solved, just as the effect of cloud on optical remote sensing.

To reduce the effects of cloud and underlying surface that cause huge errors in optical remote sensing model and passive microwave model, the combination of MODIS and AMSR-E processed with special re-sampling method is applied in an improved SCA retrieval model. The performance of improved model in daily and 8-day snow mapping shows that the effect of underestimate can be efficiently reduced. Although the error-judgment, which is caused by the effect of underlying surface over cloud covered area still exist. Further researches on the effect of underlying surface need to be conducted in near future.

## **Chapter 8 INNOVATIONS AND FUTURE WORKS**

In this chapter, the achievements during this study will be elaborated. Based on this achievements, future works snow monitoring over this study area will be discussed.

### **8.1 Innovations**

As it is mentioned in the first several chapters, research work on snow monitoring based on satellite remote sensing data over Northeast China is significant. Snow distribution over Northeast China is one piece of the jigsaw puzzle of global climate. Snow cover over Northeast China is both the result of global and local climate changes, and the primary contribution factors to the changes of circulation of atmosphere and energy balance in both local and global scale. Besides, for local scale, the information of snow cover is the most important parameters for agriculture

models as water sources, insect pests and plant diseases prediction and disaster managements.

Therefore, for the areas such as Northeast China, where is (a) the food production area and livestock breeding center of the whole country; (b) one of the three largest black soil areas, the significance of snow cover could not be described in words.

Because of above reasons, the study in the thesis has important significance in both theory and practice. The contribution of this study can be described in the following ways:

1. It is the first time that snow cover over Northeast China has been systematically studied from the ground based experiments to the application of satellite remote sensing techniques.

During the past two years, systematically study on snow properties by conducting snow sampling, field experiments and long term observations have been done to get a better understand snow physical properties. The first road trip series experiment has been performed to get the first degree data on effects of underlying surface. The second step of snow monitoring study over this area is the introduction of satellite remote sensing data and models based on the understanding of snow properties here. Only after the successful application of satellite remote sensing data on this field, it can be claimed that the whole systematic study on snow monitoring is finished. Both optical and microwave remote sensing data are applied as complement for each other. It is a great progress in comparison with results obtained in the past decades when only in situ data or MODIS data were tried in snow monitoring over this region.

2. The improved snow monitoring models are developed in the thesis. In Chapter 6 and Chapter 7, four systems are designed, which are Mass of MODIS data automatic pre-processing system, mass of AMSR-E data automatic pre-processing system, improved SCA monitoring model based on optical remote sensing data (MODIS data) and improved SD retrieval model based on both MODIS and AMSR-E data.

The processing of mass of satellite remote sensing data is always a tough task to deal with for all the researchers in remote sensing field. Someone may say that it is not a big deal to processing satellite image for their research when there are only a few images, like ten or twenty, that need to be prepared. But it does a matter when there are thousands of or even millions of images are waiting in the

list in a mid-long or long term research. How can analysts get high quality input data, which will determine the analysis results directly, for the monitoring system? How could researchers get the images responding to special and flexible requirements on spatial and temporal resolution? Manually processing method is definitely not the best choice to solve all above problems. Here in this research, automatic processing systems for MODIS and AMSR-E data are developed to deal with these issues. And till now, there is no such publication that can be found on this particular problem.

Two improved models for SCA and SD retrieval are developed as the outcomes of this research. Statistic results on improved models and initial ones prove that there are significant improvements on the estimation results of both of the two improved retrieval models.

3. The most important innovation in this thesis is the initial introduction of data assimilation.

In both of improved SCA and SD estimation models, multi-sources of satellite or in situ measurements are applied to improve the accuracy dynamically, especially in SD retrieval. Snow grain size determines the constant of our retrieval model. In the past, this constant is selected according to locations and when it is decided, in the whole processing period, the value will not be changes under the hypothesis that snow grain size of the same location is fixed. However, during our in situ measurements, the hypothesis is found to be wrong. The snow grain size in Northeast China varies from 0.2mm to more than 3mm, or even larger when the deep hoar layer generates. That the main reason that causes the cross of estimation curve and in situ measurement one. Thus, the value of 'constant' (In the existing applications of Chang's algorithm, 'a' in formula 3.5 is constant) should change according to the changes of grain size to improve SD estimation accuracy. In improved SD retrieval model, MODIS data are input into the model to amend the crucial parameter –snow grain size for SD estimation. It is the first time that MODIS data are utilized in a passive microwave model for the amending of input parameter but not for fining the spatial resolution. It can be considered as an initial application of data assimilation theory in satellite snow monitoring. The advantage of this assimilation is its convenience and efficiency in comparison with that of in situ grain size measurements. The performances of all of the two processing systems and two improved models show us that the

improvement of these models is not only on the saving of processing time and man power but also the estimation accuracy in comparison with the existing models. Because of the new method of data assimilation, now snow monitoring system can be practically applied in Northeast China.

4. Some other scientific problems are carried out and the direction is orientated for future study.

Besides the scientific problems that have been solved in the thesis, there are still some other matters that affect monitoring accuracy, such as the effect of river ice on SD retrieve. All thesis potential effects were mentioned in the analysis and discussion section in Chapter 5 and Chapter 7. Researchers who work on snow monitoring could follow the idea and try to attack the problem from these aspects.

## 8.2 Future Work

Because of the limitation on length of thesis, only the key issues that are badly need to be solves are mentioned here. Actually, there are still some other problems and further works standing in the waiting list. They are:

1. SD estimation by using optical remote sensing data. Since the water percentage in snow has great effect on microwave signals, the monitoring of snow in wet snow period should be completed by other sources than AMSR-E. However, study on SD retrieve based on optical data is still on going now. In the near future, we will work on this problem.
2. Snow information monitoring over ice area. As it is mentioned in Chapter 5, because of the effects of thin ice on microwave signals, the value of difference between 18 GHz and 37GHz is minus. It means that models based on this difference do not work on the frozen area. Alternative method is needed for snow monitoring over river ice or frozen ground.
3. Shallow snow monitoring. As it is shown in field experiments, shallow snow can hardly be detected by using the difference of 18 and 37 GHz. It is the similar question as 1.
4. Accurate retrieve of snow grain size by using MODIS reflectance. In this thesis, the retrieval model for snow grain size is a rough one. That is to say, by using this model, only increasing or decreasing trend can be determined. Because there

are so many effects on optical signals, till now perfect way to reduce all the effects and get the absolute value of grain size still in the air. Instead, the ratio of slopes shows us the changing trend and scale. As we know, normally the grain size of new fallen snow is around 0.2mm, the changing trend and scale could tell us how do we adjust the value of 'constant'  $a$ . In the future, more works should be done on snow grain size to get the specific size value.

5. The last but one of the most important thing in future snow monitoring work is the combination of GIS system. As it is known, GIS and remote sensing techniques are always interdependent, mutually promotive in the whole history of their development. The monitoring result of snow should be applied into a certain GIS system, and meanwhile, the estimation accuracy of snow will be greatly improved by using GIS system in the procedure of retrieval. For example, the application of DEM model, which is a GIS system improved accuracy of SCA models over mountain areas. In the near future, the forest GIS system is considered to be applied in the improvement of estimation accuracy over forest areas. It worth to try GIS, as well as meteorological, terrain and land use data in snow information retrieval to get higher accuracy in the time researchers have a bottle-neck in this issue.

To solve the problems carried out in this thesis, more researches, especially field experiments, should be conducted.

# References

- Aballe, A., Bethencourt, M., Botana, F., and Marcos, M. (1999). Using wavelets transform in the analysis of electrochemical noise data. *Electro. Chimica. Acta*, 44(26), 4805-4816.
- Akhoondzadch, M. & Saradjian, M.R. (2008). Comparison Of Land Surface Temperature Mapping Using Modis And Aster Images In Semi-Arid Area . *The International Archives of the Photogrammetry, Remote Sensing and Spatial Information Sciences*. XXXVII. Part B8. Beijing 2008, 873-876
- Andreadis, K. M. and Lettenmaier, D.P.(2006).Assimilating remotely sensed snow observations into a macroscale hydrology model. *Advances in Water Resources*, 29(6), 872-886.
- Armstrong, R., Brodzik, M., and Savoie, M. (2004). Enhanced Snow Cover Mapping Using Combined Optical and Passive Microwave Data. *Geoscience and Remote Sensing Symposium, IGARSS'*, 861-864
- Armstrong, R., Chang, A., Rango, A. and Josberger, E.(1993). Snow depths and grain-size relationships with relevance for passive microwave studies. *Annals of Glaciology* ,17, 171-176.
- Armstrong, R.L, Brodzik, M. J. (2002). Hemispheric-scale comparison and evaluation of passive-microwave snow algorithms. *Annals of Glaciology*, 34, 38—44.
- Ashcraft, I., and Long, D. (2005). Differentiation Between Melt and Freeze Stages of the Melt Cycle Using SSM/I Channel Ratios. *IEEE Transactions On Geoscience And Remote Sensing*, 43(6), 1317-1320.
- Baker, D.G., Skaggs, R.H. and Ruschy, D.L.(1991) Snow depth required to mask the underlying surface. *Journal of Applied Meteorology*, 30, 387 392.
- Biancamaria, S., Mognard, N., Boone, A., Grippa, M., Josberger, E. (2008). A satellite snow depth multi-year average derived from SSM/I for the high latitude regions. *Remote Sensing of Environment* ,112(2008), 2557 2568.
- Baral, D.J., and Gupta, R.P. (1997) Integration of satellite sensor data with DEM for the study of snow cover distribution and depletion pattern. *International Journal of Remote Sensing*, 18 (1 8), 3889-3894.

- Basist, A., Grody, N., and Peterson, T. (1998). Using the Special Sensor Microwave Imager to monitor land surface temperatures, wetness and snow cover. *Journal of Applied Meteorology*, 37(9), 888–911.
- Bauer, P., and Grody, N. (1995). The potential of combining SSM/I and SSMTI2 measurements to improve the identification of snow cover and precipitation. *IEEE Transactions on Geo.science and Remote Sensing*, 33, 252-261.
- Bernier, M., Fortin, J.P.(1998). The potential of times series of C-Band SAR data to monitor dry and shallow snow cover. *Geoscience and Remote Sensing, IEEE Transactions on*, 36(1), 226-243.
- Chang, A., Foster, J. , Hall,D.(1987). Nimbus-7 SMMR derived global snow cover parameters. *Annals of Glaciology*, 9, 39-44.
- Chang, A., Foster, J., and Rango, A. (1991). Utilization of surface cover composition to improve the microwave determination of snow water equivalent in a mountain basin. *International Journal of Remote Sensing*, 12, 2311–2319.
- Chang , A., and Rango, A. (2000). Algorithm Theoretic Basis Document (ATBD) for the AMSR-E Snow Water Equivalent Algorithm, Version 3.1. NASA, 2000.
- Chang, A., Foster, J., Hall, D., Rango, A., and Hartline, B. (1982). Snow water equivalent estimation by microwave radiometry. *Cold Regions Science and Technology*, 5(3), 259-267.
- Chang, A.& Tsang, L.(1992). A neural network approach to inversion of snow water equivalent from passive microwave measurements. *Nordic Hydrology*, 23(3), 173-182.
- Cao, S., Li, X., Chen, X., Wang, J., Che, T. (2006). Remote Sensing of Cryosphere. Science Press (110-112)
- Chen, J. (2007). Study on Cloud Detection methods based on MODIS data. Master Degree thesis
- Chen, J., Sun, L. (2010).Using MODIS EVI to detect vegetation damage caused by the 2008 ice and snow storms in south China. *Journal Of Geophysical Research*, 115, G00H04 (in Press).
- Che, T.,Li, X., Gao, F. (2004). Estimation of Snow Water Equivalent in the Tibetan Plateau Using Passive Microwave Remote Sensing Data (SSM/I). *Journal Of Glaciology And Geocryology*, 26(3), 261-266.
- Choudhury, B.J., and Chang, A. (1979). The solar reflectance of a snow field. *Cold Regions Science and Technology*, 1(2), 121-128.

- Cline, D., Bales, R., and Dozier, J. (1998). Estimating the spatial distribution of snow in mountain basins using remote sensing and energy balance modeling. *Water Resources Research*, 34 (5), 1275-1 285.
- Derksen, C., Walker, A., Goodison, B. (2003). A comparison of 18 winter seasons of in situ and passive microwave-derived snow water equivalent estimates in Western Canada. *Remote Sensing of Environment*, 88(3), 271-282.
- Derksen, C., Walker, A., Goodison, B. (2005). Evaluation of passive microwave snow water equivalent retrievals across the boreal forest/tundra transition of western Canada. *Remote Sensing of Environment*, 96 (2005), 315 – 327
- Derksen, C., Walker, A., and Toose, P. (2008). Estimating Snow Water Equivalent in Northern Regions from Satellite Passive Microwave Data. *Cold Region Atmospheric and Hydrologic Studies. The Mackenzie GEWEX Experience*, Berlin Heidelberg : Springer, 195-212
- Dozier, J. (1984). Snow reflectance from Landsat-4 Thematic Mapper. *IEEE Transactions on Geoscience and Remote Sensing*, GE22 (3), 323-328.
- Dozier, J. (1989). Spectral signature of Alpine snow cover from the Landsat Thematic Mapper. *Remote Sensing of Environment*, 28, 9-22.
- Dozier, J., Green, R., Nolin ,A., Painter, T.(2009). Interpretation of snow properties from imaging spectrometry. *Remote Sensing of Environment*, 113 (2009), 25–S37
- Durbha, S., King, R., Wasson, L., Pradhan, P.(2002). Virtual remote sensing: a holistic modeling approach. *Geoscience and Remote Sensing Symposium*, 2, 723-725(2002)(IGARSS '02. 2002 IEEE International Volume 2, 24-28 June 2002).
- Frei, A., and Lee, S. (2010). A comparison of optical-band based snow extent products during spring over North America. *Remote Sensing of Environment*, 114 (2010),1940-1948.
- Fu, B., Wang, C., and Zeng, Z. (2007). Geometrical correction of MODIS Data based on IDL. *Remote Sensing Information*, Vol. 2, 20-23.
- Foster, J., Chang, A. and Hall, D. (1997). Comparison of snow mass estimates from prototype passive microwave snow algorithm, a revised algorithm and a snow depth climatology. *Remote Sensing of Environment*, 62(2), 132 – 142.

- Foster, J., Hall, D., Kelly, R., Chiu, L. (2009). Seasonal snow extent and snow mass in South America using SMMR and SSM/I passive microwave data (1979-2006). *Remote Sensing of Environment*, 113(2009), 291–305.
- Foster, J., Chang, A., Hall, D., and Rango, A.(1991). Derivation of Snow Water Equivalent in Boreal Forests Using Microwave Radiometry. *Arctic*, 44, 147-152.
- Foster, J., Hall, D., Chang, A., and Rango, A.(1984). An overview of passive microwave snow research and results. *Rev. Geophys. Space Phys.*, 22 (2), 195–208.
- Gan, T.(1996). Passive microwave snow research in Canadian high arctic. *Canadian J. Remote Sens.*, 22(1), 36–44.
- Goita, K., Walker, A. and Goodison, B.(2003). Algorithm development for estimation of snow water equivalent in the boreal forest using passive microwave data. *International Journal of Remote Sensing*, 24, 1097–1102.
- Goita, K., Walker, A., Goodison, B., and Chang, A. (1997). Estimation of Snow Water Equivalent in the Boreal Forest Using Passive Microwave Data. Proceedings, GER '97 (International Symposium: Geomatics in the Ear of Radarsat), published by Natural Resources Canada and National Defence.
- Goodison, B., Waterman, S., and Langham, E.(1980) Application of synthetic aperture radar data to snow cover monitoring. Sixth Canadian Symposium on Remote Sensing, at Halifax, Nova Scotia.
- Grody, N., Basist, A. (1996). Global identification of snowcover using SSM/I measurements. *Geoscience and Remote Sensing, IEEE Transactions*, 34(1), 237-249.
- Hall, D., Kelly, R., Riggs, G., Chang, A., and Foster, J.(2002). Assessment of the relative accuracy of hemispheric-scale snow-cover maps. *Annals of Glaciology*, 34, 24-30.
- Hall, D., Riggs, G., and Salomonson, V. (1995). Development of methods for mapping global snow cover using moderate resolution imaging spectroradiometer data. *Remote Sensing of Environment*, 54, 127-140.
- Hallikainen, M. (1984). Retrieval of Snow Water Equivalent from Nimbus-7 SMMR Data: Effect of Land-Cover Categories and Weather Conditions. *Ieee Journal Of Oceanic Engineering*, OE-9, (5),372-376.

- Hallikainen, M., and Jolma, P. (1986). Retrieval of the Water Equivalent of Snow Cover in Finland by Satellite Microwave Radiometry. *IEEE Transactions On Geoscience And Remote Sensing*, Gc-24(6), 855-865.
- Hallikainen, M., Lahtinen, P., Zhang, Y., Takala, M., Pulliainen, J. (2005). Feasibility of satellite Ku-band scatterometer data for retrieval of seasonal snow characteristics in Finland, Geoscience and Remote Sensing Symposium, 2005. IGARSS '05. Proceedings. 2005 IEEE International, 3, 1936- 1939
- Hewison, T., and English, S. (1999). Airborne retrievals of snow and ice surface emissivity at millimeter wavelengths. *IEEE Transactions on Geoscience and remote sensing*, 37(4), 1871-1879.
- Hiltbrunner, D. and Mätzler, C. (1997). Land surface temperature retrieval and snow discrimination using SSM/I data. Proceedings of the EARSeL Workshop Remote Sensing of Land Ice and Snow, University of Freiburg Germany, 87-94.
- Hofer, R., and Matzler, C. (1980). Investigations on snow parameters by radiometry in the 3- to 60-mm wavelength region. *Journal of Geophysical Research*, 85 (C1), 453-460.
- IPCC (2007). Summary for Policymakers of Climate change 2007: The Physical Science Basis. Contribution of Working Group I to the Fourth Assessment Report of the Intergovernmental Panel on Climate Change (M). Cambridge University Press, Cambridge, UK.
- Immerzeel, W., Droogers, P., de Jong, S., Bierkens, M. (2009). Large-scale monitoring of snow cover and runoff simulation in Himalayan river basins using remote sensing. *Remote Sensing of Environment*, 113(2009), 40-49.
- Ji, R., Zhang, Y., Feng, R., Chen, P., Zhang, S., Wu, J. (2007). Analyzing the Changing Characteristics of Agricultural Climate Resources in Liaoning Province. *Resources Science*, 29, 74-82
- Jin, Z., Charlock, T., Yang, P., Xie, Y., Miller, W. (2008). Snow optical properties for different particle shapes with application to snow grain size retrieval and MODIS/CERES radiance comparison over Antarctica. *Remote Sensing of Environment*, 112, 3563-3581
- Ke, C., Liu, C. and Li, P. (1998). Evaluation of SMMR Data of Snow Cover in Western China Based on GIS. *Remote Sensing Technology and Application*, 13(4), 36-42

- Kelly, R., Chang, A., Foster, J., Hall, D. (2005). Using Remote Sensing and Spatial Models to Monitor Snow Depth and Snow Water Equivalent. *Spatial Modelling of the Terrestrial Environment* (pp.35-58), Chichester: John Wiley and Sons, Ltd.. 35-58.
- Kelly, R., Chang, A., Tsang, L. (2003a). A prototype AMSR-E global snow area and snow depth algorithm. *IEEE Transactions on Geoscience and Remote Sensing*, 41(2), 230–242.
- Kelly, R., Chang, A., Tsang, L., and Foster, J. (2003b). A Prototype AMSR-E Global Snow Area and Snow Depth Algorithm. *IEEE Transactions on Geoscience and Remote Sensing*, 41(2), 230-242.
- Klein, A., Hall, D., and Riggs, G. (1998). Improving snow-cover mapping in forests through the use of a canopy reflectance model. *Hydrological Processes*, 12, 1723- 1744.
- Klein, A., Hall, D., And Riggs, G. (1998b). Global Snow Cover Monitoring Using MODIS, *27th International Symposium On Remote Sensing Of Environment* June 8-12, 363-366.
- König, M., Winther, J., and Isaksson, E. (2001). Measuring snow and glacier ice properties from satellite. *Reviews of Geophysics*, 39 (1), 1-27.
- Koskinen, J., Pulliainen, J., Hallikainen, M.(1997). The use of ERS-1 SAR data in snow melt monitoring. *IEEE Transactions on Geoscience and Remote Sensing*, 35( 3), 601-610.
- Kunzi, K., Patil, S. and Rott, H.(1982). Snow cover parameters retrieved from Nimbus-7 Scanning Multichannel Microwave Radiometer (Smmr) data, *IEEE Trans. Geosci. Remote Sens*, GE-20 (4), 452 467.
- Kurvonen, L., and Hallikainen, M. (1997). Influence of land-cover category on brightness temperature of snow. *IEEE Transactions on Geoscience and Remote Sensing*, 35(2), 367–377.
- Leptoukh, G., Ouzounov, D., Savtchenko, A., Ahmad, S., Li, L., Pollack, N., Liu, Z., Johnson, J., Qin, J., Cho, S., Li, J., Kempler, S., Teng, B.(2003). HDF/HDF-EOS Data Access, Visualization and Processing Tools at the GES DAAC. *Geoscience and Remote Sensing Symposium*, 6, 3571–3573(2003) (IGARSS '03. Proceedings. 2003 IEEE International Volume 6, 21-25 July 2003).

- Li, W., Satmnes, K. and Chen, B. (2001). Snow grain size retrieved from near-infrared radiances at multiple wavelengths. *Geophysical Research Letters*, 28, 1699-1702.
- Li, Z., He, Y., Pu, T., Jia, W., He, X., Pang, H., Zhang, N., Liu, Q., Wang, S., Zhu, G., Wang, S., Chang, L., Du, J., Xin, H. (2010). Changes of climate, glaciers and runoff in China's monsoonal temperate glacier region during the last several decades. *Quaternary International*, 218(2010), 13-28
- Li, X., and CHE, T. (2007). A Review on Passive Microwave Remote Sensing of Snow Cover. *Journal Of Glaciology And Geocryology*, 29(3), 683-694.
- Liang, T., Huang, X., Wu, C., Liu, X., Li, W., Guo, Z., Ren, J. (2008). An application of MODIS data to snow cover monitoring in a pastoral area: A case study in Northern Xinjiang, China. *Remote Sensing of Environment*, 112 (2008), 1514-1526.
- López-Moreno, J.I., Goyette, S., Beniston, M. (2009). Impact of climate change on snowpack in the Pyrenees: Horizontal spatial variability and vertical gradients. *Journal of Hydrology*, 374(2009), 384-396.
- Luo, J., Pulliainen, J., Hallikainen, M. (2004). Accuracy assessment for HUT snow covered area estimation method. Proceedings of IEEE 2004 International Geoscience and Remote Sensing Symposium (IGARSS'04), 3511-3514, Anchorage, Alaska, USA, 20-24 September.
- Lyapustin, A., Tedesco, M., Wang, Y., Aoki, T., Hori, M., Kokhanovsky, A. (2009). Retrieval of snow grain size over Greenland from MODIS. *Remote Sensing of Environment*, 113 (2009), 1976-1987.
- Ma, Y., Zuo, H., Zhang, Y., Hui, X. (2005). Analyses On Variation Trends Of Atmospheric Visibility And Its Effect Factor In Multi Cities In Central Liaoning. *Plateau Meteorology*, 24(4), 623-628
- Massom, R. (1991). Satellite Remote Sensing of Polar Regions. Boca Raton, Florida: Lewis Publications.
- Masuoka, E., Tilmes, C., Devine, N., Gang, Y., Tilmes, M. (2001). Evolution of the MODIS science data processing system. Geoscience and Remote Sensing Symposium, 3, 1454-1457 (IGARSS '01. IEEE 2001 International, 9-13 July 2001).
- Matson, M., Ropelewski, C., and Varnadore, M. (1986). An Atlas of Satellite-Derived Northern Hemisphere Snow Cover Frequency. Washington,

- DC:U.S. Department of Commerce. National Oceanic and Atmospheric Administration Data and Information Service. National Environmental Satellite, Data and Information Service.
- Mätzler, C. (1994). Microwave transmissivity of a forest canopy: Experiments made with a beech. *Remote Sensing of Environment*, 48( 2), 172-180.
- Mätzler, C. (1996). Microwave permittivity of dry snow. *IEEE Transactions on Geosc. And Rem. Sens.*, 34( 2), 573 – 581.
- Mätzler, C., Wiesmann, A. (1999). Extension of the microwave emission model of layered snowpacks to coarse-grained snow. *Remote Sensing of Environment*, 70, 317–325.
- Mätzler, C. and Wiesmann, A. (2007). Microwave Emission Model of Layered Snowpacks. Documentation for MEMLS, Version 3
- Negri, A., Nelkin, E., Adler, R., Huffman, G., and Kummerow, C. (1995). Evaluation of passive microwave precipitation algorithms in wintertime midlatitude situations. *Journal of Atmospheric and Oceanic Technology* ,12, 20-32.
- Nghiem, S. and Tsai, W.(2001). Global snow cover monitoring with spaceborne Ku-band scatterometer. *IEEE Transactions on Geoscience and Remote Sensing*, 39(10), 2118-2134.
- Nolin, A. Dozier, J., and Mertes, L.(1993). Mapping alpine snow cover using a spectral mixture modeling technique. *Annals of Glaciology*, 17, 121-124.
- Painter, T., Rittger, K., McKenzie, C., Slaughter, P., Davis, R., Dozier, J. (2009). Retrieval of subpixel snow covered area, grain size, and albedo from MODIS. *Remote Sensing of Environment*, 113 (2009), 868–879.
- Parajka, J.& Blöschl, G.(2008). The value of MODIS snow cover data in validating and calibrating conceptual hydrologic models. *Journal of Hydrology*, 358, 240-258.
- Pardé, M., Goïta, K., Royer, A. (2007). Inversion of a passive microwave snow emission model for water equivalent estimation using airborne and satellite data. *Remote Sensing of Environment*, 111 (2007), 346–356
- Pulliaminen, J. (2006). Mapping of snow water equivalent and snow depth in boreal and sub-arctic zones by assimilating spaceborne microwave radiometer data and ground-based observations. *Remote Sensing of Environment*, 101, 257-269.

- Pulliainen, J., Grandell, J., Hallikainen, M.(1999). HUT snow emission model and its applicability to snow water equivalent retrieval. *IEEE Transactions on Geoscience and Remote Sensing*, 37(3), 1378 –1390.
- Pulliainen, J, Hallikainen, M. (2001). Retrieval of regional Snow Water Equivalent from space-borne passive microwave observations. *Remote Sensing of Environment*, 75(1), 76 –85.
- Rccs, G.(2005). Remote sensing of snow and ice (pp.120-139), UK: Taylor&Francis Group.
- Robinson, D., Dewey, K., Heim, R . (1993). Global snow cover monitoring - An update. *Bulletin of the American Meteorological Society*, 74(9), 1689– 1696.
- Romanov, P. and Tarpley, D. (2004). Enhanced algorithm for estimating snow depth from geostationary satellites. *Remote Sensing of Environment*, 108(1), 97-110.
- Roshani, N., Valadan Zouj, M., Rezaci, Y. , Nikfar, M.(2008). Snow mapping of alamchal glacier using remote sensing data. The International Archives of the Photogrammetry, Remote Sensing and Spatial Information Sciences, XXXVII, Part B8, Beijing 2008
- Rott, H. and Mätzler, C. (1989). Preface to microwave observations of snowpack and soil properties. *Adv. Space Res*, 9 (1), 231–232.
- Roy, V., Goita, K., Royer, A., Walker, A., and Goodison, B. (2004). Snow water equivalent retrieval in a Canadian boreal environment from microwave measurements using the HUT snow emission model. *IEEE Transactions on Geoscience and Remote Sensing*, 42(9), 1850–1859.
- Salomonson, V., Appel, I. (2004). Estimating fractional snow cover from MODIS using the normalized difference snow index. *Remote Sensing of Environment*, 89(2004), 351–360.
- Salomonson, V. & Mao, J. (2004). A Sensitivity Analysis of the MODIS Normalized Difference Snow Index. Geoscience and Remote Sensing Symposium, IGARSS'04, 3717-3720.
- Seidel, K. & Martinec, J. (2004). Remote Sensing in Snow Hydrology Runoff Modelling, Effect of Climate Change (pp.33-61), Chichester,UK:Praxis Publishing Ltd..

- Slater, M., Sloggett, D., Rees, W., and Steel, A. (1999). Potential operational multisatellite sensor mapping of snow cover in maritime sub-polar regions. *International Journal of Remote Sensing*, 20 (15), 3019-3030.
- Singh, P., Gan, T. (2000). Retrieval of Snow Water Equivalent Using Passive Microwave Brightness Temperature Data. *Remote Sensing of Environment*, 74(2), 275-286.
- Solberg, R., Hiltbrunner, D., Koskinen, J., Guneriussen, T., Rautiainen, K., and Hallikainen, M.(1997). Snow algorithms and products - review and recommendations for research and development. SNOWTOOLS WP410. Oslo: Norwegian Computing Centre.
- Song, K., Zhang, Y. (2008). Snow-cover environmental monitoring and assessment in Northeast China using passive microwave emission models. *Environmental monitoring and assessment* , 140, 223-229.
- Song, K., Zhang, Y., Jin, C., Yan, S., and Chiu, L. (2008). Seasonal snow monitoring in Northeast China using space-borne sensors: Preliminary results, *Geographic Information Sciences*, 14 (2), 113-119.
- Sonnentag, O. (2008). Book review on Image Analysis, Classification and Change Detection in Remote Sensing (With Algorithms for ENVI/IDL). *Computers & Geosciences*, 34, 93–94.
- Stahli, M., Schaper, J., and Papritz, A. (2002). Towards a snow-depth distribution model in a heterogeneous subalpine forest using a Landsat TM image and an aerial photograph. *Annals of Glaciology*, 34, 65-70.
- Standley, A., and Barrett, E.C. (1999) . The use of coincident DMSP SSM/I and OLS satellite data to improve snow cover detection and discrimination. *International Journal of Remote Sensing* ,20 (2), 285-305.
- Stiles, W., and Ulaby, F.(1980a). The active and passive microwave response to snow parameters. 1. Wetness. *Journal of Geophysical Research*, 85(C2), 1037-1044.
- Stiles, W.& Ulaby, F.(1980b). Radar observations of snowpacks. *NASA Conference Publications*, 2153, 131-146.
- Tekel, E.(2005). Operational hydrological forecasting of snowmelt runoff by remote sensing and geographic information systems integration (THESIS)

- Tarumi, T., Smal, G., Combs, R. and Kroutil, R. (2004). High-pass filters for spectral background suppression in airborne passive Fourier transform infrared spectrometry. *Analytica Chimica Acta*, 501(2), 235-247.
- Tait, A., (1998). Estimation of Snow Water Equivalent Using Passive Microwave Radiation Data. *Remote Sensing of Environment*, 64(3), 286-291.
- Tedesco, M. and Miller, J. (2007). Observations and statistical analysis of combined active passive microwave space-borne data and snow depth at large spatial scales. *Remote Sensing of Environment*, 111(2-3), 382-397.
- Tsang, L., Chen, Z., Oh, S., Marks, R., and Chang, A. (1992). Inversion of snow parameters from passive microwave remote-sensing measurements by a neural network trained with a multiple-scattering model. *IEEE Transaction. on Geoscience and Remote Sensing*, 30(5), 1015-1024.
- Varhola, A., Coops, N., Weiler, M., Moore, R.. (2010). Forest canopy effects on snow accumulation and ablation: An integrative review of empirical results. *Journal of Hydrology*, 392(2010), 219–233.
- Vikhamar, D. & Solberg, R. (2000). A method for snow-cover mapping in forest by optical remote sensing methods. EARSeL Specialist Workshop on Remote Sensing of Land and Snow, Proceedings, at Dresden.
- Vogel, S. (2002). Usage of high-resolution Landsat-7 band 8 for single-band snowcover classification. *Annals of Glaciology*, 34, 53-57.
- Walker, A., Goodison, B. (1993). Discrimination of a wet snowcover using passive microwave satellite data. *Annals of Glaciology*, 17, 307-311.
- Walker, A., Goodison, B., and Metcalfe, J. (1995). Investigation of Boreal Forest Snow Cover Variations During the BOREAS 1994 Winter Campaign. *17th Canadian Symposium on Remote Sensing*. Saskatoon, Saskatchewan, June 13-15, 1995.
- Walker, A. & Silis, A. (2002). Snow-cover variations over the Mackenzie River basin, Canada, derived from SSM/I passive-microwave satellite data. *Annals of Glaciology*, 34, 8-14.
- Wang, X., Ding, X., and Du, A. (2004). Study on Model Base System of Earthquake Damage Extraction from RS in ENVI/IDL Environment. *Geoscience and Remote Sensing Symposium*, 2252–2255(2004) (IGARSS '04. Proceedings. 2004 IEEE International Volume 4, 20-24 Sept. 2004).

- Wang, X., Xie, H., Liang, T. (2008). Evaluation of MODIS snow cover and cloud mask and its application in Northern Xinjiang, China. *Remote Sensing of Environment*, 112, 1497–1513.
- Warren, S. (1982). Optical Properties of Snow. *Reviews of Geophysics and Space Physics*, 20(1), 67-89.
- Watson, W. (2006). Automated georeferencing for Rapid Data Production. *Photogrammetric Engineering and Remote Sensing*, 72(4), 337-338.
- Wiesmann, A. and Mätzler C. (1999). Microwave emission model of layered snowpacks. *Remote Sensing of Environment*, 70, 307–316.
- Xin, Y., Li, J., and Cheng, Q. (2007). Automatic Generation of Remote Sensing Image Mosaics for Mapping Large Natural Hazards Areas. *Lecture Notes in Geoinformation and Cartography*, Springer Berlin Heidelberg, 61-73.
- Ye, J., Yan, W., Li, Z. (2007). A Method Using Adding Priority Average for Mosaic Imagery with MODIS Multitrack Data. *Remote Sensing Information*, 2007(1), 43-46
- Zhang, Y, Ban, X., Ji, R., Yuan, G., Feng, R., Zhang, S.(2004). Analysis of Climatic Resources in Liaoning Province. *Meteorological Science And Technology*, 32, 39-43
- Zhang, Y., Yan, S. and Lu, Y. (2010). Snow Cover Monitoring Using MODIS Data in Liaoning Province, Northeastern China. *Remote Sens.*, 2010, 2(3), 777-793
- Zhao, S. (2003). *Analysis of Remote Sensing Applications, Principles and Methods*, Beijing: Science Press, 2003
- Zhou, G., Wang, C., Yang, F., Li, Y. (2009). Field Collected Plant Spectrum Denoising By Logarithm Transform And Wavelet Transform. *Infrared Millim. Waves*, 28(4), 316-320